ISSN 0494-7304 0207-4508

A R T U Ü L I K O O L I

TOIMETISED

CTA ET COMMENTATIONES UNIVERSITATIS TARTUENSIS

966

PUBLICATIONS ON CHEMISTRY

XXI

TARTU 1993

TARTU ÜLIKOOLI TOIMETISED

VIHIK 966

PUBLICATIONS ON CHEMISTRY

XXI

TARTU 1993

Dedicated to the 70th Anniversary of the Academic Society of Chemistry and the 105th Anniversary of the Tartu Sanitary Laboratory

CONTENTS

ON THE ACTIVITIES OF THE ACADEMIC SOCIETY OF CHEMISTRY 1923 - 1993

T.Tenno
Institute of Physical Chemistry, University of Tartu

The Academic Society of Chemistry was founded in Tartu in 1923, the initiators of the idea being the then students of chemistry Jaan Kranig and Arnold Tols. The students were also the members of the charter commission. The foundation meeting was attended by 49 chemists, almost all the lecturers of chemistry of the University of Tartu (Paul Kogerman, Michael Wittlich, August Paris and others) among them. Doc. Paul Kogerman was elected the first President of the Society. From 1927 the head of the Society was Michael Wittlich and after him August Paris from 1928 until the activity of the Society was terminated.

The objects of the Society were given as:

1) to unite all the chemists working in their field and the academic circles interested in chemistry;
2) to promote all-round development of chemists and arouse interest in the most important issues of chemical industry in Estonia.

In the foundation year, the Academic Society of Chemistry had 63 members, in the year 1932 the number was 123, with some ten being non-chemists. The main activities went on at meetings, where the lecturers, students and guests held reports. ASC arranged trips to chemical enterprises in Estonia and Latvia. Chemists' Days were arranged together with the Society of Chemistry of Estonia.

Committees were appointed to run the activities of the Society, the most active of them being the committee of elaborating chemistry terms (Paris, Tiganik and philologist, lecturer Veske), the committee of local chemical lore (Sinka, Pääro, Sossi, Ivask), committee of chemical occupational issues (Kogerman, Wittlich, Sossi) and that of history (Kogerman, Landesen, Laur).

In the years 1932-1937 the Academic Society of Chemistry published altogether 8 issues of its own journal "Keemia Teated"

(Newsletter of Chemistry). When the preparation of university-qualified chemists terminated at the University of Tartu in 1936, quite a few lecturers headed for Tallinn. In consequence of that, the activities of the Society subsided, until in 1940 the ASC as well as many other academic organizations were dissolved.

In 1989 it was decided to restore the Society of Chemistry of Estonia which had formerly operated in Tallinn. After that chemistry students of the University of Tartu put forward a proposal to restore the Academic Society of Chemistry as the legal successor of ASC on the basis of its historical continuity.

The re-foundation meeting of the Society took place on 11th December 1991, and it was attended by 41 chemists from the University of Tartu, University of Agriculture and other research institutions of Tartu. Student of chemistry Andres Rekker made an interesting report on the activities of the Society in the years 1923 - 1940. It was found at the meeting that both lecturers and students are interested in society life in Tartu as the activities of the Society of Chemistry in Tallinn are unfortunately not within easy reach of inhabitants of Tartu. An opinion was also expressed that these two societies could exist side by side in Estonia, collaborate, and joining either of they does not rule out participation in the activities of the other.

The Board of the Society was elected as follows: Indrek Ild, Tõnis Lepiku, Mart Loog, Enn Lust, Uno Mäeorg, Vilve Nummert, Lauri Ploom, Marju Salve and Toomas Tenno. Toomas Tenno and third-year student Indrek Ild were elected President and Vice-President of the Society respectively. To run the activities of the Society the following committees were appointed:

1) the committee of conferences and the like (V.Past, U.Mäeorg);
2) the committee of club life (E.Lust);
3) the committee of foreign relation (T.Tenno);
4) the committee of the history of chemistry, museum and chronicle (T.Ilomets);
5) the committee of coordination between institutions (L.Ploom);
6) the committee of student activities (A.Rekker, M.Loog).

At the foundation meeting the Charter of the Society of Academic Chemistry was adopted and a wish was expressed to organize speciality sections within the Society, to arrange seminars, discussions, excursions and joint workshops with the Society of Chemistry of Estonia.

In 1993 the Academic Society of Chemistry will be 70. Today it has 85 members. A festive conference will be held on 9th December to

2 1935 VIHK 3

KEEMIA TEATED

AKADEEMILISE KEEMIA SELTSI ÜLESANDEL

TOIMETANUD

AUGUST PARIS
(PEATOIMETAJA)

JAAN KOPWILLEM ANTS LAUR ADOLF PARTS
LEONHARD TIGANIK

Sisukord:

TARTU
28. XII. 1935

celebrate the jubilee, and the present collection of articles is also devoted to the jubilee anniversary of the Academic Society of Chemistry. With the re-foundation of the Academic Society of Chemistry, good conditions have been created for the society activities of both chemists and chemistry students in Tartu. Articles published in the collection give a survey of the scientific research of the members of the Society.

AUGUST PARIS

AUGUST PARIS - LECTURER AT THE UNIVERSITY OF TARTU, SCIENTIST, AND ACTIVE MEMBER OF THE ACADEMIC SOCIETY OF CHEMISTRY

V. Past
Institute of Physical Chemistry, University of Tartu

ABSTRACT

The article describes life and activities of August Paris (1888-1944), the first professor of physical chemistry in the University of Tartu. He was an outstanding chemist, who was also active in public affairs, being among foundators of the Academic Society of Chemistry, for a long time he was its chairman.

1. August Paris (1888-1944) was the first professor of physical chemistry in the University of Tartu. After graduating from the Department of Chemistry of the University of Tartu in 1915, he got an opportunity to stay at the university, but he prefered working in a chemical plant. For five years A. Paris worked in one of Russia's greatest plants of fine chemistry in Moscow, where he began as a simple chemist, and finally reached the post of general director of the departments and laboratories of chemical synthesis. Arriving back in Tartu in 1920, A. Paris joined the university staff as an assistant of professor G. Landesen. After a successful doctoral promotion he became a lecturer at the Chair of Physical Chemistry in 1925. In order to prepare A. Paris for work as a professor of physical chemistry, the university sent him to do scientific work in Berlin for one year. He worked in a laboratory of a well-known scientist H. Freundlich in the Institute of Physical Chemistry of Keiser Wilhelm. In 1927 A. Paris gained the post of assistant professor of physical chemistry, in 1929 he became the elected professor.

2. In the first period of independent teaching, A. Paris lectured on physical chemistry, colloidal chemistry and electrochemistry, but from 1933 he had to begin instructing in inorganic and analytical

chemistry,and the methodology of chemistry. A. Paris's lectures stood out especially for their carefully planned structure and methodically reasonable presentation. Already as a student A. Paris was interested in creating chemical terminology in Estonian, he was an active participant in the commitee of chemical terms at the Society of Estonian Literati (Eesti Kirjameeste Selts). Being a professor he was leader of the terminology commission at the Academic Society of Chemistry.

3. Compilation and publishing of textbooks was an essential side of A. Paris's activities. Already in 1922, he and K. Loskit published a textbook on analytical chemistry in Estonian. In 1934, the first part of a manual on chemical analysis was published, the second part came out in 1941. A. Paris was the editor and one of the compilers of the book. The first part on qualitative analysis became especially popular, its reprints were published in 1940, 1945 and 1948. The older people remember a natural history and local lore schoolbook named "The Little Friend of Nature" ("Väike looduse sôber") for classes from 3rd to 6th; A. Paris was one of the authors. Simple and true-to-life stories about materials used by people, their properties and transformations in this book were intended to give an introduction to chemistry for pupils.

4. A. Paris's scientific heritage is not very bulky. Altogether 20 works were printed under his name. Many of his investigations were pioneering, and were carried on and developed by his students and younger colleagues. In the first working period, A. Paris was interested in the kinetics of chemical reactions. While working in W. Ferrein's plant he became interested in the hydratation of turpentine oil, which grew into Candidate and Doctoral Thesises. The hydratation of terpenes is a complicated heterogeneous reaction involving compounds in three phases. A. Paris managed to explain the mechanism of catalyzing and inhibiting processes accompanying the reaction. Another branch of his scientific work, research of colloidal systems' properties, took its beginning in H. Freundlich's laboratory. A. Paris has published interesting results of surveys on the orientation and structuring effects connected with the flow of colloidal solutions, on the transformations between gel and sol, etc. A. Paris especially emphasized the need to consider electrical phenomena in the discussion of processes in colloidal systems. The continuation of this direction can be observed in the research on the dielectric properties of organic compounds in the works by A. Parts and L. Tiganik, A. Paris's younger colleagues.

5. Almost 20 years A. Paris was a leading lecturer at the Department of Chemistry in the University of Tartu, from 1932 he was

director of the Institute of Chemistry. He was active in the work of the university chemists' association – the Academic Society of Chemistry, from 1928 he was its chairman. A. Paris was also the editor-in-chief of the Society's publication, the journal "Chemical Reports" ("Keemia Teated"), during the whole issuing period (1932-1937). A. Paris reacted very painfully to the closing of the Department of Chemistry at the University of Tartu, an emotional article in the last issue of "Chemical Reports" is a witness of it.

105 YEARS FROM THE FOUNDATION OF THE TARTU SANITARY LABORATORY

K. Ilmoja, Jüri Ruut
Tartu Public Health Service

ABSTRACT

In 1993 the Chemical Laboratory of the Tartu Public Health Service celebrated its 105th anniversary. The article gives a brief review of the laboratory's history and activities.

The second half of the previous century was the golden era of analytical chemistry in Tartu. At this time two scientists of international recognition worked in the University of Tartu. Carl Schmidt (1822-1894) had studied in Berlin and Göttingen Universities; he was a disciple of H. Rose, J. Liebig and F. Wöhler. Georg Dragendorff (1832-1898) had attended Rostock and Heidelberg Universities; he was a disciple of F. Schulze. Profound overviews on the life, activities and scientific research of C. Schmidt and G. Dragendorff has been published by Tullio Ilomets [1, 2].

In this period, decisive for analytical chemistry, they were among leaders in applying new quantitative volumetric and optical methods in the research of natural processes, and worked out their own methods.

Carl Schmidt worked in the University of Tartu in 1846...1892, most of the time being director of the Institute of Chemistry. His research was mainly directed to the investigation of water. It began with research on the university wells and terminated with a review of the hydrological and hydrochemical properties of the Eurasian waters which based on a huge amount of analyses from several regions.

Professor Georg Dragendorff was director of the Institute of Pharmacy in 1864...1894. His scientific interests were very broad, including problems of pharmacy and analytical chemistry, especially concerning natural compounds. His collaboration with Professor Schmidt and F. Körber, director of the Institute of Hygiene, was very active, and

resulted in tens of Doctoral and Master theses in chemistry, pharmacy and medicine, treating the fundamentals of chemical and hygienic research of air, foodstuffs and everyday materials.

Research led by G. Dragendorff covered a wide field, but it had a certain direction – to find out the amount of harmful substances in the surrounding environment. He had a great variety of published materials to be used from all over the world. He also compiled a manual for the determination of toxic compounds ("Die gerichtlich- chemische Ermittelung von Giften in Nahrungsmitteln, Luftgemischen, Speiseresten, Körperteilchen etc") which was published in 1868. The book won a great popularity, and in 1868-1895 four revised reprints were issued. The monography was also translated into Russian and French. The comparative- analytical presentation and the observations on the applicability of the methods were considered to be his strong sides.

Analysis of toxic compounds was a special subject for Dragendorff's laboratory, which proved to be a leader of international scope.

In G. Dragendorff's laboratory several reagents for analyzing alcaloids were worked out, three of them being important also nowadays: they are used as colour reagents in thin- layer and paper chromatographies. Dragendorf's reagent was invented in 1866, up to now several modifications of it have appeared. Mandelin's reagent was created by Karl Mandelin, a disciple of Dragendorff, in 1883; information on the Mark reagent was published in 1896. Dragendorff's scientific activities were very closely connected with practice, and the methods elaborated by him were used in his laboratory to analyze water, air and products on sale.

Practical work widened significantly when in the February of 1888 a municipal sanitary laboratory was founded under the leadership of G. Dragendorff. It employed one chemist and under-graduate students, so it served as a training site. The laboratory was the first sanitary establishment in Estonia and the second in contemporary Eastern Europe: the first one was in Vilnius, Lithuania.[3]

The most important jobs to do were to control food quality and falsification, also to study harmful additives in foodstuffs and everyday materials. The newest analytical methods were used. Annual reports have survived from 1888, 1889 1891 and 1892, according to which mainly foodstuffs and water, but also building materials, coal, fertilizers, pharmaceutical and chemical preparations, medical and

forensic materials, like blood, urine, poisons, etc. were analyzed. (Table 1)

Table 1

Statistics of analyses made by the Tartu Sanitary Laboratory in 1888...1892.

Item	1888	1889	1891	1872
Cream and sour cream	89	55	8	13
Milk (whole, skim,condensed,kefir)	107	92	63	10
Flour (wheat, rye)	3	1	9	63
Wheat, rice, maize	–	3	2	1
Bread	8	–	–	50
Yeast	–	2	–	24
Vinegar	21	51	2	1
Canned food	–	1	–	–
Tea	19	12	5	1
Butter	32	17	35	43
Coffee, chicory	1	–	4	–
Sugar, marmalade	7	–	4	–
Spirits, vodka, wine	1	–	2	–
Beer, lemonade	6	3	43	–
Beer additives	–	–	1	–
Cucumbers	–	–	9	–
Vegetable oil	–	–	2	–
Meat foods	5	2	–	1
Potatoes	–	5	–	–
Well water, ice	14	59	17	21
Tin	3	–	–	–
Dyes	–	1	–	3
Wall-paper	8	200	44	304
Yarn and textiles	1	217	90	202
Cigarette paper	3	–	–	–
Tar-paper, glue	2	3	–	–
Cheese fermentation preparations, cheese dyes	–	6	–	–
Fertilizers	1	4	15	14
Clay, mud, minerals	–	1	2	5
Animal feed	–	–	–	1
Leather	–	–	–	1

Item	1888	1889	1891	1872
Coal, peat	-	-	1	6
Pharmaceutical and chemical preparations	4	6	8	12
Bacteriological studies	-	-	9	-
Medical studies (urine,etc.)	54	29	21	8
Forensic studies (blood, spermium, poisons, etc.)	7	3	28	7
Altogether:	396	776	430	854

Water from springs and wells was analyzed because of spreading infections and new knowledge that dangerous diseases like cholera, typhus, etc. can be contracted from water. The bacteriological analyses were carried out by Prof. Körber's laboratory at the Institute of Hygiene of the University.

Wall- papers, textiles and yarn were widely analyzed because arsenic was used in dyes therefore, the quantitative determination of arsenic in these materials was topical. A profound review of methods for the determination of arsenic contents and their experimental comparison were done by N. Jorban, the laboratory co-worker, and it was published as a Doctoral thesis in 1889. He came to a conclusion that the most convenient method was Marsh's method modified by G. Dragendorff because of a good sensitivity and reproducibility of results.

917 samples of wall-papers and textile materials have survived, each of them having a note indicating its arsenic content. 17 % of the wall-paper samples and 23 % of the textiles contained arsenic more than 0.01 mg per 100 cm^2. The samples are kept in the History Museum of the University of Tartu.

After G.Dragendorff's leaving the laboratory activities died out. At the beginning of the 20th century, analyses were made in several laboratories of Tartu.

A new sanitary laboratory was founded at the municipal health department in 1928 [3].

After World War II the laboratory began its work as a structural unit of the sanitary-epidemiological station which had to control the sanitary and epidemiological situation in the town. At first, the chemical composition and quality of foodstuffs and drinking water were investigated in the laboratory. From 1959 chemical analyses of industrial air and later those of ambient air started, also physical factors like thermal environment and noise were controlled. From 1965

investigations of pesticide residues in foodstuffs, water and in the air of working places began.[4]

Nowadays the main working areas of the laboratory are:

- chemical analysis of water, air, soil samples and foodstuffs;
- chemical analysis of migrating toxic compounds in products, made of polymeric and some other materials;
- analysis of physical factors (noise, ventilation and thermal environment measurements).

Mainly the laboratory services the town of Tartu, and in the case of some complicated analyses the whole South-Estonian region. In the field of pesticide analysis, the Chemical Laboratory of the Tartu Public Health Service is the main analytical centre in the health-care system of Estonia.

Apart from chemical methods, physico-chemical methods, mainly chromatography, are also used. The laboratory has seven gas chromatographs, most of them having been produced in Estonia and supplied with selective detectors on the spot. Some chromatographs have been adapted for the use of capillary columns. Most of these improvements are the result of cooperation between the workers of the Bureau of Specialty Design of the Estonian Academy of Sciences, the University of Tartu and our laboratory. The laboratory has 2 HPLC devices with UV detectors. Two ion-chromatographs for the analysis of anions and cations have been completed on the spot, so have the computer-controlled automatical device to work with ion- selective electrodes, and the cold-vapor atomic absorption spectrophotometer for mercury determination. Heavy metals are determined electrolytically- a computerized device for the stripping potentiometer is used for this purpose. A great part of the above mentioned equipment is very old – for example, many chromatographs have been used for more than 20 years already.

Drinking water and water from open bodies are analyzed by using titrimetric and colorimetric methods. Ion chromatography is used for the determination of anions and cations. Heavy metals are analysed by the potential stripping measurement (soluble organic compounds in water are mineralised by UV-radiation). Phenols and some other compounds are determined by chromatographical methods. In 1993 about 1300 water samples have been analysed. The main problem of drinking water in Tartu seems to be the high concentration of nitrate-ions.

Chemical composition (proteins, carbohydrates, fats) of food is determined both in raw foodstuffs and prepared foods. The content of

vitamins and mineral salts is also analysed. According to customers' wishes, the accordance of foodstuffs to standards is controlled. In 1993, ca 800 analyses of that kind have been made.

Pesticides are mainly analyzed by means of gas chromatography, using electron captivity, flame ionization and thermoionic detectors. Thin-layer chromatography, and spectrophotometric methods are also used, efforts are being made to start with the HPLC methods.

As there exist a great number of pesticides and their metabolites, their identification is not an easy task. As we do not have any possibilities of using mass- selective detectors, we have tried to solve the problem by using simultaneously dual capillary columns of different polarity. If necessary, more columns of different polarity are used. The system is designed in our laboratory as a modification to the "Chrom-5" chromatograph (Czech Republic), the electron captivity detectors used are of Estonian origin.

We use capillary gas chromatography with the electron capture detection for the analyses of chlorinated pesticides and PCBs in fish fat, butter and human milk. Analyses of this kind are quite complicated. At first, pesticides are extracted from a sample with organic solvents, and separated from fat by means of column chromatography, followed by the gas chromatographic determination. This method enables the separation of the isomers of polychlorinated biphenyls (PCB) from the chlorinated pesticides.

In 1993, about 1100 single-component analyses have been made. In fact, the concentrations of pesticides, including chlororganical compounds, in Estonian local food are very low. But we have problems with imported foodstuffs. There are standard preparations of 90 pesticides, but we still experience difficulties in analyzing imported products due to a lack of some important standard compounds.

From different mycotoxins we control the concentrations of patulline, zearalenone, aflatoxins B_1 and M_1. In 1993, in 2 % of the analysed samples the concentrations of aflatoxin B_1 were higher than permitted (> 0.005 mg/kg).

Analyses of histamine in fish are performed by means of thin- layer chromatography. No case of exceeding the permitted concentrations occured.

For the analyses of heavy metals (Pb, Cd, Zn, Cu) the stripping voltammetry measurement is used, the concentration of mercury is determined by the cold-vapour AAS method. In 1992/93, the highest concentrations of these metals were found in imported cereals, but the

values did not exceed the permitted ones.

Conservating agents and synthetic food dyes have been a problem in imported food, big amounts of food colours were also found in domestic products.

A work- group is active in the laboratory in the field of occupational health surveys- analyses of the working zone air pollution, measurements of thermal environment, ventilation, noise, vibration, light intensity and ionizing radiation are carried out. Impurities are determined also on the communal objects and at educational establishments. For analyzing multicomponent air samples mainly gas chromatography is used, optical, volumetric and gravimetric methods are partially applied. Collecting of air samples is performed either by using active dosimeters and aspirating micropumps, or passive dosimeters which collect the impurities using the diffusion of gases, and which enable sample collecting during the whole shift.

The same group has a task of taking samples from 25 spots in the streets of Tartu to monitor the concentrations of carbon monooxide which is the most analyzed component in the ambient air.

At the present time the amount of analyses of gases (formaldehyde, etc.) emitting from synthetic materials used in dwellings, kindergartens and educational establishments has increased.

As the laboratory staff was reduced, the number of analyses made in 1992 reduced 50% compared to 1990. In 1992, 830 air samples were collected from indoor rooms, and 1553 analyses of single components were performed, concentrations in 197 samples exceeded the permitted limits. Among 911 samples of ambient air, 47 samples were above the limit.

Practical activities of the laboratory are closely connected with scientific work. The laboratory staff has published 85 publications, by 1988 the complete bibliographies of articles had appeared [5, 6, 7].

The first publication was issued in 1958. The first articles treated, dealt with the colorimetric methods in the air and water analyses, and te use of thin – layer chromatography for pesticide analyses. The use of gas chromatography began in 1966, the first article appeared in 1970, and the number of works on gas chromatography is the greatest (35) as gas chromatography is the most frequently used technique in the laboratory. Mainly, the adaptation of instruments to sanitary-chemical purposes, the use of selective detectors for air and pesticide analyses are discussed in these articles.

In 1968...1982 reviews of the contents of pesticides and

polychlorinated biphenyls in foodstuffs and breast milk appeared. The results showed a decrease of the concentrations of these components in Estonia. In resent years articles dealing with the use of the capillary gas chromatographic methods for the analysis of pesticide and PCB residues in foodstuffs have been published.

Four articles discuss the use of ion – selective electrodes for the determination of nitrate and fluoride ions in foodstuffs.

The use of ion chromatography began in 1983, the first article was printed in 1984, up to now 23 articles have been printed. The problems handled were application of ion chromatography for the analysis of drinking water, determination of nitrates in foodstuffs and determination of anions in the air. In collaboration with the Laboratory of Ecosystems of the University of Tartu, great work was done in the research of acid rains.

In 1985, the first diploma thesis was completed in the field of stripping voltammetry, by now 7 articles have been published on this theme, the determination of heavy metals in foodstuffs and water is discussed in them.

Table 2

The number of articles published by the coworkers of the laboratory in 1958...1993.

FIELD	NUMBER OF ARTICLES
Thin- layer chromatography	4
Gas chromatography	35
Ion- selective electrodes	4
Ion chromatography	23
Stripping voltammetry	7
Other methods and overviews	14
	84

The laboratory is also involved in scientific organizational work. The staff has participated in the organizing of 10 scientific conferences and the publishing of 9 collections of scientific papers. Beginning from the 90th anniversary conference in 1978, anniversary conferences have been held after every 5 years and their materials has been published. In 1986, the conference "Electrochemical and chromatographic methods of analysis in the protection of environment" took place. It was dedicated

to the 150th anniversary of Prof. G. Dragendorff, the foundator of the laboratory. The conference materials were printed in the "Acta et commentationes Universitatis Tartuensis", Vol.743. In 1988 conference on the occasion of the 100th anniversary of the laboratory took place, and in 1989 the materials were published in "Acta et commentationes Universitatis Tartuensis", Vol.844. The collection was en-titled "Perspective chromatographic and electrochemical methods in sanitary chemistry".

The laboratory has a close cooperation with the University of Tartu and the Estonian Agricultural University. The laboratory has signed a contract with the University of Tartu to educate students in the area of environmental and food analysis and to have supplementary training courses for laboratory specialists in the public health system. For example, our chemists hold lectures in ecotoxicology and run practical analytical courses in environmetal and food analysis for the last-year chemistry students of the University of Tartu, and a course of foreign substances in food for students of the Meat and Dairy Institute of the Estonian Agricultural University.

In the laboratory some students are completing their diploma theses. For example, in 1993 one chemistry student of the University of Tartu worked on the methods of the analysis of aflatoxins, and two students from the Estonian Agricultural University investigated the nitrate-ion concentrations in Estonian foodstuffs and the occurence of chlorinated pesticides in meat.

During some last years, several diploma theses on the electrochemical analysis of heavy metals have been written by chemistry students of the University of Tartu . One of the laboratory workers is completing his Master thesis on the stripping voltammetry measurement of Pb, Cd, Cu and Zn concentrations in foodstuffs.

We have used all the possibilities of raising the qualification of our workers in the application of methods used in Europe. In this we have received great help from Nordic countries. In 1992, one of our chemists took updating courses in Denmark, an other in the Finnish Customs Laboratory. We have established a very good contact with Finnish colleagues from the Finnish Customs Laboratory and The Finnish Institute of Occupational Hygiene, their specialists having held several lectures and seminars in Tartu.

REFERENCES

1. **T. Ilomets.** Trans. of Tartu State Univ., 743 (1986) 3-18.
2. **T. Ilomets.** Trans. of Tartu State Univ., 844 (1989) 3-15.
3. **O.M. Tamm, M.K. Sikk, V.V. Kalnin, K.A. Il'moya.** Materialy simpoziuma "Sovremennye metody sanitarno- gigienicheskih issledovanij i primenenie ih v praktike sanitarnogo kontrolya". Tartu, 1978. P. 5.
4. **L. Margna, L. Rootsmäe.** "Eesti Arst", 3 (1990) 194-196.
5. **L. Rootsmyae.** Bibliografiya rabot Tartuskoj sanitarno- epidemiologicheskoj stancii 1940-1970. "Nauchnaya konferenciya, posvyaschcennaya 75- letiyu kafedry gigieny Tartuskogo gosudarstvennogo universiteta i 30- letiyu Tartuskoj gorodskoj SES". Tartu, 1970. 348-360.
6. **L. Rootsmyae.** Bibliografiya rabot Tartuskoj sanitrno- epidemiologicheskoj stancii 1971-1978. Materyaly simpoziuma "Sovremennye metody sanitarno-gigienicheskih issledovanij i primenenie ih v praktike sanitarnogo kontrolya". Tartu, 1978. 192-198.
7. **L. Rootsmyae.** Trans. of Tartu State Univ., 844 (1989) 25-32.

ION SENSITIVITY OF POLYPYRROLE ELECTRODES

A. Alumaa, T. Silk, A. Hallik, A. Pruks, J. Tamm
Institute of Physical Chemistry, University of Tartu

ABSTRACT

The ion sensitivity of polypyrrole (PPy) films (2–60 μm) deposited electrochemically onto the Pt, glassy carbon and SnO_2-substrate was studied by potentiometric measurements. The influence of electrochemical pretreatment (overoxidation, reduction, potentiodynamic cycling) on the potentiometric behaviour of PPy electrodes was characterized. The equilibrium potential E_r of the PPy electrode is established after a long-time (till 200 hours) conditioning in solutions. Within this time the side products of the polymerization reaction diffuse out from the film, pores fill with the conditioning solution and the equilibrium between the PPy matrix and the solution in its pores establishes. The nature of the film substrate was found to be inessential. The E_r, lga_c-dependence (a_c – activity of $NaNO_3$ in the conditioning solution) is characterized by the slope –29 mV per decade for nontreated and –11 mV per decade for overoxidized PPy electrodes.

The short-time (3–4 minutes) potential responses of PPy electrodes conditioned in $NaNO_3$ or KCl (anion-sensitive) and in Na_2SO_4 or sodium dodecylsulphate (cation-sensitive) to the electrolyte concentration, the electrolyte nature and pH of the solution were studied. All PPy electrodes independent of electrochemical pretreatment have the short-time sub-Nernstian response. The selectivity coefficients of PPy electrodes for various ions were calculated. The sequence of the anions interfering influence for anion-sensitive PPy electrodes is mainly the same as for ion-selective electrodes with liquid membranes and corresponds to the Hoffmeister lyophilic series.

INTRODUCTION

The electronically conductive polymers, particularly polypyrrole, polyaniline and their derivatives are an area of active investigations [1]. Nowadays these polymers are the object of study for a very wide circle of chemists and physicists as the novel materials whose properties are of great theoretical interest [2]. On the other hand, they have been studied also as materials for several applications (charge-storage [3], electronics [4], electrocatalysis [5]). In some recent investigations the attention is turned to the possible use of electrodes coated with conductive polymers in electroanalysis [6]. There exist many various methods for the functioning of polymer films for analytical purposes. In order to obtain the specific activity of the films, the proper functional group may be introduced in the monomer molecules both before polymerization and by the corresponding chemical treatment of a ready film [6]. Moreover, it is possible to immobilize the suitable electroactive compound into polymer matrix during the polymerization process [6].

The electrodes modified with conductive polymer films have been studied as the possible potentiometric sensors for the determiation of various ions [7–12] and molecules [13]. The electrochemical oxydation of polypyrrole (PPy) is accompanied by the insertion of anions (A^-) as compensator of the positive charge into the polymer matrix:

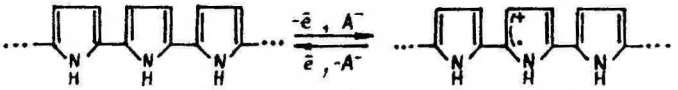

(1)

According to the reaction (1) the potential (E) of the metal electrode modified with PPy ($Me/PPy^+/A^-$) may be expressed by the Nernst equation:

$$E = E_o - \frac{RT}{F} ln[A^-] . \qquad (2)$$

In several reports [7–11] a sub-Nernstian potential response of $Me/PPy^+/A^-$ to change of $[A^-]$ in aqueous [7–11] and nonaqueous solutions [8] is obtained, from which it is concluded that E reflects the redox state of PPy chains [10].

During electrochemical reduction, aside the anion (dopant) removal from the plymer film also the cation (Me^+) incorporation into polymer is possible [14]. The latter process takes place in the case of big organic dopants, but also in thick PPy films doped with inorganic anions. The

redox transition of PPy with only cationic exchange leads to the response of electrode E to Me^+ [12] expressed as

$$E = E_o + \frac{RT}{F} \ln [Me^+] \quad . \qquad (3)$$

Beck et al. [8] have found that in thick films the mixed mechanism of redox process takes place at which E may be practically independent of the salt concentration in solution.

In this paper the potential response of PPy^+/NO_3 and PPy^+/Cl^- film coatings deposites onto glassy carbon (GC), Pt and SnO_2 to change of the electrolyte concentration has been studied in a greater detail. The potential set-up of electrodes with different electrochemical pretreatments was examined. We found that the response of E to anion concentration remains steady after the overoxidation of the PPy film in spite of it losing the redox properites. Thus the redox process of PPy^+/A^- is not the only and main factor that determines the electrode potential response to the electrolyte species in solution.

EXPERIMENTAL

The PPy films were synthesized potentiostatically (E = 0.70 V (PPy^+/Cl^-); 0.80 V (PPY^+/NO_3^- vs. sat. Ag/AgCl) from Ar saturated aqueous solutions of 0.1 M pyrrole and 0.1 M electrolyte ($NaNO_3$, KCl, Na_2SO_4, sodium dodecyl sulphate (DDS)) onto GC, Pt or glass coated with SnO_2. The film thickness (2–60 μm) was controlled by the electropolymerization charge according to the relation 0.4C/cm^2 (NO_3^-, Cl^- and SO_4^{2-} doped), and 0.2 C/cm^2 (DDS) per 1 μm [15]. A conventional three-compartment cell equipped with a platinum wire as counter electrode and a saturated Ag/AgCl electrode as reference electrode was employed for the electrochemical polymerization. The working electrodes in the form of Pt wire (0.1 cm^2), GC stick 1 mm in diameter (0.2–0.25 cm^2) and the hemispherical tip of a glass tube (0.3–0.4 cm^2) coated with SnO_2 were used. The preparation of SnO_2 electrodes consisted in heating the end of a glass tube until 450°C and exposing it within the vapour of $SnCl_4$ [16]. The electrical contact with SnO_2 was attained by means of Pt wire (0.1 mm in diameter) through the glass.

The preceding conditioning of electrodes was carried out for each electrode in a separate test-tube with 5 ml of solution containing dopant-anions. The voltammograms were measured in a conventional three-electrode cell. The measuring of the electrode potential was carried out in a two-electrodes cell.

For comparison of the potentiometric behaviour of PPy electrodes with liquid-membrane ion selective electrodes, the nitrate electrodes containing tris(bathophenanthroline)nickel(II) nitrate dissolved in o-nitrophenyl-octylether were prepared. The membranes based on the PVC matrix [17]. Two types of liquid-membrane electrodes were used: "coated wire" and liquid-contact ones.

Electrochemical experiments were carried out by the use of the polarographic analyzer system PA-2 (made in Czechoslovakia), the electrode potentials were measured using a dynamic condensator electrometer with an input impedance higher than 10 GΩ.

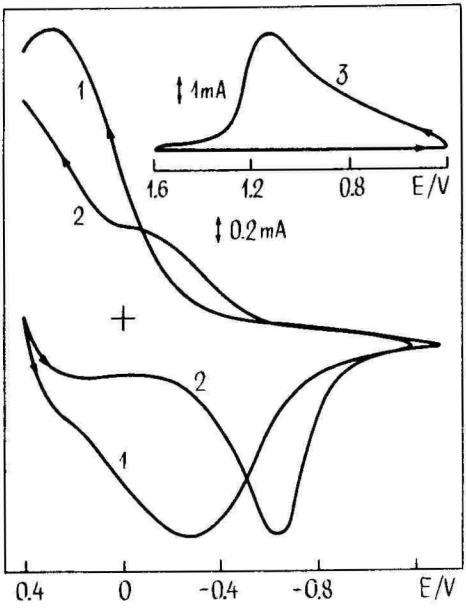

Fig. 1. Cyclic voltammograms (v = 10 mV/s) of the nitrate doped PPy films (30 μm) deposited on glassy carbon: (1) before conditioning; (2) after conditionig; (3) overoxidation.

Pyrrole (Fluka) was purified by distillation over calcium hydride under vacuum and stored in the dark under Ar atmosphere at a low temperature. All salts used were of analytical reagent grade.

The influence of the following electrochemical pretreatments on the potentiometric behaviour of the PPy electrodes was studied (Fig. 1):

1) the electrochemical overoxidation at high positive potentials (two cycles +0.4 V → 1.8 V → +0.4 V with scan rate v = 10 $mV \cdot s^{-1}$),

2) the potentiodynamic cycling (two cycles +0.4 V → −1.3 V → +0.4 V with v = 10 $mV \cdot s^{-1}$),

3) the scan from +0.4 V to −1.0 V (v = 10 $mV \cdot s^{-1}$) and electrochemical reduction at the end potential during 5 minutes.

RESULTS AND DISCUSSION

Conditioning of the electrodes

The synthesized PPy electrodes were rinsed thoroughly with bidistilled water and immersed into the conditioning solution. The electrode potential E changed with time, the nature and the rate of change depended on several factors: the electrochemical pretreatment, the film thickness, the nature of dopant-ion, the solution activity a_c and pH. The conditioning is a long-time process, within this time the side products of the polymerization reaction (H^+ ions, purrole oligomers itc.) diffuse out from the film, the film pores fill with the conditioning solution and the equilibrium between the solution and the PPy redox system establishes.

Table 1

The amount of H^+ ions, diffused out during 48 hours from PPy film doped with Cl^- ions

Film thickness, μm	Film volume, mm^3	Amount of H^+, mole
2	0.09	$2.1 \cdot 10^{-9}$
5	0.22	$2.5 \cdot 10^{-8}$
10	0.44	$3.2 \cdot 10^{-8}$
20	0.88	$3.0 \cdot 10^{-7}$

Table 1 shows that the rinsing removes the majority of side products from the thin films (d $\leq$ 2 μm), whereas the thicker films need a long-time (48–72 hours) conditioning with solution exchange.

The kinetics of electrode conditioning depends essentially upon the method of conditioning: either without solution exchange (pH of solution decreases up to 3.5) or with frequent solution exchange (Fig. 2). In the

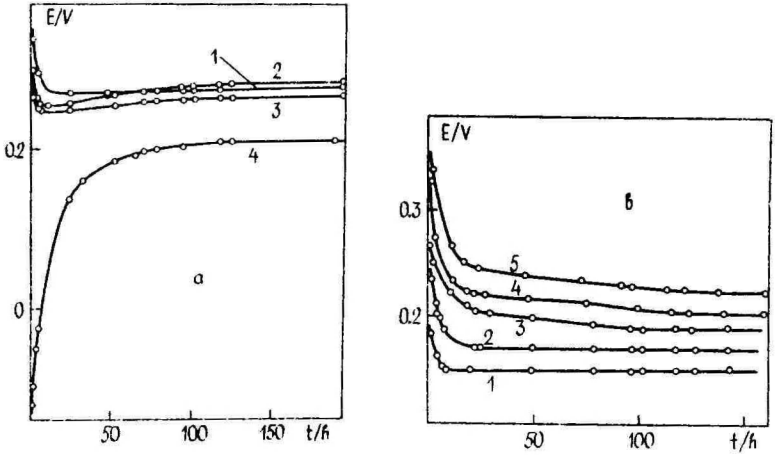

Fig. 2. The change of potential E of nitrate doped PPy electrodes during the conditioning in 0.1 M $NaNO_3$. (a) conditioning without solution exchange, the films (30 μm) were precedently pretreated in the following way: (1) nontreated (pH decreases during conditioning up to 3.5); (2) overoxidized (pH = 3.5); (3) cycled – through (pH = 4.5); (4) reduced (pH = 6). (b) conditioning with frequent solution exchange (pH = 6), the films have following thickness: (1) 3 μm; (2) 8 μm; (3) 15 μm; (4) 30 μm; (5) 60 μm.

first case we detect the decrease of E during 10–20 hours (depending on the film thickness) to be continued by a long-time increase of E and the equilibrium potential E_r is reached after 200 hours in the case of 30 μm film. If the conditioning is performed with solution exchange, the following potential increase is absent and the E_r is established in 120 hours at the same thickness. The E_r value in the first case is ~60 mV more positive due to lower pH of the conditioning solution. In the

following experimetns the PPy electrodes were conditioned with frequent exchange of solution.

The nature of the film substrate is not important. The E_r values of PPy electrodes (10 μm thick) grown on the GC, Pt and SnO_2 substrates differ less than 10 mV in the same solution.

The rate of E_r set-up depends essentially upon the film thickness, for thickness 2–3 μm 10 hours is sufficient, for 60 μm 150 hours. The equilibrium value depends upon the thickness (Fig. 3) while the range of E_r change decreases substantially with the decrease of solution pH. The E_r, d-relationship can be straightened in coordinates E_r, $\sqrt{d}$ or E_r, log d with the regression coefficient $r^2 > 0.97$.

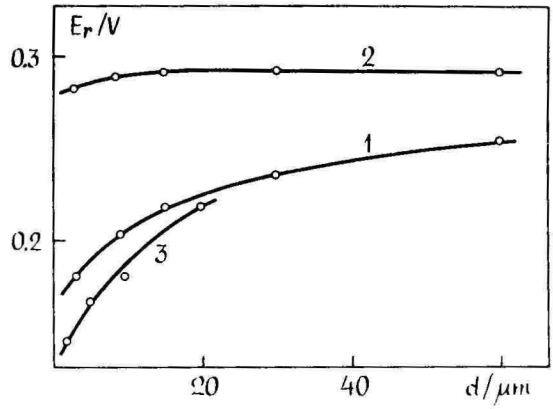

Fig. 3. The dependences of the equilibrium potential E_r of PPy electrodes on the film thickness in case of the conditioning in following solutions: (1) 0.1 M $NaNO_3$ (pH = 6); (2) 0.1 M $NaNO_3$ (pH = 3.8); (3) 0.1 M KCl (pH = 6).

It appears from the data that the conditioning is influenced by the pretreatment of PPy films. The overoxidation and the potentiodynamic cycling accelrates a little the set-up of E_r.

The reduced PPy film will be re-oxidized by the dissolved oxygen during the conditioning due to which the reaching of the equilibrium state is prolonged. The re-establishment of the redox properties of overoxidized films is excluded.

The established E_r value depends upon the activity a_c of the

conditioning solution (Fig. 4 and 5). The slope of E_r, log a_c-dependence for untreated PPy electrodes is -29 mV per decade and for overoxidized films -11 mV per decade. The final E_r value is not sensitive to oxygen presence unlike the potential value before conditioning. The established E_r of all PPy electrodes is constant for a long-time period, while this is not valid for a liquid-membrane ion selective electrode based on the PVC matrix without a stabilizing layer on solid substrate.

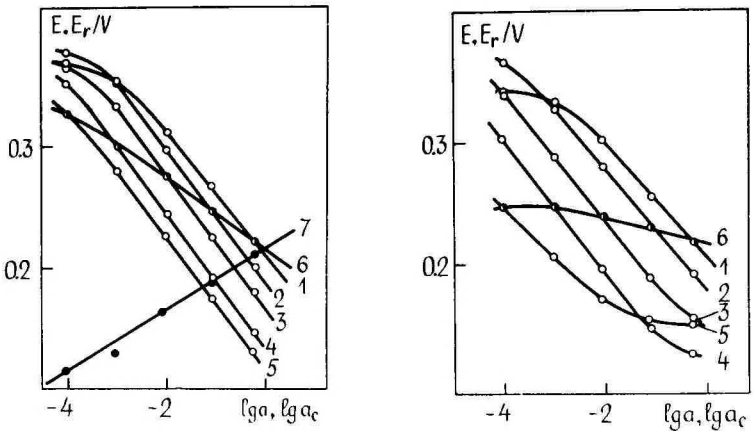

Fig. 4. The dependences of the potential short-time response E on the nitrate activity a for nontreated PPy electrodes conditioned in the $NaNO_3$ solutions with different concentrations (M): (1) 1; (2) 0.1; (3) 0.01; (4) 0.001; (5) 0.0001. (6) the dependence of the equilibrium potential E_r on the electrolyte activity a_c in the conditioning solution. (7) the dependence of the short-time response E at a = 1 on the electrolyte activity a_c in the conditioning solution.

Fig. 5. The dependence of the potential short-time response E on the nitrate activity a for overoxidized PPy electrodes conditioned in the $NaNO_3$ solutions with different concentrations (M): (1) 1; (2) 0.1; (3) 0.01; (4) 0.001; (5) 0.0001. (6) the dependence of the equilibrium potential E_r on the electrolyte activity a_c in conditioning solution.

Response of the PPy electrodes on the change of the electrolyte activity

When the conditioned PPy electrode is exposed in solution with the same electrolyte as in the conditioning solution but with its different activity, the potential E sets up and its value differs from that of E_r

which sets up by conditioning the electrode in the lastly mentioned solution (Fig. 4). The quickness of the raising of E depends on the activity of the solution where the electrode was immersed, varying from 0.5–1 min (for 1 M solution) and 2–3 min (0.1–0.001 M) up to 3–4 ($a < 10^{-3}$ M). The kinetics of the potential set-up of PPy electrodes is close to that of liquid-membrane electrodes. The potential of the PPy electrode remains constant for a certain period and then starts to change towards the potential value E_r that the electrode achieves after conditioning in this solution. The interval (till 10 min) when the potential E is constant in measuring solution depends on many factors: the ratio of the activities of conditioning (a_c) and measuring (a) solutions, the direction of solution activity change, the electrochemical pretreatment of electrode and electrode's age. The following change of E lasts some days and this results in the set-up of a new value of E_r corresponding to the measuring solution (Fig. 4). In some cases the above-given stages are not clearly distinguished: the reconditioning of the electrode may begin immediately after the E set-up that is 3–4 min after the immersion of the electrode into the measuring solution (Fig. 4, curve 1; Fig. 5, curves 1 and 5).

The reversibility of the E function caused by the change of the solution concentration depends on many factors, primarily on the thickness of the film and difference between a_c and a. So, for example, a 30 μm thick PPy film conditioned in 0.1 M solution shows the fully reversible E function by a concentration change from 1.0 M to 10^{-2} M and back to 1.0 M. At the same time after the alteration of c from 1.0 M to 10^{-4} M and back to 1.0 M, the new potential values are from 3 mV (for a 30 μm thick film) to 10 mV (for a 3 μm thick film) lower than the initial ones. Besides, the potential irreversibility increases with the electrode exposure time in the measuring solution. Irreversibility is greater also by using pretreated electrodes, particularly by cycled-through and overoxidized ones. The restoration of the initial electrode potential E_r needs additional conditioning that lasts many hours.

Fig. 4 represents the relationship between E and lga for PPy/NO_3 electrodes conditioned in solutions with various electrolyte concentrations. Analogical dependences were obtained for PPy/Cl electrodes and they both represent the anion sensitive elctrodes. The extent of the linear region depends on the concentration of the conditioning solution and also on the previous electrochemical treatment of the electrode. The linear region is shorter for pretreated electrodes. It is notable that analogically whit PPy electrodes conditioned in

solutions with $a_c > 10^{-3}$ where occurs the deviation from linearity at low concentration the same tendency is observable in the case of anion selective PVC membrane electrodes where it is related with the solubility of the ion exchanger in the measuring solution. The absolute value of the slope of the linear part of E, lg a-plot is 56 ± 2 mV per decade, only for electrodes conditioned in 1 M solution it is somewhat diminished obtaining 51 ± 2 mV per decade. These values are approximately twice greater than the absolute values of the slopes for E_r, lg a-plots (Fig. 4, curve 6). The absolute values of the slope of the linear relationship between E and lg a are lower when the thickness of the PPY film d < 10 μm, also when the films are in an overoxidized state (Fig. 5). As is seen from Fig. 5 for overoxidized and also for other pretreated films conditioned in dilute solutions ($a_c < 10^{-2}$ M), the deviation from the linear relationship takes place also in more concentrated solutions (c = 10^{-2} – 1 M). This tendency becomes particularly evident for electrodes conditioned in 10^{-4} M solution. Besides, the E function of those electrodes is essentially less reversible than that of electrodes conditioned in more concentrated solutions.

Electrodes doped with sulfate or dodecylsulfate anions and conditioned in solutions containing the above-named anions behave differently from electrodes conditioned in chloride or nitrate solutions. The former electrodes are cation sensitive.

The anion sensitive PPy electrode's response to pH change (E increases with the decreasing of pH) is slow, depending on the pH difference between conditioning and measuring solutions and on the film thickness. With the increase of the film thickness the change of E decelerates and the pH interval around pH of the conditioning solution where the E change within the first 10 min does not exceed 1–2 mV, widens. For instance, in the case of a 30 μm thick film the interval involves 3 pH units. During prolonged electrode exposure in solution (2–3 days) the reconditioning of the electrode takes place, while the potential change ΔE does not depend on the electrochemical film treatment but on the film thickness (ΔE decreases with the increasing of thickness). The pH function of the cation sensible PPy electrode consist of two parts of which the greater part is related with a fast change of E within the first minutes.

Response selectivity

The short-time response of PPy electrodes doped with NO_3^- and Cl^- ions and conditioned in solutions of $NaNO_3$ and KCl respectively are

selective relative to the charge sign of the ion. These elctrodes are anion sensitive whereas their responses are not sensitive relative to the cation nature. The change of E caused by the cation alteration of various nitrate and chloride solutions (K^+, Na^+, Cs^+, Ca^{2+}, Ba^{2+}, $N(C_2H_5)_4^+$) of the same concentration is connected only with the change of the activity coefficients. On the other hand, the response of the caiton sensitive PPy electrode doped with SO_4^{2-} and conditioned in Na_2SO_4 is not selective relative to the charge sign of the ion. Its potential E is also influenced by the anion nature. The influence decreases in the following sequence $I^- \sim Br^- \sim NO_3^- > Cl^- \sim ClO_4^- > F^-$.

In order to characterize the selectivity of anion sensitive PPy electrodes relative to various anions, the selectivity coefficients $k_{i,j}^{pot}$ were calculated (i – potential-determining ion, j – interfering ion). All methods for the determination of selectivity coefficients assume the validity of certain assumptions [18]:

- sufficiently rapid establishment of the ionic equilibrium,
- maintenance of the same conditions in the solution immediately at the membrane surface and in the bulk,
- simple membrane mechanism.

The IUPAC commission on Analytical Nomenclature [19] has recommended two basic methods:

1) measuring in separate solutions [20],

2) measuring in solutions with the fixed concentration of the interfering ion (mixed solutions) [21].

We have determined $k_{i,j}^{pot}$ using both recommended methods. The expression for $k_{i,j}^{pot}$ in the first method is the following:

$$lgk_{i,j}^{pot} = \frac{E_j - E_i}{S_i} - \frac{z_i}{z_j} lg\ a_j + lg\ a_i \qquad (4)$$

where E_j – electrode potential in solution of the interfering ion with activity a_j, E_i – electrode potential in solution of the potential-determining ion with activity a_i, z_i and z_j are the charges of ions i and j, respectively and S_i is the experimental Nernstian slope in pure solution of ion i.

For method 2 the measured dependence of electrode potential E on the lga_i in the presence of a_j = const consists of two linear parts which intercept at $a_i = a_i^*$. The expression for $k_{i,j}^{pot}$ is

$$k_{i,j}^{pot} = a_i^* / a_j^{z_i/z_j} \qquad (5)$$

It can be shown that the same result is available when we measure the electrode potentials E_i and E_{ij} in solutions containing ions i with activity a_i and ions i and j with activities a_i' and a_j, respectively. We must take into account the change of activity coefficients for ions i in the presence of ions j. The ratio of concentrations c_j and c_i in mixed solutions must be at least 100. The equation for $k_{i,j}^{pot}$ is

$$k_{ij}^{pot} = \frac{a_i \cdot 10^{\frac{E_{ij}-E_i}{S_i}} - a_i'}{a_j^{z_i/z_j}} \qquad (6)$$

The calculated values for $k_{i,j}^{pot}$ are given in tables 2 and 3.

Table 2

The selectivity coefficients for PPy^+/Cl^- not treated before conditioning in 1M KCl.

Interfering ion	Method 1	Method 2
Br^-	1.6 ± 0.2	1.5 ± 0.2
I^-	2.8 ± 0.2	2.8 ± 0.2
NO_3^-	1.8 ± 0.2	1.0 ± 0.1
ClO_4^-	1.3 ± 0.1	1.4 ±0.1
SO_4^{2-}	$3.3 \cdot 10^{-2} \pm 1.5 \cdot 10^{-3}$	$2.1 \cdot 10^{-2} \pm 5 \cdot 10^{-3}$

The calculated $k_{i,j}^{pot}$ are independent of the polymer layer thickness whithin the experimental error. According to the interfering effect we can range the ions $I^- > NO_3^- \sim Br^- \sim ClO_4^- \sim (Cl^-) \gg SO_4^{2-}$ in the case of PPy electrodes conditioned in KCl and $(NO_3^-) > I^- > Br^- > Cl^- > ClO_4^- \sim F^- \gg SO_4^{2-}$ for PPy electrodes conditioned in $NaNO_3$ and $ClO_4^- > BF_4^- > I^- > (NO_3^-) > Br^- > Cl^- \sim HCO_3^- > CH_3COO^- > SO_4^{2-} \sim F^-$ for the PVC membrane nitrate selective electrodes. As appears from the above the arrangement for the PPy electrodes is in principle the same as observed for the ion selective electrodes with liquid membranes and corresponds to the Hoffmeister

lyophilic series [22] which is based on the differences of solvation energies.

Table 3

The selectivity coefficients for PPy^+/NO_3 conditioned in 0.1M $NaNO_3$

Electrode / Interfering ion	Not treated	Overoxidized	Reduced
Cl^-	$(3.0\pm0.2)\cdot10^{-1}$	$(3.3\pm0.2)\cdot10^{-1}$	$(2.7\pm0.2)\cdot10^{-1}$
Br^-	$(4.0\pm0.2)\cdot10^{-1}$	$(3.9\pm0.2)\cdot10^{-1}$	$(2.9\pm0.2)\cdot10^{-1}$
I^-	$(4.8\pm0.2)\cdot10^{-1}$	$(4.0\pm0.2)\cdot10^{-1}$	$(3.0\pm0.2)\cdot10^{-1}$
ClO_4^-	$(1.8\pm0.2)\cdot10^{-1}$	$(2.6\pm0.2)\cdot10^{-1}$	$(1.7\pm0.2)\cdot10^{-1}$
F^-	$(1.8\pm0.2)\cdot10^{-1}$	$(2.1\pm0.2)\cdot10^{-1}$	$(8.8\pm0.2)\cdot10^{-2}$
SO_4^{2-}	$(6\pm1)\cdot10^{-3}$	$(7\pm1)\cdot10^{-3}$	$(6\pm1)\cdot10^{-3}$

Potential jumps on the phase boundaries PPy/internal solution/external solution

The lack of a quantitative difference in potentiometric behaviour between PPy electrodes which experienced different electrochemical pretreatment shows that the redox properties of PPy films do not play the main role in determing the elctrode potential function. The overoxidized PPy electrode that shows practically no electrochemical reaction between $+0.4 \div -1.0$ V is in its potentiometric behaviour principally analogous to those of nontreated, cycled-through and reduced ones (Fig. 4 and 5). The PPy electrode can be considered to be a relatively hydrophobic system whose micropores in a long-time conditioning are filled with the conditioning solution. After conditioning the PPy as a redox system is in equilibrium just with the solution included into pores and not with the external measuring solution into which the electrode is immersed for a short time.

The structure of the PPy film as a microporous hydrophobic polymeric matrix is determined by the dopant-anion but also by the electrochemical treatment of the electrode before conditioning. The potentiometric behaviour of the PPy electrode is determined, besides polymeric matrix properties also by the composition of the internal

solution in pores. On the boundary of these two phases in pores the adsorption of species of the internal solution takes place, causing an adsorption potential jump. Preferred as the adsorbates are the ions of the internal solution that are less solvated or easily desolvated (the anions). As a result of the reversible adsopriton process the hydration number of ions in pores diminishes. The equilibrium between the PPy electrode and the internal solution that sets up after a long-time primary conditioning or reconditioning depends on the electrolyte concentration. This dependence is characterized by E_r, lga_c-relationship of PPy electrodes conditioned in $NaNO_3$ solution (Fig. 4 and 5; curves 6). So the slope of the straight line for an overoxidized PPy film (that has no redox activity) is -11 mV per decade. For the other electrodes the absolute value of the slope is essentially higher but remains still below the Nernstian one. This indicates that the redox-process of PPy in reconditioning is affected by both anion (equation 2) and cation exchange (equation 3) processes. These considerations are also confirmed by the voltammetric measurements of the films before and after potentiometric measurements (Fig. 1a and b). When the redox process of a just-prepared PPy film occurs within a relatively narrow potential interval (only anion exchange) the potential interval widens essentially after conditioning.

The PPy electrode function that arises by the contact of the conditioned electrode with the measuring solution 3–4 min after the electrode immersion (the short-time response), is determined by a potential jump on the boundary of internal solution in hydrophobic micropores/external solution. This potential jump is caused by the preferred moving of anion or cation through the above-mentioned phase boundary that is primarily determined by the electrolyte nature and the concentration of the internal solution (Fig. 4, curve 7). If the internal solution contains electrolyte whose anion is easily desolvated (NO_3^-, Cl^-), the favoured process is anion moving from external to internal ($a_e > a_i$) and vice versa ($a_e < a_i$). Such kind of electrodes are anion sensitive (Fig. 4, 5) while the function selectivity is determined by the difference of the hydration energy of anions in external and internal solutions. If the internal solutions contains an electrolyte with a heavily desolvated anion (SO_4^{2-}), cation diffusion through the boundary is favoured and the electrode function is inverted. So the reason of the PPy electrode function and its selectivity is the dehydration of the internal solution ions in the adsorption process on the PPy matrix surface. Among anion sensitive PPy electrodes the most selective are those that are conditioned in solutions containing anions with low dehydration

energy.

As seen from Table 3, the film conditioned in chloride solution is selective only relative to SO_4^{2-}, at the same time conditioning in nitrate solutions transforms the film selective relative to many ions although the selectivity coefficients are not good enough, except for SO_4^{2-}. The selectivity of hydrophobic microporous anion sensitive PPy electrode relative to different anions, depends to some extent on the electrochemical treatment of an electrode before conditioning (Table 3). This influence may be connected with both porosity and a change of the PPy matrix surface active properties during treatment.

CONCLUSIONS

The potentiometric response of PPy electrodes is determined not only by its redox properties as is stated in many reports [7–11]. The long-time response of PPy electrodes is determined by the adsorption potential jump on the interface PPy matrix/internal solution and by the redox properties of PPy.

The reproducable short-time Nernstian potential response becomes feasible after a long-time conditioning of the electrode in the electrolyte solution. The length of the linear relationship between E and lga is influenced by the concentration of the conditioning solution and the electrochemical pretreatment of the PPy film before conditioning. The short-time response of PPy electrodes is determined by the moving of ions through the interface between PPy electrode as the hydrofobic microporous system filled with the conditioning solution, and the external solution. Hereby the facilities for the moving of a certain ion are based on its hydration difference in internal and external solutions. The arrangement of the anions that have an interfering influence on the anion sensitive PPy electrodes is mainly determined by the dehydration energy of ions. The short-time response of PPy electrode does not remain stable during a long-time contact with the measuring solutin due to the reconditioning of the microporous system. More durable against reconditioning are the thicker films ($d > 10\ \mu m$). The PPy electrodes preserved in the conditioning solution are usable for a long time.

REFERENCES

1. **J. Heinze.** Synth. Met., 41–43 (1991) 2805.
2. **A. Deronzier, J.-C. Moutet.** Acc. Chem. Res., 22 (1989) 249.
3. **Fengbin Li, W.J. Albery.** J. Electroanal. Chem., 302 (1991) 279.
4. **M. Schnöller, W. Wersing, H. Naarman.** Makromol. Chem., 8 (1987) 83.
5. **E. Barendrecht, A. Elzing, L.J.J. Janssen, van der Putten, W. Visscher, F. Vork.** Makromol. Chem., 8 (1987) 211.
6. **G. Zotti.** Synth. Met., 51 (1992) 373.
7. **Dong Shaojun, Sun Zhisheng, Lu Ziling.** J. Chem. Soc., Chem. Commun., (1988) 993.
8. **F. Beck, J. Jiang, M. Kolberg, H. Krohn, F. Schloten.** Z. phys. Chem., Neue Folge, 160 (1988) 83.
9. **Shaojun Dong, Guangli Che.** Talanta, 39 (1991) 111.
10. **Qibing Pei, Renyan Qian.** Electrochim. Acta, 37 (1992) 1075.
11. **A. Cadogan, A. Lewenstam, A. Ivaska.** Talanta, 39 (1992) 617.
12. **T. Okada, K. Hiratani, H. Sugihara, N. Koshizaki.** Anal. Chim. Acta, 266 (1992) 89.
13. **J.A. Vinokurov, V.V. Kondratjev.** Elektrokhimiya, 25 (1989) 1291.
14. **J.M. Pernaut, R.C. Peres, V.F. Juliana, M.-A. De Paoli.** J. Electroanal. Chem., 274 (1989) 225.
15. **F. Beck, P. Hülser, R. Michaelis.** Bull. of Electrochem., 8 (1992) 35.
16. **G. Gunawardena, G. Hills, I. Montenegro.** J. Electroanal. Chem., 184 (1985) 371.
17. **J.E.W. Davies, G.J. Moody, J.D.R. Thomas.** Analyst, 97 (1972) 87.
18. **I. Koryta.** Ion-selective Electrodes. Cambridge: Cambridge Univ. Press, 1975.
19. Recommendations for publishing manuscripts on ion-selective electrodes. Comission on Analytical Nomenclature, Analytical Chemistry Division. IUPAC. Ion-sel. El. Rev. 1 (1979) 1684.
20. **G. Eisenman, D.O. Rudin, I.U. Casby.** Science, 126 (1957) 871.
21. **E. Pungor, K. Toth.** Anal. Chim. Acta, 47 (1989) 291.
22. **K. Sollner, G.M. Shean.** J. Am. Chem. Soc., 86 (1964) 1901.

INFLUENCE OF IONS ON THE POLYPYRROLE REDOX PROCESS

A. Hallik, A. Alumaa, J. Tamm
Institute of Physical Chemistry, University of Tartu

ABSTRACT

The polypyrrole (PPy) films doped with different anions (dodecylsulfate - DDS^-; 2-naphthalene sulfonate $-NS^-$; SO_4^{2-}; ClO_4^-; NO_3^-) were electrochemically prepared. The properties of synthesized PPy films are largely influenced by the nature and size of the dopant anion. So the PPy film doped with small inorganic anions shows the similar redox-behaviour: the electroneutrality of the PPy film is conserved by the moving of the anionic species. In the case of PPy/NS and PPy/DDS, the original dopants are nonmobile and the redox-process proceeds by the incorporation - releasing of the cations. On the basis of cyclic voltammetry data the redox-properties of PPy/DDS in aqueous electrolyte solutions with various cations have been studied. The dependence between E_{pc}, E_{pa} and incorporated cation size are represented. The differential capacitance of the PPy/DDS film and its changing by electrochemical treatment of the film is estimated by the as method.

The electrochemical properties of electrochemically conducting polymers have been studied in a large number of works. Among these polymers the polypyrrole (PPy)-based electrodes are the ones most studied. It is known that the electrochemical behaviour of PPy films essentially depends on the nature and size of the so-called dopant ion and also on the nature of the electrolyte and solvents used in the preparing or treating of the polymer films. In this work our special attention is

paid to polypyrrole doped with dodecylsulphate as a big surface-active anion. The films doped with 2-naphthalene sulfonate, sulfate, perchlorate and nitrate anions are also investigated.

Polypyrrole/dodecylsulphate(PPy/DDS),polypyrrole/2-naphthalene sulfonate (PPy/NS); PPy/SO_4; PPy/ClO_4; PPy/NO_3 and some other films were prepared by the electrochemical polymerization of pyrrole in the aqueous solution containing 0.1 M pyrrole and 0.1–0.15 M corresponding electrolyte (Na-salts) onto Pt-wire. The counter electrode was Pt-ring or Pt-wire and the reference electrode – a saturated Ag/AgCl electrode. Before electrodeposition and cyclic voltammetric measurements, the solutions were deoxygenated with Ar. The thickness of films was calculated according to the relation 0.2 C/cm^2 per 1 μm for PPy/DDS and PPy/NS and 0.4 C/cm^2 per 1 μm for others. In order to determine the capacity of PPy/DDS films and the changes of film conductivity with potential, the ac method (bridge P–5021) was used. As evidenced in various studies on conducting polymers [1–7], and also found out from the results of our research group, the PPy films doped with small anions during the electrochemical redox cycle present themselves as exchangers of anionic species: upon reducing the film releases the anions and upon oxidizing the uptake of anions occurs. Such kind of behaviour is characteristic of PPy/ClO_4; PPy/NO_3; PPy/Cl; PPy/Br; PPy/PF_6; PPy/BF_4 and some other films doped with small inorganic anions. The voltammograms of those films are similar – the reducing and oxidizing proceed within a wide enough potential interval (flat curves) while the maximum of cathodic and anodic currents appear at relatively positive potential values (E_p = 0 ÷ –100 mV).

In addition to the first maximum there often occurs a smaller second reduction peak (E_p = –550 ÷ –750 mV) that usually diminishes or disappears by electrochemical cycling. The appearance of the latter maximum may be connected with the moving of the less available part of the dopant or with reducing by the cation incorporation into the film [5, 8]. The PPy/ClO_4 and PPy/NO_3 films (Fig. 1, 2) are the representative examples of such kind of polymer films. The motion of anionic species is also proved by the examination of film properties in

the solution of NaDDS. From Fig. 3 it becomes evident that during the first reduction cycle the releasing and dispersion of anions incorporated into the film by electrodeposition occurs, and upon the following oxidation cycle the reversible NO_3^- uptake does not proceed. Since the structure of the films besides the size of pores depens on the dimension of an anion doping at synthesis [6, 7, 9], the new anion DDS^-, due to its essentially bigger size as compared with NO_3^- ion, cannot easily penetrate the film either. The little cathodic maximum that will be left over, presumably corresponds to the some amount of DDS^- incorporated into surface layers (Fig. 3, the second cycle). The same is valid for PPy/ClO_4 films. It is interesting that despite the difference between ClO_4^- and DDS^- ion sizes, the redoping of PPy/ClO_4 with DDS^- (at least partially) by prolonged polarization at anodic potential, seems possible.

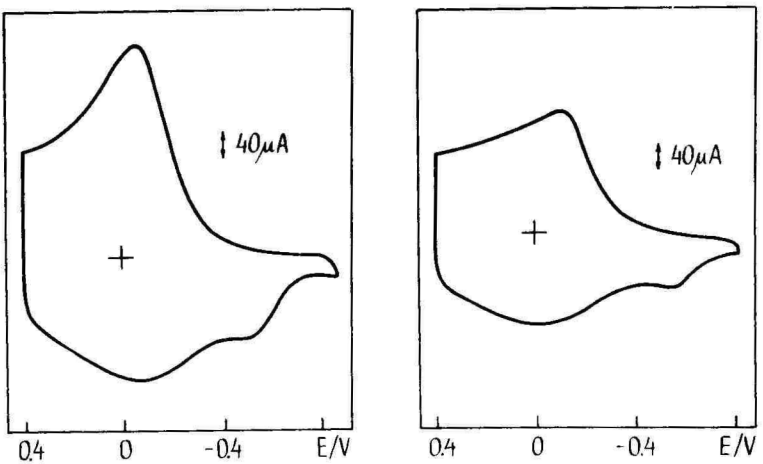

Fig. 1. Cyclic voltammogram of PPy/ClO_4 film in 0.15 M $NaClO_4$ solution. Sweep rate 50 $mV \cdot s^{-1}$.

Fig. 2. Cyclic voltammogram of PPy/NO_3 film in 0.1 M $NaNO_3$. Sweep rate 50 $mV \cdot s^{-1}$.

So it was established that the reduction currents of the above-mentioned films began to depend linearly on the duration of the electrode anodic polarization at 400 mV vs. Ag/AgCl. In the course of time the anodic maximum will be formed ($E_{p,a}$ = -380 mV). The values of $E_{p,c}$ remain almost the same, that is -750 ÷ -800 mV but the current peak (I_p) intensity depending on the polarization time considerably diminishes and a more stationary picture takes shape.

A somewhat different behaviour is shown in PPy/SO_4 films. Though the dimensions of SO_4^{2-} are close to those of ClO_4^- and NO_3^-, the differing in the properties of freshly synthesized comparable films is essential. It is indicated by the first redox cycle of a fresh PPy/SO_4 electrode (Fig. 4). The first reduction curve of the PPy/SO_4 film is,

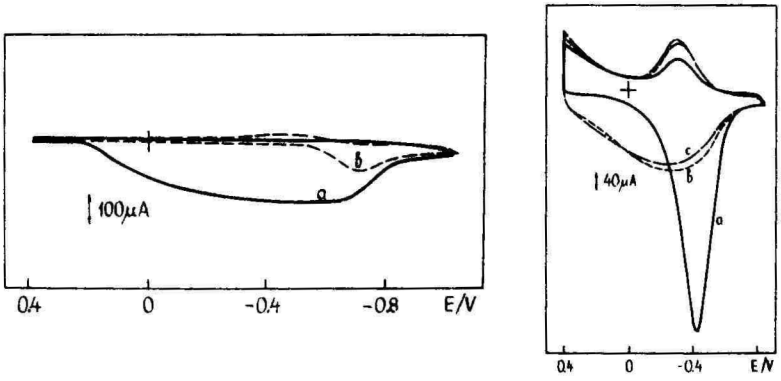

Fig. 3. Cyclic voltammogrms of PPy/NO_3 film in 0.1 M NaDDS solution. Sweep rate 50 $mV \cdot s^{-1}$; a - the first, b - the second cycles.

Fig. 4. Cyclic voltammograms of PPy/SO_4 film (synthesized from aqueous solutions containing 0.1 M pyrrole and 0.1 M Na_2SO_4) in 0.1 M Na_2SO_4. Sweep rate 50 $mV \cdot s^{-1}$; a first, b - the second and c - the tenth cycles.

differently from the other above-given ones, sharp and shifted toward the more negative potentials, $E_{pc,1}$ =-420 mV. Likewise, the values of

$E_{pa1,2}$ = -310 mV are more negative. For PPy/SO_4 films synthesized instead of 0.1 M Na_2SO_4 solution from 0.1 M H_2SO_4, the potential shift is even larger: $E_{pc,1}$ = -540 mV and $E_{pal,2...10}$ = -360 mV. This effect may be connected with a somewhat stronger connection between sulfate groups and the PPy matrix, also with the fact that the ion diffusion coefficient (D) for SO_4^{2-} is about one or two orders of magnitude less than for ClO_4^- and Cl^- [10]. The similarity of the first reduction cycle of the PPy/SO_4 film the PPy/DDS film enables to suppose, besides the anion releasing during the reduction process, also the cation uptake as it completely takes place in the case of PPy/DDS [11–16]. The potentiometric measurements of PPy/NO_3 and PPy/SO_4 films in different electrolyte solutions also indicate the occurrence of this kind of process. When the PPy/NO_3 and PPy/Cl films expose anion-sensitivity, the PPy/SO_4 shows itself as a cation-sensitive electrode [17]. At the same time the electrochemical scanning of the PPy/SO_4 film in 0.1 M NaDDS solution shows that sulfate groups are not firmly fixed into the polymer matrix and at least the majority of the original dopant separates from the matrix and disperses, Fig. 5. The following cycles

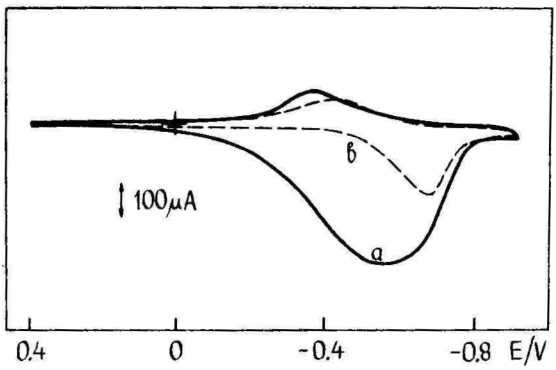

Fig. 5. Cyclic voltammograms of PPy/SO_4 film in 0.1 M NaDDS solution. Sweep rate 50 mV·s^{-1}; a – the first, b – the second cycles.

exibit a relatively small maximum $E_{pc,2}$ = -680 mV; $E_{pa,2}$ = -410 mV,

and the corresponding current values $I_{pc,2}$; $I_{pa,2}$ are bigger than in the case of PPy/NO_3 or PPy/ClO_4.

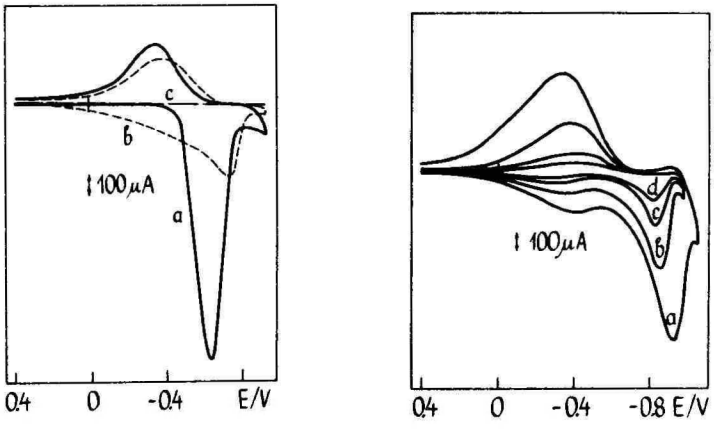

Fig. 6. Cyclic voltammograms of PPy/NS film in 0.1 M NaNS solution (a – the first, b – the second cycles) and in 0.15 M TBA Br solution (c), sweep rate 50 $mV \cdot s^{-1}$.

Fig. 7. Cyclic voltammograms of PPy/NS film in 0.1 M NaNS aqueous solution. Sweep rate a – 100, b – 50, c – 20 and d – 10 $mV \cdot s^{-1}$.

The redox behaviour of conducting polymers doped with big anions is particular. Instead of anion releasing-uptake, the cations may be the movable species and the dopant anions may prove to be only partially mobile or in many cases nonmobile. Such kind of behaviour is established for PPy films doped with polyelectrolytes (PE), dodecylbenzenesulfonate (DBS), dodecylsulfate (DDS), tosylate (TsO), pyrene sulfonate (PS), naphthalene sulfonate (NS), naphthalene disulfonates (NDS), adenosine triphosphate (ATP) and some other anions [4, 11–16, 18–28]. Besides, the concrete behaviour of the film essentially depends on the nature of the solvent used at the preparing or electrochemical switching of the film. So in the case of PPy/DDS in aqueous solutions mainly the cations move in and out of the polymer, but in ACN solutions the moving ions are the bulky anions [15, 24]. The

impossibility of the anionic charge compensation mechanism in certain conditions is easily demonstrated, for example, by using a solution containing big cations. Fig. 6 represents the voltammograms of the PPy/NS film in NaNS and tetrabutylammonium bromide aqueous solutions. The electrochemical switching of a thin film in the lastly named solutions shows that the redox process is strongly aggravated because the NS does not release from the film and the TBA cations are too bulky to penetrate the film. The behaviour of the PPy/DDS film is almost the same. It only seems that the properties of PPy/NS films are more changeable on repeated cycling and two reduction maximuma may arise (Fig. 7), also there may occur the E_{pc} shifting towards more negative potentials with a decrease in the quantity of the redoxcharge. The PPy/DDS films by electrochemical treating also experience changes but to a little extent.

In conclusion we report the data of the PPy/DDS film redox properties in various aqueous electrolyte solutions, where the anion is always the same - Cl^-. Fig. 8, 9 represent the results of the cathodic and anodic peak potentials of 2 μm thickness PPy/DDS electrodes depending on the size of hydrated and nonhydrated cations. From those data it becomes evident that the overall legitimacy of E_{pc} and E_{pa} dependence on the cation dimension cannot be established. Yet there exist some tendencies. For monovalent cations there seems to exist a slight tendency of decreasing the $E_{pc,1}$ value with the increasing of Pauling's radius (r). This indicates the possibility of cation incorporation into polymers at least partially without a hydration cell what seems reasonable because the synthesized film properties strongly differ from those of the electrochemically treated film. The second cycle shows the contrary behaviour: the hydrated volumes V_{hydr} must be taken into account. The E_{pa} values of the first and second cycles for monovalent metal cations are close and altogether are almost independent of the r values. This may be explained by the swelling of the polymer during reduction - the swollen film porosity is determined by the incorporated cation that makes the following cation moving easier. The tetraalkylammonium cations are formed of their own series. During the

first reduction cycle the incorporation of a larger TEA^+ (as compared with TMA^+) is essentially aggravated, $E_{pc,1}$ = -830 mV (high kinetical resistance of the process). The TBA^+ and triethylbenzylammonium ($TEBA^+$) cannot be incorporated into the film during the first cycle at all. It is obvious that the incorporation of bivalent and trivalent cations is favoured in comparison with the monovalent ones. This seems to be connected with their smaller Pauling's radii and stronger electrostatic interaction between M^{2+} and PPy/DDS. Besides, the $E_{pc,1}$ values for Ni^{2+}, Co^{2+} and Mg^{2+} are almost the same, only Ca^{2+} differs from the others to some extent. For the second cycle the $E_{pc,2}$ values

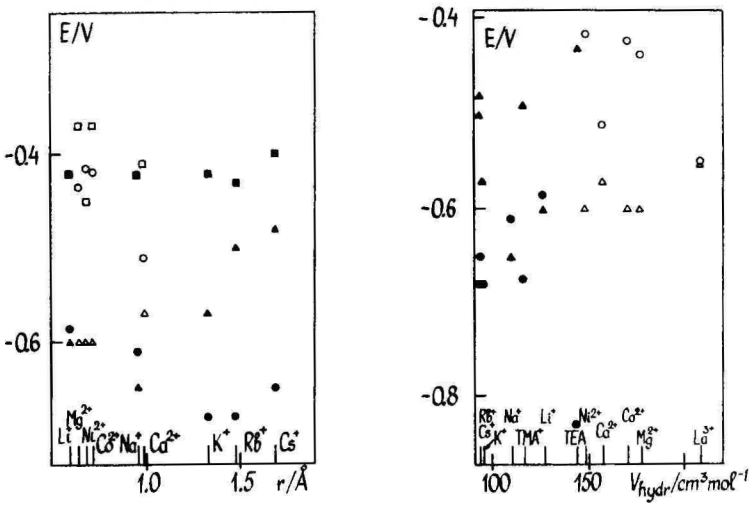

Fig. 8. Plot of $E_{pc,1}$; $E_{pc,2}$ and $E_{pa,1}$ vs. Pauling radii (r) of the cation (from cyclic voltammograms of the 2 μm PPy/DDS films in various 0.15 M chloride aqueous solutions. Sweep rate 50 $mV \cdot s^{-1}$) ○ the first reduction, △ the second reduction and □ the first oxidation cycles. ● ▲ ■ – monovalent cations; ○ △ □ bivalent cations.

Fig. 9. Plot of $E_{pc,1}$ and $E_{pc,2}$ vs. the volume of the hydrated cations (V_{hydr}). The films and measurement conditions are the same as in Fig. 8. ○ the first and ∧ the second reduction cycles. ● ▲ – monovalent cations; ○ △ – bi- and trivalent cations.

approach one another even more. The analysis of the peak separation (ΔE) shows that the redox process is more reversible when the bivalent cation participates in the charge compensation.

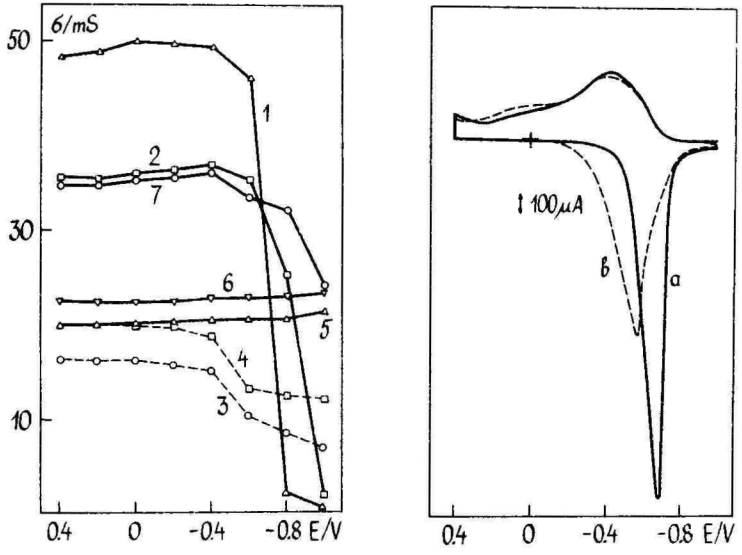

Fig. 10. Plot of 2 μm PPy/DDS films conductivity change with potential in various 0.15 M electrolyte solutions. 1 - $LaCl_3$, 2 - $MgCl_2$, 3 - TEACl, 4 - TMACl; 5 - LiCl; 6 - NaCl; 7 - $CoCl_2$.

Fig. 11. Cyclic voltammograms of PPy/DDS film in 0.15 M KCl solution. Sweep rate 50 $mV \cdot s^{-1}$; a - the first, b - the second cycles.

The film conductivity changes with potential were obtained by ac measurements at the frequency f=12 kHz (Fig. 10). Generally the decreasing of conductivity beginning at certain potentials shows that the reducing process takes place. It is observable in cases when the process is strongly aggravated (in TBA^+ and $TEBA^+$ solutions) and not clearly expressed in voltammograms. An exceptional course in conductivity is observed in Li^+, Na^+, K^+ solutions where during the reduction film its insulator properties do not become evident. Presumably, this is

related to the formation of such kind of film structure and porosity. That results from a good contact of the base matal surface and solution, i.e. the electrical resistance of the film is short-circuited by the electrolyte resistance in the pores of the polymer. In other cases the jump of conductivity always occurs.

For tetraalkylammonium salts it was found that the film conductance properties change in the similar manner – the main jump is between -400 ÷ -600 mV (TMA^+, TEA^+) and begins somewhat earlier when the cations are bigger (TBA^+, $TEBA^+$). The greatest conductance jumps were observed in the case of La^{3+}, Mg^{2+}, Ni^{2+}, and were located within the region of -600 ÷ -800 mV (Ni^{2+}, La^{3+}), -800 ÷ -1000 mV (Mg^{2+}). As approximation it may be said that the region of the reduction maxima and conductance change are close.

The question of the separation of the two types of currents – the capacitive and faradeic is discussed in many articles [8, 29]. Due to the peculiar behaviour of PPy/DDS films (the occurrence of a wide potential interval where the essential reduction process lacks) this question is interesting also for this case.

The differential capacitance of the PPy/DDS film was determined by the impedance method and from the recharging current in the potential interval where the capacitive current is prevailing. The treatment of impedance data was carried out according to the scheme in [8]. By both methods, the following tendencies are revealed.

1. C_0 values of oxidized PPy/DDS films not treated electrochemically are extremely low. In the solution of KCl for the 2 μm film at E = 400 mV before the first reduction C_0 was estimated $\sim$0.07 mF/cm^2 ($\sim$0.4 F/cm^3). The C_0 values does not essentially depend on the thickness of the film. For the 20 μm film this value is $\sim$0,1 mF/cm^2. The values of C_0 exceed the surface capacitance C_s = 0.011 mF/cm^2 (measured at frequency f = 12 kHz) only 7–10 time. Consequently, C_0 of electrochemically nontreated PPy/DDS film is not related to the whole volume of the film but to the surface layer with a certain thickness.

2. In the solution of KCl where after cycling the polymer

reduction process in a certain potential interval remains braked (Fig. 11), the C_0 retains its low values.

3. When by cycling the braking region disappears, C_0 increases essentially and extends, depending on the electrolyte to 20–60 F/cm^3 what indicates that the whole volume of the film is captivated into the process. The capacitive charge of PPy/DDS films is relatively low and does not exceed 30 %.

REFERENCES

1. **T.A. Skotheim** (Ed.), Handbook of Conducting Polymers, V.I. Marcel Dekker, N.Y., 1986.
2. **A.F. Diaz, J.I. Castillo, J.A. Logan, W.Y. Lee.** J.Electroanal. Chem., 129 (1981) 115.
3. **A.F. Diaz, J.C. Lacroix.** New J.Chem., 12 (1988) 171.
4. **T. Shimidzu, A. Ohtani, T. Iyoda, K. Honda.** J.Electroanal. Chem. 224 (1987 123.
5. **Y.-J. Qiu, J.R. Reynolds.** J.Polymer. Sci. Part A.: Polym. Chem., 30 (1992) 1315.
6. **R. Qian, J. Qiu.** Polymer Journal, 19 (1987) 157.
7. **M. Yamamura, K. Sato, T. Hagiwara.** Synth.Met., 41–43 (1991) 439.
8. **J. Tanguy, V. Mermilliod, M. Hoclet.** J.Electrochem.Soc., 134 (1987) 795.
9. **J.T. Girault, J.M. Anderson, I. Maclnnes, M. Schröder, G.Tennant, H.H. Girault.** J.Chem.Soc., Chem. Commun., (1987) 1095.
10. **V.V. Krasko, A.A., Yakovleva, Y.M. Kolotyrkin.** Elektrokhimiya, 22 (1986) 1212.
11. **J.M. Pernaut, R.C.D. Peres, V.F. Juliana, M.-A. De Paoli.** J. Electroanal. Chem., 274 (1989) 225.
12. **R.C.D. Peres, J.M. Pernaut, M.-A. De Paoli.** Synth. Met., 28 (1989) 59.
13. **M.A. De Paoli, S. Panero, P. Prosperi, B. Scrosati.** Electrochim. Acta, 35 (1990) 1145.
14. **R.C.D. Peres, J.M. Pernaut, M.A. De Paoli.** J. Polym. Sci Polym. Chem. 29 (1991) 225.
15. **J.M. Ko, H.W. Rhee, C.Y. Kim.** Makromol. Chem., Macromol. Symp., 33 (1990) 353.
16. **A. Hallik, N.A. Nekrassova, A. Alumaa, J. Tamm.** Proc. 9th Symp. on Double Layer and Adsorption at Solid Electrodes, Tartu, 1991, p. 51.
17. **A. Alumaa, T. Silk, A. Hallik, A. Pruks, J. Tamm.** Acta Comm. Univ. Tartuensis, 966 (1993) 24.

18. **Q.-X. Zhou, C.J. Kolaskie, L.L. Miller.** J. Electronal. Chem., 223 (1987) 283.
19. **L.F. Warren, D.P. Anderson.** J. Electrochem. Soc., 134 (1987) 101.
20. **K. Hyodo, M. Omae.** Electrochim. Acta, 35 (1990) 1245.
21. **C.M. Elliott, A.B. Kopelove, W.J. Albery, Z. Chen.** J. Phys. Chem., 95 (1991) 1943.
22. **V. Krishna, Y.-H. Ho, S. Basah, K. Rajeshwar.** J. Am. Chem. Soc., 113 (1991) 3325.
23. **A. Boyle, E. Genies, M. Fouletier.** J. Electroanal. Chem., 279 (1990) 179.
24. **J.M. Ko, H.W. Rhee, C.Y. Kim.** Makromol. Chem., Macromol. Symp., 53 (1992) 81.
25. **S. Panero, P. Prosperi, B. Scrosati.** Electrochim. Acta, 37 (1991) 419.
26. **M.A. De Paoli, R.C.D. Peres, S. Panero, B. Scrosati.** Electrochim. Acta, 37 (1992) 1173.
27. **R.C.D. Peres. M.A. De Paoli, R. M. Torresi.** Synth. Met., 48 (1992) 259.
28. **J. Tamm, A. Hallik, A. Alumaa.** Synth. Met., 55 (1993) 1473.
29. **S.W. Feldberg.** J. Am. Chem. Soc., 106 (1984) 4671.

VOLTAMMETRIC STUDY OF POLYPYRROLE CHLORIDE ELECTRODE

T. Silk, A. Pruks, J. Tamm
Institute of Physical Chemistry, University of Tartu

ABSTRACT

This paper presents the results of the investigation of the electrochemical properties of chloride-doped polypyrrole in various aqueous electrolytes. Much attention was given to the temporal evolution of cyclic voltammograms which is a less treated problem. It is established that the shape and evolution of voltammograms depend upon the nature of the cations and anions of the supporting electrolyte. In principle, the determining parameter is the size of ions. The differences between the observed results are explained with the different participation of anions and cations in redox switching. During the potential cycling also the structural alterations of polypyrrole film occur which affect the cation-anion participation ratio.

INTRODUCTION

The electrochemical behaviour of conducting polymers such as polypyrrole is a subject of a theoretical and practical interest [1, 2]. The comparing of results obtained by different authors [1–9] is complicated by the fact that polymer films may differ in their primary (degree of polymerization, number of 2,5 and 2,3 linkages etc.), secondary and

tertiary structure, which are influenced by the nature of the dopant, substrate, possible impurities and synthesis conditions [6]. Although some authors have observed the differences between the first and the following cyclic voltammograms [1, 4, 6–9], the detailed investigation of these phenomena is absent. Insufficient attention has also been paid up to now to the comparison of voltammograms obtained in different solutions.

This work is an attempt to fulfill this gap. The results may be used in the characterization and comparison of further investigations.

EXPERIMENTAL

All the experiments were performed in the conventional three-electrode cell under Ar atmosphere. The working electrode was a Pt-wire (area 0.1 cm^2) embedded into glass. The counter electrode was a Pt-sheet and the reference electrode a saturated silver/silver chloride electrode. All the potentials reported in this work are expressed vs. Ag/AgCl electrode.

The polymer films were synthesized potentiostatically using potentiostat P-5827M from an aqueous solution of 0.1 M pyrrole and 0.1 M KCl. The synthese potential was +0.7 V and the thickness 1 μm was achieved by passing an anodic charge 0.4 $C \cdot cm^{-2}$. During the synthesis the current density increased up to the final value $I < 2$ $mA \cdot cm^{-2}$. The cyclic voltammograms were measured using the potentiostat of a polarographic analyzer PA-2.

All the solutions were prepared from twice-distilled water. Pyrrole was freshly distilled under vacuum before use. Sodium dodecyl sulphate (NaDDS) was recrystallized before use, all the other reagents were used as received. Cyclic voltammograms were measured in 0.1 M aqueous solutions of ethylenediaminetetraacetic acid disodium salt (Na_2EDTA), NaDDS, $(C_4H_9)_4NBr$ (TBABr), $(C_2H_5)_4NBr$ (TEABr), KBr, KCl and NaCl. The KCl solutions with various pH were prepared by the addition of HCl or KOH solution.

The potential sweep rates were in the range 2-200 mVs^{-1}, but in the main the v = 50 mVs^{-1} was used. Before every potential sweep cycle the electrode was held at the initial potential E_H = +0.4 V for the time t_H = 30s.

RESULTS

Influence of the solution composition

All the measured voltammograms can be divided into 3 groups on the basis of the composition of the solution. To the first group belong curves measured in the solutions of NaCl, KCl and KBr, the second group – in the solutions of tetraalkylammonium salts and the third – in the solutions of NaDDS and Na_2EDTA (Fig. 1 and 2).

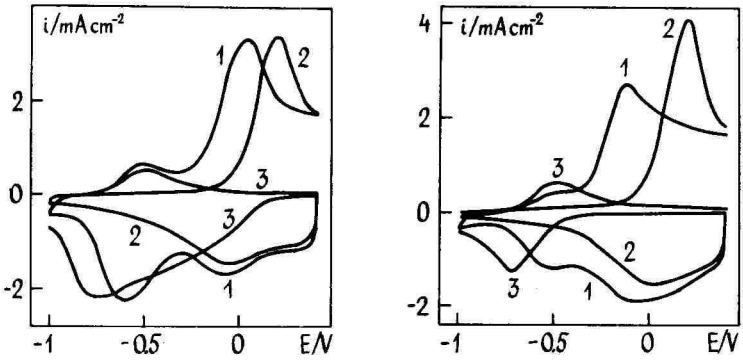

Fig. 1. Cyclic voltammograms of PPy/Cl electrode 1) in 0.1 M KCl 2) in 0.1 M TBaBr 3) in 0.1 M NaDDS 1. scan, v = 50 $mV \cdot s^{-1}$

Fig. 2. Cyclic voltammograms of PPy/Cl electrode 1) in 0.1 M KCl 2) in 0.1 M TBaBr 3) in 0.1 M NaDDS 10. scan, v = 50 $mV \cdot s^{-1}$

In general, the first group is characterized by two cathodic (C1 and C2) and two anodic (A1 and A2) current peaks. Depending on the number of potential scan and the nature of electrolyte, the positions of

the peaks were located as follows: -0,65 V < E'_{C1} < -0.43 V; _0.05 V < E'_{C2} < +0.08 V; -0.53 V < E'_{A1} < -0.40 V and -0.15 V < E'_{A2} < + 0.05 V. During the cycling current peak C2 slightly increases, but peak C1 decreases. The most change occurs during the first two potential scans (~ 25 %), although a practically stable value is achieved after 10 scans. Peak Al is weakly expressed, especially on voltammograms in NaCl solutions (disappears completely during the scans). Current peak A2 decreases somewhat and E_{A2} shifts in the negative direction.

The second group of curves shows only flat cathodic peak at -0.10 V < E''_C + 0.12 V and one considerably sharper (particularly in TBABr) anodic peak at +0.04 V < E''_A < +0.22 V. During the cycling the peak current densities increase and the potentials E''_C and E''_A shift in the positive direction.

The third group of voltammograms is characterized by the presence of one cathodic and one anodic peak a in the second group, but they are located at -0.75 V < E'''_C < -0.55 V and -0.5 < E'''_A < -0.1 V. Peak potential E'''_C is comparable to E'_{C1}. For this group a considerable decrease of current densities during the first and second scans and the lowering of current densities in the region +0.4 > E > -0.2 V are typical. The anodic current peak i relatively small and disappears practically in Na_2EDTA solutions.

Amount of redox charge

By the integration of current-potential curves we can find the amount of charge consumed in cathodic (Q_c) and anodic (Q_a) scans in the limits from +0.4 V to -1.0 V. In general $Q_c > Q_a$, since the reoxidation of reduced polypyrrole occurs relatively slowly and is not finished when the potential achieves the final value +0.4 V. To a certain extent the ratio Q_c/Q_a depends on the type of curves. In the first and second groups $Q_c \approx Q_a$, but in the third group $Q_c/Q_a = 2 \div 3$.

During the cycling we can obtain a decrease of the charge amount, except in the case of TEABr solution. The diminishing of Q_c is roughly 15 % in case of the first group and 70 % in case of the third

group. The greatest value of Q_c (up to 40 $mCcm^{-2}$) can be obtained in the first group from the first scan, the differences between Q_c in the various electrolytes in this group are small. In the other solutions Q_c has the following values: TBABr – 22.5; TEABr – 27.6; NaDDS – 30.5 and Na_2EDTA – 22.0 $mCcm^{-2}$.

Consequently, Q_c is about 20 % from the synthesis charge as noted in literature [9–11]. In general, Q_c depends upon the scan rate, especially in NaDDS solution where at low scan rates ($V < 20\ mV \cdot s^{-1}$) Q_c is considerably greater. The pH of the solution has a certain effect on Q_c values. In case of the first group of curves Q_c is greater in alkaline (pH > 8) and acidic (pH < 4) solutions than in neutral ones: at pH = 11 Q_c = 45 $mC \cdot cm^{-2}$ and at pH = 1.1 Q_c = 55 $mC \cdot cm^{-2}$. The decrease of Q_c during potential scanning is in this case greater than in neutral solutions reaching up to 50 % during the 10 scans.

Effect of the holding potential E_H and holding time t_H

In case of the first group of solutions the increase of t_H or E_H leads to the increase of peak C1 and the decrease of peak C2. During the anodic scan we establish the increase of both current peaks A1 and A2, at the same time the potential E'_{A1} shifts somewhat in the positive direction, E'_{A2}, however, to a considerable extent. It must be noticed that peak A1 increases more, so that at a higher E_H the anodic peaks become practically equal. The increase of t_H at a higher E_H (E_H > +0.6 V) reduces the current peaks, the same effect is observed in regard to Q_c.

In Na_2EDTA and NaDDs solutions t_H and E_H affect mainly the cathodic scan, the changes are in general comparable to the results in the first group. Essential is the peak shape transformation – broadening. Noticeable is the growth of Q_c, its value can become greater than in the first scan. In NaDDS solution E''_C shifts at first in the negative and then in the positive direction. The broadening of the peak is also established.

Influence of solution pH

The influence of solution pH on the measured voltammograms is mainly studied in the first group of solutions. If in neutral solutions the measured voltammograms have two cathodic and anodic peaks, then at pH > 11 and pH < 4 the cathodic scan has only one peak. in acidic solutions the peak is located close to E'_{C2}, in alkaline solution to E'_{C1}. The anodic peaks are weakly expressed at the same time. In all cases in the first scan the cathodic peak is replaced at more negative potentials than in the following scans.

The shape of voltammograms in the 0.02 M TBAOH (pH = 12.7) and in the mixture TBABr + TBAOH (pH = 10.5) was somewhat different. In pure TBAOH we obtain only one cathodic peak at E'_{C1} while at $E > E'_{C1}$ the current is practically zero. In the mixture TBABr + TBAOH on the first scan two flat peaks appear, but beginning from the second scan one flat peak remains at E'_{C2}.

Influence of scan rate

In the first group the peak separation becomes more evident at higher scan rates ($v > 50$ mV·s^{-1}). The lowering of v brings the peak potentials nearer to one another until one flat peak is formed whose potential is close to E'_{C2}. When the first scan is carried out with a high sweep ($v = 200$ mV·s^{-1}), a clearly expressed peak at E'_{C1} is obtained on the curves with low v. In this case peak C1 is greater than peak C2. The latter can become very flat. In general, the peak currents at A1, C1 and C2 depend linearly upon the scan rate. Some values of the slope of i–v dependence are given in the Table in units $10^2 \cdot A \cdot s \cdot V^{-1} \cdot cm^{-2}$.

The correlation coefficient r^2 is greater than 0.996. In mixed tetraalkylammonium salt solutions a good linearity was established with $v^{0.8}$ instead v.

Table

The slope of the dependences of peak current vs scan rate

Solution	pH	Slope di/dv		
		peak C1	peak C2	peak A2
0.1 M HCl	1.1	-	3.8±0.2	3.9±0.2
0.05 M KCl + 0.05 M HCl	1.3	-	3.7±0.1	3.5±0.3
0.09 M KCl + 0.01 M HCl	2.2	-	3.6±0.1	3.8±0.1
0.1 M KCl + HCl	4.0	2.0±0.1	3.1±0.1	4.5±0.3
0.1 M KCl	6.4	3.2±0.1	3.1±0.1	5.2±0.2
0.1 M KCl + KOH	7.3	2.5±0.1	3.0±0.1	4.6±0.1
0.1 M KCl + KOH	10.4	2.8±0.1	3.2±0.2	4.9±0.2
0.1 M KCl + KOH	11.0	2.8±0.1	-	1.2±0.2
0.1 M KCl + KOH	11.3	2.7±0.1	-	1.2±0.1
0.1 M TBABr + TBAOH	10.4	4.4±0.1*	-	4.5±0.1
0.02 M TBaOH	12.7	6.5±1.2	-	10.1±1.7

* this value corresponds to relationship $i\text{-}V^{0.8}$

Influence of potential cycling in the wide range of potential from +1.7 V to -1.0 V

This series of measurement was carried out in KCl solutions with different pH and in the mixture TBABr + TBAOH. When pH < 2 the voltammograms show in the first scan two oxidition peaks at

E_{ox1} = +0.92 V and E_{ox2} = +1.29 V. The current at E_{ox1} was about twice greater.

In the second only the second peak was present at E_{ox2} and the corresponding current was to the some extent smaller. In the region 4 < pH < 8 only one very large peak appears at E_{ox1} = +1.0 v (the corresponding oxidation charge is about half of Q_{synth}) and the peak current is practically independent of pH. In the second scan a peak appears only at E_{ox2} +1.27 V and its value is 5–6 times lower than in the first scan. If pH > 11 instead of the oxidation current peak there is only a region with a somewhat greater current density. In the TBABr + TBAOH solution two anodic current peaks appear: a weakly expressed one at E = +0.8 V and the main peak at E = +1.2 V. In the second scan only an extremely flat peak remains at +1.2 V.

After the first scan to +1.7 V the cathodic peak C2 remains, but it disappears after the second scan.

DISCUSSION

The differences between the three groups of curves result from the different sizes of ions in investigated solutions: the first group of curves is measured in the solutions, containing small cations and anions, the second group – relatively large cations (TBA^+ and TEA^+) and small anions; the third group – small cations and relatively large anions. As a rule, the redox transitions in conducting polymers are connected with the movement of the dopant anion [1, 2]. During the cathodic sweep the retaining of electroneutrality occurs by the removal of doping anions from the film and in the anodic sweep by their incorporation. If the movement of the dopant is hindered due to the steric effect the cations can be inserted to compensate the negative charge of the dopant. The differences in the shape of voltammograms can be explained by the different participation of electrolyte ions [12]. Obviously we can assume that in case of small dopant anions (such as chloride) they can move relative easily except a certain part whose release is hindered due to the

secondary and tertiary structure of the polymer. The last part of anions can be divided into blocked anions whose charge will be compensated by cation incorporation during the redox transition and into screened anions. The latter are fully isolated from the bulk electrolyte and the corresponding positively charged centers of polymer chains do not participate in the redox process. If the cations in the supporting electrolyte are relatively large (second group of solutions), they cannot incorporate, and in the redox transition the blocked anions do not participate. Thus, in the first group of solutions peak C1 can be interpreted as cation incorporation and A1 as their removal, peaks C2 and A2 correspond to anion mobility. The role of the cation participation is more important during the first scan. The changes in peak currents during the potential cycling indicate the diminishing role of the cation participation because cycling alters the structure of polymer frame [14] and a part of the blocked dopant can be released. This is in accordance with the change of Q_c in the potential region of peaks C1 and C2.

In the second group of solutions the participation of cations in the redox process is less probable; the corresponding current peaks at E_{C1} are absent. The peak currents increase during the cycling because the blocked dopant can be released. In the third group we can expect the exchange of the dopant during the cycling. The primary small dopant dissipates in solution and a relatively large electrolyte anion must be inserted in the anodic sweep. this process is sterically hindered (the ratio $Q_c/Q_a > 2$) and for this reason the differences between the first and second scan are remarkable. In this case the redox switching occurs mainly with the participation of cations except in the first cathodic sweep. Hence, Q_c is connected with the amount of blocked dopants. The different shapes of voltammograms obtained in NaDDS and Na_2EDTA solution can be explained with surfactant DDS^- anion adsorption on the film surface.

The linear relationship between the peak current and scan rate corresponds to the "surface wave" [13] indicating no diffusional limitation, i.e. the redox switching rate is determined by the rate of the reduction of the charge centers on polymer chains. The observed

relationship $i-v^{0.8}$ in alkaline TBABr solutions indicates the lowering of the diffusion rate and the overall kinetic is controlled by diffusion and the charge transfer.

The increase of t_H at the constant positive potential ($E_H > 0.4$ V) leads to the formation of a denser structure due to the slow geometrical relaxations of polymer chains [14] and as a result the redistribution of blocked and free dopant amounts and an increase of the role of cation insertion occur. The potential cycling between E = +0.4 V and E = -1.0 V induces an increase of anion mobility due to the releasing of a certain part of the blocked dopant. Whereas the redoping process (anion incorporation during the anodic sweep) is to some extent hindered – within the standard t_H = 30 sec at +0.4 V, the full amount of released anions is not able to insert – we detect a small decrease of Q_c in the first group of solutions. By the increasing of t_H this process will occur more completely (increasing of Q_c). The decreasing of Q_c and Q_a after a long-time polarization at E_H +0.7 V can be interpreted as the result of the decomposition of the primary structure of polymer chains which leads to irrersible changes in the electrochemical properties of polymer films [9, 15, 16]. The pH-effects can be interpreted ass a result of a nucleophilic attack of OH-ions on the pyrrole ring in alkaline solutions and as a result of a partial protonation of polymer in acidic media [17].

REFERENCES

1. **J. Heinze.** Topics in Curr. Chem., V. 152, 1, Springer-Verlag, Berlin 1990.
2. **G.B. Street.** In T.A. Skotheim (Ed.), Handbook of Conducting Polymers, V.1, Marcel Dekker, N.-Y. 1986, p. 265
3. **M. Salmon, A.F. Diaz, A.J. Logan, M. Krounbi, J. Bargon.** Mol. Cryst. Liq. Cryst., **83**, 265 (1982).
4. **R. Qian, J. Qiu.** Polym. J., **19** (1987) 1571.

5. **B. Tian, G. Zerbi.** J. Chem. Phys., **92** (1990) 3892.
6. **S. Skaarup, K. West, B. Zachau-Christiansen, T. Jacobsen.** Synth. Met., **51** (1992) 267.
7. **L.F. Warren, D.P. Anderson.** J. Electrochem. Soc., **134** (1987) 101.
8. **C. Odin, M. Nechtschein.** Synth. Met., **44** (1991) 177.
9. **F. Beck, M. Oberst.** Macromol. Chem. Macromol. Symp., **8** (1987) 97.
10. **A. Mohammaäi, O. Inganas, I. Lundström.** J. Electrochem. Soc., **133** (1986) 947.
11. **R.A. Bull, F.-R.F. Fan, A.J. Bard.** J. Electrochem. Soc., **129** (1982) 1008.
12. **R. Bilger, J. Heinze.** Synth. Met., **41-43** (1991) 2893.
13. **E. Laviron, L. Roullier.** J. Electroanal. Chem., **115** (1980) 65.
14. **J. Heinze, M. Störzbach, M. Mortensen.** Ber. Bunsenger Phys. Chem., **91** (1987) 960.
15. **A. Witkowski, M.S. Freund, A. Braster-Toth.** Anal. Chem., **63** (1991) 622.
16. **D. Belanger, I. Nadreau, G. Fortier.** J. Electroanal. Chem., **274** (1989) 143.
17. **Q. Pei, R, Qian.** Synth. Met., **45** (1991) 35.

ELECTRICAL DOUBLE LAYER ON THE SINGLE CRYSTAL ANTIMONY, BISMUTH AND CADMIUM ELECTRODES IN SURFACE INACTIVE ELECTROLYTE SOLUTIONS

E. Lust, A. Jänes, K. Lust, M. Salve
Institute of Physical Chemistry, University of Tartu

ABSTRACT

The electrical double layer on the single crystal Bi, Sb and Cd electrodes has been studied in the surface-inactive elecrolyte solutions. The values of the zero charge potential, capacities of inner layer and other fundamental electrochemical parameters have been established. The applicability of the Gouy - Chapman - Stern - Grahame theory has been tested by various methods.

INTRODUCTION

It is commonly accepted that the electrochemical properties of a solid metal surface significantly depend not only on the chemical composition but also on the crystallographic structure of the surface of a metal studied [1, 2]. In discussing the electrical double layer (edl) at metal single crystal electrodes in contact with an electrolyte solution, one has to go back as far as 1956–1957 when potentials of zero charge ($E_{\sigma=0}$) for low index planes of zinc were published [3, 4]. However, the importance of the physical state of the surface on the edl for solid electrodes was pointed out already in 1928 by Frumkin [5]. Owing to the dependence of the electronic work function on the orientation of the single crystal faces [6], a difference in their edl parameters would be expected. Nowadays the influence of the electrode surface structure on the edl properties at the metal/electrolyte interface has been proved experimentally on a notable number of s-p and s-d metals. However, for a complete understanding of the observed dependences there is still a lack of sufficient literature data about many metals, including antimony

and cadmium. Unlike bismuth, studies of the antimony edl have been performed mainly on polycrystalline electrodes [7–9], except our previous data [10].

Bismuth and antimony are electronanalogues, considered as semimetals which crystallize in the same rombohedral system and are characterized by the existence of two types of bonds (covalent – by s^2p^3 and metallic – by hybride sp^3d^2 orbitals) in the lattice [11]. In this case, the surface atoms of various single crystal planes have different types of binding orbitals and different numbers of unpaired electrons which causes the adsorption anisotrophy of solvent molecules, organic compounds and inorganic anions on the different single crystal Bi and Sb electrodes. The existence of two types of bonds between the atoms in the lattice causes considerable differences between the semimetallic properties of different single crystal planes of Bi and Sb electrodes, in which case the metallic side (electronic distribution in the interfacial region and its response to charging in interaction with all the other system components) of an interface may have an important effect, especially on the properties and structure of the inner part of edl.

Unlike the zinc single crystal electrodes [2, 12, 13] until now only a few studies have been devoted to the influence of the crystallopgraphic orientation on the edl and adsorption of ions and organic compounds on the Cd single crystal faces [14–17]. Zn and Cd are electronanalogues and they are crystallized in the same hexagonal close-packed system.

The present paper is devoted to a comprehensive study of the influence of the surface structure of Sb, Cd and Bi single crystal plane electrodes on the edl parameters in the aqueous surface-inactive electrolyte solutions.

PREPARATION OF SINGLE CRYSTAL FACE ELECTRODES AND SURFACE INACTIVE ELECTROLYTE SOLUTIONS

The electrodes were bismuth, antimony and cadmium single crystals, grown in the Institute of Problems of Microelectronics Technology and Superpure Materials, Russian Academy of Sciences by a modified Czochralski (Vertical Bridgman) method (Bi) [18, 19] or by the Horizontal Bridgman (zone refiring) method (Sb, Cd) [18–20]. The crystal growth and characterization techniques and other experimental problems have already been described in ref. [18–20].

The electrodes are discs of 3.60 ± 0.05 mm diameter and 4 mm

thickness which were prepared by cutting from the monocrystalline Bi, Sb and Cd, using the anodic dissolution method in aqueous KI + HCl (Bi, Sb) or in aqueous H_3PO_4 (Cd) solutions [10, 21–23]. The crystallographic orientation was determined by X-ray, using a special crystal holder and goniometric head. The crystal was cut along the chosen crystallographic orientation with the precision $\pm 0.3°$. The isolation of the faces was carried out by a thin polystyrene film (dissolved in toluene) covering the part of no interest, and then the sample was placed into a Teflon holder [2, 10, 12–14, 23, 24]. The surface was polished to a mirror finish by using standard metallographic procedures. The final surface preparation was obtained by alternative electrochemical polishing in the aqueous KI + HCl solutions (Bi, Sb) or in the aqueous H_3PO_4 solutions (Cd). Thereafter, the second X-ray diagram was done to determine the precise angle, and only the samples, whose precision on the orientation was better than $\pm 0.2°$, have been used for the electrochemical investigations. After the last stage of surface preparation, electrodes were very well rinsed with ultra purified water and cathodically polarized in the working solutions. The basal face (111) of Bi and Sb and the (0001) face of Cd were prepared by cleaving the single crystal at the temperature of liquid nitrogen.

The water for preparing solutions was purified by triple destillation (the quartz system was used at last once) and purified additionally by using the special method described in ref. [25]. Solutions were prepared volumetrically using either LiF, NaF, KF, $NaBF_4$, $LiClO_4$ or $NaClO_4$ purified by triple recrystallization from water followed by vacuum heating to dryness. NaF and KF were calcined at 700°C immediately prior to the measurements. The change in the $LiClO_4$ solution pH in the range 2.0–6.0 was effected by the addition of a calculated amount of $HClO_4$ solution prepared from triply destilled concentrated perchloric acid and the solution pH was controlled with the pH-meter. Electrolytic hydrogen has been previously bubbled for 1–2 h through the electrolyte in the cell and was bubbled for the whole time of the experiment. The temperature was kept at 293K and the reference electrode was an aqueous saturated calomel electrode.

PRECISION OF EXPERIMENTAL DATA

For the accurate determination of the precision of the experimental data the statistical treatment of the data for the aqueous surface inactive

electrolyte solutions for the single crystal Bi, Cd and Sb electrodes has been carried out. The experimental investigations were carried out for the different single crystal electrodes (with the some indexes) whose geometrical surface area was established by using optical methods with the accuracy better than ± 2 %. The total number of independent experiments was $n > 8$. Thereafter the mean values of differential capacity $\bar{C}$, charge density $\bar{\sigma}$, Helmholtz layer capacity $\bar{C}_H$ and their standard deviations S_x, standard error of the mean $S_{\bar{C}}$ ($C_{\bar{\sigma}}$) and coefficient of variation V at the fixed E=const (or at σ=const) and at the fixed c=const were calculated by using the HP 85 computer and the General Statistics Pac. The calculated $\bar{C}(E)$–, $\bar{C}(\sigma)$–, $\bar{C}_H(\sigma)$– and $\bar{C}^{-1}$ (C_D^{-1})– curves are shown in Fig. 1–10. Some statistical characteristics for the C(E)– curves for Bi(111) and Cd(0001) are given in Table 1.

As follows from the Table 1 and Fig. 1–4, in the case of the moderate surface inactive electrolyte solutions ($c_{NaF} > 0.03$ M) for the whole region of σ the experimental values of C can be established better than ± 2 %. But the precision of experimental C decreases as the concentration of the solution decreases, and for the dilute solutions ($c_{NaF} < 0.01$ M) the maximum values of error ($5 \div 8$ %) can be established in the region of σ where the derivation dC/dE is large. In the region of surface charge densities $\sigma < 0.5$ $\mu C \cdot cm^{-2}$, the error of C (2–4 %) is only somewhat higher than for the more concentrated solutions. Comparison of the statistically treated $\bar{C}(E)$– and $\bar{C}(\sigma)$–curves (Fig. 1 and 2) shows that the $\bar{C}(E)$– curves are more erratic than the $\bar{C}(\sigma)$– curves, calculated at σ = const. The main reason for this effect is the slight variation of $E_{\sigma=0}$ (± 5 mV) from one experiment to another.

The first group of reasons for the imprecisions are induced by the possible errors in the preparing of electrodes with the exact geometrical surface area (S_{el}). For example, if the surface area of the Bi(111) single crystal electrode changes from 0.0989 to 0.1046 cm^2 ($d_{el} = 0.360 \pm 0.005$ cm), calculated value of the capacity for the 0.005 M NaF solution decreases from 10.36 to 9.80 $\mu F \cdot cm^{-2}$.

As we can see from Fig. 1–4, the experimental values of $\bar{C}$ in the region of the diffuse minimum are constantly higher than the ones calculated by the Gouy – Chapman – Stern – Grahame (GCSG) theory.

Table 1

Statistical characteristics for the Bi and Cd electrodes in the 0.1 M NaF aqueous solution

Electrode	-E, V	$\bar{C} = \frac{1}{n}\sum_{i=1}^{n} C_i$	$S_x = \sqrt{\left(\sum_{i=1}^{n} C_i^2 - n\bar{C}^2\right) / (n-1)}$	$V = (S_x/\bar{C})100\%$	$C_{\pm}$, $\mu F \cdot cm^{-2}$
Bi(111)	1.60	18.58	0.189	1.02	18.42–18.73
	1.20	17.20	0.110	0.63	17.07–17.41
	1.00	17.83	0.142	0.80	17.71–17.95
	0.80	18.45	0.137	0.74	18.33–18.56
	0.65	18.90	0.100	0.58	18.81–18.99
	0.50	21.26	0.333	1.57	20.87–21.43
Cd(0001)	1.60	17.0	0.201	1.04	16.6–17.4
	1.20	23.5	0.198	1.03	23.1–23.9
	1.00	25.8	0.159	0.91	25.5–26.1
	0.96	27.0	0.156	0.89	26.7–27.3
	0.90	30.2	0.358	2.06	29.6–30.8

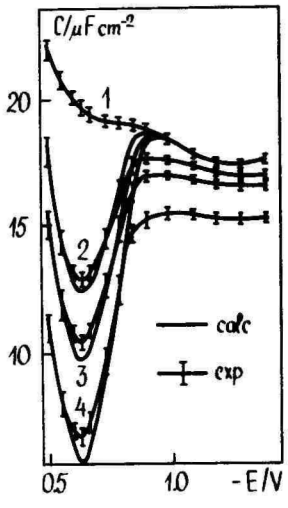

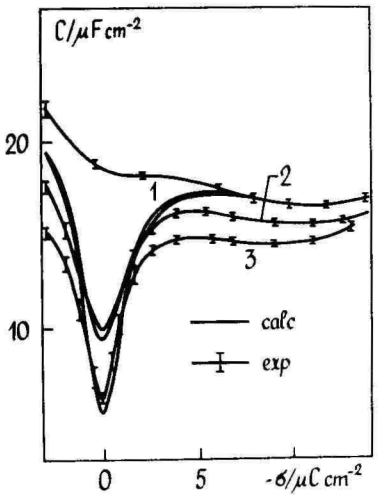

Fig. 1. C(E)- curves at ν = 210 Hz for Bi(111) in aqueous solutions of NaF, M: 1 - 0.1; 2 - 0.01; 3 - 0.005 and 4 - 0.001.

Fig. 2. C(σ)- curves at ν = 210 Hz for Bi(111) in aqueous solutions of NaF, M: 1 - 0.1; 2 - 0.01; 3 - 0.005 and 4 - 0.001.

Undoubtedly, however careful the surface preparation of the single crystal Bi, Sb and Cd electrodes was, they are not drawn flat to the atomic level, and so their "apparent" surface area S_{app}, measured by optical methods does not coincide with the "true" one S_{real} i.c. $S_{app} < S_{real}$. The geometrical roughness entails a crystallographic (energetic) inhomogeneity of single crystal surfaces which at the same time is due to the difference between the properties of the individual faces of the same metal. As shown in [2, 10–17, 21–27] at the potential of the diffuse minimum, the differential capacity of a polycrystalline electrode (for the real moncrystalline electrode with surface defects) in the dilute solutions is greater than on the perfect single crystal faces at $E_{\sigma=0}$.

The other group of reasons for the imprecisions in the measurements are induced by the possible errors in the preparing of solutions with the exact concentration, by the incomplete dissociation of an electrolyte and by the very slight specific adsorption of ions. For example, in the case of Bi(111) at σ=0, the calculated value of C increases from 10.10 to 10.40 $\mu F \cdot cm^{-2}$ when the concentration c_{NaF}

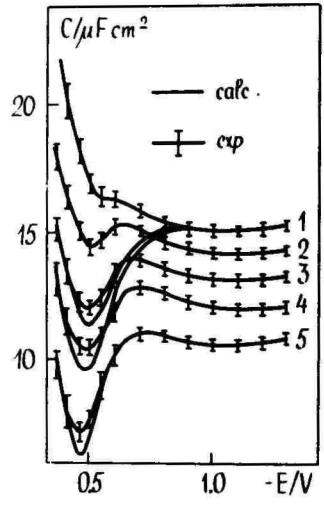

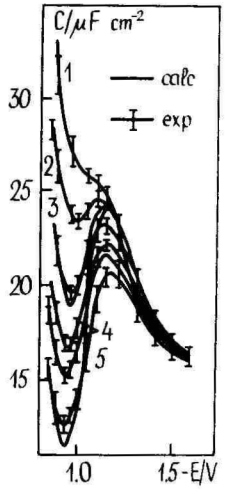

Fig. 3. C(E)- curves at ν = 2100 Hz for Sb(111) in aqueous solutions of NaF, M: 1 - 0.1; 2 - 0.03; 3 - 0.01; 4 - 0.0055 and 5 - 0.0005.

Fig. 4. C(E)- curves at ν = 210 Hz for Cd(0001) in aqueous solutions of NaF, M: 1 - 0.1; 2 - 0.05; 3 - 0.02; 4 - 0.01; 5 - 0.07 and 6 - 0.0045.

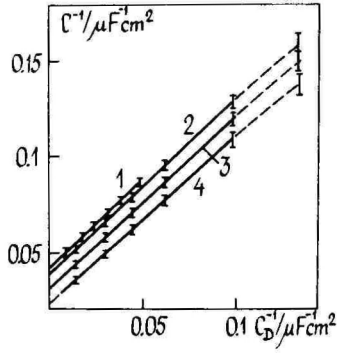

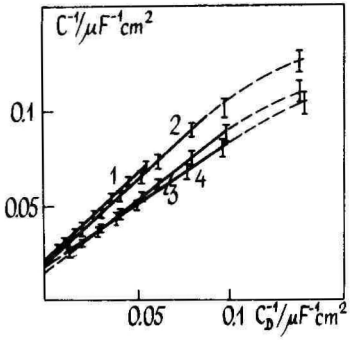

Fig. 5. The Parsons-Zobel plots at σ = -2 μC·cm^{-2} (1) and σ = 0 (2-4) for single crystal planes of Bi: 1; 2 - (001); 3 - (01$\bar{1}$), 4 - (111).

Fig. 6. The Parsons-Zobel plots at σ = -2 μC·cm^{-2} (1) and σ = 0 (2-4) for the single crystal planes of Sb: 1; 2 - (001); 3 - (111) and 4 - (2$\bar{1}\bar{1}$).

Table 2

The edl parameters on the single crystal planes of Bi, Sb and Cd

Electrode	$-E_{min}$, V 0.005 M NaF	$-E_{\sigma=0}$, V	f_{P-Z}	$C_H^{\sigma=0}$ $\mu F \cdot cm^{-2}$	$\delta E_{min}/\delta lgc$, $mV \cdot M^{-1}$
Bi(111)	0.650±0.005	0.650±0.005	1.04±0.02	25.6±0.2	50
Bi($\bar{1}0\bar{1}$)	0.575±0.010	0.575±0.010	1.07±0.03	25.7±0.3	15
Bi(001)	0.595±0.005	0.585±0.005	1.06±0.02	28.3±0.2	20
Bi($01\bar{1}$)	0.595±0.010	0.590±0.010	1.05±0.03	27.0±0.2	15
Bi($2\bar{1}\bar{1}$)	0.585±0.010	0.575±0.010	1.14±0.03	26.8±0.3	20
Sb(111)	0.450±0.005	0.450±0.005	1.06±0.02	23.0±0.4	10
Sb(001)	0.370±0.005	0.360±0.005	1.04±0.02	26.2±0.5	20
Sb($01\bar{1}$)	0.390±0.010	0.380±0.010	1.18±0.05	25.9±0.9	30
Sb($2\bar{1}\bar{1}$)	0.350±0.020	0.330±0.020	1.25±0.07	25.0±1.0	50
Cd(0001)	0.97±0.01	0.950±0.01	1.09±0.03	38.0±1.5	20
Cd($01\bar{1}0$)	1.01±0.01	1.00±0.01	1.12±0.05	47.6±1.8	10
Cd($21\bar{1}0$)	1.02±0.01	1.01±0.01	1.20±0.07	48.6±1.4	10

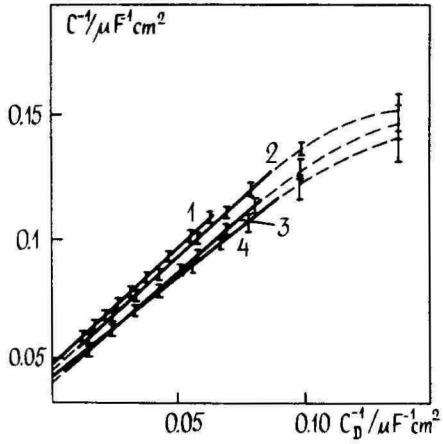

Fig. 7. The Parsons-Zobel plots at $\sigma = -2\ \mu C \cdot cm^{-2}$ (1) and $\sigma = 0$ (2–4) for the single crystal planes of Cd: 1; 2 – $(01\bar{1}0)$; 3 – (0001) and 4 – $(21\bar{1}0)$.

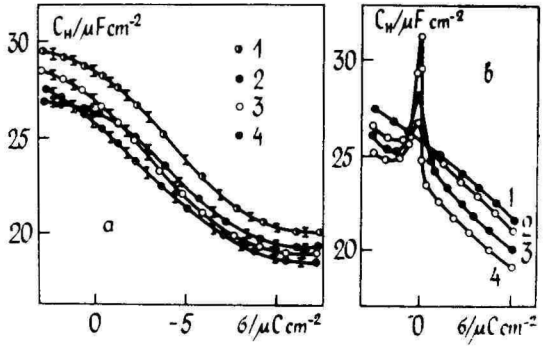

Fig. 8. $C_H(\sigma)$– curves in the 0.1 M in aqueous solutions of NaF for the 1 – (001); 2 – $(\bar{1}0\bar{1})$; 3 – $(01\bar{1})$ and 4 – (111) single crystal planes of Bi (a).

$C_H(\sigma)$– curves for Bi(111) in the aqueous solutions of NaF, M: 1 – 0.1; 2 – 0.01; 3 – 0.02; 4 – 0.005 and 5 – 0.001 (b).

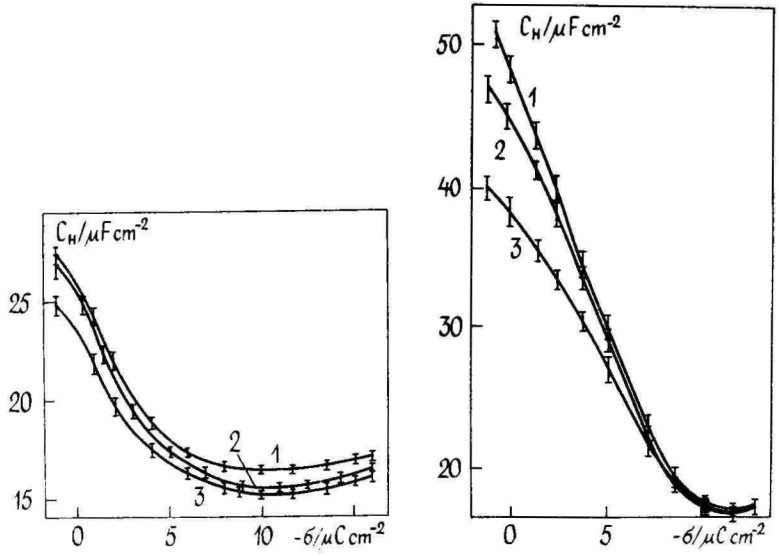

Fig. 9. $C_H(\sigma)$– curves in the 0.1 M aqueous solutions of NaF for 1 – (001); 2 – $(2\bar{1}\bar{1})$ and 3 – (111) single crystal planes of Sb

Fig. 10. $C_H(\sigma)$– curves in the 0.1 M aqueous solutions of NaF for 1 – $(01\bar{1}0)$; 2 – $(2\bar{1}\bar{1}0)$ and 3 – (0001) single crystal planes of Cd.

changes from 0.00475 to 0.00525 M. The comparison of the experimental data for the NaF, $NaBF_4$ and $LiClO_4$ solutions shows (Fig. 11) that the weak adsorption of anions (BF_4^-, ClO_4^-) causes a considerable discrepancy between the experimental capacity curves in the region of E_{min}. For example, the values of C are 0.2 ÷ 0.3 $\mu F \cdot cm^{-2}$ higher for the 0.005 M $LiClO_4$ solution than for the 0.005 M NaF solution, and with the decreasing of the concentration of the solution the observed differences are increased. But a small experimental error in C ($\Delta C = \pm 0.15$ $\mu F \cdot cm^{-2}$) would entail a large imprecision in C_H ($\Delta C_H = \pm 1.3$ $\mu F \cdot cm^{-2}$) and with the decreasing of the concentration of the solution the error in the determination of C_H increased. For example, if $c_{NaF} = 0.001$ M and $\Delta C = \pm 0.2$ $\mu F \cdot cm^{-2}$, $\Delta C_H = \pm 5$ $\mu F \cdot cm^{-2}$. At higher charge densities ($\sigma < -3$ $\mu C \cdot cm^{-2}$) the same

experimental error on C does not entail a noticeable imprecision on C_H (if $\Delta C = \pm 0.15\,\mu F \cdot cm^{-2}$, $\Delta C_H = \pm 0.20\,\mu F \cdot cm^{-2}$). These conclusions are in a good agreement with our experimental results (Fig. 1–3, 8–10) and with the mathematical remarks of works [26, 27] and the analysis of the mercury data [26–28].

Consequently, these experimental errors cannot be interpreted unambigously, inasmuch as the following different reasons for the deviations of the experimenta values of C from the theoretical ones have been proposed: the geometrical roughness or crystallographic (energetic) heterogeneity of electrodes, the sligh specific adsorption of an electrolyte, the contribution of which difficult to estimate.

The above-mentioned imprecisions in the experimental measurements are the most important origin of the deviation of experimental capacity curves from the ones calculated by the GCSG – theory (Fig. 1–4) if we accept that there is no error in the diffuse layer theory. These imprecisions and their mathematical consequences [10, 26–29] explain the irregularities observed on the $\bar{C}_H(\sigma)$– curves at low charge densities (Fig. 8–10), and on the $\bar{C}^{-1}$ (C_D^{-1})– curves at low electrolyte concentrations (Fig. 5–7).

ELECTRICAL DOUBLE LAYER IN THE AQUEOUS NaF AND KF SOLUTION

The edl differential admittance was measured in the ac frequency υ interval from 110 to 11000 Hz. As for the PC-Bi [30] and PC-Cd [7–9], a slight variation (3 ÷ 8 %) as a function of frequency υ, in the 0.1 M NaF, KF, $LiClO_4$ and $NaBF_4$ solutions, allows the measured admittance at the first approximation to be identified with the differential capacitance C (Fig. 12–13). As for the PC-Sb in aqueous and ethanolic solutions [7–9], the differential capacity dispersion for the single crystal Sb electrodes over the whole potential E range is 8–12 %, with the a.c. frequency varying from 710 to 5100 Hz. At $\upsilon < 710$ Hz, in the region of $-0.75 < E < -0.55$ V, the maximum of pseudocapacity on the C(E)– curves has been observed. The height of this maximum decreases as ν increases and at $\upsilon > 710$ Hz this maximum has not been observed (Fig. 13).

As can be seen from Fig. 1–4, 12, 13, the influence of the diffuse

layer on the total capacity of the edl is visible for concentrations

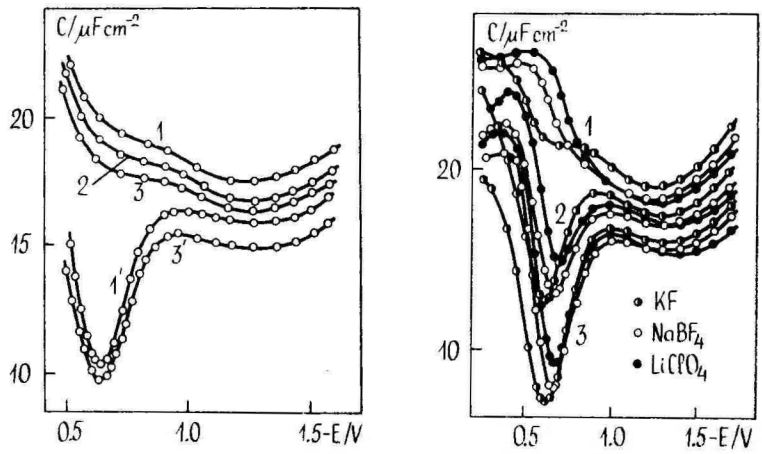

Fig. 11. C(E)- curves for Bi(001) in the 0.1 M - (1); 0.01 M - (2) and 0.001 M - (3) NaF, $NaBF_4$ and $LiClO_4$ aqueous solutions.

Fig. 12. C(E)- curves for Bi(111) in the 0.1 M (1-3) and in the 0.005 M (1'-3') aqueous solution of NaF at ϑ, Hz: 1; 1' - 210; 2; 2' - 1100; and 3; 3' - 11000.

$c_{NaF} < 0.05$ M for the Bi and Sb electrodes, and for $c_{NaF} < 0.1$ M for Cd single crystal plane electrodes. The potential of the diffuse layer capacity minimum E_{min} for the single crystal Bi(111) and Sb(111) electrodes is independent of c_{NaF} with a relative accuracy of ± 5 mV, when c_{NaF} changes from $1 \cdot 10^{-3}$ to $2 \cdot 10^{-2}$ M. As for the PC-Bi, PC-Sb and PC-Cd [7-9, 21, 30, 31], it may be assumed that no significant specific adsorption of F^- occurs at E_{min} and the value of E_{min} may be identified with $E_{\sigma=0}$ for the single crystal Bi(111) and Sb(111) electrodes. The C(E)- curves for the Bi($\bar{1}0\bar{1}$), Bi($01\bar{1}$), Bi(001), Bi($2\bar{1}\bar{1}$), Sb(001), Sb($01\bar{1}$), Cd(0001), Cd($01\bar{1}0$) and Cd($11\bar{2}0$) show a slight concentration dependence on the E_{min} values at $c_{F^-} > 0.002$ M. This suggests that a very slight specific adsorption of F^- ions occurs at the potential of zero charge, and the values of $E_{\sigma=0}$ given in Table 2 have been obtained by the extrapolation of the dependence E_{min} on the $\sqrt{c} = 0$. The values of $E_{\sigma=0}$ for the single crystal electrodes in the NaF solutions are in good agreement with the values given in ref. [24, 25]

for the KF solutions and the value of $E_{\sigma=0}$ for the Cd(11$\bar{2}$0) plane is in agreement with the one given in ref [14]: -0.99 V. According to the experimental results (Table 2) for the single crystal planes (001), ($\bar{1}0\bar{1}$), (01$\bar{1}$) and (2$\bar{1}\bar{1}$) of bismuth in the aqueous NaF solutions, the differences between the values of the zero charge potential $E_{\sigma=0}$ do not exceed 20 mV, but the value of $E_{\sigma=0}$ for plane (111) is approximately 60 mV higher than the $E_{\sigma=0}$ of other planes. The same tendency is valid for the (11$\bar{1}$), (001), (2$\bar{1}\bar{1}$) and (01$\bar{1}$) planes of Sb, where $\Delta E_{\sigma=0}$ for the (001), (2$\bar{1}\bar{1}$) and (01$\bar{1}$) planes does not exceed 50 mV, but the value of $E_{\sigma=0}$ for the Sb(111) is approximately 70 mV higher than the $E_{\sigma=0}$ of other planes. In our opinion this is mainly caused by the specific surface state of the bismuth and antimony atoms of face (111) in the lattice. The surface atoms of planes (001), ($\bar{1}0\bar{1}$), (01$\bar{1}$) and (2$\bar{1}\bar{1}$) contain partially filled orbitals s^2p^3 with unpaired bonding electrons [11]. The surface atoms of plane (111) have only partially filled hybrid sp^3d^2 orbitals [11] which from stronger bonds with water molecules than it takes place in the case of other single crystal planes of Bi and Sb [32,33].

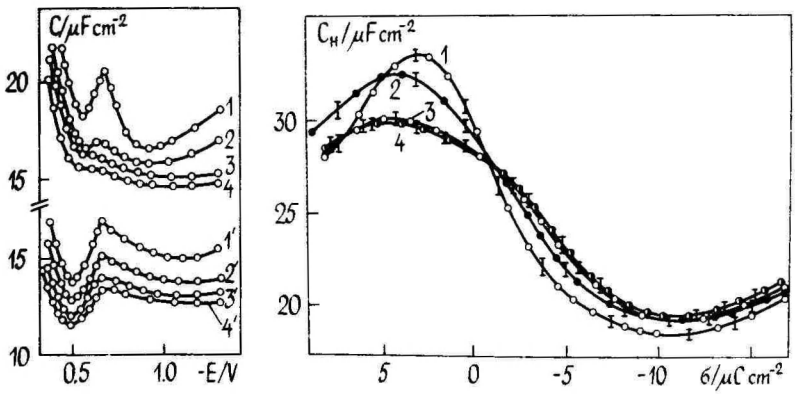

Fig. 13. C(E)- curves for Sb(111) in the 0.1 M (1-4) and in the 0.01 M (1'-4') aqueous solution of NaF at ω, Hz: 1; 1' - 110; 2; 2' - 510; 3; 3' - 2100 and 4; 4' - 5100.

Fig. 14. $C_H(\sigma)$- curves for Bi(111) in the 0.1 M aqueous solutions of 1 - $LiClO_4$; 2 - $NaBF_4$; 3 - NaF and 4 - KF.

At the same electron configuration (s^2p^3), the dependence of the $E_{\sigma=0}$ values on the reticular density of atoms D is rather weak and we can see only a slight correlation between $E_{\sigma=0}$ and D. The difference of the zero charge values $\Delta E_{\sigma=0} > 90$ mV for the (001) and (111)

single crystal planes of Sb are somewhat higher than for the (001) and (111) planes of Bi ($\Delta E_{\sigma=0} > 70$ mV). For the (0001) and (1120) faces of Cd the $\Delta E_{\sigma=0} > 40$ mV is somewhat lower than for the (0001) and (1120) of zinc ($\Delta E_{\sigma=0} > 110$ mV) [12, 17].

ELECTRICAL DOUBLE LAYER IN THE AQUEOUS $NaBF_4$ AND $LiClO_4$ SOLUTION

The investigation of the adsorption behaviour of BF_4^- and ClO_4^- ions have been carried out with the purpose of throwing some more light on the structure of the inner layer. The BF_4^- and ClO_4^- anions are large, compact, symmetrical ions whose solvation in aqueous solution is negligible [34, 35] and whose ion – solvent interactions are quite similar [34–36].

The experimental investigations into aqueous solutions of ions, which exert a "structure-breaking" effect of water e.g. BF_4^-, ClO_4^- show some peculiarities in the curves in $NaBF_4$ and $LiClO_4$, compared to those in NaF solutions (Fig. 11, 14 and Table 3):

1) a moderate shift of E_{min} to more negative potentials with an increasing concentration of salt and the dependence of E_{min} on the concentrtion of salt (Esin-Markov effect);

2) higher values of the capacity at E_{min} and the disappearance of diffuseness in 0.05 M solutions;

3) higher values of the reciprocal slope of the Parsons and Zobel plots for the $NaBF_4$ and $LiClO_4$ solutions than for the NaF solutions.

On the basis of these peculiarities the conclusion may be drawn that there is a weak adsorption of anions which increases in the sequence of ions $F^- < BF_4^- < ClO_4^-$ and electrodes Cd(0001) < Bi(111) < Cd(11$\bar{2}$0) < Cd(01$\bar{1}$0) < Bi($\bar{1}$0$\bar{1}$) < Bi(01$\bar{1}$) < Bi(001) < Bi(2$\bar{1}\bar{1}$). The same order of the adsorption activity of anions is given on mercury [34–36] and on the Ag(111), Ag(001), Au(001), Au(111) and Au(210) electrodes [2, 37–40].

As we can see from Table 3, the values of the Esin-Markov coefficient $|\delta E_{min}/\delta \ln c| < 58$ mV and, accordingly the discreteness of the distribution of specifically adsorbed ClO_4^- and BF_4^- anions may be ruled out in the region of $\sigma \sim 0$. Therefore it seems that the "squeezing out" effect of the solvent has a major effect on the

Table 3

The edl parameters in $NaBF_4$ and $LiCl)_4$ aqueous solutions

Electrolyte	Electrode	$-E_{\sigma=0}$, V	f_{P-Z}	$C_H^{\sigma=0}$ $\mu F \cdot cm^{-2}$	$\delta E_{min}/\delta lgc$, (mV/M^{-1})
$NaBF_4$	Bi(111)	0.665±0.01	1.12±0.02	26.6±0.3	15
	Bi($\bar{1}0\bar{1}$)	0.630±0.01	1.17±0.30	27.1±0.4	20
	Bi(001)	0.640±0.01	1.19±0.03	28.9±0.3	25
	Bi(01$\bar{1}$)	0.650±0.01	1.15±0.02	28.0±0.4	20
	Bi(2$\bar{1}\bar{1}$)	0.625±0.015	1.21±0.04	27.7±0.3	30
$LiClO_4$	Bi(111)	0.700±0.010	1.19±0.03	27.2±0.3	25
	Bi($\bar{1}0\bar{1}$)	0.650±0.015	1.23±0.03	25.5±0.4	30
	Bi(001)	0.655±0.010	1.24±0.03	29.5±0.3	35
	Bi(01$\bar{1}$)	0.670±0.015	1.24±0.03	28.6±0.4	35
	Bi(2$\bar{1}\bar{1}$)	0.650±0.015	1.26±0.04	28.0±0.4	40
	Sb(111)	0.490±0.015	1.22±0.04	25.1±0.7	20
	Cd(0001)	1.00±0.01	1.14±0.04	45.2±1.5	15
	Cd(01$\bar{1}$0)	1.04±0.01	1.17±0.05	52.2±1.7	20
	Cd(11$\bar{2}$0)	1.04±0.01	1.22±0.05	48.5±1.6	20

adsorption energy of ClO_4^- and BF_4^-, the adsorption being stronger the less tense the water in the double layer or the lower the chemisorption energy of the face. In ref. [16, 23, 24, 32] the following order for the water adsorption on the different crystal faces of Cd and Bi was assumed: (0001) > (1120) >(0110) > (111) > (101) > (001) > (011) > (211). This sequence is in a good agreement with the one established for the BF_4^- and ClO_4^- anions in this work, and for the Cl^-, Br^-, I^- and SCN^- anions in ref. [41].

The lower values of the Esin-Markov coefficient $|\delta E_{min}/\delta \ln c|$ in the case of the ClO_4^- and BF_4^- anion adsorption may be drawn that these anions are separed from the metal surface by the first layer of adsorbed H_2O molecules.

An additional argument for the weak specific adsorption of the ClO_4^- and BF_4^- ions might be the higher values of the reciprocal slops of the Parsons-Zobel plots f_{P-Z} in $LiClO_4$ and $NaBF_4$ solutions, compared to those in NaF solutions. As already shown in ref. [34–38, 42], the linear dependences of C^{-1} vs $(C_D)^{-1}$ at σ=const in the case of weak specific adsorption may be interpreted by the equation

$$C^{-1} = (C_H)^{-1} + (C_D)^{-1}(1 + \delta\sigma^1/\delta\sigma), \qquad (1)$$

where σ^1 is the charge of the specifically adsorbed ions. Accordingly, the higher values of f_{P-Z} at $\sigma > 0$ for the $LiClO_4$ and $NaBF_4$ than for the NaF solutions appear to be true to the effect of the specifically adsorbed charge on the diffuse layer capacity. But differently from the NaF solutions where the values of f_{P-Z} decreased by increasing the surface charge densities σ (the influence of crystallographic inhomogeneity of the surface on the double layer structure diminishes [23, 24, 29], the corresponding values of f_{P-Z} for the $NaBF_4$ solution increased with the increasing of positive values of σ, and this is some definite evidence for the presence of the weak specific adsorption of the ClO_4^- and BF_4^- ions on the surface of the single crystal Bi electrodes.

THE APPLICABILITY OF THE GOUY - CHAPMAN - STERN - GRAHAME THEORY

The applicability of the Gouy – Chapman – Stern – Grahame (GCSG) theory has been tested by various methods. The so called

theoretical differential capacity potential $\bar{C}(E)$–; the capacity charge density $\bar{C}(\sigma)$– curves and the Parsons-Zobel plots (the $C^{-1}(C_D^{-1})$– curves where C_D is the diffuse layes capacity, obtained by the Gouy - Chapman theory) were calculated for the Bi, Sb and Cd single crystal electrodes. According to the Fig. 5–7 the Parsons-Zobel plots for the Bi, Cd and Sb single crystal electrodes in the aqueous NaF solutions can be considered linear when c_{NaF} decreases from 0.1 to 0.001M. The values for the fitting (roughness) coefficient f_{P-Z} estimated from the inverse slope of these dependences, reflecting surface geometrical roughness and crystallographic heterogenity and as shown before, the accuracy of the determination of the surface area and solution concentration, are given in Table 2. In the absence of the last two components of the mistakes, the fitting coefficient f_{P-Z} would correspond to R·f, where f represents the crystalline heterogenity and R the geometrical roughness of the surface, accordingly. As shown theoretically in [1, 2, 26] and proposed from the experiments in [43, 44], for model polycrystalline twoplane electrodes, the coefficient f_{P-Z} depends on the differencies of the zero charge potential $\Delta E_{\sigma=0}$ of the individual planes and on the electrolyte concentration c. The values of f_{P-Z} increases as $\Delta E_{\sigma=0}$ increases and c_{NaF} decreases.

According to the data of Table 2, for the singular low-index Bi(111), Bi(001), Bi($\bar{1}0\bar{1}$) Bi(01$\bar{1}$) Sb(111), Sb(001), Cd(0001) and Cd(01$\bar{1}$0) single crystal electrodes $f_{P-Z} < 1.12$, which is an indication of a high degree of homogeneity of the surface of the electrodes studied. The higher values of f_{P-Z} for the high-index (stepped) Bi(2$\bar{1}\bar{1}$) Sb(2$\bar{1}\bar{1}$) and Cd(2$\bar{1}$0) planes can mainly be explained by the microscopic (geometrical) roughness and the energetic inhomogenity of these electrodes.

It is seen in Fig. 5–7 that $C^{-1}(C_D^{-1})$– plots at lower c_{NaF} become nonlinear for all systems studied. As shown before by the error analysis the small experimental error in C would entail a large imprecision in C_H or C_D and, consequently, the determination of f_{P-Z} at $c_{NaF} < 10^{-3}$ M is ruled out for single crystal plane electrodes.

The inner layer capacity charge density $C_H(\sigma)$– curves were calculated according to the Grahame model (concerning existance of the compact layer with concentration – independent properties) and by the Valette – Hamelin method [26] from the well-known equation applicable to the edl model in the absence of specific adsorption of ions [28]

$$\frac{1}{C} = \frac{1}{FC_H} + \frac{1}{FC_D}, \qquad (2)$$

where F is the fitting coefficient. The monotonic $C_H(\sigma)$- curves were obtained for the values of the fitting coefficient F, which were varied from 1.05 to 1.25 for Bi, from 1.07 to 1.30 for Sb and from 1.10 to 1.30 for Cd, when the c_{NaF} decreases from $5 \cdot 10^{-1}$ to $1 \cdot 10^{-3}$ M. As shown before, the inner layer capacity, as well as the fitting coefficient, reflecting surface geometrical roughness and crystallographic heterogenity, the accuracy of the determination of the "true" surface area and the solution concentration is a very sensitive parameter and at low charge densities ($\sigma < 3\ \mu C \cdot cm^{-2}$) and electrolyte concentrations ($c < 10^{-2}$ M) a small experimental error in C would entail a larger imprecision on C_H or F. Accordingly, the higher values of F (or C_H) observed for our lowest concentrations ($c < 0.03$ M) at low charge densities, would have their origin mostly in the mathematical form of relation [2] (i.e. experimental errors in C) and the higher experimental values of F (or C_H) observed for Bi, Sb and Cd faces, however do not correspond only to the roughness of the electrode surface. As for mercury, only the results for $c > 0.05$ M should be used to determine C_H at low charge densities. The established values of C_H for 0.1M NaF, $LiCl_4$ and $NaBF_4$ aqueous solutions, corrected by the fitting (roughness) coefficient are presented in Table 2 and 3. The corresponding values of F vary from 1.05 to 1.09 for Bi, from 1.07 to 1.12 for Sb and from 1.08 to 1.13 for Cd, when c_{NaF} decreases from $5 \cdot 10^{-1}$ to $5 \cdot 10^{-2}$ M.

Recently various theoretical correction to the Gouy-Chapman expression for the diffuse layer capacity have been proposed mainly near $E_{\sigma=0}$, which appeared to be quite appreciable even at rather low concentrations. These estimates resulted in a suspicion that the method used by Grahame for the GCSG theory examination was not sensitive enough. Moreover, as a result of the $C_H(\sigma)$- curves for various NaF concentrations with the use of Grahame's experimental data [28], an obvious concentration dependence of the curve was found near $E_{\sigma=0}$ [27, 45–47]. This variation was attributed to the violation of the Gouy-Chapman theory for the diffuse layer properties. But as shown before, as an error of ± 2 % on the experimental values of C presented itself, it is not possible to establish the values of C_H with needful accuracy and, accordingly, the experimental verification of the corresponding model theories for edl must be ruled out. Therefore, more distinct

criteria must be elaborated and more sensitive and precise experimental methods for the development of the modern theories of a very complicated phase boundary solid electrode/electrolyte solution must be used.

For the higher charge densities ($|\sigma| > 3\ \mu C \cdot cm^{-2}$, for instance) imprecision on C does not show on C_H, because C_D is large. This is a direct consequence of the hyperbolic form of the relation (2). As it was found, the structure the Bi, Sb and Cd monocrystalline electrodes in the solutions of indifferent electrolyte at the first approximation can be described by the GCSG theory i.e. by the superposition of the inner and diffuse layer contributions, connected in series. But as for the PC-Bi [24, 30], PC-Cd [14, 21] and Hg [27, 28], a noticeable concentration dependence on C_H (Fig. 8–10) was observed for the single crystal plane Bi, Sb and Cd electrodes at $|\sigma| > 3\ \mu C \cdot cm^{-2}$. This effect was typically interpreted as a result of nonuniform electrode polarisation or analogous reasons. On the basis of the experimental results (Fig. 1–4 and 8–10), the concentration dependence of C (or C_H) increases in the sequence of electrodes Cd(0001) < Cd(11$\bar{2}$0) < Cd(01$\bar{1}$0) < Hg < Bi(111) < Bi(001) < Bi(01$\bar{1}$) < Bi($\bar{1}$0$\bar{1}$) < Sb(111) < Sb(001) < Sb(01$\bar{1}$), as the metallic nature of the electrodes decreases. In our opinion, these deviations from the GCSG theory, observed far from $E_{\sigma=0}$, must be connected with some secondary processes on the compact layer properties, in view of the expected smallness of the diffuse layer contribution. The retarded relaxation of the compact layer as a reason of this deviation from the theoretical predictions, as well as some variation of solvent dielectric properities under the influence of the electrode field may be suggested [45–47].

As shown in Tables 2 and 3 the values of the inner layer capacity for the (111), (001) and (01$\bar{1}$) planes of Sb are somewhat lower than for the corresponding planes of Bi, which can be explained by the weakes hydrophility of Sb electrodes of by the higher contribution of the metal phase to the differential capacity of Sb single crystal plane / surface inactive electrolyte than to the Bi / electrolyte interface [7–10, 33]. Judging from the higher values of C_H for the Cd electrodes than for the Hg and Bi single crystal planes, it appears, that the hydrophility of Cd is somewhat higher than of Bi or Hg. As follows from the experimental data (Fig. 8–10 and Table 2 and 3), for the single crystal planes (001), (01$\bar{1}$) and (2$\bar{1}\bar{1}$) of Bi and Sb and for (0001) and (01$\bar{1}$0) planes of Cd (unlike from Sb(111), Bi(111) and Cd(21$\bar{1}$0)) in all region of σ, the most compact principal plane has the smallest and the most open plane has the

largest interfacial capacity. These conclusions are in good agreement with the theoretical calculations [48] where the metal is represented as a "jellium" (with a pseudopotential lattice) and the electrolyte solution as an ensemble of hard sphere ions and dipoles.

REFERENCES

1. **A.N. Frumkin.** Potentsialy nulevogo zaryada. Moskva: Nauka, 1979. P. 115.
2. **A. Hamelin, T. Vitanov, E. Sevastyanov, A. Popov.** J. Electroanal. Chem., 145 (1983) 225.
3. **H.L. Heifetz, B.S. Krasikov.** Dokl. Akad. Nauk SSSR, 109 (1956) 586.
4. **B. Krasikov, V. Sisoeva.** Dokl. Akad. Nauk SSSR, 114 (1957) 825.
5. **A.N. Frumkin.** Eng. Exacten Naturwiss., 7 (1928) 270.
6. **R.P. Johnson, W. Shockley.** Phys. Rev., 49 (1936) 436.
7. **M.E. Haga, V.E. Past.** Elektrokhimiya, 5 (1969) 618.
8. **R.J. Pullerits, M.E. Moldau, V.E. Past.** Double Layer and Adsorption at Solid Electrodes. IV. Tartu Univ., 1975 P. 257.
9. **V. Past, R. Pullerits, M. Moldau.** Trans. Tartu State Univ., 757 (1986) 140.
10. **E.J. Lust, A.A.-J. Jänes.** Elektrokhimiya, 28 (1992) 803.
11. **W.B. Pearson.** The Crystal Chemistry and Physics of Metals and Alloys. Wiley-Intersience, 1972. P. 280.
12. **V.V. Batrakov, B.B. Damaskin, Yu.P. Ipatov.** Electrokhimiya, 10 (1974) 144.
13. **V.V. Batrakov, B.B. Damaskin.** J. Electroanal. Chem., 65 (1975) 361.
14. **A. Korotkov, E. Bezlepkina, B. Damaskin, E. Golov.** Elektrokhimiya, 22 (1985) 1298.
15. **R. Naneva, V. Boston, A. Popov, T. Vitanov.** J. Electroanal. Chem., 274 (1989) 179.
16. **E. Lust, J. Ehrlich.** Double Layer and Adsorption at Solid Electrodes. IX. Tartu Univ., 1991. P. 112.
17. **R. Naneva, T. Vitanov, N. Dimitrov, V. Bostanov, A. Popov.** J. Electroanal. Chem., 328 (1992) 287.
18. **W.D. Lawson, S. Nielsen.** Preparation of Single Crystals. London: Butterworths, 1958.
19. **V.N. Vigdorovich, G.A. Uhlinov, V.V. Marychev.** Trans. Moskow. Institute of Problems of Microelectronics Thecnology, 8 (1972) 68.
20. **A. Chernov, E. Guvargizov, H. Bagdasarov.** Modern Crystallography. Crystal Growth. Moscow Science Ed., 1980. Vol. III.
21. **D.Y. Leikis, V.A. Panin, K.V. Rybalka.** J. Electroanal. Chem., 40 (1972) 9.

22. **E.C.W. Parryman.** Metal Ind., 79 (1951) 23.
23. **E.J. Lust, U.V. Palm.** Elektrokhimiya, 21 (1985) 1256.
24. **U.V. Palm, M.P. Pärnoya, M.A. Salve.** Elektrokhimiya, 13 (1977) 1073.
25. **N.P. Berezina, N.V. Nikolayeva-Fedorovich.** Elektrokhimiya, 3 (1967) 3.
26. **G. Valette, A. Hamelin.** J. Electroanal. Chem., 45 (1973) 301.
27. **A. Hamelin, L. Stoicoviciu.** J. Electroanal. Chem., 271 (1989) 15.
28. **D.C. Grahame.** J. Am. Chem. Soc., 76 (1954) 4819; 79 (1957) 2093.
29. **E.J. Lust, A.A.-J. Jänes, K.K. Lust.** Elektrokhimiya, 26 (1990) 1627.
30. **M. Salve, U. Palm.** Trans. Tartu State Univ., 332 (1974) 71.
31. **U. Palm.** Trans. Tartu State Univ., 757 (1986) 3.
32. **E.J. Lust, U.V. Palm.** Elektrokhimiya, 21 (1985) 1381; 22 (1986) 407; 22 (1986) 696.
33. **A. Jänes, E. Lust, R. Pullerits.** Double Layer and Adsorption at Solid Electrodes. IX. Tartu Univ., 1991. P. 53.
34. **D.J. Schiffrin.** Trans. Faraday Soc., 67 (1971) 3318.
35. **S. Trasatti.** J. Chem. Phys., 5 (1975) 561.
36. **A. de Battisti, S. Trasatti.** J. Electroanal. Chem., 59 (1975) 137.
37. **G. Valette.** J. Electroanal. Chem., 122 (1981) 285.
38. **G. Valette.** J. Electroanal. Chem., 224 (1987) 285.
39. **A. Hamelin, Z. Borkowska, J. Stafiej.** J. Electroanal. Chem., 189 (1985) 85.
40. **A. Hamelin, L. Stoicoviciu.** J. Electroanal. Chem., 236 (1987) 267.
41. **K. Lust, M. Salve, E. Lust.** Double Layer and Adsorption at Solid Electrodes. IX. Tartu Univ., 1991. P. 116.
42. **B.B. Damaskin.** J. Electroanal. Chem., 1975. 65. 799.
43. **E.J. Lust, U.V. Palm.** Elektrokhimiya, 22 (1986) 565; 24 (1988) 557.
44. **E.J. Lust, M.A. Salve, U.V. Palm.** Elektrokhimiya, 23 (1987) 561.
45. **M.J. Sparnaay.** Rec. Trac. Chim., 77 (1958) 872.
46. **M.A. Vorotyntsev, A.A. Kornyshev.** Elektrokhimiya. 20 (1984) 3.
47. **A.A. Kornyshev.** Electrochimica Acta, 36 (1991) 1660.
48. **E. Leiva, W. Schmickler.** J. Electroanal. Chem., 205 (1986) 323.

APPLICATION OF CHRONOCOULOMETRY IN ADSORPTION STUDIES AT BISMUTH/ALCOHOL INTERFACE

M. Väärtnõu
Institute of Physical Chemistry, University of Tartu

ABSTRACT

The application of chronocoulometry for the adsorption studies on bismuth electrode has been investigated. The details of experimental and computational procedures are described. It was found on the basis of the results of the adsorption of thiourea that chronocoulometry has some advantages in comparison with differential capacity measurements but the results obtained by these two methods were quite close.

INTRODUCTION

Chronocoulometry is an experimental method for the direct measurement of electrode charge. The method is not very widely used for adsorption studies nowadays. In recent years, however, adsorption of some organic compounds on solid electrodes has been studied [1, 2]. As follows from these works, the electrode charge values obtained by chronocoulometry are closer to the equilibrium ones than those calculated from differential capacity measuremetns. Since the differential capacity results for bismuth in nonaqueous solutions are often frequency-dependent and the extrapolation to zero frequency is a quite labour-consuming and not very exact procedure, the application of chronocoulometry on bismuth can be considered perspective.

EXPERIMENTAL

The device for coulometric measurements (coulometer) was constructed and built in the "Abakus" firm. The construction and technical characteristics of the device were described earlier [3]. Additional equipment consists of on oscilloscope and a computer. The working procedure is as follows. The initial parameters (the potential interval, length of potential step etc.) are given to coulometer by an Apple II personal computer, then the coulometer produces the corresponding potential impulses (ΔE), measures the momentary current values (i), integrates the current-time dependence to yield the electrode charge (σ), and, in the end, sends the results back to the computer. Our coulometer is capable of producing two different kinds of potential steps (Fig. 1a): (a) the stairs-like and (b) returning to the initial potential value (E_{st}) after each impulse. The i values are measured in the time interval Δt and the i,t-dependence (Fig. 1b) can be watched on the oscilloscope screen. On an ideally polarized electrode, all registered current is the double layer charging current and the integration of i in the time interval Δt yields the electrode charge.

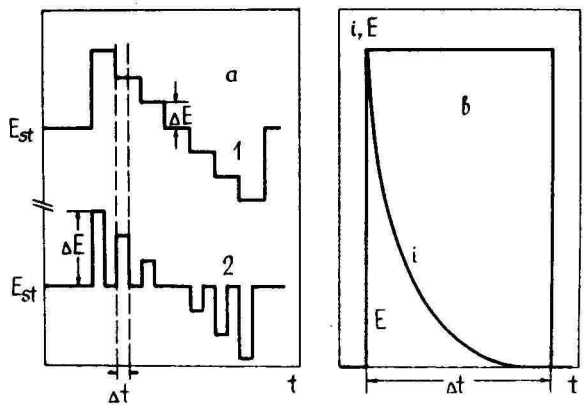

Fig. 1. Potential steps produced by coulometer (a) and the current-time dependence during a single potential step (b).

In real systems, however, an electrode is never totally ideally polarizable. Because of high ohmic resistance between electrodes in non-

aqueous solutions the current impulse is quite long (up to 100 ms for

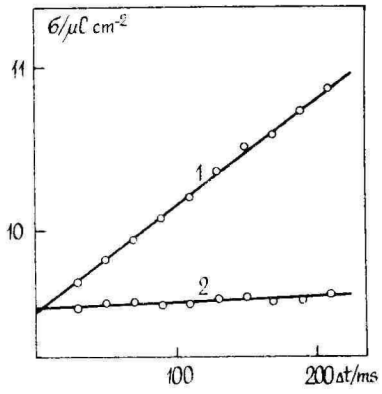

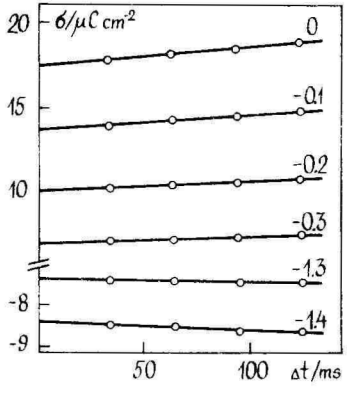

Fig. 2. Plot of measured electrode charge density against potential impulse length for an equivalent circuit. 1 faradaic current modelled by 1 MΩ resistor; 2 – faradaic current is absent.

Fig. 3. Plot of measured electrode charge density against potential impulse length for 0.1 M $LiClO_4$ solution in ethanol. Potential values are given near each line.

higher electrode charges) and the time of measuring cannot be shorter. It is therefore possible that the faradaic current is added to the double layer charging current and, consequently, the obtained charge values are higher than the real ones. Strictly speaking, only the change in the faradaic current during the potential impulse is important because the coulometer is capable of eliminating a constant faradaic current from the charging current. The inclusion of the faradaic current is detected by the dependence of measured charge values on the impulse length. The extrapolation to the zero impulse length was used [1, 2] on that occasion. We made experiments with an equivalent circuit using a resistance connected parallel to the condenser representing the double layer capacity. Various resitors were used to obtain faradaic current values corresponding to these values in actual measurement on an electrode. As can be seen from Fig. 2, there is a significant charge-time dependence in the case of 1 MΩ parallel resistor (i = 1 μA for E = 1 V) and no dependence when the parallel resistor is excluded. But in all cases, a good linear charge-time dependence occurs and the extrapolated charge values are exactly the same as measured in the

absence of the parallel resistor. Therefore, the same extrapolation procedure must be used in the case of actual measurements and the σ values, probably very close to the equilibrium ones, should be obtained. It must be noted that in real systems for adsorption studies i values are usually no higher than 0.1 -0.3 μA and the dependence of measured σ values from Δt is expected to be considerably less than in Fig. 2. In Fig. 3, the corresponding results for $LiClO_4$ solutions in ethanol are presented. As can be seen, the linear charge-time dependence is still maintained and, consequently, the extrapolation procedure can be considered as correct. It must also be noted that in the cases when can use shorter impulses (higher solution concentrations, the absence of adsorption, low electrode charges) σ values without extrapolation are also acceptable, but in any case, the use of $\sigma(\Delta t = 0)$ values is more correct.

Preparing of electrodes, solutions and electrochemical cell for a coulometric experiment did not differ from analogous procedures for capacity measurements. The second potential step method (see Fig. 1a) was used for the sake of reducing the amount of calculations. Each curve was measured five times with the same impulse length, after that the computer instantly calculated the mean σ values which were saved on a disk. Four different impulse lengths were used, namely 35, 65, 95 and 125 ms for ethanolic solutions. For higher alcohols when the ohmic resistance of solutions is larger, longer time intervals should be applied. So each curve was taken 20 times that covered the time necessary for the deareation of the next solution. For adsorption studies, series of solutions with different concentration were measured.

COMPUTATIONS

A pack of computer programs was written for further calculations. At first, the necessary data were selected. Secondly, the extrapolation to $\Delta t = 0$ was performed. Thirdly, the charge scale was corrected, so that $\sigma = 0$ corresponded to the zero charge potential, and the area of the electrode was taken into account. Fourthly, the program for calculating $\Delta\xi$ (the Parsons function) from C, E-curves was changed so that analogous calculations from σ, E-curves could be performed. Further calculations (of the amount of adsorption, isotherm and compact layer parameters) did not differ from those used before.

RESULTS

It is of interest to establish how much the results obtained by chronocoulometry differ from capacity-based results on the bismuth electrode. We have used chronocoulometry for studying Cl^- ions adsorption from ethanolic solutions [3]. In the present work, the adsorption of thiourea on the bismuth drop electrode from ethanol was studied. The adsorption behaviour of thiourea is formally much like to that of anions and the same calculation procedures can be applied [4]. The σ, E-curves for eleven solutions were obtained. The solutions contained 0.1 M of $LiClO_4$ and various content of thiourea, from 0 to 0.2 M. The σ, E-curves are presented in Fig. 4. The curves look like

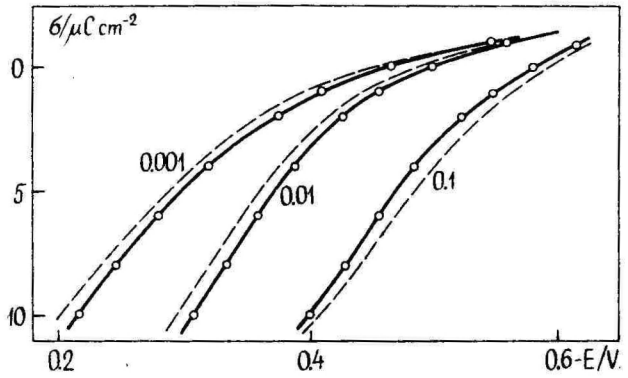

Fig. 4. Plot of electrode charge against potential on bismuth in solutions 0.1 M $LiClO_4$ + c M thiourea. The values of c are given in the figure. Dotted lines represent the curves obtained from differential capacity measurements.

those for anion adsorption. They coincide at potentials more negative than −1.2 V that indicates the desorption of thiourea at these potentials. As can be seen from Fig. 4, σ values obtained by chronocoulometry are somewhat higher than those obtained by the integration of differential capacity curves, but the differences are smaller than on a gold electrode. It is also worth noting that the two different potential step methods yielded completely coinciding results.

The σ, E-curves were treated accordingly to the standard procedure for anion adsorption [5]. The E values for integer σ values were calculated using an interpolation procedure and $E-E_{m=0}$ vs. σ

curves were integrated to yield $\Delta\xi$ for integer σ values ($\Delta\xi = \xi - \xi_{m=0}$; $\xi = \gamma + \sigma E$; γ is the surface tension). The differentiation of $\Delta\xi$, lg m-curves yields Γ, the surface excess of thiourea. In Fig. 5, some of Γ, σ-curves are presented. As can be seen from Fig. 5, there are no great differences between Γ values obtained from differential capacity measurements and by chronocoulometry.

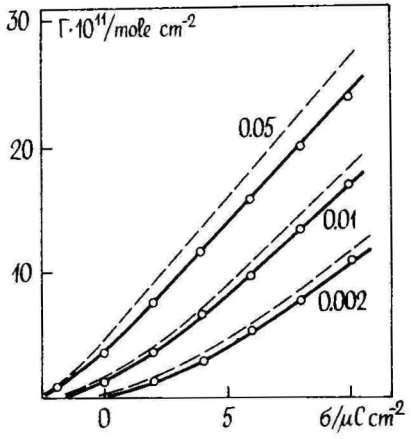

Fig. 5. Plot of surface excess of thiourea against electrode charge at bismuth/ethanol interface. The values of c are given in the figure. Dotted lines represent the curves obtained from differential capacity measurements.

The simple virial isotherm

$$\ln(\Gamma/c) = \Delta G_A^o/(RT) - 2B\Gamma \qquad (1)$$

describes the adsorption of thiourea well in ethanol (Fig 6a) and the potential step in the inner layer depends linearly on Γ (Fig. 6b). So, the main adsorption parameters ΔG_A^o (the standard Gibbs energy of adsoprtion) and B (the coefficient of mutual repulsion) as well as the inner layer parameters, can easily be obtained. Using the data in Fig. 6a, the following adsorption parameter values were obtained: $\Delta G_A^o = 86.5\ kJmol^{-1}$ and $B = 1.3\ nm^2 ion^{-1}$. These values differ quite little from those obtained earlier from differential capacity measurements [6].

The inner layer parameters in the presence of adsorbed thiourea molecules, as proposed first by R. Parsons [4], have later been widely used for the separate determination of the inner layer dielectric permeability (D_{02}) and thickness (x_2). However, the model [4] is quite primitive and yields unrealistic results in some cases [6]. However, the application of an improved model [6] changed the parameters only slightly. Nevertheless, the calculations were carried out to establish if the results obtained by chronocoulometry will be the same. The improved model [6] was used. The results are given in a table.

As can be seen from Table 1, the results are qualitatively the same that were obtained earlier. So it may be once more confirmed that the

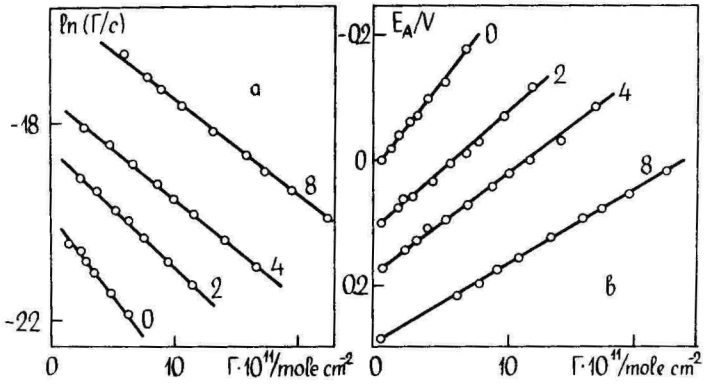

Fig. 6. Plot of function ln(Γ/c) (a) and potential drop in double layer against surface excess of thiourea at bismuth/ethanol interface. The electrode charge is given near each line in μCcm^{-2}.

low values of x_2 are caused by the deficiencies of the model rather than by experimental inaccuacies.

Table 1

Inner layer characteristics for bismuth/ethanol interface calculated from adsorption results of thiourea

Parameter	$\sigma < -1\ \mu Ccm^{-2}$	$\sigma \approx 0$	$\sigma > 3\ \mu Ccm^{-2}$
D_{02}	5.0	5.1	6.9
x_2, Å	3.7	2.4	2.4

CONCLUSION

The results of the present work and the previous one [3] show us that the adsorption results obtained by chronocoulometry and differential capacity do not differ significantly for the bismuth electrode. In adsorption studies, however, chronocoulometry has several advantages:

a) the method is considerably less labour-consuming because it is fully automatized;

b) since the measuring is very fast, the electrode is a greater part of the time under a potential where it is most stable and, concequently, the possibilities of electrode oxidation and other surface changes are small;

c) extrapolation to zero time impulse is much more exact than extrapolation to zero frequency in capacity measurements.

The disadvantages of the method are to following:

a) determination of zero charge potential is not possible;

b) differential capacity curves are qualitatively much more informative than σ, E-curves.

REFERENCES

1. **J. Richer, J. Lipkowski.** J. Electrochem. Soc., 133 (1986) 121.
2. **J. Richer, J. Lipkowski.** J. Electroanal. Chem., 251 (1988) 217.
3. **V. Semevsky, P. Pärsimägi, M. Väärtnõu, A. Alumaa.** Proc. 9th Symp. on Double Layer and Adsorption at Solid Electrodes. Tartu, 1991. P. 175.
4. **R. Parsons.** Proc. Roy. Soc., 261A (1961) 79.
5. **B. Damaskin, U. Palm, E. Petyärv, M. Salve.** J. Electroanal. Chem., 47 (1973) 127.
6. **U. Palm, B. Damaskin, M. Väärtnõu, E. Petyärv.** Proc. 4th Symp. on Double Layer and Adsorption at solid electrodes. Tartu, 1975. P. 220.

ELECTROCHEMICAL REDUCTION OF OXYGEN ON GLASSY CARBON AND ON A THIN LAYER OF GOLD IN ALKALINE SOLUTION

K. Tammeveski, T. Tenno
Institute of Physical Chemistry, University of Tartu

ABSTRACT

The kinetics of the oxygen reduction reaction on a glassy carbon electrode and on a thin layer of gold evaporated onto glassy carbon have been studied in alkaline electrolyte. Typical two-wave curves were obtained on both electrodes. The half-wave potential of the first wave of oxygen reduction on gold was about 0.15 V more positive than on the glassy carbon electrode. The anodic treatment of the glassy carbon electrode leads to a higher current value of the first wave, but has a negligible effect on the current of the second wave.

INTRODUCTION

It is generally assumed that the electrochemical reduction of oxygen proceeds through two pathways in alkaline solution:

1) the direct $4e^-$ reduction

$$O_2 + 2H_2O + 4e^- \rightleftharpoons 4OH^- \qquad F^\circ = +0.401\ V \qquad (1)$$

2) the $2e^-$ process involving the formation of hydrogen peroxide as an intermediate product

$$O_2 + H_2O + 2e^- \rightleftharpoons HO_2^- + OH^- \qquad E^\circ = -0.065\ V \qquad (2)$$

Hydrogen peroxide formed by reaction (2) can be further reduced to hydroxide ions

$$HO_2^- + H_2O + 2e^- \rightleftharpoons 3OH^- \qquad E^\circ = +0.867\ V \qquad (3)$$

or catalytically decomposed

$$2HO_2^- \rightarrow O_2 + 2OH^- \quad (4)$$

These reactions should give various combinations, depending on the electrode material, the applied potential and composition of the solution [1]. According to the previous studies [2-6], the electroreduction of oxygen on carbon materials and on gold in alkaline solution proceeds through the intermediate formation of hydrogen peroxide i.e. series process is operative. Due to the fact that a further reaction of HO_2^- requires the rupture of the O–O bond, high overpotential is needed. As a result, two distinguished waves can be observed at voltammetry curves.

EXPERIMENTAL

Polarization curves for the electroreduction of oxygen have been obtained by linear sweep voltammetry, using the rotating disc electrode technique. The rotating assembly had a speed controller and the rotation rate was varied from 360 to 4600 rpm. The potential scan (10 mv/s) was applied with a potentiostat SVA-1.

The glassy carbon electrodes SU-2000 (0.41 cm in diameter) were mechanically polished with thin emery paper and then with alumina to achieve a mirror finish. The glassy carbon electrodes were mounted in a teflon holder. Thin layers of gold were applied by means of vacuum evaporation at 2×10^{-5} torr. Before evaporation the glassy carbon surface was treated with concentrated alkali and isopropanol to avoid contamination with grease. The calculated thickness of the gold layer was about 50 nm.

The electrochemical measurements were conducted in a 100 cm^3 three-compartment cell. Pt-foil was used as a counter electrode and Hg/HgO, 0.1 M KOH as a reference electrode. All potentials are given versus this reference electrode. Before each measuring cycle the working electrode was scanned between potentials +0.2 to -1.2 V to obtain reproducible results. The experiments were carried out in 0.1 M KOH electrolyte, which was prepared from analytical grade KOH (Merck) and bidistilled water. No further purification of the electrolyte was done. The solutions were saturated with air oxygen.

RESULTS AND DISCUSSION

Current-potential curves for the electroreduction of oxygen on a thin layer of gold in 0.1 M KOH solution are shown in Fig. 1. Two-wave voltammograms are observed as expected from the previous reports for O_2 reduction on gold electrode. The current values have been gained by subtracting a background current from the measured disc current. A current plateau is formed in the potential range of the first wave from -0.35 V to -0.65 V. The second wave is not well developed.

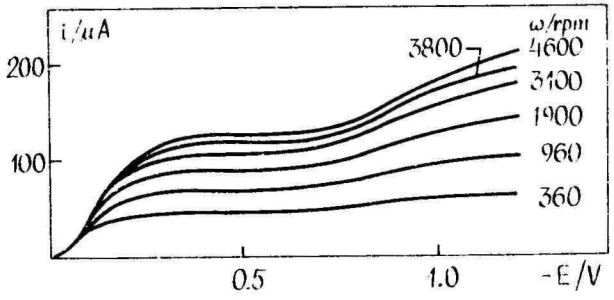

Fig. 1. Oxygen reduction on a thin gold layer in air saturated solution of 0.1 M KOH. Sweep rate 10 mV/s.

The Koutecky-Levich plots obtained from the experimental data, shown in Fig. 2, are used to distinguish between the contributions of the diffusion and the kinetic current to the overall disc current. For the first order reaction with respect to dissolved oxygen, the disc current density is related to the rotation rate by the expression

$$1/i = 1/i_k + 1/B\omega^{1/2} \qquad (5)$$

where i_k is the kinetic current density, B is related to the diffusion limiting current density by the expression $i_d = B\omega^{1/2}$ and ω is the rotation rate of the disc electrode. B is given by

$$B = 0.62nFc_{O_2}D_{O_2}^{2/3}\nu^{-1/6} \qquad (6)$$

The theoretical value of B in 0.1 M KOH calculated from equation (6) is 0.092 mA/cm^2(rad/s)$^{1/2}$, for n = 4 and ν = 0.01 cm^2/s, using data for oxygen solubility (c_{O_2} = 0.25 × 10^{-6} mol/cm^3) and diffusion coefficient (D_{O_2} = 1.9 × 10^{-5} cm^2/s). The number of electrons

excanged per molecule of oxygen can be calculated from the experimental values of B.

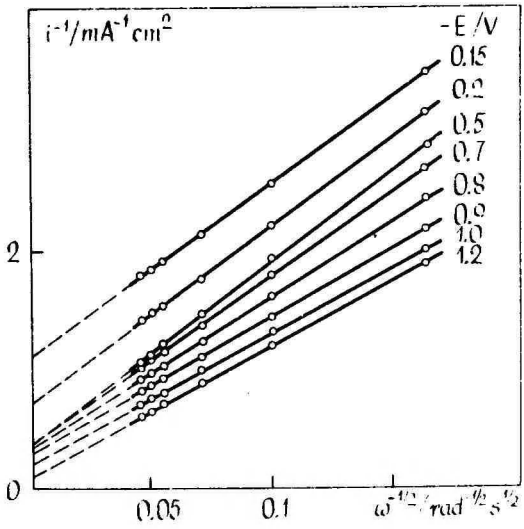

Fig. 2. Plots of i^{-1} vs·$\omega^{-1/2}$ obtained from the i, E-curves of Fig. 1 at various potentials.

It was found that in the potential region of the first wave, the minimum value of n is 2.6. This is not in accordance with the expectancy that only $2e^-$ process to hydrogen peroxide takes place. It is evident that another reaction must occur besides $O_2 \rightarrow HO_2^-$. It should be either the direct reduction to hydroxide ions or a further reduction of the formed hydrogen peroxide. The number of transferred electrons at the potentials of the second wave is close to 4. Fig. 3 shows the dependence of i vs. $\omega^{1/2}$. These plots are not in accordance with the Levich equation and have greater intercepts than zero by extrapolating to $\omega \rightarrow 0$. Similar results were reported in [2], but the current values of the second wave have been taken there from a more positive potential than we did.

In the case of combined diffusion and kinetic control, the dependence of current versus potential is given by

$$i = i_o(1-i/i_d)\exp[-\alpha nF(E-E_r)/RT] \qquad (7)$$

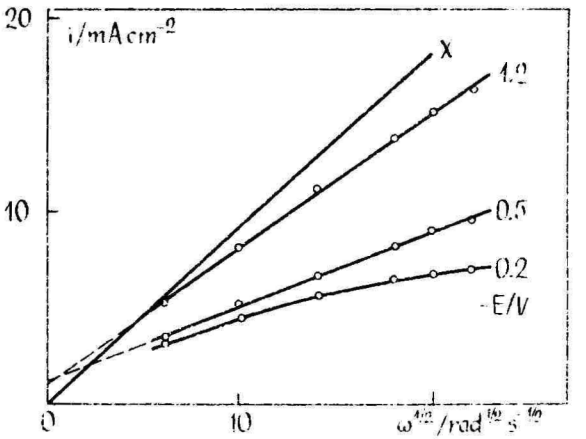

Fig. 3. Plots of i vs. $\omega^{1/2}$ derived from the disc current data of Fig. 1. x – theoretical limiting current density for $4e^-$ reduction.

A plot of $\log[i/(i_d-i)]$ vs. potential is shown in Fig. 4. In the linear region at higher overpotentials the Tafel slope is 130 mV/dec. This

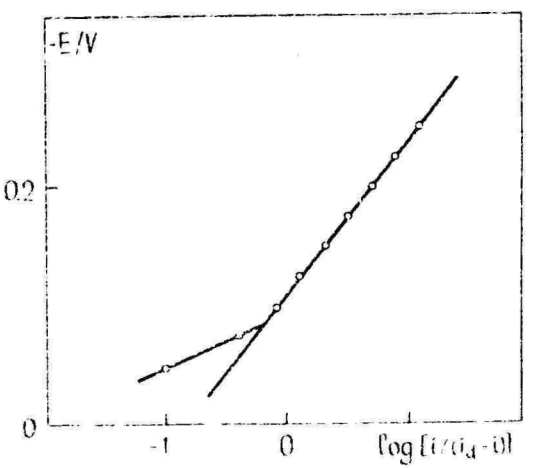

Fig. 4. Tafel plot for oxygen reduction on a thin layer of gold in 0.1 M KOH solution at ω = 1900 rpm, i_d = 0.68 mA·cm^{-2}.

indicates that the reaction rate is determined by the first electron transfer by Eq. (8).

$$O_2 + e^- \rightarrow O_2^- \qquad (8)$$

When we used the anodic sweep direction starting from potential -1.2 V the currents of the second wave had nearly the same value but those of the first wave were considerably higher as compared with the cathodic sweep. Starting the anodic scan from potential -0.7 V, only a negligible hysteresis of the current was observed between negative and positive sweep directions. Such effect should be explained by changes in the surface state at more negative potentials. A half-wave potential was only slightly affected by the direction of the potential scan.

Hydrogen peroxide forms as an intermediate product of oxygen reduction on gold. Therefore a real necessity exists to obtain experimental data for HO_2^- reduction in O_2-free solutions. Fig. 5 presents voltammetry curves for HO_2^- reduction on a thin layer of gold measured in He-saturated 0.1 M KOH solution containing 3mM HO_2^-.

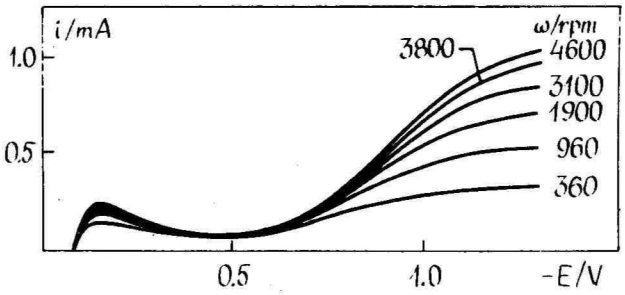

Fig. 5. Voltammetry curves for HO_2^- reduction on thin Au-layer in He-saturated 0.1 M KOH containing 3 mM HO_2^-. Sweep rate 10 mV/s.

It should be noted that a current maximum appears at potential -0.15 V. The peak current depends on the rotation rate, but in fact these data are not well enough reproducible for further analysis. In the potential range from -0.25 V to -0.7 V the reduction reaction of HO_2^- is retarded. At more negative potentials than -0.7 V, a gradual rise of the current is observed.

The HO_2^- reduction wave is corresponding to the second wave of

O_2 reduction reaction in Fig. 1. The Koutecky-Levich plots for HO_2^- reduction reaction are shown in Fig. 6.

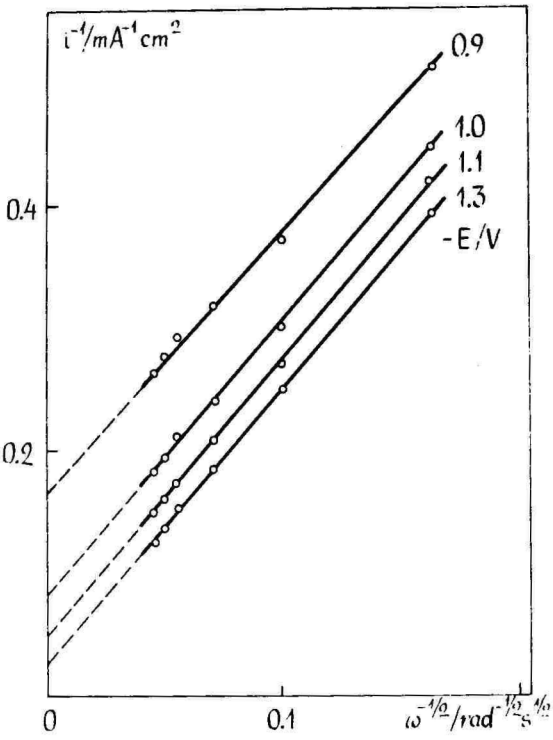

Fig. 6. Dependence of i^{-1} on $\omega^{-1/2}$ derived from the data of Fig. 5 at various potentials.

The parameter B calculated from Eq. (6) is 0.405 $mA/cm^2(rad/s)^{1/2}$, using the following data n = 2, F = 96500 C/mol, ν = 0.01 cm^2/s, D = 1.2 × 10^{-5} cm^2/s and C = 3 × 10^{-6} mol/cm^3. The experimental value of B obtained from the slopes of the straight lines in Fig. 6 is 0.44 $mA/cm^2(rad/s)^{1/2}$ i.e. the deviation from the theoretical value is less than 10 %. However some uncertainity remains due to the fact that there can be found different data for the diffusion coefficient of HO_2^- in literature.

In order to obtain information about the support material, the electroreduction of oxygen has been investigated on glassy carbon too. There are a lot of experimental data indicating that the electrocatalytic

activity of the glassy carbon electrode depends to a considerable degree on the surface treatment. In this work anodic treatment was done by holding working electrode at various anodic potentials for 5 min. Polarization data for the oxygen reduction reaction on glassy carbon are shown in Fig. 7. The current reaches the maximum value at potential -0.45 V.

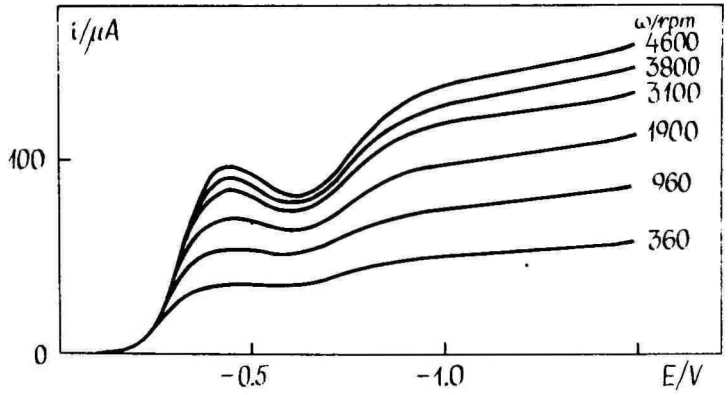

Fig. 7. Current-potential curves for oxygen reduction on glassy carbon in 0.1 M KOH. Sweep rate 10 mV/s; Po_2 = 0.21 atm.

At more negative potentials a drop of the current is observed, which is more evident at higher rotation rates. This behaviour is connected with the decreasing electrocatalytic activity of the electrode surface. The anodic treatment leads to an increase of the first wave current, but does not have an essential effect on the current value of the second wave. A remarkable change of the first wave current is seen after anodization at potentials greater than +1.0 V. This is in good correlation with the oxidation data of glassy carbon, where considerable increase of current is seen at potentials E > +1.0 V. Fig. 8. shows a plot of i^{-1} vs. $\omega^{-1/2}$ derived from current-potential curves in Fig. 7. It is seen in Fig. 8 that the slope of straight lines is changing i.e. the number of the transferred electrons is not constant. In comparison the experimental value of B with the theoretical value of B calculated by Eq. (6), the number of exchanged electrons may be established. In the potential region of the first wave on a highly oxidized electrode n = 2

was obtained. At very negative potentials the number of transferred electrons is rising over 3. This is in contradiction with the results

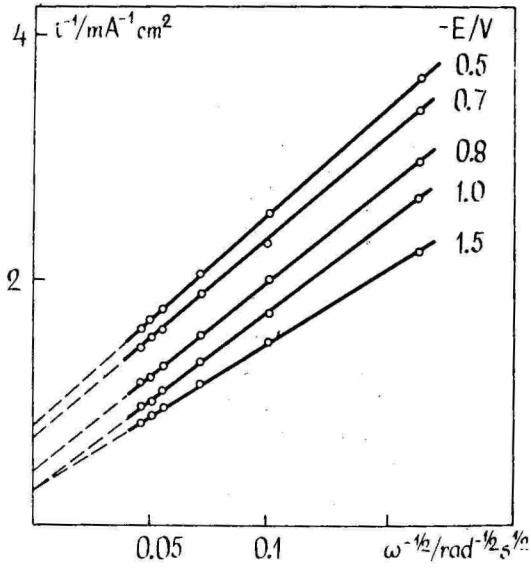

Fig. 8. Plots of i^{-1} vs. $\omega^{-1/2}$ for oxygen reduction on glassy carbon in 0.1 M KOH.

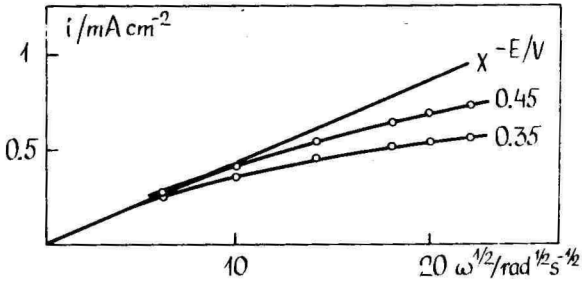

Fig. 9. Levich plots for oxygen reduction on glassy carbon in 0.1 M KOH solution. x – theoretical limiting current density for $2e^-$ reduction.

obtained in [7]. There was pointed out that only $2e^-$ reduction to hydrogen peroxide proceeds in the potential region of the second wave. It should be noted that even at potential -1.5 V the dependence of i^{-1} vs. $\omega^{-1/2}$ extrapolated to the infinite rotation rate does not pass the zero intercept. Levich plots of oxygen reduction on glassy carbon are given in Fig. 9. At the potential of the maximum current of the first wave the plots of i vs. $\omega^{1/2}$ do not obey the Levich equation. Tafel slope calculated from the dependence of $\log i/(i_d - i)$ vs. potential has the value of 85 mV/dec.

ACKNOWLEDGEMENTS

We thank Dr. Arnold Rosental (Institute of Physics, Estonian Academy of Sciences, Tartu) for preparing thin metal layers.

REFERENCES

1. **M.R. Tarasevich, A. Sadkowski and E.B. Yeager** in B.E. Conway, J.O'M. Bockris, E. Yeager, S.U.M. Khan and R.E. White (Eds.) Comprehensive Treatise of Electrochemistry. New York: Plenum Press, 1983. Vol. 7. P. 301.
2. **C. Paliteiro, A. Hamnett, J.B. Goodenough.** J. Electroanal. Chem., 234 (1987) 193.
3. **C. Paliteiro, A. Hamnett, J.B. Goodenough.** J. Electroanal. Chem., 233 (1987) 147.
4. **R.W. Zurilla, R.K. Sen, E. Yeager.** J. Electrochem. Soc., 125 (1978) 1103.
5. **N.R. Vilambi, E.J. Taylor.** J. Electroanal. Chem., 270 (1989) 61.
6. **R. Jiang, S. Dong.** J. Electrochem. Soc., 136 (1989) 3325.
7. **R.J. Taylor, A.A. Humffray.** J. Electroanal. Chem., 64 (1975) 63.

DETERMINATION OF SELENIUM BY CATHODIC STRIPPING VOLTAMMETRY

H. Keis, Y. Piibar
Institute of Physical Chemistry, University of Tartu

ABSTRACT

The behaviour of selenium(IV) in differential pulse cathodic stripping voltammetry is investigated. The effect of pH, deposition potential, pulse amplitude and copper concentration on the stripping peak at the mercury film glassy carbon electrode are examined. The detection limit was found to be 1 $\mu g \cdot l^{-1}$ with deposition time of 10 min.

Several papers published in recent years have dealt with the polarographic behaviour [1–4, 13] and stripping voltammetric determination of selenium [4–12, 14–19]. Because only selenium(IV) is electroactive, electrochemical tehniques can be used for speciation. For the behaviour of Se(IV) at the mercury electrode two possible mechanisms are proposed. Speranskaya [2, 3] assumed two steps for reduction, the first of which leads to the formation of elemental Se, reduced to hydrogen selenide in the following step. A more accepted plating reaction is considered to involve the reduction of selenium(IV) to mercury(II) selenide at a potential more negative –0.05 V vs. Ag/AgCl [1, 4–7]:

$$H_2SeO_3 + 4H^+ + Hg + 4\bar{e} \rightarrow HgSe + 3H_2O \qquad (1)$$

It is generally accepted that in acidic solution reduction occurs in two

stages, the first involving the formation of hydrogen selenide

$$H_2SeO_3 + 6H^+ + 6\bar{e} \rightarrow H_2Se + 3H_2O \quad (2)$$

and in the second, anodic reaction forms mercury(II) selenide:

$$H_2Se + Hg - 2\bar{e} \rightarrow HgSe + 2H^+. \quad (3)$$

At a more negative potential the stripping process occurs in the reverse of the reaction [3]. All processes are pH dependent and favoured in acidic media. Because it is possible to accumulate a HgSe film at a stationary electrode, many studies have applied cathodic stripping voltammetry (CSV) on the mercury electrode [4–10, 12, 14, 15], stripping chronopotentiometry on the mercury film electrode (MFE) [11] and anodic stripping voltammetry on gold electrodes [7, 17–19]. Peak currents are highly dependent on the deposition potential E_d and E_d = -0.2 – -0.7 V [5–12] and -0.065 V is recommended as an optimal [15] for CSV. A sufficient increase of the selenium signal in the presence of copper has been reported in several papers when the determination was done by DPCSV at the HMDE [5–8, 9]. The effect of the copper addition is explained as the formation of an intermetallic compound with selenium Cu(Hg)Se which could change both the potetnial and the size of the signal.

EXPERIMENTAL

Differencial pulse cathodic stripping voltammetry was used with the Tacussel Polaropulse PRG5 analyser with a glassy carbon CY-2000 rotating discus electrode, frequency 4600 rot·min^{-1}. The reference electrode is a saturated calomel electrode (SCE) and the counter electrode is a platinum plate with the area of 1 cm^2. The standard stock solution of selenium(IV) was prepared from Titrisol ampoules (Merck) (1 g·l^{-1} in 1 M hydrochloric acid) and tripledestilled water. The standard solution 1 mg·l^{-1} in 1 M HCl was prepared weekly and boiled in a water bath to avoid the oxidation of selenium(IV). A mercury film

was previously plated onto the glassy carbon electrode in the solution of $\sim 1 \cdot 10^{-3}$ or $1 \cdot 10^{-4}$ M Hg^{2+} in 0.1 M $HClO_4$ on a potential -0.8 V (SCE) with the deposition time t = 1–5 min. Measurements were provided in acidic media containing 0.01–1 M $HClO_4$ and(or) HCl, deoxygenated with Ar.

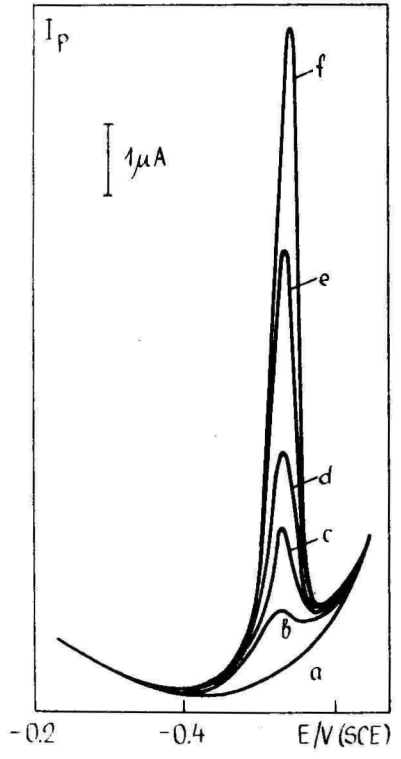

Fig. 1. Dependence of peak current on deposition time for $1 \cdot 10^{-7}$ M Se(IV) in 0.1 M HCl. t = 0 (a); 1 (b); 2 (c); 3 (d); 6 (e) and 10 (f) min, respectively. E_d = 0 V, 100 mV pulse width, 5 $mV \cdot s^{-1}$ scan rate.

The CSV peak of selenium occurs near E = -0.5 V (Fig. 1). The Dependence of the peak current on the deposition potential E_d is shown in Fig. 2. In all used supporting electrolytes the best sensitivity and the

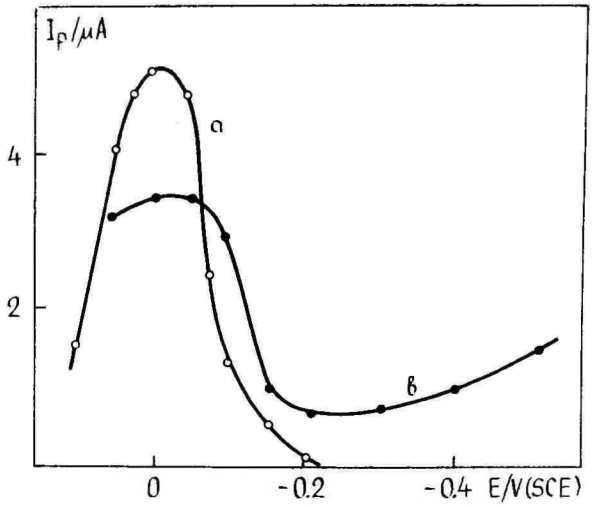

Fig. 2. Effect of deposition potential on peak current for $2 \cdot 10^{-7}$ M Se(IV) in 0.1 M HCl (a) and after addition of $2 \cdot 10^{-6}$ M Cu(II) (b). E_d = 0 V, t = 2 min.

reproducibility of the selenium signal was achieved with Ed ≃ 0 V (SCE). The decrease of the peak current using more positive deposition potentials can be explained with a calomel formation on the mercury surface: the cathodic peak of reduction Hg_2Cl_2 appears in 0.1 M HCl beginning from E_d = -0.03 V. The reducing of the selenium peak using more negative deposition potentials can be explained by the inhibition of an anodic process, the formation of HgSe (reaction 3) with an increasing -E. The selenium peak potential shifts cathodically with the increasing pH with a slope of about 60 mV, pH dependence of the signal is similar to the one described by Batley [13]. The peak height increase with the concentration of HCl (pH = const), but more serious on sensitivity and peak width has the mercury film quality. On the thin film electrode $b_{1/2}$ = 50–65 mV and sensitivity of about 0.4 μA: $10^{-7}M^{-1}min^{-1}$. The sharp peak ($b_{1/2}$ = 40–45 mV) and sensitivity up to 1.2

$\mu A \cdot 10^{-7} M^{-1} \cdot min^{-1}$ correspond to the thick film electrode. The peak height is highly dependent on the pulse amplitude ΔE. With the increasing of $-\Delta E$ from 20 to 50 and 100 mV the peak height arises 12 and 36 times, respectively. Because the background current does not grow worse sufficiently with the pulse amplitude, $\Delta E = -100$ mV was used mostly to obtain the best sensitivity. It was found that after some measurements the size of the signal decreased. Te quantity of reproducible measurements depends on the concentration of selenimu(IV) and electrolysis time and is less when the concentration and t are high. At the same time if $[Se^{4+}] \leq 10^{-7}$ M, more than 10 measurements can be done without the decreasing of the signal using a short deposition time to keep i_p less than 5 μA.

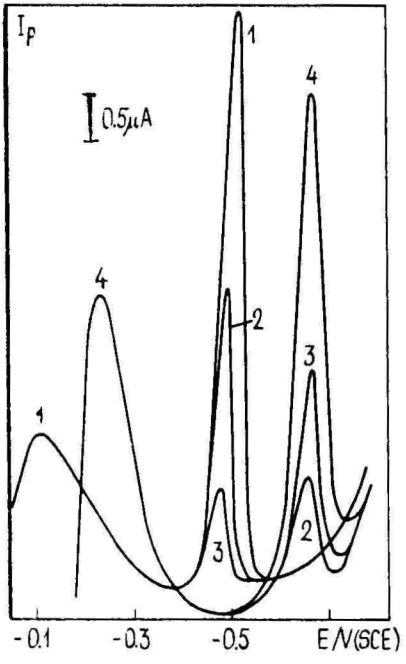

Fig. 3. Influence of Cu(II) on peak current for $5 \cdot 10^{-7}$ M Se(IV) in 0.1 M HCl. Concentration of Cu(II): 1 - 0; 2 - $5 \cdot 10^{-7}$; 3 - $10 \cdot 10^{-7}$; 4 - $30 \cdot 10^{-7}$ M. $E_d = 0$ V, t = 1 min.

Influence of added copper to the sample seems to be more complicated on MFE than on HMDE. When the deposition potential near O V is used, the increasing of Cu(II) concentration reduces the selenium signal at -0.5 V and the peak with $b_{1/2}$ = 60–70 mV appears at -0.65 V (Fig. 3), presumably by changing the nature of the adsorbed intermetallic compound. So the ratio of Se(IV) and Cu(II) 1:1 decreases the peak approximately 50 % and in the conditions of 1:6 or more, only the second peak is measurable (Fig. 4). The maximum height of the last

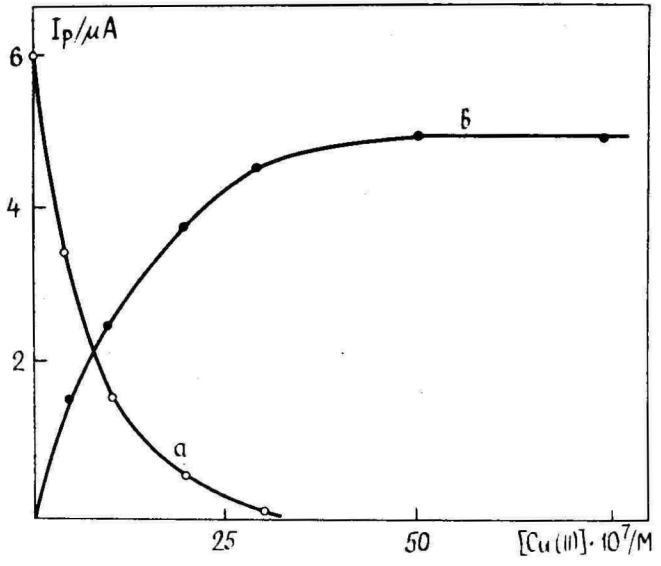

Fig. 4. Dependence of peak current for $5 \cdot 10^{-7}$ M Se(IV) on concentration of Cu(II). a - at 0.5 V, b - peak at -0.65 V. E_d = 0 V; t = 1 min.

one is less but due to the higher values of $b_{1/2}$, the peak area is nearly same as it is at -0.5 V without added copper. The deposition potential dependence of the selenium peak current is shown in Fig. 2 in the conditions of 10 fold excess of Cu(II). It must be noted that copper

deposition onto the electrode is possible only at more negative potentials than -0.2 V: anodic stripping peak's E = -0.18 V in 0.1 M HCl, chronovoltammetric peak of depostion Cu (see Fig. 3) lies near -0.25 V. Obviously at E_d = 0 - 0.1 V the HgSe deposits and the intermetallic compound with copper can be formed during the scan of the potential. When the deposition is provided at -0.5 V, the increasing of pH value causes a noticeable rise of sensitivity, the signal moves to a more negative potential and $b_{1/2}$ increases: for pH = 3.2 E_p = -0.85 V and $b_{1/2}$ = 85 mV. On the other hand, the signal in these conditions is less reproducible and can be used for analysis only when a fresh mercury film is plated before each new electrolysis. So to determine Se(IV) it is nessecary to remove Cu(II) from the sample and to measure the peak on -0.5 V or to add an excess of copper and to register the signal on -0.65 V, both at pH values below 2.

CONCLUSION

Selenium(IV) above 10^{-8} M can be determined by using differential pulse cathodic stripping voltammetry on mercury coated glassy carbon rotating disc electrode in acidic media. The deposition potentials near 0 V (SCE) make possible the maximal sensitivity in both, the absence and presence of copper in the smaple solution.

REFERENCES

1. **J.J. Lingane, L.W. Nedrack.** J. Am. Chem. Soc., 71 (1979) 196.
2. **E.F. Speranskaya.** Zh. Anal. Khim., 17 (1962) 347.
3. **E.F. Speranskaya.** Zh. Anal. Khim., 19 (1963) 9.
4. **G.D. Christian, E.C. Knoblock, W.C. Burdy.** Anal Chem., 3 (1963) 1129.
5. **U. Baltensperger, J. Hertz.** Anal. Chim. Acta., 172 (1985) 49.

6. **S.B. Adeloju, A.M. Bond, H.C. Hughes.** Anal. Chim. Acta., 148 (1983) 59.
7. **S.B. Adeloju, A.M. Bond, M.H. Briggs, H.C. Hughes.** Anal. Chem., 55 (1983) 2076.
8. **G. Jarzabek, Z. Kublik.** Anal. Chim. Acta., 143 (1982) 121.
9. **G.P. Bound, S. Forbes.** Analyst, 103 (1978) 176.
10. **B.L. Dennis, J.L. Moyers, G.S. Wilson.** Anal. Chem., 48 (1976) 1611.
11. **H. Eskilsson, C. Haraldsson.** Anal. Chim. Acta., 198 (1987) 231.
12. **L. Campanella, T. Ferri, R. Morabito, A.M. Paoletti.** La Chimica et L'industria, 69 (1987) 90.
13. **F.G.E. Batley.** Anal. Chim. Acta., 187 (1986) 109.
14. **R. Ahmad, J.O. Hill, R.J.Magee.** Analyst, 108 (1983) 835.
15. **B. Deldime, J. Harman.** Anal. Lett., 13 (1980) 105.
16. **L.S.K. Opanskaya, A.T. Russo.** Zh. Anal. Khim., 27 (1975) 738.
17. **R.W. Andrews, D.C. Johanson.** Anal. Chem., 47 (1975) 294.
18. **R.W. Andrews, J.H. Larochelle, D.C. Johnson.** Anal. Chem., 48 (1976) 212
19. **R.W. Andrews, D.C. Johnson.** Anal. Chem., 48 (1976) 1056.

SIMULTANEOUS DETERMINATION OF TIN AND LEAD IN AQUEOUS SOLUTIONS BY POTENTIOMETRIC STRIPPING ANALYSIS

Jüri Ruut, V. Pihl, V. Past
Tartu Public Health Service, University of Tartu

ABSTRACT

Lead and tin are analyzed simultaneously by means of the potential stripping analysis (PSA). Analytical signals of Sn and Pb, which appear at the same potential when 0.1 M HCl is used as a supporting electrolyte, can be separated after adding either ammonium oxalate, ammonium citrate or ammonium acetate.

INTRODUCTION

In the Chemical Laboratory of Tartu Public Health Service, trace amounts of heavy metals (Zn, Cd, Pb, Cu) are determined by the potentiometric stripping analysis (PSA) which requires simple instrumentation and ensures a good sensitivity. One can find information on the method in literature [1, 2, 3]. When canned food is investigated, one can expect the co-occurence of tin and lead in the material. Unfortunately, the PSA method using pure 0.1 M hydrochloric acid as a supporting electrolyte does not allow the separation of the stripping plateaus of thin and lead. This may lead to serious mistakes as permitted levels in food for Sn and Pb differ more than 100 times. To solve this problem, ammonium salts were investigated as an addition to the supporting electrolyte.

In literature [4], a method is described which uses methanol as an added reagent to analyze lead and tin in juices. De-gassing of the solution was applied before the analysis which made the method unsuitable for us.

EXPERIMENTAL

Apparatus

The PSA system consists of a potentiostat PA3, a XY-recorder XY-4103 (both Laboratorni Pristroje, Prague), a TTA-80 titration assembly with a glassy-carbon electrode F3500 as a working electrode, a reference saturated calomel electrode K4040, and an auxiliary Pt-electrode P1312 (all Radiometer, Copenhagen). The potential between the working and reference electrodes was amplified by a high-impedance- input electrometer unit (University of Tartu, Estonia) and transferred simultaneously to the recorder and an analogue-digital converter with the following signal processing in the computer memory. The system is controlled by a timer unit.

Reagents

Hydrochloric acid used as a supporting electrolyte is prepared from technical grade acid by means of molecular distilling. The other reagents are of analytical grade. Sn^{2+}, Pb^{2+}, and Cd^{2+} working solutions are made of $SnCl_2 \cdot 2H_2O$, $Pb(NO_3)_2$ and $Cd(NO_3)_2$, respectively. Saturated solutions of ammonium salts are made of solid ammonium oxalate, citrate and acetate.

Analytical procedures

The working electrode is prepared by polishing its surface with 3 μm diamond powder, followed by coating in mercury aqueous solution (0.05 g $Hg(NO_3)_2$/l) in four 1-minute cycles with the plasting potential being -950 mV. The quality of the mercury layer is controlled visually.

The working solution is electrolyzed during 1 minute. The initial solution contains 0.1 M HCl as the supporting electrolyte, afterwards it is modified by adding 1 ml of saturated solution of either ammonium citrate, ammonium oxalate, or ammonium acetate. pH values for the modified solutions were 2.1, 3.2 and 5.5, respectively.

Background curves are registered, after that $5.27 \cdot 10^{-5}$M Cd^{2+}, $4.85 \cdot 10^{-5}$M Pb^{2+}, and $3.68 \cdot 10^{-4}$M Sn^{2+} are added. 200 μl of each. Standard additions of Pb^{2+} and Sn^{2+} are made and the stripping curves taken in pure 0.1 M HCl solution and in the supporting electrolyte containing ammonium salts.

RESTULTS AND DISCUSSION

In pure 0.1 M hydrochloric acid solution, tin and lead show slightly different stripping potentials when they are analyzed separately, –0.55 V for Pb and –0.58 V for Sn. Responses to standard additions show good linearity (Fig. 1).

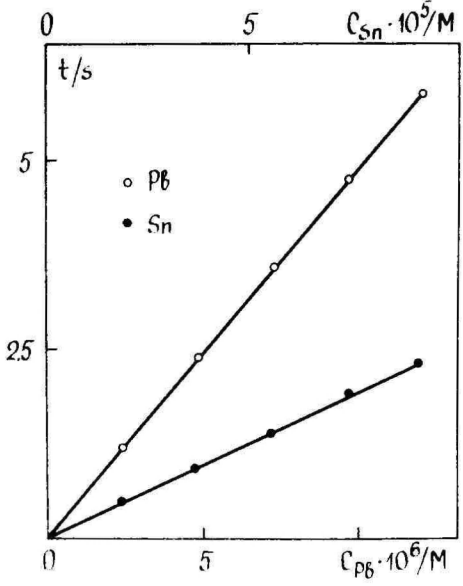

Fig. 1. Stripping time. vs concentrations of Sn and Pb. Standard additions of 200 μl $4.85 \cdot 10^{-5}$ $Pb(NO_3)_2$ and $3.68 \cdot 10^{-4}$M $SnCl_2$ are made.

The difference in stripping potentials gets lost as lead and tin ions are in the solution together, only one plateau can be observed at –0.55 V potential (Fig. 2a). When standard additions are made to either Sn or Pb, standard curve plots remain the same as they were in the previous cases when metal ions were added separately.

After adding 1 ml of saturated ammonium oxalate solution to the solution containing $2.64 \cdot 10^{-6}$M Cd^{2+}, $2.43 \cdot 10^{-6}$M Pb^{2+}, and $1.84 \cdot 10^{-5}$M Sn^{2+} the stripping potentials of tin and lead shift to –0.65 V and –0.55 V, respectively; cadmium has a stripping plateau at –0.75 V (Fig. 2a). When standard additions are made with $4.85 \cdot 10^{-5}$ M Pb^{2+} solution, plateaus of tin have a decreasing tendency as lead

concentration grows (Fig. 3), the plateau of cadmium remains constant. The effect of decreasing of the analytical signal of tin upon the addition of lead ions is not observed on using ammonium citrate or ammonium acetate.

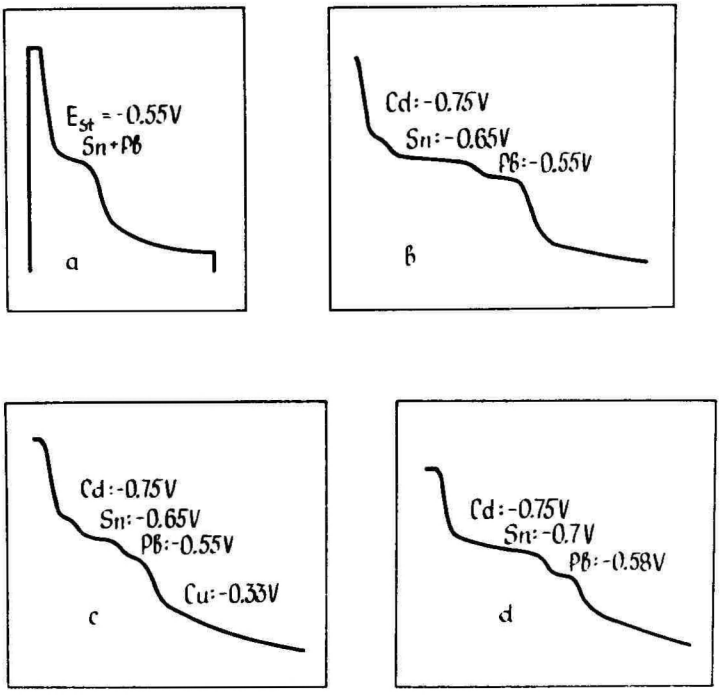

Fig. 2. Time vs potential curves using pure supporting electrolyte (0.1M HCl) (a) and the solution containing ammonium oxalate (b), ammonium citrate (c) and ammonium acetate (d).

Adding of 2 ml ammonium citrate solution makes tin and lead plateaus shift to –0.65 V and –0.55 V, respectively, the plateau of cadmium is located at the potential of –0.75 V (Fig. 2c). As the salt used contains certain amounts of copper, a stripping plateau of Cu appears at –0.33 V after adding ammonium citrate.

When 1 ml of ammonium acetate is added, the plateau of Pb is located at –0.58 V, for Sn at –0.70 V and for Cd at –0.75 V. It means that Cd and Sn plateaus become hardly distingushable from each other, although Sn–Pb separation is the best (Fig. 2d).

Hence, every method proposed here has it own faults. In addition, as dry ashing is used in our laboratory for real food samples, great losses of tin are likely to be present, so that the analysis results of tin contents may be strongly reduced. However, the exact determination of lead is possible while using any of the salts as an addition to the supporting electrolyte.

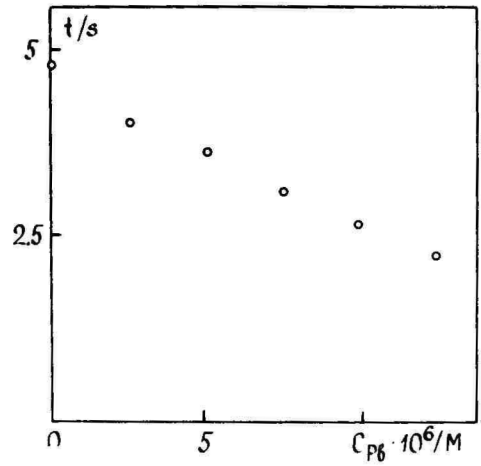

Fig. 3. Stripping time for tin vs Pb^{2+} concentration. 200 μl additions of $4.85 \cdot 10^{-5}$M lead ions are made, decreasing of tin signals can be seen.

REFERENCES

1. **D. Jagner.** Anal. Chem., 51 (1979) 342-345.
2. **L.-G. Danielsson et al.** Anal. Chim. Acta, 127 (1981) 147.
3. **T. Anfält et al.** Anal. Chim. Acta, 103 (1978) 379.
4. **S. Mannino.** Analyst, 197 (1982) 1466.

COMPUTER-AIDED POTENTIOMETRIC STRIPPING ANALYSIS

M. Miil, Jüri Ruut, V. Pihl
Tartu Public Health Service

Abstract

A system which allows to perform potential stripping analysis (PSA) and process analysis data by computer is described. The system uses a potentiostat, an electrometer unit, a 12-bit analogue-digital converter and a AT-286 computer.

INTRODUCTION

Potentiometric stripping analysis is used for heavy metal determination in the Tartu Public Health Service Chemistry Laboratory. This method has been thoroughly described by Jagner and co-workers [1]. The traditional methods to measure the analytical signal are quite tedious. Therefore, a computer-aided signal processing was found to be suitable to overcome this problem.

Here we describe a simple system which includes a common PSA apparatus and a 12-bit analogue-digital converter (ADC) computer interface. The analytical signal is stored and processed in the memory of the computer, the results are shown on the graphic display. Similar systems have been described before [2, 3, 4] but we found it more useful to develop our own system. The data acquisition and the treatment program are written in the Pascal programming language.

EXPERIMENTAL AND APPARATUS

The PSA system consists of a PA3 potentiostat, a XY-recorder 4103 (both Laboratorni Pristroje, Prague), an electrolytic cell with a reference saturated calomel electrode K4041, a working glassy-carbon

electrode F3500, and an Pt-auxiliary electrode P1312 (all Radiometer, Copenhagen). The system is controlled by a timer block. The analytical signal is amplified by a high- impedance- input (at least 10^{12} Ω) electrometer block (University of Tartu, Estonia) and transferred to the ADC and the recorder.

The electrometer has the input potential range ±2 V, the output potential range ±10 V, and the signal rise time from 10 % to 90 % 1.0/0.1 ms.

The analogue-digital converter consists of a 12-bit digital-analogue converter, 8 comparator elements for the analogue potential and the controller schemes which altogether form a 4-channel 2-band potential measuring device. In every channel the input potential is applied to 2 comparators. In one channel the input potenital is reduced 4 times, in the other channel it remains unchanged. The input potential is measured against the comparison potentials set by the computer according to the converting programmed algorithm which may be a sequential iteration method, linear or tracking methods. In this case a tracking algorithm is applied where the comparison potential tries to follow the input potential. Transforming speed depends on the computer speed and in this case (IBM PC AT 286 16 MHz) is 5 μs per comparing cycle which allows to track the potential change at the rate of 0.501 V/ms at maximum resolution (12 bit). The program allows a greater tracking speed (5.1 V/ms) while using the 8-bit resolution. Up to 32.000 integers can be read into the computer memory, after that they are compressed to 1024 integers. The signal curve is averaged using the so-called sliding mean method and is calculated by the following formula:

$$Y_i = \sum_{k=-m}^{m} Y\,[i + k]/(2m + 1), \qquad (1)$$

where m ≥ 0 and can be given by the operator forms a base width for filtration which determines the extent of signal smoothing. 1st and 2nd derivatives are found and smoothed. Algorithm for derivation is similar to finding the sliding mean, with the only difference that Y_i is obtained as a difference of points of the processed section [-m..m] which have the greater weight the farther they are situated from the central point (k=0). Similarily to averaging, the operator can input the coefficient m, and also the scaling coefficient. The beginning and end of the plateaus are determined by the 2nd derivative maximum and minimum provided that the value of the 1st derivative is greater than the one given by the operator. Potential vs. time can be displayed graphically. After

determing the plateau lengths and stripping potentials, the program compares the plateau heights with these of the ones for the outputs and results of different metals in a table. Afterwards the changes in concentrations and volumes are computed.

RESULTS AND DISCUSSION

Work of the system containing on XY-recorder as a signal storing device and the standard equipment is widely tested and found to be satisfactory, so we compare those results with the ones got while using digital data processing.

Standard additions of $4.85 \cdot 10^{-5}$M $Pb(N)_3)_2$ are made to 0.1 M HCl solution by 200 μl, the plating time is 60 s, the plating potential -1100 mV, results are obtained both on the computer and the recorder. The results are given in Tab. 1. As we see, plateau lengths are practically indentical ($R^2 = 0.9999$).

Table 1

Comparison of plateau lengths obtained by computer processing and by manual processing from recorder curves

Computer (ms)	Recorder (s)
1404	1.4
2584	2.6
3800	3.8
5320	54

Fig. 1 shows a stripping curve for $2.4 \cdot 10^{-6}$M Pb^{2+} solution, the 1st and 2nd derivatives of the curve. Plateau length found by the algorithm described above is shown by the markers. The plot obtained is shown in Fig. 2.

When using short plating times (60 s) and the concentrations of determined metals ($10^{-9}..10^{-8}$M) in the cell are small, the plateaus canbe easily identified. However, background subtracting from the obtained curve should be used to obtain correct results. Alas, this is not foreseen yet and must be worked out. On the recorder similar curves cannot be detected.

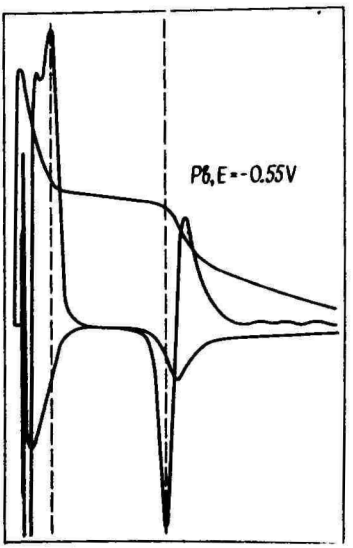

Fig.1. Stripping curve for $2.4 \cdot 10^{-6}$M Pb^{2+} solution. Computer screen reproduction.

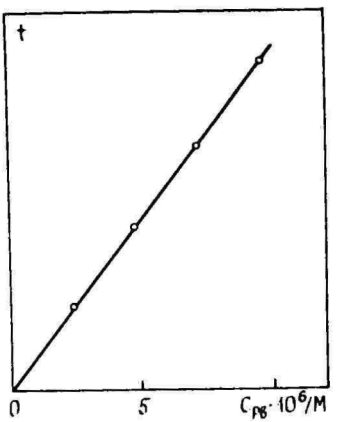

Fig. 2. Stripping time vs concentration for Pb^{2+} ions. Standard additions of $4.85 \cdot 10^{-5}$ $Pb(NO_3)_2$ are made by 200 μl steps.

REFERENCES

1. **D. Jagner and A. Graneli.** Anal. Chim. Acta, 83 (1976) 19.
2. **A. Cladera et al.** Talanta, 37 (1990) 689.
3. **L. Renman et al.** Anal. Chim. Acta, 188 (1986) 137.
4. **J. Mortensen et al.** Anal. Chim. Acta, 103 (1978) 379.

AMPEROMETRIC SENSOR WITH IMMOBILIZED BACTERIA

K. Orupõld, A. Mashirin, T. Tenno
Institute of Physical Chemistry, University of Tartu

ABSTRACT

Microbial sensors based on an oxygen sensor have been studied. The used differential device includes an amperometric bacterial sensor specific for glucose, based on *Pseudomonas putida PAW* 85 immobilization into agarose gel and a compensating oxygen sensor. A theoretical model of the microbial sensor based on a Clark type oxygen sensor has been developed.

INTRODUCTION

In recent years more and more microbial cells as an alternative for enzymes have been used in selective sensors because of several advantages e.g. the elimination of extraction and purification procedures, multistep transformation, increased stability [1].

In the studied sensors the organic compound is metabolized by immobilized bacteria and their oxygen consumption is measured amperometrically.

The oxygen transport in the biosensor, taking into account the continuous character of the oxygen fluxes at the interface between different membranes is showed in figure 1. The shceme is based on the model of the oxygen sensor introduced by T. Tenno et al [2]. The oxygen decrease in the bacterial layer is nonlinear due to the oxygen consumption in the enzymatic reactions. This decrease can be described by solving equation of diffusional flows for the elementary volume in layer "b". Taking into consideration a model of the oxygen sensor and the agarose membranes with an enzymatic reactions occuring there, the steady state oxygen flow to the cathode j_k is the following:

$$j_k = \frac{c_e - j_b\left(\frac{l_o}{P_o} + \frac{l_b}{2P_b}\right)}{\frac{l_s}{P_s} + \frac{l_m}{P_m} + \frac{l_b}{P_b} + \frac{l_o}{P_o}}, \quad (1)$$

where c_e – effective concentration of oxygen; j_b – density of the oxygen flow consumed by bacteria; l_s, l_m, l_b, l_o – thickness of the electrolyte layer, membrane of oxygen sensor, bacterial membrane and external membrane; P_s, P_m, P_b, P_o – permeability of the electrolyte layer, membrane of oxygen sensor, bacterial membrane and external membrane.

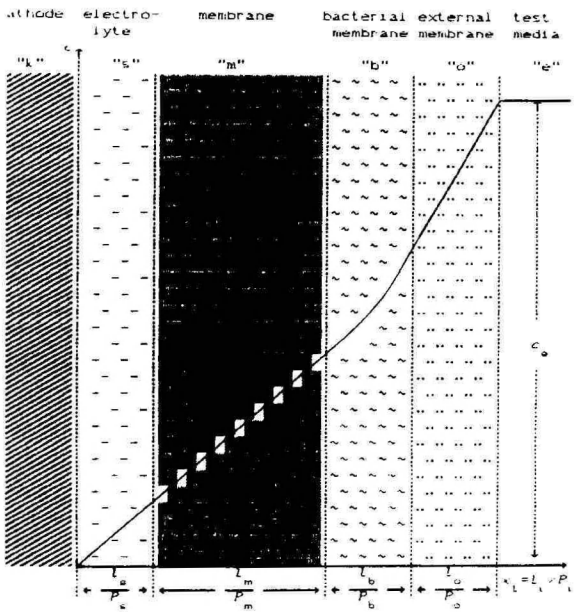

Fig. 1. The steady state of the oxygen distribution for the diffusional layers of microbial sensor. $x_i = l_i/P_i$ – effective thickness of diffusional layer.

Since an output current of the sensor I is determined by the equation

$$I = nAFj_k \quad (2)$$

the current of the sensor is proportional to the oxygen consumption by bacteria.

Figure 2 shows the steady state for the flow of glucose. According to the Fick's equation the density of the diffusional flow of glucose can be written as:

$$j_g = \frac{c_{g_o} - \bar{c}_{g_b}}{\frac{l_b}{2P_b'} + \frac{l_o}{P_o'}}, \tag{3}$$

where c_{g_o} – effective concentration of glucose; $\bar{c}_{g_b}$ – the average concentration of glucose in layer "b".

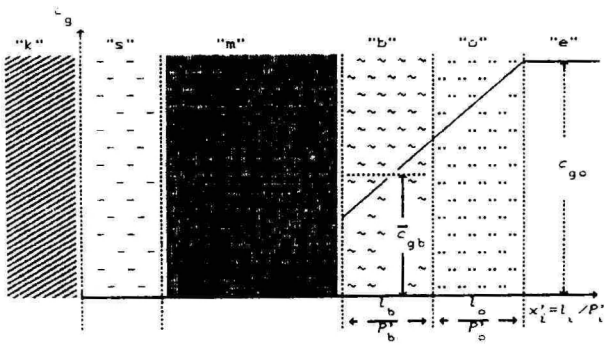

Fig. 2. The steady state of the substrate flow.

The density of the flow of glucose consumed by bacteria j_{g_b} can be expressed with the aid of the Michaelis-Menten type of equation, additionally taking into consideration the possibility to have a relatively high concentration of bacteria:

$$j_{g_b} = \frac{kc_b\bar{c}_{g_b}l_b}{c_b + \bar{c}_{g_b} + K_M}, \tag{4}$$

where K_M and k have the usual meanings; c_b – the concentration of bacteria in the agarose membrane.

Equations (3) and (4) result the following equation for the $\bar{c}_{g_b}$

$$\bar{c}_{g_b} = -\frac{p}{2} \pm \sqrt{\left(\frac{p}{2}\right)^2 - q}, \tag{5}$$

where

$$p = \left(\frac{l_b}{2P_b'} + \frac{l_o}{P_o'} \right) k c_b l_b + c_b + K_M - c_{go} , \tag{6}$$

$$g = -(c_b + K_M)\, c_{go} . \tag{7}$$

An output signal of the sensor can be given by:

$$\delta I_g = \frac{I_o - I}{I_o} , \tag{8}$$

where I_0 is the biosensor response without glucose.

It follows from equations (1) and (2) that the output signal is therefore:

$$\delta I_g = \frac{j_b}{c_o} \left(\frac{l_b}{2P_b} + \frac{l_o}{P_o} \right) . \tag{9}$$

When oxygen is presented in a sufficient excess its consumption can be related to the concentration of glucose by the stoiciometric coefficient of the glucose oxidation reaction:

$$j_b = x_{o_2} j_g . \tag{10}$$

In steady state $j_b = j_{g_b}$, thus the equation (10) may be written as:

$$j_b = x_{o_2} j_{g_b} . \tag{11}$$

Taking into account equation (11), an output signal δI_g is then:

$$\delta I_g = x_{o_2} \frac{j_{g_b}}{c_e} \left(\frac{l_b}{2P_b} + \frac{l_o}{P_o} \right) . \tag{12}$$

EXPERIMENTAL

The bacteria *Pseudomonas putida PAW* 85 were grown under aerobic condition at 30°C in a glucose containing medium. Before immobilization the bacteria were centrifuged, washed twice and resuspended in phosphate buffer (pH 7.2). A bacteria-agarose membrane

was prepared from a mixture of the 2 % agarose solution and of bacterial suspension at 36°C. The mixture was put on a Clark type oxygen sensor designed at Tartu University. The bacterial membrane was covered with agarose gel.

The tested glucose solutions (in phosphate buffer pH 6.86) were stirred and saturated with air. All measurements were carried out at temperature 25°C in a volume 200 ml.

The experiment was made using a differential device to eliminate the possible effects of oxygen variation. This glucose sensitive device included a biosensor consisting of a sensor on which bacteria have been immobilized and a compensating sensor covered with a nonbacterial agarose membrane. The difference of stabilized outputs was recorded at different concentrations of glucose in test media.

RESULTS

The relative change of the current of a microbial sensor $(I_0 - I)I_0$, where I_0 is the biosensor response in the absence of glucose, was observed as a output signal of the sensor. This signal was studied as a function of the glucose concentration. It was linear in the glucose concentration range of 10^{-5} -1.6×10^{-4} mol/l. At the higher concentrations the dependence was nonlinear having no meaning for the analytical measurement of the organic substrate. To find out the general shape of the above said dependence was important for the modelling of microbial sensors and investigation of characteristics.

Figure 3 shows the results by using sensors with different thicknesses of layer "o". It appeared, that the linearity range can be shifted by the variation of thickness and diffusional characteristics of membranes. The decrease in the rate of external diffusion resulted in a broadering of the range of glucose concentration for which the sensor has a linear dependence of the signal on the glucose concentration.

The curves depicted in figure 4 for repetition after one and four weeks illustrate the stability of sensors obtained with this arrangement.

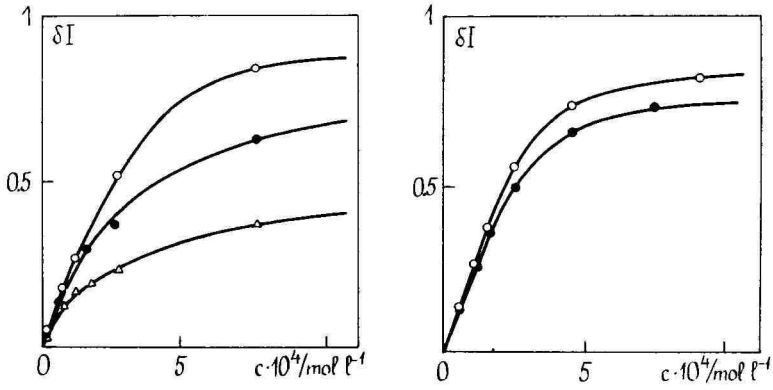

Fig. 3. The dependences of the stabilized response of microbial sensor on the glucose concentration at different thicknesses of external agarose membrane. Δ - l_1, ● - l_2, ○ - l_3, where $l_1 < l_2 < l_3$.

Fig. 4. Stability of the response of microbial sensor ○ - repeated after 1 week, ● - repeated after 4 weeks.

CONCLUSIONS

On the basis of experimental data and created theoretical model it should be possible to optimize and improve the characteristics of the sensor with changing its designing features.

We started with the sensor specific for glucose having in mind the potential interest of obtaining sensors for environmental monitoring. The amperometric sensors with different immobilized microbes represent a promising tool for analytical procedures. Using the same method the sensors for several other compounds can be developed.

AKNOWLEDGEMENT

The authors thank the Estonian Science Foundation for financial support of this work and the Institute of Molecular and Cellbiology of Tartu University for providing bacteria.

REFERENCES

1. **Riedel, K., Renneberg, R., Wollenberger, U., Kaiser, G., Scheller, F. J.** Chem. Tech. Biotechnol., 44 (1989) 85.
2. **Tenno, T.T., Mashirin, A.A., Past, V.E.** Dvoynoy Sloy i Adsorbtsya na Tverdykh Elektrodakh., 7 (1985) 320.

INVESTIGATION OF THE OUTPUT SIGNAL TEMPERATURE DEPENDENCE OF SOME pH AND AMMONIA SENSORS

M. Arulepp, V. Loodmaa, A. Tüür
Institute of Physical Chemistry, University of Tartu

ABSTRACT

The temperature dependence of the output signal of pH and ammonia sensors causes the need to use constant temperature measurements or temperature compensators. For using the sensors at different temperatures or constructing temperature compensators it is necessary to know exact values of output signal temperature dependences. Temperature dependences of the potentials of two type glass electrodes and output signals of sensors, which were built on the base of these electrodes, have been investigated in this work.

The temperature dependence of the output signal of the potentiometric sensors and its compensation are very aggravating problems. The temperature dependence of a sensor consists of the dependences of its parts: a glass electrode, the buffer solution and a silver-silver chloride reference electrode. The most important and complicated of them is the temperature dependence of the potential of the glass electrode. The potential of the glass electrode E depends on solution pH by the Nernst equation

$$E=E^0+\frac{RT}{F}2.3pH.$$

If the standard potential E does not depend on temperature, the dependence of E will be determined by 2.3RT/F. The standard potential of the glass electrode consists of some parts:

$$E^0 = E^{0'} + E_{dif} + E_{in},$$

where $E^{0'}$ is the asymmetric potential, E_{dif} is the diffusion potential and E_{in} is the potential of inner reference electrode. The values $E^{0'}$ and E_{dif} depend on temperature. The dependence of E on temperature is given by the equation (1)

$$E = f(T^2)$$

So the glass electrode has some temperature dependence even under isopotential conditions. The temperature of the sensor parts may be different. This temperature difference causes a potential difference and an output signal change during considerable time.

The dependence of the output signal of two types of class electrodes, a pH sensor and an ammonia sensor on temperature has been studied. The bulb shaped end electrodes from Gomel were used to construct pH sensors and the plane glass membrane electrodes from St. Petersburg University were used in ammonia sensors. Reference electrodes were silver silver chloride electrodes in 0.1 M KCl solutions. Glass electrodes and pH sensors had been investigated in standard buffer solutions with pH values 1.08; 1.68; 4.01; 6.86; 9.18 and ammonia sensors in 0.01 M NH_4Cl solution and in the sample which consists of 1 mg NH_3 per litre. Eight glass electrodes and five sensors had been studied. The average results are presented on Fig. 1 and in Table.

As it can be seen from the presented data, the potential values of glass electrodes were not exactly 0 even under iso-pH conditions, although the slopes of E, pH-curves were in agreement with the Nernst equation.

The investigation of constructed pH sensors shows full agreement with the glass electrodes data (Fig. 1). If the inner solution pH was 4.01, the temperature coefficients of the pH sensors output signals were 0.34; 0.29; 0; 0.50 and -0.87 $mV \cdot K^{-1}$ if the outer solution pH values were 1.08; 1.68; 4.01; 6.86 and 9.18 correspondingly. By the interpretation of these results one must take into consideration the dependence of the pH values of buffer solutions on temperature which is the greatest in case of the borax buffer solution [1].

Table

The differences of output signals ($E_{35°}$–$E_{15°}$) of St. Petersburg University electrodes in the temperature region of 15–35°C

pH in electrodes	$E_{35°}$–$E_{15°}$, mV			
	1.68	4.01	6.86	9.18
1.68	-3	-15	-23	-32
4.01	+3	-3	-16	-22
6.86	+14	+8	-4	-8
9.18	+22	+5	-1	-3

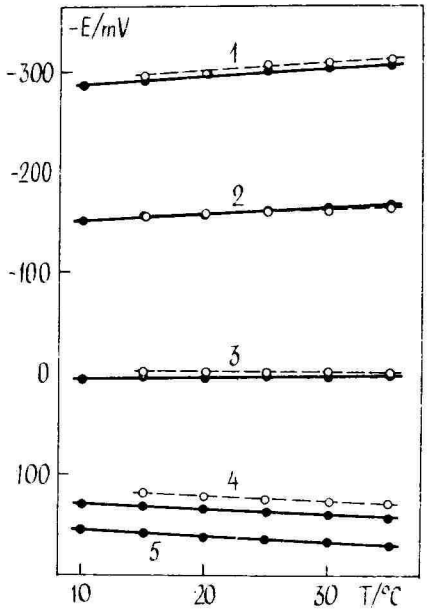

Fig. 1. The dependences of potentials of the glass electrodes on temperature. pH value in glass electrodes is 4.01. pH values of outer solution are: 1–9.18; 2–6.86; 3–4.01; 4–1.68; 5–1.08. The continuous line – Gomel electrode; the interrupted line – Petersburg electrode.

The constructed and investigated ammonia sensors had a buffer solution with pH value 4.01 inside glass electrodes and 0.01 M NH_4Cl solution iside the sensor. Both solutions contained 0.1 M KCl. The construction of sensors and some data have been published earlier [2, 3].

If the ammonia sensor is immersed in 0.01 M NH_4Cl solution, the dependence of the output signal on temperature is about 0.025 $mV \cdot K^{-1}$. Such small dependence is connected with two effects. If the pH value of the outer solution is higher than inside the class electrode, the glass electrode potential value turns more negative with the rise of the temperature. The pH value of 0.01 M NH_4Cl solution at 25°C is 5.73. On the other hand, the pH value of 0.01 M NH_4Cl solution diminishes 0.4 units with the temperature growing from 15°C to 35°C. The last effect causes the change of the glass electrode potential towards less negative values.

If the ammonia sensor is immersed in solution where the NH_3 content is 1 $mg \cdot l^{-1}$, the sensor's output signal temperature coefficient in the range 15-35°C is 2.1 $mV \cdot K^{-1}$. So a great change of the signal to less negative values is connected with the diminishing pH of the solution from 7.54 to 6.84 if the temperature grows from 15°C to 35°C. The change of the class electrode's potential to more negative values (Fig. 1) cannot compensate for the effect of the pH change of the buffer solution.

When the sensor and sample temperatures are different, the sensor signal changes during a long time, because the different parts of the sensor have different temperatures. The investigated sensor's output signal was stabilized during one hour, if the sample temperature changed ten degrees. After about 10 minutes the signal had the extreme value. If the sample was 0.01 M NH_4Cl solution, the rising of temperature by 10°C caused a 10-15 mV shifting of the output signal to more negative values, which can be explained by the shifting of the NH_3/NH_4^+ balance to the left and the diffusing of a complementary amount of ammonia into the sensor. When the temperature was lowered by 10°C, the change of the signal was smaller.

When the temperature of the solution which consists of 1 mg NH_3 per litre was changed, the sensor's output signal change was contrary to the situation in NH_4Cl solution. The result of one experiment can be seen from Fig. 2.

The sharp minimum on curve 2 can be explained by the diffusion of NH_3 from the sensor into the solution because of the gas solubility growth with the lowering of temperature. If the temperature inside the

sensor lowers during 10-15 min, the potential of the glass electrode and the sensor's output signal will shift to more negative values .

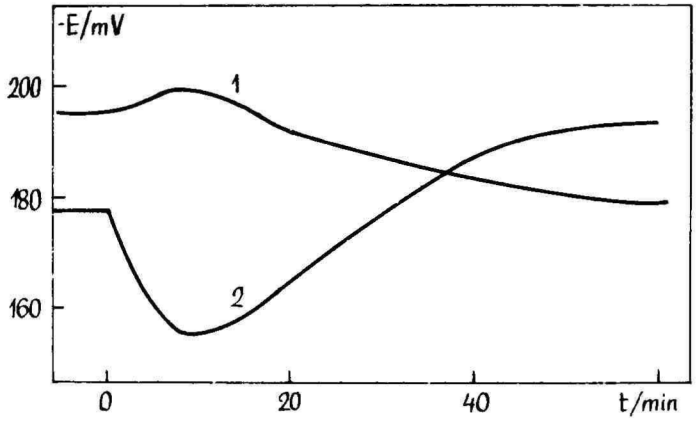

Fig. 2. The change of ammonia sensor's output signal in the solution, which consists of 1 $mg \cdot l^{-1}$ NH_3. 1 – the temperature changes from 15 to 25°C; 2 – the temperature changes from 25 to 15°C.

REFERENCES

1. **N. Linnet.** pH Measurements in Theory and Practice, Radiometer A/S. Copenhagen 1970.
2. **M. Arulepp, A. Tüür, V. Loodmaa.** Trans. Tartu Univ., 905 (1990) 127.
3. **V. Loodmaa, M. Arulepp, A. Tüür.** Double Layer and Adsorption at Solid Electrodes IX, Extended Abstracts, Tartu, 1991, p. 104.

DYNAMIC MODEL OF GASEOUS MIXTURE

T.Tenno, A.Mashirin
Institute of Physical Chemistry, University of Tartu

ABSTRACT

Equilibrium state of a gaseous component in a gaseous mixture is described as a process of conservation of the average kinetic energy of a molecule. The model is derived on the bases of the kinetic-molecular theory of the ideal gases. The conception of the conservation of momentum and average kinetic energy of colliding molecules before and after collision is taken as a bases. It is shown that the average kinetic energy of each gas in the mixture is not equal. The basic concepts of Dalton's law of partial pressures is discussed.

Let us examine the mixture of ideal gases A and B. When two molecules collide, the interaction between them has an effect on the direction of the normal components of velocities v_{an} and v_{bn} (figure 1). The tangent components of velocities v_{at} and v_{bt} conserve their initial values:

$$v'_{at} = v''_{at}, \qquad v'_{bt} = v''_{bt}, \tag{1, 2}$$

where v'_{at} and v''_{at} are the tangent components of the velocity of molecule A before and after collision, v''_{bt} and v''_{bt} are the tangent components of the v
elocity of molecule B before and after collision.

In the case of the elastic collision of two molecules, the energy and momentum of the molecules are generally changed. At the same time the total kinetic energy and momentum of the two particles are conserved and we can write for the normal components of velocity [1]:

$$m_a v'_{an} - m_b v'_{bn} = m_b v''_{bn} - m_a v''_{an}, \tag{4}$$

$$\frac{m_a v_{an}^{/2}}{2} + \frac{m_b v_{bn}^{/2}}{2} = \frac{m_a v_{an}^{//2}}{2} + \frac{m_b v_{bn}^{//2}}{2}, \qquad (3)$$

where m_a and m_b are masses of the molecules of gases, $v_{an}^{/}$ and $v_{an}^{//}$ are the normal components of the velocity of molecule A before and after collision, $v_{bn}^{/}$ and $v_{bn}^{//}$ are the normal components of the velocity of molecule B before and after collision.

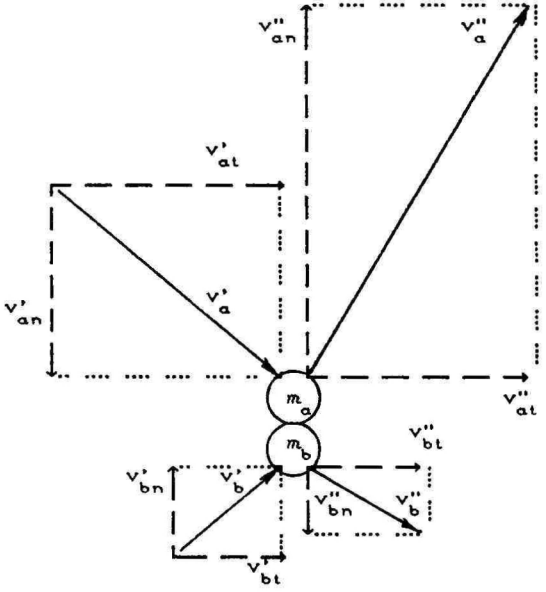

Fig. 1. Schematic representation of an elastic collision between two molecules A and B: where $v_a^{/}$ and $v_b^{/}$ - velocities of molecules befor collision; $v_a^{//}$ and $v_b^{//}$ - velocities of molecules after collision.

The conservation of the kinetic energy and momentum of molecules by collision is essentially a process of their reproduction. The redistribution of kinetic energy and momentum between molecules by collision is determined by the relation of masses and the initial velocities of the colliding molecules.

Solving together equations 3 and 4 we get the following equations for the normal component of velocities of the colliding molecules:

By the individud collision of two molecules of different gases, the transfer of energy from molecule A to B or in the opposite direction is

$$v''_{an} = \frac{2v'_{bn} + v'_{an}(1 - m_a/m_b)}{1 + m_a/m_b}, \tag{5}$$

$$v''_{bn} = \frac{2v'_{an} + v'_{bn}(1 - m_b/m_a)}{1 + m_b/m_a}, \tag{6}$$

possible. The condition of the state of energetic equilibrium of two gases in the gas mixture is a process of equilibrial exchange of energy between their molecules. Ideal from that point wiev is the case when by the collision of two molecules each of them conserves the previous kinetic energy and momentum.

$$E'_a = E''_a = E_a, \qquad E'_b = E''_b = E_b, \tag{7}$$

where E'_a and E''_a is the energy of molecule A before and after collision, E'_b and E''_b is the energy of molecule B before and after collision, E_a and E_b is equilibrial values of the energy of molecules.

The tangent components of the energy of molecules for both gases are conserved because the corresponding values of the velocities do not change. Therefore, after the collision the former values of the normal components of the energy of molecules must be conserved:

$$E'_{an} = E''_{an}, \qquad E'_{bn} = E''_{bn} \tag{8}$$

where $E'_{an} = m_a v'^2_{an} / 2$, $E''_{an} = m_a v''^2_{an} / 2$, $E'_{bn} = m_b v'^2_{bn} / 2$ and $E''_{bn} = m_b v''^2_{bn} / 2$ normal components of the energys E'_a, E''_a, E'_b, E''_b correspondingly.

In the equilibrium state, the modulus of the normal components of velocities before and after collision has to reproduce, i.e. to be equal:

$$v'_{an} = v''_{an}, \qquad v'_{bn} = v''_{bn}. \tag{9}$$

Under the conditions 9 from equations 5 and 6 it follows that the ratio of normal components of the velocities of different gases had to be inversely proportional to the ratio of their masses:

$$\frac{v'_{an}}{v'_{bn}} = \frac{m_b}{m_a}, \qquad \frac{v''_{an}}{v''_{bn}} = \frac{m_b}{m_a} \tag{10}$$

We have to mention that the tangent direction of the pair of

molecules under examination by collisions with other molecules may have a normal component. Therefore, the conditions of reproducibility will extend also to the tangent components of the velocity for whole gas mixture. At that the reproduced normal and tangent components of energy of molecules inversely proportional their masses. The result of the composition of normal and tangent components the total reproduced energy of a pair of molecules of different gases in the mixture also inversely proportional to their masses.

$$\frac{E_a'}{E_b'} = \frac{m_b}{m_a}, \qquad \frac{E_a''}{E_b''} = \frac{m_b}{m_a}, \qquad \frac{E_{ae}}{E_{be}} = \frac{m_b}{m_a} \tag{11}$$

Let us consider a gas system containing a large number of particles N_a and N_b. We can assume that the condition of energy conservation for a pair of molecules will also extend to the ratio of the average kinetic energy of the molecules of these gases. Therefore, the average kinetic energies of different gases in the mixture are inversely proportional to the masses of molecules:

$$\bar{E}_a / \bar{E}_b = m_b / m_a, \tag{12}$$

where $\bar{E}_a = m_a\bar{v}_a^2 / 2 = \frac{3}{2}kT_a$ *and* $\bar{E}_b = m_b\bar{v}_b^2 / 2 = \frac{3}{2}kT_b$ are the average kinetic energies of cases A and B; $\bar{v}_a$, $\bar{v}_b$ are the mean square velocities of the molecules; k is the Boltzmann constant; T_a, T_b are the temperatures of cases A and B.

Consequently, the condition of the internal energetic equilibrium of a gaseous mixture is an additional dispersion of the kinetic energy of molecules being inversely proportional to their masses. At that the average kinetic energies and temperatures of the gases are not equal and differ from their values before mixing (i.e. they were equal before mixing).

The obtained deduction on the dispersion of the average kinetic energies of molecules of different gases contradicts the general (universal) application of the representation of the equal average kinetic energy and equal temperature of gases in the gaseous mixture.

The average energy of gas molecules on their mixing is determined by the law of conservation of the energy:

$$n_a\bar{E} + n_b\bar{E} = n_a\bar{E}_a + n_b\bar{E}_b \,, \tag{13}$$

where $\bar{E} = \frac{3}{2}kT$ is the average kinetic energy of the given gas before mixing; T is the temperature of gases before mixing; $n_a = N_a / V$, $n_b = N_b / V$ are the concentrations of molecules of cases A and B in the volume of gas mixture V.

The left part of equation 13 gives us the sum of energies of gas molecules before mixing and the right part - after it. When solving equations 12 and 13 together, we can get the expressions for the average energies of gas molecules:

$$\bar{E}_a = \frac{\bar{m}_{ab}}{m_a} \times \bar{E} \,, \qquad \bar{E}_b = \frac{\bar{m}_{ab}}{m_b} \times \bar{E} \,, \tag{14}$$

where $\bar{m}_{ab} = (n_a + n_b) / (n_a/m_a + n_b/m_b)$ is the average of the molecule mass of the sa called "hypothetic mean molecule" of the two gases mixed.*

Equations 13-14 are describing the redistribution of the average kinetic energies between gases after their mixing in the equilibrium state of the average momentum:

$$m_a\bar{v}_a = m_b\bar{v}_b, \tag{15}$$

where $\bar{v}_a$ and $\bar{v}_b$ are the average velocities of gas molecule.

The average energy of the "mean molecule" of a gas mixture could be expressed as follows:

$$\bar{E}_\Sigma = (n_a\bar{E}_a + n_b\bar{E}_b) / (n_a + n_b) \tag{16}$$

When replacing average energies $\bar{E}_a$ and $\bar{E}_b$ to equation 16, we can see the equality of the energies of all gases before mixing to the average energy of the "mean molecule" of the gas mixture.

While the energy of gas molecules is determines their temperature,

---

* In a general case, the equation of the mass average for a mixture can be expressed:

$$\bar{m} = \sum n_i / \sum (n_i / m_i) \,,$$

where n_i and m_i are correspondingly the concentration and mass of gas i; $6i = a, b, \ldots$ is the notation of gases.

$$\bar{E}_{\Sigma} = \bar{E} \tag{17}$$

we can calculate the temperatures of gases in mixtures T_a and T_b, as well as the average temperature T_{Σ} by analogous equations:

$$T_a = \frac{\bar{M}_{ab}}{m_a} \times T, \qquad T_b = \frac{\bar{m}_{ab}}{m_b} \times T \tag{18}$$

$$T_{\Sigma} = \frac{n_a T_a + n_b T_b}{n_a + n_b} \tag{19}$$

The average temperature of a gas mixture is equal to the temperature of gases before mixing:

$$T_{\Sigma} = T \tag{20}$$

Only the average temperature of a gas mixture is measured in the experiment, so we concluded that all the gases preserved their own temperatures they had before mixing. The concept of the additional dispersion of the average energy and temperature of a gas mixture according to the single gases parameters needs coordination with the specifications of Dalton's law. Dalton's law in its classical redaction has the form: "the whole pressure of a gas mixture is equal to the sum of partial pressures of the mixed components". In this redaction, the partial pressure of a gas is defined as the pressure this gas component can influence if it has the same volume V that the whole gas mixture has (i.e. the a single gas from the mixture behaves as "monogas", one-component gas) [2, 3]. At the base of this redaction of Dalton's law lies the presumption of the uniform temperature T for a single gas, being both alone in the volume V and in a mixture with other gases.

The partial pressure of a gas in the observable case can be expressed by the equation of the gas state for a single gas:

$$p_a = n_a k T_a, \qquad p_b = n_b k T_b \tag{21}$$

where p_a and p_b are the partial pressures of gases A and B.

As shovn above, the temperature of a gas in the mixture is a function of the ratio of masses of different gas molecules. According to equation 18 of temperatures T_a and T_b we can express the partial pressures as follows:

The acquired expressions of partial pressures of gases in gas

$$p_a = n_a k \times \frac{\bar{m}_{ab}}{m_a} \times T, \qquad p_b = n_b k \times \frac{\bar{m}_{ab}}{m_b} \times T \qquad (22)$$

mixtures differ from their conventional forms, because they take into account the additional dispersion of energy and temperature which are caused by the mass ratios of different gases. Those expressions do not contradict the classical redaction of Dalton's law, because the sum of the partial pressures of gases in the mixture will be equal to the sum of their pressures when they are as monogases before mixing:

$$p_a + p_b = \left(\frac{n_a}{m_a} + \frac{n_a}{m_b} \right) \times \bar{m}_{ab} kT = n_a kT + n_b kT = p_a' + p_b' \qquad (23)$$

where p_a' and p_b' are the partial pressures of gases before mixing.

Consequently, the quantity of the "partial pressure of a gas" can be observed beyond the quantities of partial molar values which are depend only on the amount of the substance, because the quantity of the partial pressure depends on the energy of this substance as well. We have to mention also that Dalton's law has no "retroaction". The fact that the sum of the partial pressures of gases in a mixture is be preserved, we could not draw the opposite conclusion that every partial pressure for a gas as a "monogas" is its value.

Conclusions

1. Observation of the laws of conservation of the momentum and energy of molecules in a gas mixture can be made with the additional dispersion of energy of molecules and the temperature of gases in the mixture which is inversely proportional to their masses of molecules. The temperatures of single gases will have their own values, differing from the average temperature of the gas mixture.
2. On the dispersion of the temperature of gases in the mixture, the ratio of the partial pressures of gases will differ from the ratio of mole fractions of gases in the mixture.
   The partial pressure for the given gas is a function of the mole fractions and masses of all gases in the mixture. The standpoint of Dalton's law which says that the partial pressure of a gas is proportional to its mole fraction in the gas mixture, can be reobserved.

REFERENCES

1. **Yavorsky B.M., Detlaf A.A.** Spravochnik po fizike. M.: Nauka, 1979, p.p.43,67-69.
2. **Belikov P.N.** Fiziczesky slovar, T.2. M.: ONTY NKTP, 1937, p.30.
3. **Atkins P.W.** Physical Chemistry, 4 ed. Oxford.: Universiy press, 1990, p.11.

FACTORS AFFECTING THE EQUILIBRIUM DISTRIBUTION OF A GASEOUS COMPONENT IN A HETEROGENOUS SYSTEM

A.Mashirin, K.Hellat, T.Tenno
Institute of Physical Chemistry, University of Tartu

ABSTRACT

Parameters of the state of gas mixtures determining the equilibrium distribution of a gaseous component in the two- phase system will be observed. The kinetic theory of ideal gases, which considers the difference in kinetic energies of molecules caused by the difference of masses of gas molecules, is used as a basis for the model describing of the state of a component in the gas mixture. The effect of the concentration of a gaseous component to the equilibrium distribution between phases will be grounded. The main standpoints of Henry-Dalton's law are discussed.

The system under examination consists of two phases, one of which is the mixture of ideal gases A and B. We assume the average kinetic energies of gas molecules A and B and their temperatures to be inversely proportional to their masses [1]. This assumption of the difference of average kinetic energies of different gases in the mixture is in contradiction with the well-known standpoint about the equality of their energies. A ground for our assumption is the conservation of average kinetic energies of different components in a gas mixture [1].

Taking the above-mentioned assumption into account, we can express the partial pressures of components A and B (p_a and p_b) from the gas state equation, [1]:

$$p_a = n_a k T_a, \qquad p_b = n_b k T_b, \tag{1}$$

where $n_a = N_a / V$ and $n_b = N_b / V$ are the concentrations of molecules of components A and B in the volume of gas mixture V; N_a and N_b are the numbers of molecules of components A and B

respectively in the volume of gas mixture V; k is constant of Boltzmann; T_a and T_b are temperatures of components A and B.

By the complementary distribution of the average kinetic energies of molecules there is the dependence of temperatures of gaseous components A and B on the masses of their molecules, m_a and m_b and also upon their concentrations [1]:

$$T_a = \frac{\overline{m}_{ab}}{m_a} \times T \qquad T_b = \frac{\overline{m}_{ab}}{m_b} \times T, \tag{2}$$

where $\overline{m}_{ab} = (n_a+n_b) / (n_a/m_a + n_b/m_b)$ is average of the mass of a hypotetic "mean molecule" of the two-component gas mixture; T is the temperature of components before their mixing.

Taking into account the additional dispersion of temperature in the gas mixture, the expressions for partial pressures considering the ratio of the masses of components are as follows:

$$p_a = n_a k \times \frac{\overline{m}_{ab}}{m_a} \times T, \qquad p_b = n_b k \times \frac{\overline{m}_{ab}}{m_b} \times T, \tag{3}$$

By the difference of the masses of molecules ($m_a \neq m_b$) the ratio of partial pressures of gases A and B is not equal to the ratio of molar fractions (n_a/n_b):

$$\frac{p_a}{p_b} = \frac{n_a}{n_b} \times \frac{m_b}{m_a} \neq \frac{n_a}{n_b} \tag{4}$$

It is in contradiction with Dalton's law according to which the ratio of partial pressures can be expressed:

$$\frac{p_a}{p_b} = \frac{n_a}{n_b} \tag{5}$$

and is not depending on the difference of the masses of molecules of gases.

The Henry-Dalton law about the equilibrium distribution of a gas component between two phases - gaseous and liquid has many well-known redactions. In the source [2] we can find it formulated with some probability degree:

"The partial pressure of a gas, being in the equilibrium with the solution of itself, is commonly proportional to the concentration of the same gas in the solution":

$$p_i = k_h c_i, \tag{6}$$

where p_i is partial pressure of a component in the gaseous phase; k_h is Henry's coefficient; c_i is equilibrium concentration of the component in the solution.

All redactions of Henry-Dalton's law use the concept of partial pressure. By discrepancy between partial pressure and mole fraction of a gas component in the gas mixture, we have to answer the question what is the contribution of the partial pressure to the formation of equilibrium concentration of gas in the liquid phase. When the physical factor of the solution of oxygen is directly its partial pressure, we would get the smaller oxygen concentration in the solution dissolving oxygen from the air than the same dissolving it from pure oxygen.

The calculated value of the partial pressure of air oxygen in standard conditions (air containing 20,94 volume % of oxygen, t = 20°C, atmospheric pressure 101325 Pa and the humidity of air α = 100%) taking into account the additional dispersion of temperature and kinetic energy of molecules is p_{02} = 18692 Pa. When calculating the partial pressure of oxygen under the same conditions from the oxygen mole fraction data in the air, we will get p_{02} = 21217 Pa. Consequently, when oxygen is dissolved from the air, the concentration of oxygen in water would be nearly 13% lower, compared to the concentration we get upon dissolving pure oxygen from the gaseous phase which contains oxygen in the same quantity of moles per unit of volume as in the air.

More lower solubility of oxygen in water we assumed to measure when oxygen is dissolved from the helium-oxygen gaseous mixture. We prepared two different mixtures with the same oxygen content (20% mole fraction): one with helium and the other with nitrogen and examined the solubility of oxygen from these gas mixtures in water. The calculated values of the partial pressures of oxygen under standard conditions (t = 20°C, p = 101325 Pa, α = 100%) in mixtures with helium and nitrogen are accordingly: $p_{02(He)}$ = 3000 Pa and $p_{02(He)}$ = 17500 Pa.

So we will get the difference in the concentration of oxygen about 6 times if the solubility is determined by the partial pressure of oxygen in the gas mixture and in pure gas. The experimental data of oxygen solubility from mixtures with helium and nitrogen showed the

differences in solubilities not exceeding the values of estimation error.

We also examined the effect of the partial pressure of oxygen from the mixtures nitrogen-oxygen and helium-oxygen (with the oxygen content of 20% mole fraction) on the output signals of a Clark type sensor. Output currents, measured with the sensor in both gas mixtures had the same values, fluctuating only in the limit ranges of measurement error (3–5% from the measured value). So we can suppose that the physical factor affecting the solubility of a gas from the gaseous phase to the membrane surface of the oxygen sensor and causing its output current is not the partial pressure of the gas component but the content (mole fraction) of the gas in the mixture.

Canadian scientists Maharajh and Walkley got a lowering in the solubility of oxygen in water by the presence of a second gas - nitrogen [3]. These results were criticized by Mayers and Quinn [4] and Wilson [5] who showed that the reduction of oxygen solubility ignores a considerable body of literature evidence. The solubility coefficients for oxygen in water obtained over the past eighty years show no significant difference (range about 2,5%) in their values [5]. Taking the above mentioned results into account, we can say that the equilibrium concentration of a gas in the solution is not directly determined by its partial pressure in the gaseous phase but depends on the mole fraction of the component in the gas mixture. The partial pressure in Henry-Dalton's law will be only the measure of the quantity of molecules (concentration) in the gaseous phase.

Henry-Dalton's law as a special case for the gas-liquid system may be written in the general form of Henry's law: two different phases containing of the molecules of component under investigation and having the equilibrium state between the phases at the constant temperature will have a constant concentration ratio not depending on the concentration values.

Conclusions.

1. Conception about the additional energy and temperature dispersion of gaseous components in the gas mixture needs the corresponding coordination with Henry-Dalton's law.
2. Physical substance affecting the equilibrium distribution of a gaseous component between the gaseous and liquid phases is concentration.

3. Henry's law may correspond to the distribution of a gas component in the heterogenous system proportional to the concentration of the gas in the gaseous mixture. The partial pressure of a gas in the gaseous phase is only the measure of its concentration.
The standpoint of the use of partial pressure as an acting factor of the equilibrium state in Henry's law must also be revalued.

REFERENCES

1. **Tenno T., Mashirin A.** Acta et Comm. Univ. Tartuensis, 966 (1993) 133.
2. **Moelwyn-Hughes E.A.** Physical Chemistry, 1961. M.:Izd.inostr.lit., 1962, p.684.
3. **Maharajh D.M., Walkley J.** Lowering of the Saturation Solubility of Oxygen by the Presence of Another Gas. Nature, 236 (1972) 165.
4. **Myers A.L., Quinn J.A.** Applicability of Henry's Law: An Analysis of the Data of Maharajh and Walkley. Nature, 239 (1972) 32.
5. **Wilson T.R.S.** Lowering of the Saturation Solubility of Oxygen by the Presence of Another Gas. Nature, 239 (1972) 31.

MULTI-ELEMENT ANALYSIS BY INDUCTIVELY COUPLED PLASMA ATOMIC EMISSION SPECTROMETRY

L. Paama[a], L. H. J. Lajunen[b], P. Perämäki[b]
[a]Institute of Chemical Physics, University of Tartu,
[b]Department of Chemistry, University of Oulu

ABSTRACT

The simultaneous multi-element analyses were carried out using the sequential PU 7000 (Philips) inductively coupled plasma atomic emission spectrometer (ICP-AES). The spectrometer was equipped with a Gilson 221 autosampler and controlled by a Philips P 3230 computer. The determination of nine main and minor elements in geological and ceramic materials were studied. The detection limits for all the elements varied between 0.02 to 0.12 mgdm^{-3} and the relative standard deviation values varied between 0.3 and 3 %.

The multi-element analyses of samples by ICP-AES is generally a simple task. This is due to the versatility of the ICP-AES technique and freedom of chemical interferences. In addition, the use of computers has simplified or even eliminated many of the tasks that were previously required for ICP-AES analysis [1]. A book on the fundamental studies and instrumentations for atomic absorption and atomic emission spectroscopies has been published by professor Lauri H.J. Lajunen [2].

The plasma atomic emission instrument consists of two main units (Figure 1): the signal generator and the signal processor. The signal generator consists of the plasma source and the sample introduction system (an autosampler, a pump, a nebulizer and a tube for sample introduction). The signal processor comprises the optics and electronics and the data acquistion unit [2].

The chief analytical advantages of the ICP over other emission sources are derived from the ICP's ability to vaporize, atomize, excite and ionize efficiently and reproducibly a wide range of elements present in many different sample types. While flames and furnaces have the

upper temperature range in the area of 3000°C, the gas temperature in the centre of the ICP is about 6000°C.

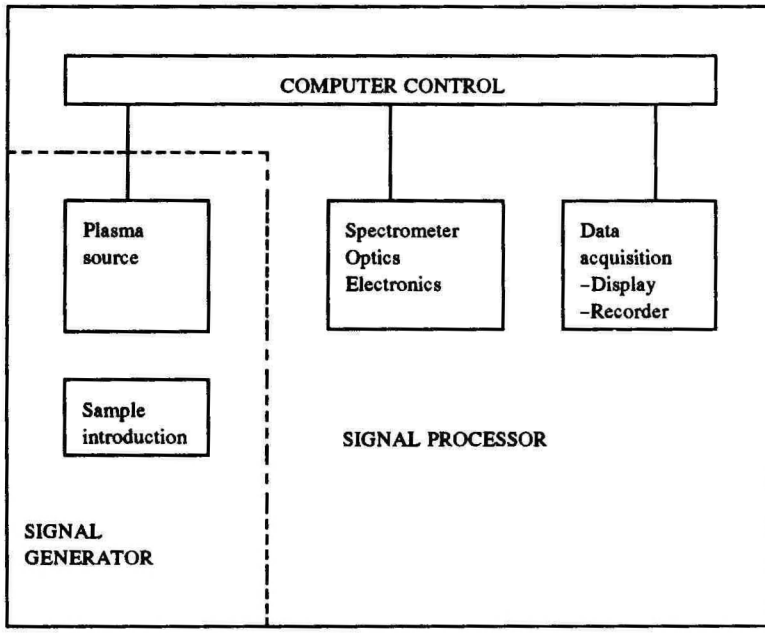

Fig. 1.

Chemical interference are largely eliminated due to high plasma temperature. Physical interferences can be easily compensated for by taking adventage of the ICP's multielement capability. While spectral interferences are the main source of errors in ICP-AES analyses, the use of high-resolution spectrometers and advanced background correction techniques, together with the possibility of using alternative emission lines, allows for interference-free analyses of the majority of samples.

A typical layout of the ICP-AES instrument is shown in Figure 2.

Several papers deal with the effects of different solvents on plasma parameters, mainly temperature, used in sample introduction. The presence of a low concentration of mineral acids decreased emission intensities by decreasing the excitation temperature according to the report of E. Yoshimure and H. Suzuki [4]. The presence of organic acids on the other hand appeared to increase the temperature of the plasma and the emission intensity of the analyte lines [5]. The effects of desolvation were found to be very selective: with aqueous solutions the

results depended on the analyte exitation energy relative to the bond energies of water, and plasma temperature were found to be much more affected when desolvation was applied to organic rather than aqueous solutions [6]. Similar results have been published by Nixon D. [7]. It seems plausible that the intensities of low excitation potential lines remaining nearly constant with desolvation and the intensities of higher excitation potential lines markedly changed, desolvation has a direct effect on the excitation of relevant excitation states even though the atmom population is clearly reduced with desolvation. Desolvation appears not only to affect the atom-ion equilibrium but also the fraction of atoms excited.

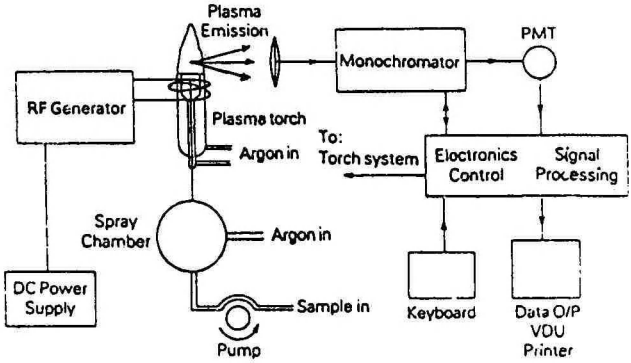

Fig. 2. Schematic diagram of ICP-AES system [3].

The detection limits of the majority of elements are within the range of 0.1–10 μgdm^{-3} and the precision of analysis by ICP-AES is usually within the range a 0.5–2 % RSD (relative standard deviation) [1, 2, 6].

Fusion techniques have been applied fon the dissolution of the geological and ceramic materials: Na_2CO_3 or $K_2CO_3 + H_3BO_3$, $Na_2CO_3 + MgO$ and $Li_2CO_3 + H_3BO_3$ [6, 8, 9].

EXPERIMENTAL

Instrumentation and Reagents. A sequental PU 7000 Philips (Unicam Analytical Systems, Cambridge, England) inductively coupled plasma atomic emission spectrometer (ICP-AES) was used for the measurements. The design of this spectrometer includes a 40.68 MHz free-running oscillator for driving the plasma, an echelle grating for the wavelength separation and a grid nebulizer for sample aspiration. The spectrometer is equipped with a Gilson 221 Autosampler and controlled by a Philips P 3230 computer. The results are printed out by a Philips NMS 1461 printer [10].

The stock solutions, containing 1000 $mgdm^{-3}$ of each element, were prepared using the following reagents (pro analysi, Merck): Al metal, $CaCO_3 \cdot Cu(NO_3)_2 \cdot 2H_2O$, Fe metal, $MgCl_2 \cdot 6H_2O$, $MnCL_2 \cdot 4H_2O$, $Pb(NO_3)_2$ and Zn metal. Commercial standard solution was used for silicon (Art. 19798, Merck). The calibration standards were prepared by serial dilution of the stock solution with water and concentrated nitric acid (Suprapur, Merck) was added to standard solutions (5 % HNO_3 v/v).

The US Geological Survey reference material GXR-2 and the pulverized ceramic glaze were used for the testing of analytical methode [11].

Sample Decomposition [12]. Pulverised samples were weighted (0.1 ± 0.0002 g) into a platinum crucible and 1g of $Li_2B_4O_7$ (pro analysi, Merck) was added. The sample was heated in a muffle furnace (Phoenix, Model Sigma1) on 1100°C and kept 30 min. The crucible was allowed to cool and put in a 250 cm^3 plastic beaker. The melt was dissolved in 150 cm^3 of 5 % (v/v) HNO_3 (suprapur, Merck) and the sample was transferred into 250 cm^3 volumetric flask and diluted to the volume with water. Blank samples were also prepared following the instructions described above.

Optimum operating conditions for the sequential ICP-AES.

Plasma power	1.0 KW	Nebulizer pressure	280 kPa
Coolant flow	13 dm^3min^{-1}	Read delay	60 s
Sample uptake	1.0 cm^3min^{-1}	Integration time	3 s
		Number of integrations	3

RESULTS AND DISCUSSION

The sensitivities (S_i) of the different emission lines of the element were measured to find out suitables lines for the measurements (Table 1). The sensitivity was calculated using the formula

$$S_i = dI/dc = Ic_{max} - Ic_{min}/c_{max}$$

where I - intensity, c - concentration.

Table 1.

Wavelengths and sensitivities of the different emission lines

Element Line	State	Wave-length, nm	Sensitivity	Concentration range, $mgdm^{-3}$
Si 1	I	251.611	14507	0.2 - 20
Si 2	I	288.157	311	0.2 - 20
Al 1	I	309.271	15825	0.05 - 10
Fe 2	II	259.940	51708	0.02 - 10
Ca 2	II	396.847	3477784	0.07 - 10
Mg 1	II	279.553	1835689	0.05 - 10
Mn 2	II	259.373	214329	0.02 - 10
Pb 1	II	220.353	202	0.2 - 20
Pb 2	I	283.306	766	0.2 - 20
Pb 3	I	280.199	1979	0.2 - 20
Cu 1	I	324.754	102880	0.02 - 10
Cu 2	II	224.700	3588	0.02 - 10
Zn 2	II	202.548	142347	0.05 - 10
Zn 1	I	213.856	1521	0.05 - 10

[a] I = atomic line, II = ionic line

For optimization of the ICP-AES spectrometer the plasma source was peaked with the lead emission line Pb 3 at 280.199 nm. The sensitivities of emission lines Si2 at 288.157nm, Pb1 at 220.353nm, Pb2 at 283.306nm, Cu2 at 224.700nm and Zn1 at 213.856nm were very low and therefore emission lines Si1 at 251.611nm, Pb3 at 280.199nm, Cu1 at 324.754nm and Zn2 at 202.548nm were used for the measurements.

The performance of the instrument was tested by repeated

measurements of the water sample containing 1.0 $mgdm^{-3}$ of Al, Fe, Ca, Mg, Mn, Cu, Zn and 2.0 $mgdm^{-3}$ of Si and Pb. (Table 2).

Table 2

Sequential determination of nine elements

Element Line	Concentration (c) $mgdm^{-3}$		RSD%
	Added	Found C ± S	
Si 1	2.0	2.10 ± 0.012	0.57
Al 1	1.0	1.08 ± 0.007	0.65
Fe 2	1.0	1.09 ± 0.002	0.18
Ca 2	1.0	0.98 ± 0.005	0.51
Mg 1	1.0	1.10 ± 0.005	0.45
Mn 2	1.0	0.99 ± 0.007	0.71
Pb 3	1.0	2.15 ± 0.015	0.69
Cu 1	1.0	1.02 ± 0.012	1.17
Zn 2	1.0	0.98 ± 0.006	0.62

The method was tested by determing the elements in the US Geological Survey reference material GXR - and in the ceramic glaze sample (Table 3) [11]. The following calibration ranges were used in the analyses: Si 0.2 - 100, Pb 0.2 - 100, Al 0.2 - 100, Fe 0.1 - 10, Ag 0.1 - 10, Mn 0.1 - 10, Cu 0.1 - 10, Zn 0.1 - 10 $mgdm^{-3}$.

The detection limits for the elements were measured and calculated according to the IUPAC recommendation: BL + 3s (BL - blank sample, s - standard deviation). Four replicates were made.

The detection limits for the nine elements were: Si 0.07, Pb 0.06, Al 0.12, Ca 0.04, Cu 0.03, Fe 0.09, Mn 0.02, Zn 0.08, and Mg 0.09 $mgdm^{-3}$.

The satisfactory results were obtained from the analysis of the US Geological Survey reference material GXR-2. Reasonable agreement with the recommended values was obtained. The relative standard deviation (RSD) values varied between 0.3 and 3 % for all the elements measured.

The studies demonstrated that the ICP-AES technique permits a rapid sequential determination of the elements at different concentration levels and sample dilution is not needed. The results show that both the

accuracy and precision of the method are good.

Table 3

The analytical results for geological reference material CXR-2 and ceramic glaze sample

Elements	CXR-2, %		Ceramic glaze, %	RSD, %
	Recommended	Found		
Si	22.20±0.79	20.46±0.57	18.89±0.21	1.11
Pb			23.36±0.28	1.19
Al	18.57±0.06	19.10±0.62	4.08±0.05	1.23
Fe	1.86±0.06	1.83±0.08	2.70±0.05	1.85
Ca	0.93±0.07	0.90±0.01	0.98±0.01	1.02
Mg	0.84±0.09	0.87±0.01	0.78±0.01	1.23
Mn	0.10±0.004	0.10±0.006	0.034±0.001	2.94
Cu	0.008±0.001	0.008±0.001	0.63±0.005	0.79
Zn	0.053±0.006	0.057±0.004	0.065±0.004	0.67

[b] The historical glaze sample was taken from the St. John Church in Tartu, Estonia.

[a] Four replicates were made

The authors wish to thank the reseaschers of Department of Chemistry University of Oulu for their helpful support during the course of this study.

REFERENCES

1. **C.B. Boss, K.J. Freeden** (ed.). Concepts, Instrumentation and Techniques in Inductively Coupled Plasma Atomic Emission Spectrometry, Perkin Elmer, Norwack, CT 1990.
2. **L.H.J. Lajunen.** Spectrochemical Analysis by Atomic Absorption and Emission. Cambridge: Royal Society of Chemistry, 1990.
3. **T.C. Dymott** (ed). Spectrometer Design for Inductively Coupled Plasma-Optical Emission Spectrometry. Cambridge: Philips Analytical, 1990.
4. **E. Yoshimura and H. Suzuki.** Analyst, 115 (1990) 167.
5. **T.D. Hettipathirana, P.P. Wade, M.W. Blads.** Spectrochim. Acta, Part B. 45 (1990) 271.

6. **D. Littlejohn, R. Jowetti, S.T. Sparkes et al.** J. Anal. Atom. Spectrom., 6 (1991) 137R.
7. **D.E. Nixon.** J. Anal. Atom. Spectrom., 5 (1990) 531.
8. **V. Carbonell, A. Sanz, A. Salvador et al.,** J. Anal. Atom. Spectrom., 6 (1991) 233.
9. **M.S. Cresser, J. Amstrong, J. Dean et al.,** J. Anal. Atom. Spectrom., 7 (1992) 1R.
10. Philips Scientific, PU 7000 ICP Spectrometer, Operating Manual (Version 2.0. J. Philips Scientific, Cambridge, 1990.
11. **E.S. Gladney, J. Roelandts.** Geostandards Newslet. 14 (1990) 21.
12. **P. Perämäki, L.H.J. Lajunen, L. Paama et al.** Elemental Analysis of Glazes and Brick Materials by Inductively Coupled Plasma Atomic Emission Spectrometry, University of Oulu, Report Series in Chemistry, Report 38 (1993) 1.

SPECTROCHEMICAL DETERMINATION OF TRACE METALS IN BERRIES BY ATOMIC EMISSION AND ABSORPTION

L. Paama[a], P. Perämäki[b], L.H.J. Lajunen[b], K. Laine[c], T. Pakkonen[c], E. Saari[c], P. Havas[c]
[a]Institute of Chemical Physics, University of Tartu,
[b]Department of Chemistry, [c]Department of Botany,
University of Oulu

ABSTRACT

Trace metal contents of nine elements (Ca, Mg, Mn, Fe, Al, Cr, Ni, Cd and Cu) were determined in lingonberries and blueberries collected in Finnish Lapland and Kola (Russia) in 1990. The aim of the study was to investigate the possible environmental contamination of the berries at different collection sites.

An automated sequential inductively coupled plasma-atomic emission spectrometer (PU 7000, Philips), direct current plasma-atomic emission spectrometer (Spectraspan III b, Beckman) and Zeeman/3030 graphite furnace atomic absorption spectrometer (Perkin Elmer) were used for the determination of micropollutants of heavy metals.

INTRODUCTION

The Lapland Forest Damage Project was established in 1989 to intensify research into forest damage connected with air pollution in Finnish Lapland. The Finnish Forest Research Institute has invited a number of leading Finnish researchers from various research institutes and universities to participate in this project [1, 2].

Trace metal contents of nine elements: Ca, Mg, Fe, Al, Cr, Ni, Cd and Cu were determined in bilberries (*Vaccinium myntillus L*) and lingonberries (*Vaccinium vitis-idaea L*) collected in Finnish Lapland and in the Kola Peninsula [3]. The study was carried out in the University of Oulu. The aim of the study was to investigate the possible

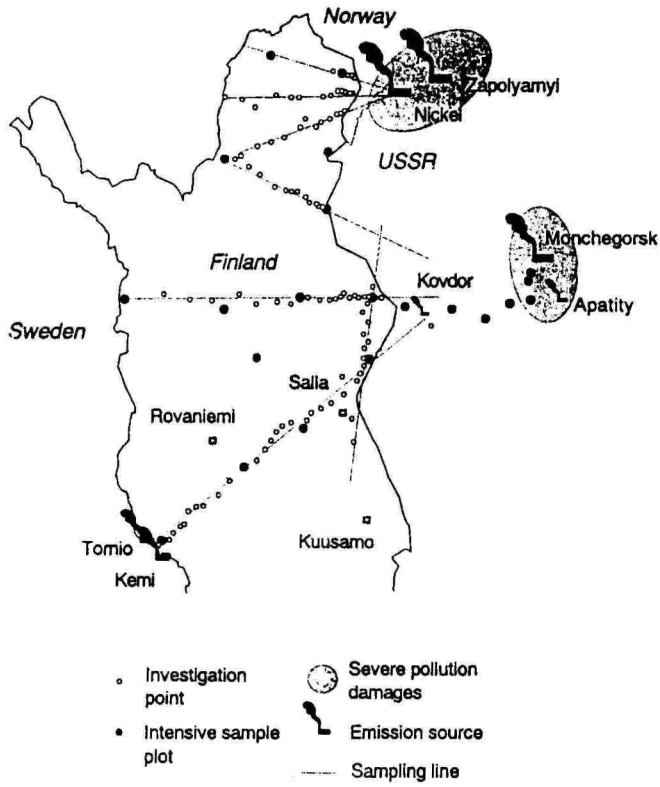

Fig. 1. The Lapland Forest Damage Project sample plot lines.

environmental contamination of the industrial pollution from the Kola Peninsula in Russia [4].

Berry samples were collected in 1990 on seven gradient sampling lines across Finnish Lapland towards the towns of Nickel and Monchegorsk (fig. 1) [1]. Same samples were collected from the Russian side towards Monchegorsk.

The mineral element composition of Finnish foods was studied by Varo P., Lähelmä O. et al in 1980 [5]. The chemical composition of wild berries subjected to atmospheric industrial pollution in Kola was studied by Kruglikova J. in 1990 [6]. No clear trends in trace metal levels towards the assumed pollution sources were found.

The automated sequential inductively coupled plasma-atomic emission spectrometry (ICP-AES), direct current plasma atomic emission spectrometry (DSP-AES) and graphite furnace atomic absorption spectrometry (GF-AAS) were used for the analyses. The ICP-AES, DSP-AES and GF-AAS techniques are a natural choice for the multi-element determination of trace metals in biological materials [7, 8, 9, 10].

Sample digestion was carried out with a microwave digestion system using special teflon high pressure vessels [3, 11].

The validity of the analytical methods was monitored by analysing two reference materials: wheat flour and potato powder provided by the ARC Central Laboratory of Finland [12].

EXPERIMENTAL

Instrumentation

A sequential PU 7000 inductively coupled plasma-atomic emission spectrometer Philips (Unicam Analytical Systems Ltd, England) was used for measurements [9]. The design of this spectrometer includes a 40, 68 MHz free-running oscillator for driving the plasma, an echelle grating for wavelength separation and a grid nebulizer for sample aspiration. The spectrometer is equipped with a Gilson 221 Autosampler and is controlled by a Philips NM S 1461 printer.

For the determination of Ni, Cu, Al a direct current plasma atomic emission spectrometer SectraSpan IIIB (Beckman) was used.

Table 1

Operation parameters for the sequential ICP-AES and DCP-AES

ISP-AES		DCP-AES
Plasma power	1.0 kW	approx. 280 W
Coolant flow	13 dm^3 min^{-1}	
Sample uptake	1.0 cm^3 min^{-1}	2.0 cm^3 min^{-1}
Nebulizer pressure	40 psi (28 kPa)	
Read delay	30 s	manual operation
Integration time	3 s	3 s
Number of integration	3	3

The determination of very low concentrations of Cd, Cr, Ni was carried out with a Perkin-Elmer Zeeman 3030 graphite furnace atomic absorption spectrometer equipped with a Perkin-Elmer AS-60 autosampler [13, 14, 15]. The results were printed out on an Perkin-Elmer PR-100 printer.

Table 2

Measuring wavelengths for ISP-AES and DSP-AES.

Methods	Element Line	Wavelength nm	State*	Standard concentration range $mgdm^{-3}$
ISP-AES	Ca 3	317,934	II	0.2–50
	Mg 3	285,214	I	0.2–50
	Fe 2	259,940	II	0.02–5.0
	Mn 2	258.374	II	0.04–10.0
DSP-AES	Ni 4	341,476	I	0.02–5.0
	Al 2	396,152	I	0.01–5.0
	Cu 1	324,754	I	0.02–5.0

* I atomic line, II ionic line

The operation parameters and measuring wavelengths of all techniques are summarized in Tables 1, 2 and 3.

Samples were difested by using a Milestone ML-S-1200 microwave digestion system. The system includes: a microwave unit ML-S 1200, an exhaust module EM 5, and an automatic capping module ACM 100. The system is equipped with PTFE/PFA (polytetrafluoroethylene/perfluoroalcholoxil) standard SV 140 vessels P/N 33262. The full microwave power of the instrument is 1200 W [12].

Reagents

The stock solutions containing 1000 mg dm^{-3} of each element were prepared using the following reagents (pro analysi, Merck): Al metal, $CaCO_3$, $Cu(NO_3)_2 \cdot 3H_2O$, Fe metal, $MgCl_2 \cdot 6H_2O$, $MnCl_2 \cdot 4H_2O$, $NiCl_2 \cdot 6H_2O$, Cd metal and $Cr(NO_3)_3 \cdot 9H_2O$. The mixed calibration standards were prepared by serial dilution of the stock solution with water. Concentrated nitric acid (suprapure, Merck) was added to the

Table 3

Analytical operation conditions and furnace programme of GF-AAS

Parameter	Cd	Cr	Ni
Wavelength, nm	228.8	357.9	232.0
Light source*	HCL	HCL	HCL
Lamp current, mA	6	25	22
Bandpass, nm	0.7	0.7	0.2
Atomisation**	P	P	P
Chemical modificer	MgPd/Mg	-	-

* HCL = Hollow Cathode Lamp
** P = pyrolytically coated graphite tube with totally pyrolytic L'vov platform inserted

standard solution to obtain a concentration of 5 % HNO_3 (v/v). The validity of the analytical methods was monitored by analysing two reference materials: Potato Power No. 234 and Wheat Flour No. 137 provided by the ARC Central Laboratory of Finland.

Sample digestion

Reference materials and berry samples were accurately weighed (0.25 ± 0.0002 g) into SV 140 digestion vessels and 5 cm^3 concentrated nitric acid (surapur, Merck) was added. The vessels were sealed and they were heated according to the following programme: 10 % for 2 min, 30 % for 5 min and 50 % for 2 min. To ensure the uniform heating, the samples were turned and the programme was repeated. Then the vessels were cooled in ice, 5 cm^3 H_2O_2 (pro analysi Merck) was added and the vessels were heated using the 30 % power setting for 5 min. The samples were heated again and the second digestion step was repeated.

The blank samples containing 5 cm^3 HNO_3 and 5 cm^3 H_2O_2 were handled like berry samples. The decomposed samples and blank solutions were transferred quantitatively into 25 cm^3 volumetric flasks.

Great care was taken to avoid contamination during sample preparation. The deionized and distilled water used was further purified to 18 MΩ resistivity before use (Water 1 Apparatus, Barnstead, Sybron Corporation).

RESULTS AND DISCUSSION

The analytical operation parameters for the ICP-AES, DCP-AES and GF-AAS determinations are shown in Tables 1, 2 and 3. The calcium emission line Ca3 at 317,934 nm was used for the source peacing with the ISP-AES technique. The 3 s criterion was used (Table 4) for the determination of the detection limits of the methods. According to the IUPAC recommendations, the detection limit is the mean value of the blank plus three times its standard deviation [7].

Table 4

Detection limits for determination of trace metals in berries

Element line	n	BL μgcm^{-3}	s	DL*	DL ± CL $\mu g \cdot g^{-1}$ in dry w
Ca 3	7	0.042	0.200	0.102	8.8±1.7
Mg 3	7	0.027	0.011	0.057	4.9±0.8
Fe 2	7	0.006	0.003	0.015	1.3±0.2
Mn 2	7	0.008	0.003	0.017	1.5±0.2
Ni 4	8	0.004	0.0024	0.011	0.97±0.1
Al 2	10	0.021	0.017	0.025	2.2±0.2
Cu 1	10	0.006	0.005	0.021	1.8±0.2
Cd	15	$3.5 \cdot 10^{-5}$	$2.1 \cdot 10^{-5}$	$9.8 \cdot 10^{-5}$	0.009±0.001
Cr	15	$2.3 \cdot 10^{-4}$	$3.5 \cdot 10^{-5}$	$3.3 \cdot 10^{-4}$	0.029±0.004
Ni	15	$8.3 \cdot 10^{-4}$	$1.4 \cdot 10^{-4}$	$1.2 \cdot 10^{-3}$	0.110±0.015

* BL – blank; s – standard devision; a) DL – detection limit (DL = BL + 3_S); b) CL – confidence limit – t 0.95 ns

The following detection limits were obtained with the ICP-AES and DCP-AES techniques: Ca 0.10, Mg 0.06, Fe 0.015, Mn 0.017, Ni 0.011, Al 0.025 and Cu 0.021 $mgdm^{-3}$.

The methods were validated by analysing two certified reference materials: Potato Powder No 234 and wheat Flour No 137. Reasonable agreement with the certified values was obtained (Table 5).

Table 5

Concentration of the elements determined in reference samples

Element	Potato Power No 243 $\mu g \cdot g^{-1}$			Wheat Flour No 137 $\mu g \cdot g^{-1}$		
	Recommended*	Result**	n	Recommended	Result	n
Ca	91 ± 6	83 ± 9	16	210 ± 5	186 ± 12	15
Mg	747 + 16	663 ± 50	19	570 ± 20	483 ± 39	15
Fe	22.0 + 2.0	19.6 ± 2.7	19	51 ± 6.05	47.8 ± 5.9	16
Mn	6.1 + 0.32	7.3 ± 1.2	19	13.0 ± 0.32	11.1 ± 0.9	14
Al	-	2.1 ± 1.0	17	-	4.0 ± 1.2	16
Cu	3.87 _ 0.18	4.2 ± 1.4	17	2.48 ± 0.31	2.6 ± 0.03	11
Ni	0.193 + 0.043	0.153 ± 0.061	12	0.191 ± 0.06	0.012 ± 0.03	11
Cr	0.096 + 0.018	0.096 ± 0.061	17	-	0.055 ± 0.03	14
Cd	0.035 + 0.0016	0.043 ± 0.017	18	0.030 ± 0.004	0.044 ± 0.013	14

* Recommended value from the ARC Central Laboratory of Finland

$$(C + s\ tg95/n)$$

**concentrations $\mu g\ g^{-1}$ calculated on dry weight.

204 bilberry samples were collected from 54 sites and 150 lingonberry samples from 46 sites (usually four separate replicates per site from Finnish Lapland). Some lingonberry samples were collected from the Russian side towards Monchegorsk (Figure 1). The results of the analyses of berry samples calculated on mg kg^{-1} wet weight and presented in Table 6.

Table 6

Mineral element composition of the berries of Lapland and Kola, $mgkg^{-1}$ (wet weight)

Elements	Lapland				Kola	
	Bilberry, n = 204		Lingonberry, n = 150		Lingonberry, n = 8	
	Means	Ranges	Means	Ranges	Means	Ranges
Ca	207	127 - 364	234	153 - 357	258	209 - 300
Mg	83	51 - 131	100	75 - 142	105	79 - 132
Fe	3.0	0.1 - 7.6	2.1	1.4 - 3.9	3.0	2.4 - 3.8
Mn	56	7 - 118	48	24 - 104	48	10 - 78
Al	2.6	1.3 - 4.9	3.5	1.6 - 7.3	3.8	2.5 - 5.7

Ele-ments	Lapland				Kola	
	Bilberry, n = 204		Lingonberry, n = 150		Lingonberry, n = 8	
	Means	Ranges	Means	Ranges	Means	Ranges
Cu	0.8	0.3 - 2.4	0.9	0.3 - 1.7	1.6	0.6 - 5.1
Ni	0.11	0.006 - 0.44	0.08	0.02 - 0.28	1.08	0.13 - 3.78
Cr	0.03	0.001 - 0.68	0.01	0.004 - 0.006	0.01	0.004 - 0.06
Cd	0.003	0.002 - 0.0012	0.001	0.001 - 0.007	0.003	0.001 - 0.013

The level nickel in lingonberries near Monchegorsk (two sites) was 40 times higher than the average for Finnish Lapland. The level of copper was five times higher and the level of manganese was lowest close to Monchegorsk (Figure 2) [4]. The results of the analyses indicated that the concentration of manganese in berries decreased if the pollution of berries by Ni, Cu, Cd was observed. The toxic effect of aqueous aluminium did not exist.

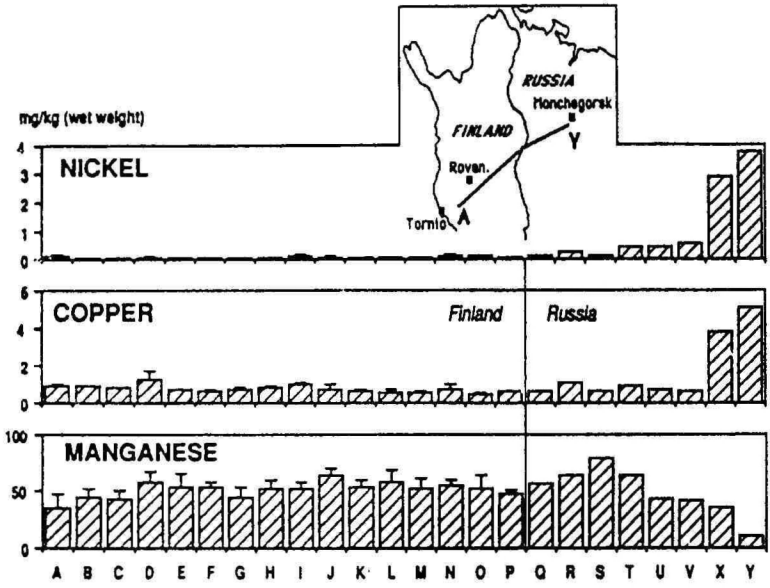

Fig. 2. Nickel, copper and manganese levels in fruits of lingonberry (*Vaccinium vitis-idaea* L.) on gradient sampling line no. 1 (Torino-Monchegorsk). Mean and standard deviation.

The concentrations of Cu, Ni, Cr, Cd, Al, Fe in the bilberry and lingonberry samples collected from Finnish Lapland were at the same level found earlier by Varo and coworekrs in 1980 [5].

ACKOWLEDGEMENTS

The authors would like to thank the researchers from the Finnish Forest Damage Project.

REFERENCES

1. **Tikkanen E., Mikkola K.** In: Research into Forest Damage Connected with Air Pollution in Finnish Lapland and the Kola Peninsula of the USSR. Ed. by E. Tikkanen and M. Varmola. FFRJ, Rovaniemi 1991, p. 30.
2. **Mikkola K., Nöjd P.** In: The Lapland Forest Damage Project. Interim report. Ed. by H. Kauhanen and M. Varmola. Research Papers 413, Rouvaniemi 1992, p. 13.
3. **Paama L., Perämäki P., Lajunen L., Laine k. et al.** 41-th Finnish Chemical Congress. 12–14.11; 1991 Helsinki Finland. The Abstracts Espoo 1991, p. 13.
4. **Laine K., Lajunen L., Perämäki P., Paama L. et al.** Symposium on the State of the Environment and Environmental Monitoring in Northern Fennoscandia and the Kola Peninsula. Oct. 6–8, 1992, Rovaniemi, Finland. Extended Abstracts. Rovaniemi, 1992, p. 297.
5. **Varo P., Lähelmä O., Nuustamo O., Saari E.** Acta Agriculturae Scandinavica. 1980. 22. P. 89–113.
6. **Kruglikova J.** In: Research into Forest Damage connected with Air Pollution in Finnish Lapland and the Kola Peninsula of the USSR. Ed. by E. Tikkanen and M. Varmola. FFRJ Ravaniemi 1991, p. 153.
7. **Lajunen L.H.J.** Spectrochemical Analysis by Atomic Absorbtion and Emission. The Royal Society of Chemistry. England, 1992. 275 p.
8. **Perämäki P. and Lajunen L.H.J.** J. Anal. Atom. Spectr. 7 (1992) 7. P. 735.
9. Philips Scientific, PU7000 ICP Spectrometer, Operating Manual (Version 2,0); Philips Scientific, Cambridge, 1990, p. 101.
10. **Taylor A., Branch S., Crews H., Halls D.** J. Anal. Atom. Spectr. 7 (1992) 67 R.
11. Vademecum for Digestion Methods Development, Milestone Vademecum. Feb. 1990.
12. 1989 Annual Book of ASTM Standards. American Society for Testing and Materials, Philadelphia. PA, 1989.

13. Atomic Absorbtion Databook. Philips Scientific. Cambridge, 1988.
14. **Siira J., Kokkonen P., Perämäki P. et al.** Bothnian Bay Reports. 5 (1991) 3.
15. **Cresser M., Amstrong J., Dean J., et al.** J. Anal. Atom. Spectr. 7 (1992) 1 R.

METHODS OF VAPOUR SAMPLING AND ANALYSIS - STYRENE AS AN EXAMPLE

L. Saarinen
Institute of occupational Health, Helsinki

ABSTRACT

Analysis of air pollutants is discussed. Air impurities are gathered, using solid sorbents. Thermal or solvent desorption follows the final analysis is made using the gas chromatograph with flame-ionization and mass-selective detectors. Analysis of styrene is described as an example.

Exposures of individuals to toxic substances in ambient or occupational environments requires accurate sampling and measurement of aerosols and gases. The sampling and analysis techniques have developed rapidly during the past twenty years. Acceptable and validated methods are available for several hundred substances.

Also technology in the analytical laboratory has changed considerably. With the computerization and the development of more selective and sensitive instrumentation, the analyst has been able to detect and identify very small quantities of materials never seen before. This has brought about a keen awareness of the widespread distribution of toxic hazards and also the need to study the long term effects of low level exposures.

Basically the air monitoring involves sampling and analysis. Both of these processes go hand in hand and are dependent on each other for the proper assessment of environmental risk. In this presentation emphasis has been placed on the sampling and gas chromatographic analysis of the vapour phase of the air pollutants. Problems have been illustrated using styrene measurements as an example.

Styrene causes health risks in industrial use and adverse inconvenience even in very low concentrations. Styrene is used as a

solvent and reactive component in polyester resins. The monitoring of styrene is of particular interest to personnel working in the glass fiber industry. Another problem of importance are emissions in dwellings after incomplete hardening of plystyrene-polyester used in repair work or as a component in construction elements.

Due to relatively small amounts of organic contaminants in the air, most chromatographic methods for the measurement of these compounds require a concentration step before the actual analysis. The frequently used methods for organic vapours are solvent scrubbing, cryogenic concentration, and adsorption on a solid sorbent.

Activated charcoal

Activated charcoal is one of the most widely used sorbents for the collection of organic vapours in the air. The standard sampling device is the tube that contains charcoal. The adsorbed analyte is extracted out from charcoal with some solvent such as dimethyl formamide, carbon disulfide or ethyl ether.

The method has several advantages; the sampling device is small, portable, and involves no liquids. Mos of the interferences can be solved in the subsequent analysis by altering gas cromatographic conditions such as column packing or temperature program to separate other simultaneous solvents.

There are only a few disadvatages with this method. During sampling under very humid conditions, water may interfere and decrease the adsorption capacity of the sampling tube and a breakthrough may occur. Furthermore, the desorption efficiencies are not constant and sometimes difficult to control.

When monitoring styrene, the safe sampling volume for the 150 mg charcoal tube is 3–10 dm^3 air in the occupational exposure ranging from 20 to 400 mg/m^3. The real breakthrough volume is circa 20 dm^3 in the styrene concentration of 2000 mg/m^3. In ambient and indoor environments the concentration range of interest is 0.001 to 1 mg/m^3, and the safe sampling volume is respectively bigger. Charcoal is an excellent sorbent for styrene and samples have good storage properties. The desorption efficiency is more than 95 per cent if the amount of styrene per sample exceeds 0.5 mg.

In indoor and ambient styrene monitoring, the collection and storage of microgram amounts on charcoal is safe. However, in carbon disulfide liquid desorption system, activated charcoal causes a serious loss of styrene, which is not seen in large samples. If carbon disulfide

is used, one should prepare standards with the equal amount of sorbent according to the phase equilibrium method. After the desorption charcoal should be removed from vials. It is recommended to use other sorbent-desorbent systems.

Alternative sorbents

Besides the almost universal activated coconut charcoal, also petroleum-based carbon and synthetic graphitized molecular sieves are widely used to collect nonpolar organic solvent vapours. They also adsorb polar vapours but there are frequently difficulties in desorption, and the recovery remains poor. Molecular sieves have thermal desorption applications with low boiling point compounds ($C < 5$) in the ambient air monitoring.

Silica gel is a polar sorbent and its surface contains hydroxyl groups. Thus polar substances have a strong attraction towards silica gel. Since water is highly polar, silica gel retains atmospheric moisture, sometimes preferentially over other substances. It is an excellent sorbent in the dry air, but the affinity for moisture limits the use of silica gel. It is suitable for the collection of compounds such as aniline, cresol, ethylamine and morpholine among others. Amines are usually soluble in water and are therefore not significantly affected by the retention of water on silica gel.

When charcoal and silica gel cannot be used because of poor recovery or storage stability, porous polymers are considered. These are relatively inert, hydrofobic and they have a surface area of 100 to 600 m^2/g. The weak attractive forces facilitate good desorption for the subsequent analysis but also affect seriously the breakthrough volumes and the linearity of the sampling method. Most porous polymers do not retain properly volatile compounds such as low boiling point solvents or water. Several methods have been validated for porous polymers and compounds which have had problems when collected with charcoal or silica gel. For example, diphenyl and pyridine derivatives have collected on Tenax, and methyl methacrylate and nicotine on XAD-2. Despite the relatively low adsorpiton to styrene the XAD-2 sorbent is sometimes used because it gives excellent recoveries in carbon disulfide.

Diffusional samplers

One of the innovations of the early seventies was the sampling of organic vapours without the use of mechanical air pumps. The first paper describing the diffusional monitor was published in 1973. Since

then there have been a number of publications demonstrating that the diffusion monitor can be used in circumstances in which pumps and charcoal tubes were previously used.

The diffusional monitor is comprised of a velocity barrier, a static air column, and a sorbent layer at the bottom of the air column. The monitor represents a dynamic, non-mechanical system. The driving force is based on the difference between the contaminant concentration at the barrier ant the sorbent surface and this difference is maintained by the continuous adsorption of the vapours by the sorbent.

According to Fick's law of diffusion the mass uptake (M) is a direct function of the badge sampling rate (DXA/L), the ambient concentration (C) and the sampling time (t).

$$M = D \times A/L \times C \times t$$

When the collected mass is measured in the laboratory, the time defined during sampling and the sampling rate have been determined in advance, so the concentration can be calculated. The response times of diffusive monitors are usually a few seconds i.e. monitors respond to changes in the concentration of most organics in the air very quickly. There are commercially available many tipes of diffusional samplers loaded either with carbon, XAD-2 or Tenax which can be used to collect styrene as well as most other similar solvent vapours from the air.

Desroption and analysis

The advantages of solvent desorption are that it uses only standard laboratory equipment and it produces solutions which are easily handled. The disadvantage is that the desorption efficiency of analytes varies from one sorbent-desorbent system to another and as a function of loading.

Charcoal has got capacity many times bigger than Tenax and XAD-2 to hold the molecules. According to Langmuirs adsorption isoterms, the trace amounts are strongly bound to the sorbent. In liquid desorption the poor recovery is common for compounds less than 0.5 mg per 150 mg charcoal. For example, samples of styrene near the lower detection limit of the method i.e. 5 microgram per sample, have recovery circa 40 per cent. This is partly due to the strong adsorption and also due to the side reactions in carbon disulfide solution in the presence of activated charcoal. Recovery of styrene is nearly 100 per cent with Tenax and XAD-2.

A newer method which has the advantages of high sensitivity and

the absence of solvent peak utilises the adsorption on porous polymers and direct thermal desorption into the gas chromatograph. This technique has gained acceptance among many applications in ambient air analysis, occupational hygiene, odor analysis and water analysis. Among many adsorbents the most popular has been 2,6-diphenyl-p-phenylene oxide or Tenax because of its high temperature stability and its insensitivity to moisture.

In the conventional method ambient air is drawn through a sorbent tube containing 0.2 to 2 gram Tenax. After sampling the tubes are submitted for analysis by the capillary gas chromatography/mass spectroscopy/data system. After adding internal standard, the organic compounds are removed from Tenax by heating the sample to 250 to 300 °C under the flow of helium. The desorbed vapours are collected in the cryogenic trap which is then heated to transfer the sample to the capillary column. Only high resolution columns are applicable because of the complexity of air samples. The gas chromatography column is programmed to allow the separation of compounds, while mass spectrometer is scanning. Data is recorded by the computer for subsequent processing. Component identification is normally accomplished by using the retention time and mass spectral characteristics. For example the Wiley 130K data base of nearly 40 000 spectra of different compounds is able to solve many of the qualitative identification problems in ambient or industrial environment.

The adjustment of analytical conditions for hudreds of different compounds with different vapour pressure, affinity to sorbent, and thermal stability is a challenging task in any laboratory trying to harmonize or standardize methods used in environmental analysis.

The choice of sorbent is difficult and it is often a compromise. A long experience with Tenax has taught that heating at 250 °C for ten minutes gives quantative desorption up to C15-compounds and the degradation products of Tenax are still neglible. With some graphitized molecular sieves in similar conditions, desorpiton is good up to C10-compounds bud aldehydes interfere in this system. Both sorbents seem to be inert with styrene and desorption efficiencies are above 95 per cent.

Detection limits

In solvent extraction the analyte of interest is diluted and only 0.1 to 1 % of the sample is injected to the gas chromatography for analysis. In capillary gas chromatography we are obliged to omit the most part of

the sample because of the split technique. Generally only 3 to 5 per cent of the injected amount reach the column. The survey of ambient and indoor air demands more sensitive methods.

The sensitivity of the flame ionization detector in gas chromatography is circa 0.1 nanogram for most organic compounds. Mass specific detectors have the detection limit in few nanograms in SCAN mode and few tenths of nanogram in SIM mode.

The thermal desorption methods have a great advantage as the entire sample can be injected into the capillary column. This means that a sample of one nanogram in one liter of air can be analyzed. When only small air volumes are needed, it allows us to use diffusional samplers. Without a pumping device we are free to increase the number of samples and the representativeness of our studies.

The future

The determination of people's exposure to harmful substances has been a challenging and continuously changing task for many years. Sampling and analytical methods have been adapted to meet the needs for the identification of risks as well as for the compliance with the legal provisions.

The ability to see the previously invisible components has both advantages and disadvanatages. It is good that we can identify components that are truly deleterious but on the other hand, we have to be prudent not to initiate hunts for no other reason than the possibility of detecting the material.

In the future there will be more use of diffusive samplers, both those which are exposed in the field but analyzed in the laboratory and those which provide a quick and reliable reading in the field. Methods of collecting reactive chemicals on nonvolatile surface coatings are becoming more frequent. As an analytical chemist I hope there will also be more methods which allow us to determine more components at a time to simplify our efforts in the laboratories.

REFERENCES

1. **Brown, R. and Purnell, C.** Collection and Analysis of Trace Organic vapous Pollutants In Ambient Atmospheres, The Performance of Tenax-GC Adsorbent Tube. J. Chromatogr. 178 (1979) 79.
2. **Brown, R., Saunders, K. and Walkin, K.** A Personal Sampling Method for

the Determination of Styrene Exposure. Am. Ind. Hyg. Assoc. J. 48 (1985) 760.

3. Determination of Volatile Organic Compounds (VOCs) in Indoor Air, Method IP-1B, Solid Adsorbent Tubes, in Compendium of Methods for the Determination of Air Pollutants in Indoor Air, U.S. Environmental Protection Agency. Research Triangle Park, 1990.
4. **Geuskens, R., Jongen, M., Ravensberg, J., van der Tuin, J., Leenheers, L. and van der Val. J.** Comparison of Active and Diffusive Sampling Methods for Environmental Monitoring of Styrene. Appl. Occup. Environ. Hyg. 5 (1990) 364.
5. MDH 43, Styrene in Air, Methods for the Determination of Hazardous Substances. London: Health and Safety Executive, 1985.
6. NIOSH, Manual of Analytical Methods. 3rd ed. National Institute of Occupational Safety and Health. Cincinnati, 1984.
7. NIOSH. Organic solvents in air. Method no.: P&CAM 127, in NIOSH Manual of analytical Methods, National Institute of Occupational Safety and Health, Cincinnati, 1977.
8. NIOSH, Styrene, Method No.: S30, in NIOSH Manual of Analytical Methods, National Institute of Occupational Safety and Health, Cincinnati, 1977.
9. Hydrocarbons, Aromatic Method 1501, in NIOSH Manual of Analytical Methods, Third edition. National Institute of Occupational Health, Cincinnati, 1984.
10. **Rothweiler, H., Wäger, P. and Schatter.** Comparison of Tenax and Carbotrap for Sampling and Analysis of Volatile organic Compounds in Air, Atmospheric Environment 25 (1991) 231.
11. **Saarinen, L., Rothberg, M. and Bäck, B.** Comparison of Diffusive Samplers and Charcoal Tube Method under Field Conditions, in Diffusive Sampling, ed.: Berlin, A. et al., Royal Society of Chemistry, London, 1987, 259.
12. **White, L. Taylor, D., Mauer, P. and Kupel, R.** A Convient Optimized Method for the Analysis of Selected Solvent Vapors in the Industrial Atmosphere. Am. Ind. Hyg. Assoc. J. 31 (1970) 225.

APPLICATION OF CHROMATOGRAPHICAL METHODS FOR ANALYSIS OF BIOACCUMULATIVE ORGANOCHLORINE COMPOUNDS IN ENVIRONMENTAL SAMPLES

Juhan Ruut
Tartu public Health Service

ABSTRACT

In the presentation are reviewed current sample preparation methods in PCB analysis in complex biological and environmental matrices, and possibilities of separating single PCB isomers by applying gaschromatographical methods.

INTRODUCTION

The analytical methods for the determination of persistent organochlorine compounds (pesticides, polychlorinated biphenyls PCBs) can generally be divided into three distinct phases: 1) sample preparation and extraction; 2) sample clean-up and fractionation; 3) final determination.

The main purpose of the current paper is to introduce novel separation methods of prganochlorine pesticides (OCPs) and PCBs during the second and third steps of the whole analytical procedure to avoid possible overlappings and resulting misidentification at the final step.

1. SAMPLE CLEAN-UP AND FRACTIONATION METHODS

There are a substantial number of variations of the four basic methods for the separation and clean-up techniques for the extracts of organochlorine compounds: 1) liquid-liquid partition; 2) treatment with

concentrated sulphuric acid or saponification by 1 M KOH in ethanol; 3) gel permeation chromatography (GPC); 4) column chromatography on different adsorbents. A new approach in environmental analysis for sample clean-up is using dialysis membranes which enables non-destructive reduction of fat more than 99 % with lipid samples as large as 20 g in one step [1].

Nowadays the most widely used methods are GPC and column chromatography as they enable single-step clean-up and the fractionation of target compounds. Much research has been devoted to the separation of OCPs and PCBs by solid adsorbents. With silica colums only, satisfactory separations have been reported; it has been observed that good results can be obtained by combining silica and aluminium oxide in one column [2]; however, aldrin, p,p-DDE and heptachlor still co-elute with PCBs. In fact, the impossibility of cleaning-up and separating different groups of organic compounds for multiresidue analysis by the single-column adsorbent system has cleared out, therefore, the latest systems have developed use combinations of different adsorbents (both in the open column and HPLC modes). Besides the traditional adsorbents (florisil, silica gel, alumina, diatomaceous earth), some new ones have recently appeared – graphitized porous carbon, which separates chlorinated compounds based on the degree of chlorination as well as molecular planarity [3, 4], and aminopropyl-bonded silica HPLC columns (CH_2-column) – solutes elute from the amino column according to the number of aromatic rings [5].

In recent years, on-line HPLC has received an increasing attention because of its higher inherent reproducibility and its potential for automatization [6, 7, 8]. Quite sophisticated approach is the use of on-line coupling LC with capillary GC (for a review, cf, ref. [9]).

2. SEPARATION OF INDIVIDUAL PCB CONGENERS BY GC-ECD

Gas chromatography with the ^{63}Ni-electron capture detection (GC-ECD) analysis is the most common analytical techique for the analysis of OCPs and PCBs. Previously, analyses were accomplished using packed columns and yielded only the total PCB concentration, usually expressed in concentration units of commercially available mixtures (Aroclors). Then the analysis of PCBs as single CB congeners received attention (there are 209 PCB congeners, some 120 have been found in

environmental samples, of which 36 have identified as priority compounds [10]) and researchers started to use capillary columns. Different stationary phases were tested, but it proved that no single capillary column could separate all the isomers of interest [11]. The most widely used stationary phase is SE-54 (5 % diphenyl, 1 % vinyl polydimethylsiloxane [12], but only 15 of 36 priority congeners can be analyzed accurately on SE-54 [13]. Some researchers have resorted to multidimensional GC to separate closely eluting congeners using two columns with different polarity [14, 15]. Recently, a capillary coated with a liquid crystalline stationary phase has become commercially available. These phases provide greatly enhanced separations of rigid molecules, based upon molecular shape parameters [16].

Table 1.

Review of analytical methods

No	Individual steps of sample preparation	GC determination
1.	Soxhlet extraction (toluene) Open silica column, deactivated with 10 % water (hexane). Fat and polar compounds are retained Aminopropyl HPLC column (250 × 10 mm, 5μm) eluent hexane, 3 frications: I Clorinated benzenes and aliphatics, II Diaromatics, III Polyaromatics (n > 2) (backflushed) Porous graphitized carbon HPLC column (100 × 4.7 mm Hypercarb), diaromatics only I eluent hexane, 2-4-ortho PCBs, II hexane/CH_2Cl_2 (1:1), mono-ortho PCBs, III Toluene, non-ortho PCBs (backflushed)	GC/MS analysis* with a 25 × 0.22 mm SE-54 fused silica capillary column [17]

No	Individual steps of sample preparation	GC determination
2.	Blood sample O1 ml) is directly injected on acid silica gel over neutral alumina column. I 1 % CH_2Cl_2 in hexane, PCBs excluded PCB-77, II 50 % CH_2Cl_2 in hexane, PCB-77	non specified [18]
3.	10 g of milk are mixed with 15 g of silica gel (40–60 mesh) and topped to 15 g of 10 % water deactivated silica gel (70–230 mesh). Eluent 150 ml petroleum ether (PE) - CH_2Cl_2 (80:20) 4 × 4 mm HPLC column is filled with activated carbon dispersed on 5μm silica deactivated 20 %, in a 80:20 ratio (total carbon amount is 25 mg), I 5 × 20 ml PE, interfering PCBs, II 3 × 20 ml 1 % toluene in PE, momo-ortho PCBs, III 4 × 5 ml 50 % toluene in PE, non-ortho PCBs	GC/MS on fused capillary column DB-1 (30 m × 0.25 mm) [19]
4.	Concentrated-H_2SO_4 clean-up 4.5 g of 3 % deactivated silica gel, I hexane PCBs, DDE, II hexane/ether (1:1), DDT, DDD, HCH, chlordanes, etc. SP-1 activated coal/Chromosorb (PCB fr.) I hexane/CH_2Cl_2 (1:1) 2-4-ortho PCBs, DDE II Toluene Carbopack C/Celite (II fr.) I hexane, mono-ortho PCBs, II Toluene, non-ortho PCBs	Dual column GC, not specified [20]

*For a review on GC/MS applications in pesticide and PCB analyses, cf. ref. [21].

REFERENCES

1. **J.N. Huckins, M.W. Tubergen, J.A. Lebo, R.W. Gale, T.R. Schwartz.** J.A.O.A.C. 73 (1990) 290.
2. **P. de Voogt, J.C. Klamer, H. Govers.** J. Chromatogr. 363 (1986) 407.
3. **O. Chiantore, I. Novak, D. Berek.** Anal. Chem. 19 (1988) 638.
4. **C.S. Greaser, A. Al-Haddad.** Anal. Chem. 61 (1989) 1300.
5. **Y. Zebühr, C. Näf, D. Broman, K. Lexen, A. Colmsjö, C. Östman.** Chemosphere. 19 (1989) 39.
6. **R.J. Dolphin, F.W. Willmott, A.D. Mills.** J. Chromatogr. 122 (1976) 259.
7. **E.A. Hogendoorn, G.R. van der Hoff, P. van Zoonen.** J. HRC. 12 (1989) 784.
8. **E.A. Hogendoorn, C.E. Goewie, P. van Zoonen.** Fesenius J. Anal. Chem. 339 (1991) 348.
9. **K. Grob Jr., B. Schilling.** HTC & CC 8 (1985) 7.
10. **V. Mcfarland, J. Clarke.** Environ. Health Perspectives. 81 (1989) 225.
11. **S. Bøwadt, B. Larsen.** J. HRC. 15 (1992) 377.
12. **M. Mullin, C. Pochini, S. McCrindle, M. Romkes, S. Safe, L. Safe.** Environ. Sci. Technol. 18 (1984) 468.
13. **D. Schulz, G. Petric, J. Duinker.** Environ. Sci. Technol. 23 (1989) 852.
14. **G.S. Durell, Th.C. Sauer.** Anal. Chem. 62 (1990) 1867.
15. **J.C. Duinker, D.E. Schulz, G. Petrick.** Anal. Chem. 60 (1988) 478.
16. **F.R. Guenther, S.N. Chesler, R.E. Rebbert.** J. HRC. 12 (1989) 821.
17. **Y. Zebühr, C. Näf, C. Bandh, D. Broman, R. Ishaq, H. Pettersen.** DIOXIN '92, 12th International Symposium on Dioxins and Related Compounds, 24.-28. August 1992. University of Tampere. P. 193.
18. **R.F. Gierczak, D.J. Hallett.** DIOXIN '92, 12th International Symposium on Dioxins and Related Compounds, 24.-28. August 1992. University of Tampere. P. 55.
19. **H. Steinwandter.** Fresenius J. Anal. Chem. 343 (1992) 378.
20. **S.S. Atuma, Ö. Andersson.** DIOXIN '92, 12th International Symposium on Dioxins and Related Compounds, 24.-28. August 1992. University of Tampere. P. 11.
21. **P.T. Holland.** Pure & Appl. Chem. 62 (1990) 317.

FORMATION OF PARTIALLY SOLVATED GRIGNARD REAGENTS IN TOLUENE

A. Tuulmets
Institute of Organic Chemistry, University of Tartu

ABSTRACT

Toluene solutions of alkylmagnesium halides containing one mole or less of an organic base per magnesium atom and particularly the kinetics of their formation reaction have been investigated in this laboratory during the last decade. Reports on the subject together with several unpublished data are reviewed in this paper.

The reaction proceeds in two steps. In the first rapid stage a monosolvated Grignard reagent forms, then a slow completion of the reaction occurs. The latter stage is catalized by the solvated Grignard reagent. The dependences of the rate constant on the alkyl group, halide, and organic base for both stages of the reaction are determined. Under certain conditions oscillation of the reaction rate was observed. The mechanism of the catalyses plausibly consists of an exchange of the organic base between the solvated Grignard reagent and the organomagnesium halide formed on the surface of magnesium metal, followed by the subsequent dissolution of the compound.

INTRODUCTION

Although conventional Grignard reagents are known to be prepared in diethyl ether or in other donor solvents, since long ago organomagnesium compounds have also been obtained in hydrocarbon media in the absence of donors or without any solvent at all. Such preparations are investigated rather extensively and repeatedly reviewed [1–4].

The employment of big-scale organomagnesium syntheses in industry requires the replacement of easily inflammable solvents, e.g. ethers, by safer hydrocarbons of high boiling points. The process in hydrocarbons is economical since the reaction medium is cheap, non-

hygroscopic and fire hazards are low.

In general the reactions of the unsolvated organomagnesium halides resemble qualitatively those of the conventional Grignard reagents. However, several differences have been observed. The unsolvated reagents are active as polymerization catalysts, particularly in combination with titanium halides, whereas ethereal reagents are inactive. Unsolvated reagents have also given good results in the syntheses of various organometallic compounds.

The use of the unsolvated organomagnesium halides is limited to primary alkyl and aryl compounds. Branched alkyl halides, vinyl, allyl and benzyl halides do not react under these conditions or produce Wurtz-type coupling products. Methyl-, ethyl-, and propylmagnesium halides only form with low yields. Because of their scarce solubility in hydrocarbons, the unsolvated organomagnesium compounds may be used but in the form of dispersions or slurries that complicates both the dosage and the transportation of the reagents.

The main part of the shortcomings of the unsolvated organomagnesiums may be overcome by the use of small admixtures of solvating compounds provided their content in the reagent is permissible. In the presence of small amounts (one mole or less per mole of halide) of complexing agents, e.g. ethers, tertiary amines etc., even secondary, tertiary or benzyl halides react smoothly with magnesium metal in mild conditions with the formation of organomagnesium compounds in good yields [1–6]. Also light metal alkoxides [2, 7] or tetraethoxysilane in catalytic amounts [8, 9] may be used to promote the formation of organomagnesium halides in non-donor media. The reagents obtained exhibit surprisingly high solubilities at least in aromatic hydrocarbon solvents.

Whereas the Grignard reagents in donor solvents are solvated at least by two solvent molecules per atom of magnesium, the reagents obtained in the presence of catalytic amounts of donor substances are but partially solvated. As the solvating agent is firmly bound to the Grignard reagent, such solutions possess almost all the advantages of unsolvated organomagnesium halides in non-solvating media. Apart from this, partially solvated Grignard reagents exhibit several properties different from those of both conventional Grignard reagents and unsolvated organomagnesium compounds.

The reactions of monosolvated alkylmagnesium bromides with ketones in benzene or toluene increase considerably the yield of the addition products in comparison with the reactions in ethers [10, 11].

The rate of the reaction of ethylmagnesium chloride with ethylethoxysilanes increases drastically when free ethyl ether is replaced by toluene [12]. It has been reported that the molar ratio of ethyl ether to ethyl chloride predetermined the ratio of monomers formed in a continous organomagnesium synthesis of ethylchlorosilanes and thus enabled to control the process [13].

Although partially solvated Grignard reagents have been exploited in big-scale industrial processes [14], their chemical and physical properties as well as the outlines of their formation reaction have been insufficiently investigated and only fragmentarily known.

In our laboratory the kinetics of the formation of organomagnesium halides in the presence of small admixtures of organic bases has been investigated during a decade [15–19]. Our interest to partially solvated Grignard reagents was first evoked by our finding [20] that in mixtures of toluene with organic bases the rates of the formation of n-butylmagnesium halides depend relatively little on the composition of the mixture except the values of the ratio base to organic halide less than two moles to one mole, where the decrease of the ratio causes a dramatic decrease in the rate constant. We realized that this was the region of the solvent composition where the catalytic properties of the base could be observed almost purely. Further work was prompted also by an industrial research laboratory interested in the kinetic investigation of the Grignard reagent formation process in the presence of catalytic amounts of diethyl ether. We succeeded in establishing the kinetic course of the reaction, the influence of the nature of the organic base and of the structure of the organic halide on the rate of the reaction, and an unexpected catalytic action of the partially solvated Grignard reagent.

The reaction kinetics was followed by a thermographic method or using the method of samples [15]. Considering the unsolvating medium we have confined ourselves to toluene as a very typical and widely used aromatic hydrocarbon solvent.

The most important and formerly unknown feature of the reaction is that the formation of the Grignard reagent in toluene in the presence of small amounts of an organic base (less than one mole per a mole of the organic halide) proceeds in two stages [15]. After a rapid formation of the monosolvated Grignard reagent a slow completion of the reaction occurs under the influence of the solvated alkylmagnesium halide.

Although we focused our attention on the slow stage of the reaction, the rapid initial stage was investigated at the same time [15–19]. The kinetic curves were obtained from the corresponding thermograms of the process [15]. When the reaction rate permitted to withdraw a sufficient number of aliquots, the kinetic curves were obtained by plotting of the data of Grignard reagent titration against time.

The measurements were made at the constant initial concentration of alkyl halide, the molar ratio of base to halide being varied from 0.17 up to an equimolar composition. Under such conditions the kinetics of the rapid stage of the reaction appeared to be of a complicated character. However, a certain part of the process could be described according to the first-order kinetics. The rate constants were calculated by means of a differential method from the slope of the linear part of a plot of ln $(\Delta T/\Delta t)$ vs. τ, where ΔT stands for the temperature rise during the time interval Δt (see ref. [15]) and τ indicates the time corresponding to the intermediate of this time interval.

With the increase of the relative content of the base, the length of the linear portion of the curve diminishes. At the end of the rapid stage the yield of the Grignard reagent corresponds to the molar amount of the organic base. Consequently, in the rapid stage of the reaction the monosolvated Grignard reagent forms, and after the added portion of the base is exhausted, the reaction slows down. An analogous yield of the monoetherate of sec butylmagnesium bromide corresponding to the added amount of the ether, and the following cease of the reaction when carried out in hexane, are described by Smith [4]. After the rapid stage of the reaction the formation of the Grignard reagent in toluene does not discontinue but the reaction is very slow.

We can also conclude that the obtained rate constants should be considered as pesudofirst-order rate constants, the reaction is catalyzed by the base, and the reaction is of the first order in organic halide and also of the first order in the base, because the latter is consumed during the reaction by binding with the organomagnesium compound formed in the reaction.

The values of the first-order rate constants linearily depend on the ratio base to halide, however, nearly at the equimolar ratio a dramatic increase in the reaction rate occurs [15, 16]. At a relative content of the base from one to two mole per mole of the halide, a steep increase in the reaction rate continues. At higher concentrations of the base the rate

of the reaction is mainly determined by the viscosity of the medium [20].

The slope of the dependence of the first-order rate constants on the relative base content in the reaction mixture can be considered as a second-order catalytic constant inherent to the base. In Table 1 these characteristics for several bases are given [15, 16, 18]. However, we are not capable of explaining the sequence on the ground of the structure or other properties of the bases.

Table 1

Catalytic Constants for Organic Bases*

Base	Et_2O	dig-lyme	Et_3N	THF	Bu_2O
$k_{II} \cdot 10^2$ l·mole^{-1} sec^{-1}	3.48	2.06	1.25	0.50	0.10

* Determined from the initial stage of the reaction of n-butyl bromide with magnesium in toluene at 30 °C.

Monosolvated Grignard reagents formed in the rapid stage of the reaction are very soluble in toluene. Saturated at 20°C solution of the complex n-BuMgBr·Et_2O is about 3.7 molar in n-butylmagnesium bromide [21]. An analogous solution of n-butylmagnesium chloride complex is at least 4.4 molar in basic magnesium but the content of magnesium chloride is less than the stoichiometric one. This is the case also in unsaturated solutions whereas n-butylmagnesium bromide complex appeared to be of a stoichiometric composition at any concentration.

THE SLOW STAGE OF THE REACTION

After the organic base added in a deficiency is consumed in the formation of the monosolvated Grignard reagent, a relatively slow process occurs until the organic halide is completely converted into an organomagnesium compound. This product of the reaction might be considered as an unsolvated organomagnesium halide, however, its

solubility in toluene is remarkable, whereas unsolvated organomagnesium compounds are reported to be practically insoluble [2–4]. Consequently, a complexation with the monosolvated Grignard reagent occurs. Thereby a disproportion of the Grignard reagent takes place and the content of magnesium halide in the solution diminishes with the decreasing solvation. An investigation of toluene solutions of partially solvated Grignard reagents is still in progress, however, some rough estimates are available by now. For example, at the fourfold molar excess of n-butyl bromide to diethyl ether in the initial reaction mixture, the saturated product solution is nearly one molar in dibutyl magnesium and the composition of the complex is approximately $R_2Mg \cdot 1.4MgBr_2$. Magnesium chloride evidently precipitates intensively. An analogous system obtained from n-butyl chloride and diethyl ether in a molar proportion three to one was also about one molar in dibutyl magnesium, however, the concentration of magnesium chloride was nearly two times lower.

A distinctive feature of the slow stage of the reaction is a linear increase of the Grignard reagent concentration in the course of the process. The slope of a linear kinetic curve increases with an increase in the relative content of the organic base in the reaction mixture (Fig. 1).

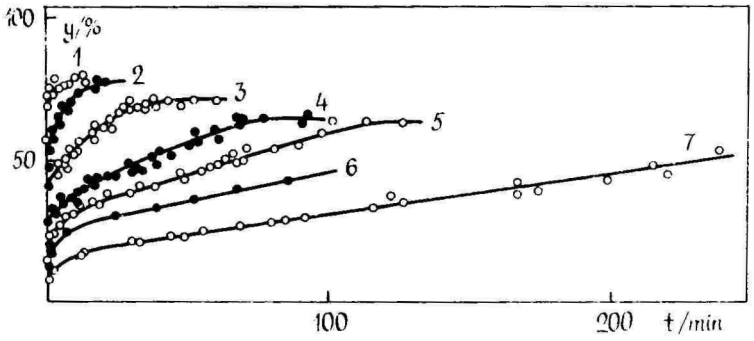

Fig. 1. The time-dependence of the yield of n-butylmagnesium bromide at molar ratios of diethyl ether to n-butyl bromide: 1 – 0.85; 2 – 0.68; 3 – 0.51; 4 – 0.41; 5 – 0.34; 6 – 0.27; 7 – 0.17. From ref. [15].

This pattern of the process holds equally when an excess of halide to base is used or a new portion of halide is added after the formation of the monosolvated Grignard reagent. Hence, under these conditions the

reaction of organic halide with magnesium is of the zeroeth kinetic order and is catalized by the monosolvated Grignard reagent [15].

The dependence of the zeroeth-order rate constants on the concentration of the catalyst is determined by the halide and organic base. The values of the rate constants for alkyl bromides exert an approximately square dependence on the base content in the reaction mixture while those for alkyl chlorides depend linearily on the diethyl ether content [15, 17, 19]. In the case of diglym, the dependence is of the fourth power of the base content [17].

The alkyl group in the reagent has a moderate influence on the reaction rate (Table 2). With diethyl ether and tetrahydrofurane the following sequence was found [18, 19] EtBr > n-BuBr > i-BuBr ≈ s-BuBr. On the contrary, halogen atom strongly influences the rate of the reaction. Alkyl chlorides react considerably more rapidly and the corresponding catalysts reveal a powerful catalytic effect in the reactions of both alkyl chlorides and bromides [19] (see Table 2). These findings appear to be somewhat surprising because in pure ethers the chlorides compared with bromides have a markedly lower reactivity [20]. It cannot be excluded that the high catalytic activity of alkylmagnesium chloride etherates may be in connexion with a lower content of magnesium halide in their solutions. It has been found that the addition of magnesium bromide to ethylmagnesium bromide – diethyl ether complex considerably suppresses the catalytic ability of the latter [18].

Unexpectedly, the variation in organic bases only slightly affects the catalytic power of monosolvated Grignard reagents. However, in the case of n-butylmagnesium bromide the following sequence was observed [17] Et_2O > THF ≈ diglym > Bu_2O. A more pronounced effect of bases becomes evident in the yields of the Grignard reagent. By the end of the reaction the yield of the Grignard reagent does not reach 100 %. The analyses of reaction mixtures showed that alkyl bromides reacted completely, however, with some formation of the Wurtz reaction products. The Wurtz-type reaction proceeds also in the rapid stage of the reaction, however, it is more essential in the slow stage. In the case of primary alkyl bromides and diethyl ether as a catalyst the Grignard reagents form with 60–80 % yields. When diethyl ether is replaced by any other base considered in this work (THF, triethylamine, dibutyl ether), during the slow stage of the reaction mostly the Wurtz reaction products form and the overall yield of the Grignard reagent is low. The same takes place when secondary or tertiary bromides are used [15–18]. In contrast to this alkylmagnesium chlorides can be obtained in high

yields (up to 95 %) at least with diethyl ether in composition of the catalytic complex [21]. This is surprising again because alkyl chlorides have been reported to tend to form the Wurtz-type and other byproducts more easily than bromides and iodides do in the absence of solvating admixtures [2, 7].

Table 2

Rate Constants of the Formation of Alkylmagnesium Halides[a]

Reagent	Catalyst[b]			
	EtMgBr	n-BuMgBr	i-BuMgBr	n-BuMgCl
EtBr	1.08	0.40	0.13	-
n-BuBr	0.77 (1.53)[d]	0.50	0.29	osc., 4.0[c]
i-BuBr	0.40 (0.42)[d]	0.25	0.15	osc., 4.5[c]
n-BuCl	0.18[c] (0.08)[c, d]	0.23[c]	0.08[c]	4.42
i-BuCl	osc.	osc.	osc.	0.90[c]

[a] In toluene at 30°C, k. 10^4 mole·l^{-1}·sec^{-1}; [b] $RMgX \cdot Et_2O$, 0.5 M; [c] Initial rate determined from an autocatalytic curve; [d] THF instead of Et_2O.

As a practical inference of our investigations, it should be emphasized that in the region of small additions, this is diethyl ether that ensures the highest rate of the process and the best yield of the Grignard reagent. The use of chlorides is also recommendable.

OSCILLATING GRIGNARD REAGENT FORMATION

Kinetic investigations of the formation of partially solvated Grignard reagents were carried out in two ways. Usually the corresponding amount of an alkyl halide was introduced into the reaction mixture. The rapid stage of the reaction was immediately followed by the slow one, that kinetics was of the zeroeth order. The two stages of

the reaction were also investigated separately. Preliminarily, the catalyst (a monosolvated Grignard reagent) was prepared and then another portion of alkyl halide was added. In this way the reaction between an alkyl halide and magnesium metal was investigated in the presence of a chosen catalyst [19].

When an alkyl halide different from the one from which the catalyst had been prepared was used, irregular oscillations of the rate of the product formation were observed [19]. In the case of an insignificant difference in alkyl groups the amplitude of oscillation remained within the limits of an experimental error and the relationship between the yield and time could be approximated by a straight line corresponding to the zeroeth order kinetics (Table 2). However, the oscillations achieved a markedly greater amplitude while the reagents differed from each other by halides or at least one of the alkyl groups was branched. A typical example of a such kind of a process is presented in Fig. 2. The oscillation in the rate of the alkylmagnesium bond formation always strictly corresponded to the oscillation in the rate of magnesium halide formation. When the experimental conditions were kept constant, the oscillations were reproducible (Fig. 2). The alteration of the amount of the catalyst in the reaction mixture caused an alteration of the character of oscillations, however, we could not reveal any regularities in the concentration effect of the catalyst. Analogical phenomena occured when tetrahydrofuran was used as an organic base.

Sometimes an autocatalytic pattern of the process was observed instead of oscillations. In order to characterize these processes the initial rates of the reaction were determined (Table 2).

The available experimental material confirms our hypothesis about the catalysis by the solvated organomagnesium compounds. If the catalysis was carried out by uncomplexed ether then with an increase in the concentration of the organomagnesium compound a decrease in reaction rate proportional to a decrease in the equilibrium concentration of free ether in the reaction mixture should occur. These circumstances do not allow an appearance of a linear, yet an autocatalytic pattern of the reaction. Moreover, alkylmagnesium chlorides are more effective Lewis' acids compared with the corresponding bromides [24] and therefore can more strongly bind ether and thereby lower the reaction rate. However, the alkylmagnesium chlorides appeared to be very effective catalysts.

To our knowledge the formation of a partially solvated Grignard reagent is the first known example of such kind of an oscillating reaction

where the catalyst is dissolved and the solid surface acts as a reagent.

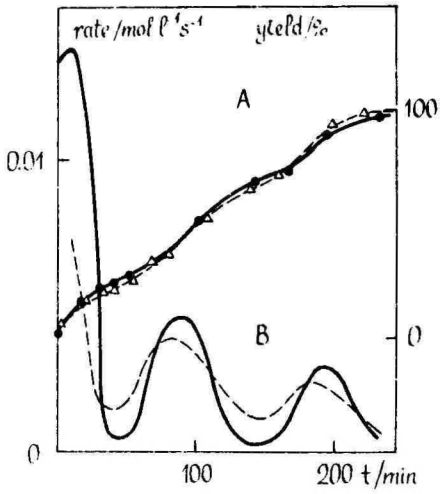

Fig. 2. Two parallel runs of a reproducibly oscillating process in toluene. Catalyst: ethylmagnesium bromide – ethyl ether (0.5 M). Reagent: isobutyl chloride. A – dependence of the yield of isobutylmagnesium chloride vs. time. B – dependence of the reaction rate vs. time. From ref. [19].

So far as the system appears to be very complicated due to its heterogenity and as the details of the mechanism of the Grignard reagent formation are not completely known, it is not yet possible to explain unambiguosly the origin of oscillations in this reaction.

It is found that different monosolvated Grignard reagents have different catalytic activity. It is also known that both the catalyst and a considerable part of the reaction product are present in the solution. Consequently, the unsolvated product of the reaction is complexed with the solvated alkylmagnesium halide. Thus, during the reaction a permanent redistribution of the organic base between dissolved particles occurs. When the redistribution and recomplexing processes are not fast, the system does not reach an equilibrium immediately and the oscillations in the reaction rate may appear.

On the other hand, it is necessary to remove the reaction products from the surface of magnesium metal in order to enable the development of the process. This causes the presence of free (active) and blocked

(inactive) reaction centres on the magnesium surface and oscillations may arise analogically with the catalytic reactions with solid catalysts. Very likely to this kind of oscillations may be attributed those sporadically observed in the course of rapid stage of the Grignard reagent formation from alkyl bromides prone to form Wurtz-type products [22]. Oscillations in the reaction rate have also been indicated for n-butylmagnesium bromide formation in 25 % diethyl ether- n-hexane mixture [23]. It has to be mentioned that the solubility of organomagnesium compounds in aliphatic hydrocarbons is very low [4].

SOME MECHANISTIC ASPECTS OF THE REACTION

The appearance of oscillation phenomena described above permits to cast light upon some details of the mechanism of the Grignard reagent formation. If the oscillations in rapid reaction may be explained by the accumulation of the reaction products on the surface of magnesium metal, it follows that the formation of the organomagnesium compound and subsequent to this solvation and dissolution of the latter proceed at comparable rates. Hence, in certain cases, particularly when the dissolution process is embarrassed, the reaction may become mass-transport limited. This seems to be a rather common situation, e.g. Whitesides and coworkers [25, 26] established that the reaction of alkyl iodides and of the majority of alkyl bromides with magnesium is diffusion or mass-transport limited in ethers while that of chlorides is slower and therefore not limited by diffusion. Although their work was accomplished with scrupulosity, the authors had committed themselves to the idea of the rate limiting diffusion of alkyl halides. In this connexion their extensive experimental material does not allow to distinguish between the limitation by mass-transport to the surface of magnesium and in the opposite direction. In light of recent findings the latter seems to be more plausible.

The protracted oscillations in the slow stage of the reaction can hardly be related to diffusion phenomena. A more acceptable explanation should be based on a slow redistribution of the organic base between particles dissolved in toluene (vide supra). An exchange of the organic base between a partially solvated organomagnesium compound in solution and an unsolvated alkyl- or arylmagnesium halide on the surface of magnesium metal seems to be essential for the catalysis by the solvated Grignard reagent and rate limiting for the overall process.

Considering that the formation of the Grignard reagent is possible in the absence of organic bases provided that a sufficiently high temperature, a vigorous stirring etc. enable to remove the reaction products from the surface, the role of the organic bases seems to consist in the solvation and dissolution of the organomagnesium compound.

The latter conception permits uniquely to comprehend both the catalysis by a free organic base and by a partially solvated Grignard reagent. An exchange of the organic base between the catalyst and a newly formed organomagnesium particle is also compatible with the zeroeth order kinetics of the process, because the rate of the reaction is determined by the rate of the liberation of the surface, the solvated particle dissolves immediately and the concentration of the catalyst remains unchanged.

When the catalyst is prepared from an halide different from the one used as a reagent, the composition of the catalyst alters during the reaction and an autocatalytic or oscillating course of the process may appear (vide supra).

In the case of a "normal" reaction a slight dependence of the zeroeth order reaction rate on the nature of the organic moiety of the reagent [18, 19] can be related to the variation in the complexing abilities of organomagnesium compounds, the latter being effectively controlled by steric requirements of both the compound and the organic base (cf. ref. [24]).

REFERENCES

1. **M.S. Kharash, O. Reinmuth.** Grignard Reactions of Non-Metallic Substances, London: Constable, 1954.
2. **D. Bryce-Smith.** Bull. Soc. Chim. Fr. 1963, 1418.
3. **B.J. Wakefield.** Organometal. Chem. Rev. 1 (1966) 131.
4. **W.N. Smith.** J. Organometal. Chem. 64 (1974) 25.
5. **E.C. Ashby, R. Reed.** J. Org. Chem. 31 (1966) 985.
6. **T. Leigh.** Chem. and Ind. 1965, 426.
7. **E.T. Blues, D. Bryce-Smith.** Chem. Ind. 1960, 1533.
8. **K.A. Andrianov, O.I. Gribanova.** J. Gen. Chem. (Russ.). 8 (1938) 552.
9. **K.A. Andrianov.** J. Gen. Chem. (Russ.). 16 (1946) 487.
10. **P. Canonne, G. Foscolos, G. Lemay.** Tetrahedron Lett. 1979, 4383.
11. **P. Canonne, G. Foscolos, H. Caron, G. Lemay.** Tetrahedron, 38 (1982) 3563.

12. **A. Tuulmets, M. Hörak, T. Kõopere, J. Ruotsi.** Organic Reactivity (Tartu) 19 (1982) 102.
13. **B.A. Klokov.** Deposited Doc., **1982** SPSTL 67, 212 and 407, Khp-D82, Chem. Abstr. 98 (1983) 143856; 99 (1983) 71184; 101 (1984) 23970.
14. Oligoorganosiloksany: Svoistva, Poluchenie, Primenenie. M.V. Sobolevskii (Ed.). Moscow: Khimiya, 1985.
15. **A. Tuulmets, M. Hörak, E. Pill, A. Riikoja.** Organic Reactivity (Tartu), 22 (1985) 93.
16. **A. Tuulmets, M. Hörak, K. Sarv, E. Aaresild.** Organic Reactivity (Tartu), 22 (1985) 332.
17. **A. Tuulmets, M. Hörak, E. Aaresild, K. Sarv.** Organic Reactivity (Tartu), 22 (1985) 460.
18. **A. Tuulmets, M. Hörak, E. Hansen, V. Palm.** Organic Reactivity (Tartu), 24 (1987) 412.
19. **A. Tuulmets, M. Hörak, A. Ong, M. Limberg.** Organic Reactivity (Tartu), 25 (1988) 116.
20. **A. Tuulmets, M. Hörak, E. Jakob, M. Vapper.** Organic Reactivity (Tartu), 18 (1981) 225.
21. **A. Tuulmets, P. Kullamaa.** Will be published elsewhere.
22. **A. Tuulmets, M. Hörak,** unpublished data.
23. **V.A. Palm, M.P. Khyrak.** Doklady Akad. S.S.S.R. 130 (1960) 1260.
24. **A. Tuulmets.** Reakts. Sposobn. Organ. Soedin. (Organic Reactivity, Engl. Ed.) 11 (1974) 81.
25. **H.R. Rogers, G.M. Whitesides et al.** J. Am. Chem Soc. 102 (1980) 217, 226, 231.
26. **K.S. Root, J. Deutch, G.M. Whitesides.** J. Am. Chem. Soc., 103 (1981) 5475.

SYNTHESIS OF SOME γ-LACTONES VIA GRIGNARD REAGENTS

I. Liblikas, E. Mõttus, A. Nilson
Estonian Agricultural University

ABSTRACT

From succinic acid anhydride and the Grignard Reagent γ-ketoacids were obtained. The prepared γ-ketoacids were reduced with $NaBH_4$ to get γ-hydroxyacids from which γ-lactones were obtained in 51 - 61 % yields.

Disubstituted γ-lactones were isolated from the reaction mixture before reducing the salts of monosubstituted γ-ketoacids using of Na_2CO_3.

The yields ratios of mono- and disubstituted γ-lactones in various co-solvents were measured. Ether alone was found to be the best.

γ-lactones have become an important class of ecochemicals over the past several years. Interest in the chemistry of γ-lactones has emerged in recent years because of the biological activities of a number of them. Many of the substituted γ-lactones show characteristics of antifeedant or antifungal activity or serve as communication means for many insect and mammal species. In everyday human practice they are used as components of odorants.

There is good evidence that γ-lactones are used by some animals, particulary insects, as a component of pheromones.

γ-lactones are distributed as pheromone components among various insect species. γ-caprolactone has been identified as a component of the sex pheromone emitted by females of the Trogoderma species: *Trogoderma granarium* [Levinson et al., 1978, Adamovic et al., 1979, Nunez M. et al., 1990), *Trogoderma glabrum* [Yarger et al., 1975], *Trogoderma inclusum* [Insecoe et al., 1976].

The pyralid moth *Eldana saccharina* produces a long-range attractant lactone from a wing gland [Kunesch et al., 1981]. Five years

later Phealan et al. identified some more γ-lactones as wing pheromones from *Ephestia elutella males*.

A number of γ-lactones are animal repellents. These compounds possess animal anti-mating effects, especially for dogs [Meyly, 1976].

With these points in mind we have worked on the synthesis of γ-lactones.

The preparation of γ-lactones is often associated with badly available synthons and a complicated experimental procedure. Most of the well-known approaches involve many steps that cause the drop of final overall yields.

Here we report an efficient synthetic route to the synthesis of γ-lactones via the Grignard Reagent action on succinic acid anhydride and the subsequent treatment of the initially formed γ-ketoacid with sodium borohydride and lactonization. It appears to be a convenient method for synthesis on γ-lactones using easily available reagents and simple synthetic procedures. The yields of the products are acceptable.

The investigation of the reaction between the Grignard Reagent and succinic acid anhydride has been the subject of some publications.

Some earlier spproaches involved the application of arylmagnesium halides. The application of these synthones for the synthesis of γ-aroylketoacide was described by G. Komppa and W. Rohrmann [1934] and C. Weizmann et al [1935].

Preparation of 3-aroplpropionic from the action of the Grignard Reagents on succinic acid anhydride has been studied [Paddar et al., 1955, 1957].

The preparation of mono-substituted γ-alkyllactones from succinic acid anhydride and dialkylcadmium derived from the Grignard Reagent was reported by Molina et al. [1974]. The ketoacids formed in this reaction were reduced using sodium borohydride to obtain γ-lactones in a 45 % yield.

In the present study the γ-lactones were prepared as shown in the general sheme:

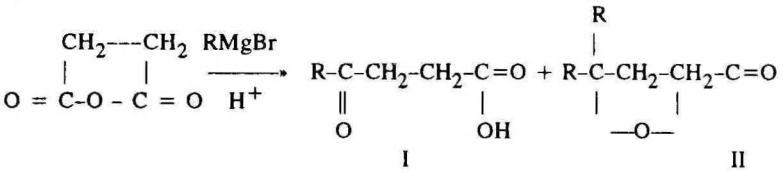

After the hydrolysis of the Grignard reaction products, the disubstituted γ-lactone (II) was separated from γ-ketoacid (I) by

transferring the latter to the aqueous phase by means of Na-salt with sodium carbonate.

γ-ketoacid was reduced to γ-hydroxyacid with simultaneous lactonization to γ-lactone by means of Na-salt with sodium borohydride in aqueous solution according to the shceme:

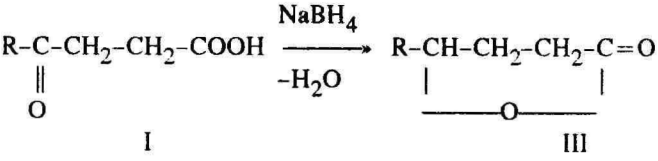

Monosubstituted γ-lactones were obtained in yields over 50 %, based on succinic anhydride. Table 1 summarizes the results of these experiments.

Table 1

Formation of mono- and disubstituted γ-lactones in the reaction of some Grignard Reagents with succinic acid anhydride.

RMgBr /mol/	Succinic acid anhydride /mol/	Disubsti-tuted γ-lactone /g/	Mono substituted γ-lactone /g/	Yield of monosub-stituted γ-lactone /%/
EtMgBr				
0.55	0.5	14.5	33.5	59
0.55	0.5	16.7	34.6	60
0.33	0.3	10.0	19.0	51
BuMgBr				
0.33	0.3	10.6	23.9	56
0.66	0.6	23.0	45.0	53
HexMgBr				
0.33	0.3	12.1	29.2	57
0.55	0.5	29.3	46.0	54
OcMgBr				
0.33	0.3	28.3	32.2	54
0.55	0.3	40.4	59.3	60

The reactivity of the Grignard Reagents toward the carbonyl group varies in solvents with different polarity and solvating ability. Addition of several co-solvents: p-xylene, benzene, diglyme, tetrahydrofurane to ether was tested for the investigation of the optimum reaction conditions for the preparative synthesis of γ-lactones.

For the investigations of the solvent effect on the formation of mono- and disubstituted products in the reaction of the Grignard Reagent with succinic acid anhydride, synthesis was performed where anhydride was suspended in various solvents and the Grignard Reagent was added to ether. The reaction mixture was hydrolyzed and reduced with sodium borohydride according to procedure 2. Yields of the reaction products were detected by the quantitative gas-chromatographic analysis. The results are summarized in table 2.

Table 2

The effect of co-solvents on the reactivity
of the Grignard Reagent toward the carbonylgroup

Co-solvent	Yield of mono-substituted γ-lactone /%/	Ratio between mono- and disubstituted γ-lactones	Grignard Reagent used /%/
p-Xylene	45.6	1.60	80.8
Benzene	50.6	1.76	90.6
Diglyme	33.4	2.40	49.3
Tetrahydrofurane	19.3	1.20	38.5

EXPERIMENTAL SECTION

Reaction procedure 1.

The Grignard Reagent RMgBr (0.55 mol) in ether (250 ml) was added dropwise to succinic acid anhydride (0.5 mol) in ether (500 ml) under an argon atmosphere while the mixture was refluxed. A solution of the Grignard Reagent RMgBr was previously prepared from alkylpromide (0.55 mol) and Mg turnings in ether (250 ml) in the usual manner. The reaction mixture was refluxed for additional 2 hrs and kept overnight at room temp.

Precipitated Mg-salt was hydrolyzed with 10 % hydrochloric acid. The organic layer was separated, combined with the etheral extract of

the aqueous layer.

The etheral layer was shaken vigurously for 0.5 hr with sodium carbonate to transfer ketoacid from the etheral layer to the aqueous layer as a Na-salt.

The disubstituted γ-lactone from the Grignard reaction mixture was separated with the etheral layer. This compound was of no interest to us for futhare use and etheral layer indicated a little presence of starting alkyl bromide.

For reduction the Na-salt of ketoacid remained the aqueous layer the aqueous solution of sodium borohydride (0.25 mol) was added dropwise to a slowly stirred solution at room temp. The excess of sodium borohydride and formed boric compound was destroyed by adding 1:1 diluted sulphuric acid. The hydroxylalkanoic acid converted to γ-lactone spontaneously.

The reaction mixture was extracted with ether, the combined etheral solutions washed with aqueous sodium chloride, dried and concentrated to leave the γ-lactone which was no more purified.

The isolated products were analyzed by a gas-chromatograph equipped with the flame ionization detection (FID) and 2.5 m X 2.5 mm columns packed with 5 % OV 17 and Carbowax 20 M on Chromaton Super.

The structural assignement of the reaction products was based on the IR and NMR data. The experimental results are summarized in table 1.

Reaction procedure 2.

0.1 mol of succinic acid anhydride was suspended in 100 ml of a solvent: p-xylene, benzene, diglyme or tetrahydrofurane.

The Grignard Reagent EtMgBr was added to a resulting mixture dropwise and with vigurous stirring over a 2 hr period. After the reaction the mixture was kept overnight, the precipitated Mg-salt was hydrolysed with 10 % hydrochloric acid. The organic layer was separated and combined with the ether extract of the aqueous phase. The organic solution was concentrated.

Reduction is carried out with 1.4 g sodium borohydride in an alkaline (sodium carbonate) solution. The formed boric compounds were destroyed with 1:1 sulphuric acid and products separated with ether.

Dodecanol-1 as an internal standard for the quantitative analysis was added, and the amounts of the reaction products were detected by the gas chromatograph equipped with catharometric detection and 1.4 m

X 2.5 mm column packed with Carbowax 20 M on Chromaton Super. Four parallel syntheses were carried out in each solvent. The experimental data are summarized in table 2.

REFERENCES

1. **Adamovics J.A., Robinson K.J.** High-performance liquid chromatography of various insect pheromone. J. Chromatogr., 179 (1979) 192–194.
2. **Inscoe M.N., Beroza M.** Insect-behavior chemicals active in field trials. Pest management with insect sex attractants and other behavior-controlling chemicals. ASC symp. ser 23. Washington, 1976. 147–173.
3. **Kunesh G., Zagatti P., Lallemand J.Y., Debal A. and Vigneron J.P.** Tetrahedron Lett., 22 (1981) 5271.
4. **Komppa Gust. and Rohrmann W.** Über eine allgemeine Reaction zur Darstellung von Ketosäuren, ungesättigten Säuren und disubstitutuierten Lactonen. Ann., 509 (1934) 259–268.
5. **Levinson A.R., Levinson H.Z., Shwaiger H., Cassidy R.F., Silverstein R.M.** Olfactory behavior and receptor potentials of the khapra beetle. *Trogoderma granarium (Coleoptera: Dermestidae)* induced by the major components of its sex pheromone, certain analogues, and fatty acid esters. J. Chem. Ecol., 4 (1978) 95.
6. **Meyly, Walter C.** Anti-mating effects of γ-alkyl-γ-butyrolactones and δ-alkyl-δ-valerolactones. Can. pat., 969471, CA 83 (1976) 131142.
7. **Molina P., Soler A., Cambronero J.** Sintesis total de gammalactones. "IonII. Esp., 34(397) (1974) 557–561.
8. **Nunez M. Teresa, Martin Victor S.** Efficient oxidation of phenyl groups to carboxylic acids with ruthenium tetraoxide. A simple synthesis of (R)-γ-caprolactone, the pherommone of *Trogoderma granarium*. J. Org. Chem., 55 (1990) 1928–1933.
9. **Paddar F.G., Lanson S. El-Assal and Adiba Habashi.** β-Aroylpropionic acids. VII. The action of Grignard reagents on succinic anhydride, methylsuccinic anhydride, and β-aroyl- and -β-aroyl-α-methylpropionic acids and their esters. J. Chem. Soc., 1957, 1690–1699.
10. **Paddar F.G., Lanson S. El-Assal and Adiba Habashi.** 3-Aroyl-propionic acids. IV. The action of Grignard reagents on succinic anhydride: 3-aroylpropionic acids and their esters. J. Chem. Soc., 1955, 456–460.
11. **Weizmann C., Blum-Bergmann O. and Bergmann F.** The reaction of Grignard reagents with some succinic anhydrides. J. Chem. Soc., 1935, 1370–1371.
12. **Yager R.G., Silverstein R.M., Burkholder W.E.** Sex pheromone of the female dermestid beetle *Trogoderma Glabrum*. J. Chem. Ecol., 1 (1975) 323.

PRECOCENE-2 AS A VOLATILE FROM *Ageratum houstonianum* VARIETIES

E. Mõttus, S. Kuusik, V. Nõmm, T. Lepiku
Estonian Agricultural University

ABSTRACT

Ageratum houstonianum consists of more than 12 volatile components, precocene-2 among of them. The latter accounted for about 31-60 % of the toal and varied during growth and development.

INTRODUCTION

Insects and plants have evolved together, and many secondary substances in plants are known to stimulate or inhibit insect development, feeding and host attraction or repellency. After the discovery and deployment of various juvenile hormone analogs as mimics of natural juvenil hormones, W.S. Bowers [1976] discovered two anti-juvenile hormone compounds, 7-methoxy and 6,7-dimethoxy-2,2-dimethyl-chromene (named Precoene-1 and Precoene-2) from the bedding plant, *Ageratum houstonianum*. Numerous species of paurometabolous insects evidenced precocious metmorphosis and sterilisation on treatment with the precocenes [W.S. Bowers, 1991].

Precocene-2 possesses both morphogenetio and sterilisant activity. G. Matolosy and al. [1981] found that many compounds with similar structural features, but lacking the chromene ring, exert chemosterilisant activity only. Among them, 1,2,4-trimethoxy-5-propenyl-benzene (asarone) showed a remarkable activity. Various scientists have reported more different behavioral activity of extracts from *A. houstianum*, antifeedant and repellent effects included [S.A. Quershi, 1988].

Little is known as yet about the ecochemical activity of volatiles

from *Ageratum houstonianum*. In the work presented here, the relative amount of precocene-2 and some other volatiles were detected during plant development in two varieties of the plant.

EXPERIMENTAL

Plant. Two varieties of *Ageratum houstonianum* were selected for the tests: Eureca and White. Both of them are widely used in Estonia as decorative plants.

For experiments were collected A) young plants after two months of vegetation; B) buds, stems and leaves after 81 days of vegetation; C) buds, stems and leaves after 125 days of vegetation.

Analysis. Gas cromatograph Model 3700 was used. Conditions were the following: Detector PID, carrier gas He, flow rate 30 ml/min. Three columns were used. We mainly operated with SE-30, 2 m × 3.5 mm, temperature 138–150°C. Other columns with XE–60 (1 m × 3.5 mm) or a capillary column 25 m × 0.25 mm with OV–1 were also used.

The highest peak on chromatograms belonged to precocene-2. It was identified by the addition of a known sample to the listed columns. Quantitative analysis was carried out by the method of inner standard. The known amound of tridecyl acetate was added to hexane od the EtOH extracts of the plant parts.

RESTULTS

Some results of the analysis are listed in Table 1.

As it is seen, precocene-2 in different parts of the plant varies during growth and development, being the highest at the end of the vegetation period. It is evident that the higher concentration of Precocene-2 in plants is due to higher amounts of it in the buds. Despite being at different stages of development, the buds contained the highest concentration of precocene-2.

As a minimum about 12 other components were detectable in extracts of the plant in our conditions. Their amounts varied significantly in different varieties of *Ageratum houstonianum* (Eureca or White) and

possibility, at different growth stages. In case of buds, precocene accounted for 31-60 % of the detected 10 compounds.

Table 1

Concentration of precocene-2 in different parts of the variety "Eureca" of *Ageratum houstonianum*

Parts of plant	Vegetation period in days		
	60	81	125
Roots	0.024	ND	ND
Stems	ND	0.004	0.001
Leaves	ND	0.03	0.041
Buds	ND	0.09	0.064
Whole plan	0.057	0.026*	0.051*

Remarks: ND – not detected; * calculated value

ACKNOWLEDGEMENT. We thank Vaike Põdersoo of the Botanical Gardens of the University of Tartu for providing different varieties of the plant.

REFERENCES

Bowers W.S., D.M. Soderlund, D.M. Chemistry and action of the precocenes. In: Regulation of Insect Development and Behaviour. Wroclaw, 1981. Part 1. P. 309-322.

Bowers W.S. Insect Hormones and Antihormones in Plants. In: Herbivores: their interactions with secondary plant metabolites, 2E, 1991. Volume 1: The chemical participants. P. 431-455.

Matolosy G., Farag A.I., Varjas L., Belai I., Darwish Y.M. Morphogenetic and Chemosterilisant Activity of Asaone analogues. In: Juvenile hormone Biochemistry. 1981 P. 393-413.

Quershi S., Mohiuddin S., Quershi R.A. Repellenot values of some common indigenous plants against red flour beetle, *Tribolium castaneum* (Herbst). Pakistan J. Zool. 1988. 20, 3. P. 201-207.

CHANGES OF CONTENT CARBOXYL GROUPS ON DIFFERENT KINDS OF PAPER DURING ACCELERATED AGING

J. Lehtaru
Department of Chemistry, University of Tartu

Abstract

These 12 different kinds of paper were tested in the Tartu University Library (Estonia).

Content of moisture, fillers, lignin, carboxyl groups and cold water pH were determined.

The purpose of this investigation was to determine the changes of the content of carbonyl groups on different kinds of paper under accelerated aging and compare those results with the changes of cold water extract pH and find suitable paper for restoring. All the paper samples were tested before and after accelerated aging for 72 and 240 hours at 100°C and at 50% RH.

INTRODUCTION

Hydrolytic degradation has historically been looked upon as the most important reason for the breakdown of cellulose during the aging of paper. What is important in this context is that the degradation processes, both the acid and the oxidation hydrolysis [1], are often very strongly related. The rate of the hydrolysis of cellulose thus increases strongly when it is oxidized. The acidhydrolysis leads similarly to the formation of reducing end-groups that can easily be oxidized to carboxyl groups which induce the autohydrolytical breakdown of cellulose. Hemicellulose is hydrolyzed more rapidly than cellulose, and the acidic degradation products, which are formed, accelerate the hydrolysis. A higher content of non-cellulosic material in the fibre leads to a higher

content of carboxyl groups.

If one starts from a fibre material with a higher content of carboxyl groups, this leads to an increased content of transition metals in the paper, because of the ion exchange with the acidic groups, and these transition metals (Fe, Mn, etc.) catalyze the oxidation process including the oxidation of sorbed SO_2 to H_2SO_4 (from environmental contamination).

Oxidation bleaching, by e.g. Cl_2, hypochlorite or oxygen is harmful because of the fact that the carboxyl content increases. The formation of chlorinated residual products (chlorinated lignin, chlorinated extractive substances) in the fibre during chlorine-based pulp bleaching makes possible the formation of HCl and a subsequent hydrolytic attack.

Photochemical attack leads mainly to the oxidation process of cellulose. An increase in the moisture content or in temperature increases the rates of both hydrolytic and oxidation degradation processes.

The breakdown and aging of paper therefore depends in a complex way on the chemical environment, the composition of the raw material etc. and can therefore in principle not be predicted from kinetic investigations (Arrhenius-extrapolation) unless the aging process is completely dominated by a single degradation process, e.g. the acid hydrolysis. Nevertheless, this seems to be the case since a correlation still seems to exist between accelerated and natural aging [2].

SAMPLES

1. White handmade paper
   (Made in India)
   Weight: 67 G.SM.
   Date: 14.02.76.
2. Chromatography-electrophorese paper
   (Made in USSR)
   Weight: 85 G.SM.
   Date: 09.02.74.
3. Micalent paper (thin transparent repair paper)
   (Made in USSR)
   Weight: 15–20 G.SM.
   Date: 16.06.70.
   Treated with poly (vinyl alcohol) solution

4. Chalk paper
(Made in USSR)

Weight: 240 G.SM.
Date: 14.11.88.

5. Newsprint paper
(Made in Russia)

Weight: 45–48 G.SM.
Date: 28.08.92.

6. Writing paper
(Made in Russia)

Weight: 63 G.SM.
Date: 19.03.89.

50% unbleached sulfitcellulose
50% bleached sulfitcellulose

7. Book paper 1832
(Manufactured and printed in Russia, Moscow)
8. Book paper 1869
(Manufactured and printed in Germany, Leipzig)
9. Book paper 1917
(Manufactured and printed in Germany, Bonn)
10. Book paper 1936
(Manufactured and printed in Germany, Berlin)
11. Book paper 1948
(Manufactured and printed in USSR, Omsk)
12. Book paper 1955
(Manufactured and printed in East-Germany, Berlin)

METHODS OF TEST

Determination of Moisture

There are a few principal methods for determining the moisture content of paper:

1) drying methods
2) distillation methods
3) titration methods [3]
4) infrared methods [4]

Drying method is the most commonly used procedure for determining the moisture content of paper because of its easiness and

simplicity. In these methods paper is exposed to relative humidity, and the decrease in weight occasioned by loss of moisture is determined. The common procedures are drying in an electrically heated oven, for general use, temperature of $105 \pm 2°C$ is recommended (TAPPI T 412)

Calculation:

$$m(\%) = \frac{W_1 - W_2}{W_1} \times 100,$$

where W_1 – weight of air dry paper sample; W_2 – weight of dried paper sample [3].

In the present work the moisture content was determined by the drying method. Results are given in Table 2.

Determination of Amount of Filler

The amount of the filler in paper is found from the ash content. The percentage of ash is always less than the percentage of the filler added to the paper stock or furnish since the complete retention during the forming of a sheet is rarely achieved.

On the other hand, the amount of ash may be greater than that corresponding to the filler content, because inorganic residues introduced to the pulp in processing (particularly alum) contribute to the ash content.

The ash content will be less than the amount of the filler in paper if the filler loses weight during ashing. For example, calcium carbonate is converted to calcium oxide (at 925°C) and clay satin white lose water of hydration [3].

Procedure

Paper samples in porcelain crucibles were ignited in an electric muffle furnace at $575 \pm 25°C$, cooled in desiccator, and weighed to 0,1 mg. The heating, cooling and weighing were repeated until the weight was constant.

Ash content (F) was calculated [5] from

$$\textit{Ash content (\%)} = \frac{\textit{weight of ash} \times 100}{\textit{weight of sample (100 - m)}} \times 100$$

Results are given in Table 2.

Determinant of Lignin

Lignin is stained or coloured in the presence of HCl or H_2SO_4 by a large number of reagents (phenols, amines) (Table 1) [6].

Aniline sulfate and dimethyl p-phenylene diamine have been used for testing groundwood papers. Sulfanic acid as a solid or as a solution (20 g of sulfanilic acid, 40 g of urea, 40 g of glycerol and 900 g of water) gives an intensive yellow colour after 5 min. when applied to moist groundwood. This method has been treated in detail to moist groundwood. This method has been treated in detail by Brayns [3]. Phloroglucinol method is used primarily to indicate the presence of lignin.

In the present work lignin was determined by the Brayns method. The following paper samples gave an intensive yellow colour No. 5, 6, 11, 12 and papers No. 8, 9, 10 gave a pale yellow colour.

Table 1

Colour reactions, which indicate the presence of lignin

Reagent	Colour	Reagent	Colour
phenol	greenish gray	aniline	yellow
o-cresol	greenish gray	o-aminophenol	yellow
m-cresol	gray	m-aminophenol	yellow
p-cresol	green	p-aminophenol	brownish yellow
resorcinol	gray	o-nitroaniline	yellow
hydroxyquinone	sorell-green	m-nitroaniline	orange
phloroglucinol	bright red or magenta colour	p-nitroaniline	orange
pyrogallol	green		
o-nitrophenol	yellowish green		
m-nitrophenol	yellowish green		
p-nitrophenol	yellowish green		

Determination of carboxyl groups

There are many methods for determining the carboxyl groups content of paper.

1) **Alkalimetric method**

Cellulose is treated with 0.01 M $NaHCO_3$ and 0.1 M NaCl mixture and the excess of alkali is titrated with 0.01 M HCl in the presence of methyl red indicator. It is a sample method but gives higher content of $COOH^-$ groups. In alkali conditions, carbonyl groups are oxidized to carboxyl groups [7].

2) Calcium acetate, zinc acetate method

A method based the exchanged reaction between carboxyl groups and calcium acetate results in the formation of acetic acid. Acetic acid is titrated with 0.01 M NaOH solution in the presence of phenolphthalein indicator. This method gives a lower content of $COOH^-$ groups because carboxyl groups, which are bound with lactate compounds, are not determined. The presence of carbonyl groups is ineffective [8].

3) Determination of $COOH^-$ groups by reaction with silver nitrophenolate ($AgOC_6H_4NO_2$)

$COOH^-$ groups react equivalently with siver ions. Carboxyl groups are determined by the decreasing of silver ions. The presence of reducing groups (carbonyl groups) gives incorrect results [9].

4) Determination of $COOH^-$ groups by alkaline dyes

Reaction with methylene chloride is most widely used. Decrease of the concentration of methylene chloride indicates the $COOH^-$ groups content [10].

5) Determination of $COOH^-$ groups by reactions with amines

Presence of carbonyl groups gives incorrect results [6].

6) Spectroscopic (IF) (UV) methods

Spectroscopic methods give approximate results [6].

In this work the content of $COOH^-$ groups in cellulose was determined by the exchange reaction with calcium acetate which reacts quantitatively with $COOH^-$ groups in cellulose. The result of this reaction is the forming acetic acid.

$$2Cell.COOH + (CH_3COO)_2Ca = (Cell.COO)_2Ca + 2CH_3COOH$$

(calcium acetate must be very pure and freshly prepared) Acetic acid is titrated with 0.01 M *NaOH* in the presence of phenolphthalein indicator.

Calculation

1) How many $COOH^-$ groups (g) is equal to 1 ml 0.01 M NaOH solution

$$P = \frac{45.01 \times 0.01M \times 1.000}{1000} = ... (g)$$

E_{COOH} = 45.01 (equivalent weight)

2) $COOH^-$ groups content (g) in air-dry cellulose

$$B = \frac{P(a-b) \times V_1}{V_2} = ... (g)$$

where a – ml of 0.01 M NaOH required for the titration of $COOH^-$ groups in cellulose; b – ml of 0.01 M NaOH required for the titration in case of the absence of cellulose; V_1 – ml of $(CH_3COO)_2Ca$ (50 ml); V_2 – ml of titrated $(CH_3COO)_2Ca$ solution (25 ml)

3) $COOH^-$ groups content (%) in absolutely dry cellulose

$$\frac{B}{G \times (100-m)} \times 100 = ... (\%),$$

where G – air-dry cellulose sample weight; m – content of moisture in cellulose

Procedure

1) Paper sample was treated with 0.5% HCl solution for 40 min. to avoid the formation of salts with $COOH^-$ groups

2) Cellulose was neutralized with water (congo red reaction)

3) Paper sample was dried in the air and defibred

4) Paper sample (~ 1g weighed to ± 0.01g) was placed in a flask (100–200 ml), added 50 ml 0.1 N calcium acetate solution and allowed to stand 12 hours (with stirring it several times).

5) 25 ml of the above-mentioned solution was taken from the flask with a pipette and titrated with 0.01 M NaOH solution in the presence of phenolphthalein indicator until the end point was reached (the yellow colour of the solution turned to violet-pink)

6) Parallel titration was performed without paper sample [11].

Results are presented in Table 2.

Accelerated aging

The aging stability of paper is usually characterized by exposing it to the so-called accelerated aging procedure [1, 2, 12, 13].

Although the Arrhenius approach towards estimating paper permanence appears simple and straightforward, predictions of permanence may be just as misleading as those obtained in the single temperature method. More than one reaction contributes to the

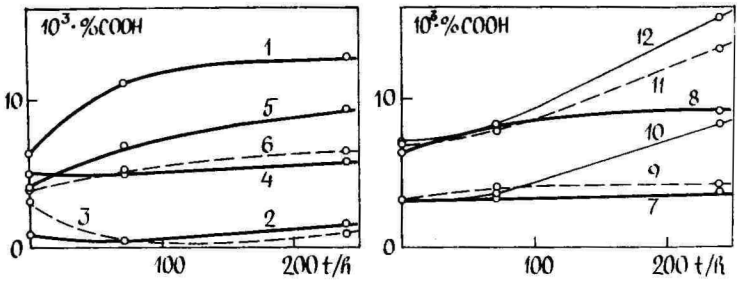

Fig. 1. Dependence between $COOH^-$ content and time of accelerated aging

degradation of paper, while the Arrhenius concept is applicable in a simple manner only to single reactions. It became very clear that much information had to be developed on the effect of moisture in the accelerated aging of paper. In order to develop of humidities and temperatures [14].

In this work conditions were chosen to maintain the moisture content of paper as closely as possible at the existing level when paper is conditioned at 50% RH and 19°C. Twelve different sorts of paper samples sealed into glass tubes were aged in an oven at 100°C for 72 hours and 240 hours the contents of carboxyl groups determined. Results are given in Table 2. (Fig. 1).

In the end, pH of the cold water extract was measured (TAPPI (T435) and ASTM (D778)). Results are presented in Table 3. (Fig. 2).

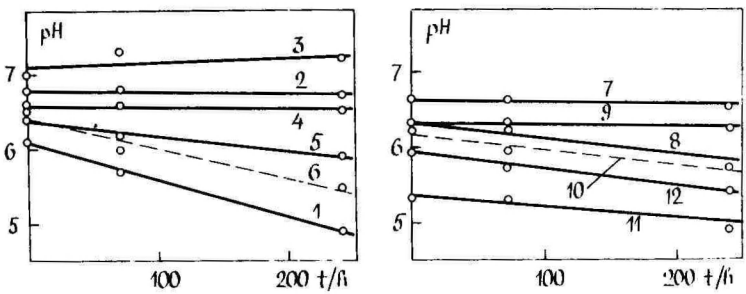

Fig. 2. Dependence between pH of cold water extract and time of accelerated aging

Table 2

Content of moisture, filler, lignin and carboxyl groups

No. of paper samples	Content of moisture m (%)	Content of filler F (%)	Lignin	Content of $COOH^-$ groups (10^{-3}%) before and after accelerated aging		
					72 h	240 h
1	5.47	4.94	–	6.4017±0.1874	11.1136±0.0469	12.8626±0.0932
2	5.55	0.17	–	0.8460±0.1892	0.4373±0.1897	1.5080±0.1904
3	3.76	0.22	–	3.0981±0.1829	0.3887±1.9440	0.9230±0.2034
4	3.05	36.39	–	4.9396±0.1798	4.9810±0.1816	5.7826±0.1800
5	5.77	0.83	+	4.0140±0.1873	6.8853±0.1358	9.3257±0.1807
6	3.30	15.82	+	3.7853±0.1815	5.3009+0.1792	6.4951±0.1799
7	3.62	1.16	–	3.1491±0.1820	3.1695±0.1821	3.7089±0.1869
8	3.46	21.04	+	6.2404±0.1785	8.1058±0.1762	9.0883±0.0830
9	3.64	17.81	+	3.1278±0.1815	3.9694±0.1788	4.1796±0.1829
10	3.07	25.60	+	3.0468±0.1816	3.4199±0.1813	8.2991±0.1770
11	4.96	13.81	+	6.7086±0.1743	7.6077±0.1859	13.0948±0.1752
12	5.27	23.76	+	6.9150±0.1802	7.9771±0.1934	15.1621±0.1735

DISCUSSION OF RESULTS

Tables 2, 3, 4 present the numerical data for the tests.

Table 3

pH of the cold water extract before and after accelerated aging

No. of paper samples	pH of the cold water extract before and after accelerated aging		
		72 h	240 h
1	6.1	5.7	4.9
2	6.8	6.8	6.7
3	7.0	7.3	7.2
4	6.6	6.6	6.5
5	6.4	6.2	5.9
6	6.5	6.0	5.5
7	6.6	6.6	6.5
8	6.2	6.2	5.7
9	6.3	6.3	6.2
10	6.2	5.9	5.7
11	5.3	5.3	4.9
12	5.9	5.7	5.4

The content of moisture, fillers, lignin and carboxyl groups are given in Table 2. Data on the carboxyl content of different paper samples indicate a small increase tendency [1], except for micalent paper (No. 3). This paper had been impregnated with polyvinyl alcohol which left the acidic properties and retained stability even during accelerated aging [15].

Increase of carboxyl content in chromatography-electrophorese paper (No. 2) and chalk paper (No. 4) is insignificant. Calcium carbonate, the most widely used coating in chalk paper has been found to increase the stability of paper under accelerated aging [12, 16].

Papers No. 7, 9, give the smallest change of the COOH groups content out of book papers. Papers No. 1, 12, 5 indicate the biggest rise of the carboxyl content. (Table 4., Fig 3).

Results of the pH (cold water extract) measurements are given in Table 3. If the pH values of papers (No. 2, 4, 7, 9) decrease only 0.1

pH unit, then the rest of the paper samples indicate a bigger decrease tendency. Changes of pH of micalent paper are comparable with the changes of carboxyl content.

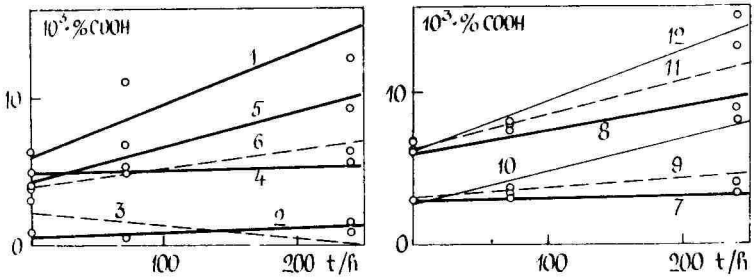

Fig. 3. Dependence between $COOH^-$ content and time of accelerated aging

For explaining the correlation between changes in the carboxyl groups content and cold water extract pH, slopes were calculated (tan α = x/y) and results are given in Table 4 (Fig. 3, 4).

Papers are presented in the order of slope size and it is observed whether the order of slopes is the same or not. Papers (No. 1–6) gave a surprisingly good correlation, but there are unremarkable changes, in the order of book papers.

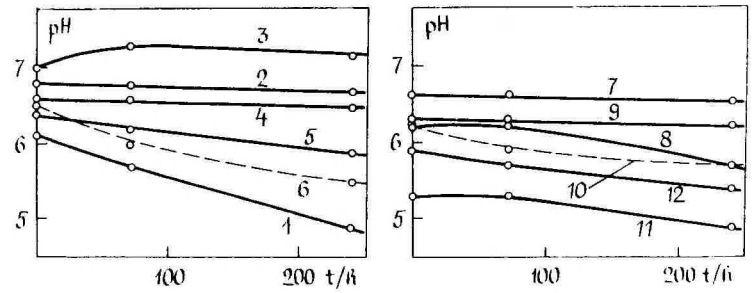

Fig. 4. Dependence between pH of cold water extract and time of accelerated aging

Table 4

Correlation between changes in carboxyl groups content and cold water extract pH

No. of paper samples	Slope of dependence between $COOH^-$ content and time	No. of paper samples	Slope of dependence between caold water extract pH and time
1	0.36	1	-0.50
5	0.24	6	-0.41
6	0.13	5	-0.21
2	0.04	2	-0.02
4	0.03	4	-0.02
3	-0.09	3	0.05
12	0.33	12	-0.23
11	0.22	8	-0.20
10	0.21	10	-0.20
8	0.16	11	-0.15
9	0.06	9	-0.05
7	0.02	7	-0.02

CONCLUSIONS

1) Changes in the content and changes of carboxyl groups in cold water extract pH gave comparable results.

2) The content and increase tendency of carboxyl groups are small.

3) The analytical tools presently available are not likely to be capable of measuring, or detecting changes in carboxyl due to natural or accelerated aging.

4) A far more useful approach than Arrhenius plots should be to probe the reactions that occur during natural aging, and devise accelerated aging conditions that cause the same reactions to occur.

REFERENCES

1. **Wilson W.K.** Restaurator, 3 (1979) 37.
2. **Fellers C.** "Ageing / Degradation of Paper." "FoU-projektet for

papperskonservering." Stockholm 1989 Report N. 1E 132 p.
3. **Browning B.L.** "Analysis of Paper.", Dekker inc, NY 1969, 335 p.
4. **Kuusela R.** "Infrared Moisture Measurement of Paper, Board and Pulp." Kuopio Un. 1990, 176 p.
5. Овдейчук В.П. "Лабораторный практикум по техническому контролю целлюлозно-бумажного произволство." Москва: "Лесная промышленность 1979. 231 ст.
6. Роговин З.А. Химия целлюлозы и его спутников." Москва-Ленинград: "Госхимиздат" 1953, 678 ст.
7. **Wilson W.K.** "Bestäming av karboxylgrupper i cellulosa." Svensk papperstidn. 51 (1948) 45–49.
8. Карливан В.П. "Методы исследования целлюлозы." Рига "Зинатне" 1981. 234 ст.
9. **Sooke A.** "Base-Combining Capacity of Cotton." J. Res. Nat. Bur. Stand., 26 (1941) 205–211.
10. **Davidson G.F.** J. Text. Inst., 39 (1948) 65.
11. **Davidson G.F.** J. Text. Inst., 39 (1948) 102.
12. **Barrow W.J.** "Deterioration of Book Stock Causes and Remedies." The Virginia State Library, Richmond 1959, 70 p.
13. **Wilson W.K.** Restaurator, 4 (1980) 1.
14. **Graminski E.L.** Restaurator, 2 (1978) 175.
15. **Baer N.S.** Restaurator, 2 (1972) 5.
16. **Wilson W.K.** Restaurator, 1 (1969) 79.

ALDOLASE AND SORBITOL DEHYDROGENASE IN BOVINE LIVER AND HEART MUSCLE

A. Karus
Department of chemistry, Estonian Agricultural University

ABSTRACT

Aldolase and sorbitol dehydrogenase from bovine liver and heart muscle were studied. Both consist of four subunits. The Effects of pH, t°, EDTA and $ZnCl_2$ to the activity of enzymes were determined. Also the isoenzymspectrum of aldolase and sorbitol dehydrogenase in liver and heart muscle were described.

Recently biochemical and specially enzymological methods have been employed by agricultural sciences and among these by animal breeding. It is due to great informativity of enzymological tests, in particular of the multiplicity of enzymes [1]. Aldolase (D-Fructose-1,6-bisphosphate-D-glyceraldehyde-3-phosphatase; EC 4.1.2.13) and sorbitol dehydrogenase (L-Iditol: NAD^+ 5-oxidoreductase; EC 1.1.1.14) are enzymes of different metabolic ways of carbo-hydrates. Aldolase catalyses the reversible splitting of fructose-1,6-bisphosphate to two triosephosphates. Aldolase occurs in three parent forms A, B and C and their hybrids. Aldolase A is the classical muscle enzyme, B – liver aldolase and C – brain aldolase. Sorbitol dehydrogenase operates specifically with NAD^+ and catalyses the reversible oxidation of several acyclic polyols to ketoses. The enzyme occurs in the livers of all mammalian species but there are few reports about the multiplicity of sorbitol dehydrogenases from bovine tissues.

METHODS.

Enzymes. Aldolase A and B were prepared by the Scopes method [2]. Sorbitol dehydrogenase was prepared and purified as described elsewhere [3].

Assays. Aldolase activity was assayed by the modified method of Sibley and Lehninger [4]; Sorbitol dehydrogenase activity was assayed by the UV-method [5].

Electrophoresis. Disc PAGE electrophoresis was performed in 7.5% vertical gels. The strips were stained for aldolase activity by a histochemical procedure [6] and for sorbitol dehydrogenase activity by the method of Sudovtsov and Zharmuhhamedova [7].

Molecular weight. The molecular weight of subunits was assayed by the method of SDS-PAGE electrophoresis and the molecular weight of enzyme was assayed by the method of gel filtration on sephadex G-200.

RESULTS AND DISCUSSION.

The bovine muscle aldolase (A) had a specific activity of 2.4 nkat/mg protein. Aldolase B (from bovine liver) had a specific activity of 46 pkat/mg protein. Aldolase is composed of four subunits. The molecular weight of aldolase is 160 $\pm$ 6 kD.

The bovine muscle sorbitol dehydrogenase was identical with the sorbitol dehydrogenase from bovine liver and had a specific activity ranging from 10.1 to 10.7 nkat/mg protein. Sorbitol dehydrogenase (M = 112 $\pm$ 6 kD) consists of four subunits with molecular weight 26.7 $\pm$ 1.2 kD.

The effect of pH on the velocity of reactions. Aldolase: the effect of pH on the rate of the splitting of fructose-1.6-bisphosphate is shown in Fig. 1. Optimum pH for aldolase A was 7 – 8 and for aldolase B - 7.4. The effect of pH on the activity of sorbitol dehydrogenase on the rate of the oxidation of sorbitol by NAD^+ (optimum) pH 9.0) and on the rate of the reduction of fructose by NADH (optimum pH 7.2) are shown in Fig. 2.

The effect of temperature on the velocity reactions is shown in Fig. 3. Optimum t° to realize maximum of the activity of aldolase was 37–41° C and for sorbitol dehydrogenase 31–35° C. Low optimum t° characterizes the thermolability of sorbitol dehydrogenase.

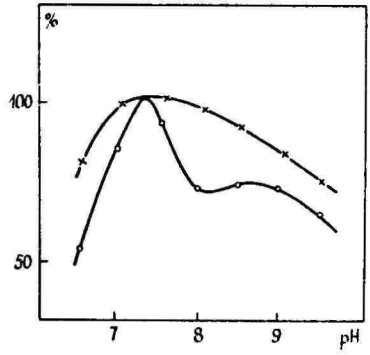

Fig. 1.

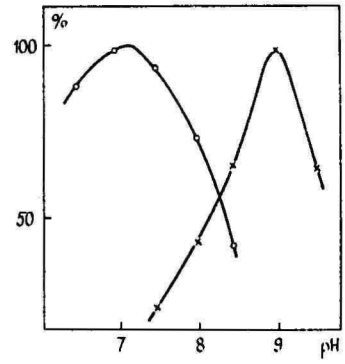

Fig. 2.

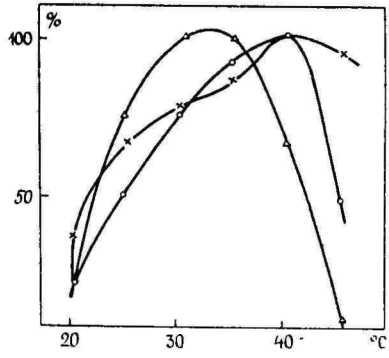

Fig. 3.

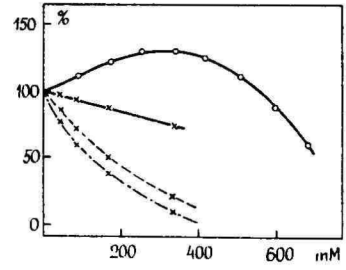

Fig. 4.

Several compounds inhibit sorbitol dehydrogenase. As Maret and Auld (B) are of the opinion that the active centre of sorbitol dehydrogenase contains Zn^{2+}, the effects of EDTA and $ZnCl_2$ on the activity of sorbitol dehydrogenase were probed (Fig. 4). EDTA inhibits competitivly the enzyme at pH 9.0. The activity of the enzyme in the presence of $ZnCl_2$ was maximum at the concentration ranging from 320 to 350 μM $ZnCl_2$. These results suggest that the enzyme contains

possibly Zn and coincides with the conclusions of Jeffrey, Jornwall [9], Maret and Auld [8].

The difference in the mobilities of isoenzymes suggested a possibility of the resolution of these proteins by electrophoresis. Aldolase activity was detected by means of an activity stain. Our method (see Methods) is relatively more sensitive to aldolase A than to aldolase B (with FDP as substrate). The aldolase activity in heart migrated as a single band. The aldolase activity in liver migrated as a single band with a different velocity. Aldolase hybrids were not observed. The sorbitol dehydrogenase activity in heart was migrated as two bands. The sorbitol dehydrogenase from bovine liver was resoluted into four isoenzymes. Two of these were identical with the sorbitol dehydrogenase from heart.

Abbreviations employed in this paper: NAD, oxidized nicotinamide adenine dinucleotide; NADH, reduced nicotinamide adenine dinucleotide; EDTA, ethylene diamine tetraacetic acid; FDP, fructose-1,6-diphosphate sodium salt.

REFERENCES

1. **Graml R.** Einfluß von Markergenen auf Milchzusammessetzung. – Diss. ... D. der Landwirtschaft. München-Weihenstephan, 1982. 320 S.
2. **Scopes R.K.** Anal. Biochem., 114 (1981) 8.
3. **Karus A.L.** Physico-chimitsheskaja characteristica sorbitol degidrogenasõ, võdelennoi is petsheni i serdetshnoi mõshtsõ korov. Mosk. vet. akademija im.K.I.Skrjabina, M.1990, 10 s. Dep. VNIITElagroprom.: ser. Zhivotnovodstvo/biolog.osnovõ/. 1990, N.217, VS-90. Opubl. 1990. N. 8. s. 5. (in russian)
4. **Sibley J.A., Lehninger A.L.** Determination of aldolase in animal tissues // J. biol. Chem., 177 (1949) 859.
5. **Gerlach U., Hiby W.** Sorbit-Dehydrogenäse / in Bergmeister H.U. Methoden der enzymatischen Analyse. Weinheim: Chemie, 1 (1974) 601.
6. **Loyda S., Goßrau R., Schiebler T.** Gistochimia fermentov. Laboratornõe metodõ. M: Mir, 1982. – 270 s. (in russian)
7. **Sudovtsov V.E., Zharmuhhamedova T.J.** Physico-chimitsheskie characteristiki sorbitoldegidrogenasõ is tsitoplasmõ kletok petsheni bõka. Vopr. med. chimii. 33 (1987) 81–84. (in russian)
8. **Maret W., Auld D.S.** Biochemistry. 27 (1988) 1622.
9. **Jeffrey J., Jornwall H.** Proc. Nat. Acad. Sci. USA., 80 (1983) 901.

A COMPARATIVE STUDY OF ESTONIAN CURATIVE MUDS

T. Ilomets, A. Koorits, S. Peil, A. Pärn, S. Salm, K. Utsal, V. Utsal and I. Veermäe

Department of Chemistry, University of Tartu,
Estonian Agricultural University

ABSTRACT

The paper is a comparative description of three more important curative muds of Estonia – the peloid of the Haapsalu Bay, the peloid of the Kuressaare Suurlaht, and the sapropel of the Värska Bay. The humic acids, fulvic acids and hymatomelanic acids extracted from these curative muds were compared on the basis of their chemical, physico – chemical and physical characteristics. Their combustion heat and oxydation rates were calculated from the elemental composition. Also the aminoacids and carbohydrates were established. The mineral content was determined X-Ray-difractometrically. The samples were also characterised thermographically.

Estonia is rich in curative mud – a unique natural resource. Curative mud has long been known as a means of treatment in folk medicine, but the official medicine has used it since 1824 when it was applied for the first time in the village of Rootsiküla, the island of Saaremaa. The actual initiator of mud cure was K. H. Hunnius, a physician of Haapsalu. In 1825 he opened there an establishment for providing mud baths and mud cure. Similar establishments were also founded in Pärnu (1838) and Kuressaare (1840). The founder of chemical research into the local curative muds, a former professor of chemistry of Tartu Univesity D. H. Grindel was the first one to start chemical research into our curative muds. His paper which appeared in 1824 contained data on the composition of the sea mud of Rootsiküla. Thus, in 1994 we will mark the 170th anniversary of mud treatment and

of its scientific studies in Estonia [1, 2, 3, 4].

From the point of view of colloid chemistry, curative muds belong to the so-called periodical colloidal structures [5]. As concerns their formation, such colloids are considered to be coagulation systems. They form as a result of the worsening of the aggregative stability of a dispersed system. A specific property of coagulation structures is thixotropy. Structures got destroyed by an agency of external mechanical action (stirring, shaking, etc.), but they are able to restore themselves after a certain time. As to the physico-chemical and mechanical properties, these structural systems lie between ideal elastic substances and Newton liquids. Systems having coagulation structures posess low strength, certain plasticity and elasticiy. Such systems also exhibit creep i.e. the ability to slowly develop, in the course of flow, a considerable residual deformation practically without a noticable destruction of the three-dimensional network.

Syneresis is another property which is often found in systems having coagulation structures. It implies a spontaneous decrease in the dimensions of gel with the simultaneous separation form it of the dispersion medium contained in cells. Syneresis occurs because in gelation the small number of contacts that does not correspond to the maximum condensed state of a structure is formed between structural elements. The same factors which promote coagulation also cause and favour syneresis. Coagulation structures can retain their stability under certain conditions only. Changes in the solvate layer or in the electric double layer influence the forces of attraction between particles which either start peptization (restoration of the aggregative independence of particles) or promote further coagulation. As a result of the latter, aggregation increases until the system is not able to form gel any more, and thus a precipitate will be formed. For instance if the water jacket reduces until reaching a certain point, the system will lose its ability to restore the previous state.

Very little is known about the structures and composition of the particles forming coagulation structures. Yet, we can guess that they are rather complicated. The curative muds of Haapsalu, Kuressaare Suurlaht and Värska can be treated as typical lyophilic system retaining their original native properties within a certain range of medium conditions. Their gel is probably made up of unsymmetrical (isodiametric) polydispersal particles having

1) a crystalline, highly dispersal mineral phase
2) an amorphous colloidal mineral part

3) a high-molecular organic part

4) a low-molecular organic part

5) a stabilizing layer surrounding the whole aggregate (solvate layer, electrical double layer).

Water acts as a dispersion medium, containing:

1) dissolved mineral salts

2) low-molecular organic compunds

3) dissolved oligemeric and soluble high-molecular compounds.

The dispersion medium established in the layer of curative mud is called mud solution.

The rheological properties of curative muds can be described by means of the maximum shearing stress Θ (mg/cm^2). The flow starts when the shearing stress F exceeds the critical limit value Θ which results in the destruction of the structure, i.e.

$$F - \Theta \geq O$$

Such a flow is called plastic flow and the critical (intimate) shearing stress Θ - the yield point. The critical shearing stress reflects the structural strength of the system, also being a quantity enabling us to compare it with other similar objects. The changes taking place in the system and having on effect on its structure, are very well reflected by Θ (e.g., such phenomena as the influence of centrifugation, the aging of gel, etc.).

The studying of sedimentation curves is another means of getting information about the differences and changes in the colloidal structures of curative muds.

The ration of the components of curative muds, their nature and colloid chemical properties depend on the deposit area of mud and on its types. High-molecular organic huminic substances have a strong effect on the properties of curative mud. According to their solubility in alkali (NaOH, etc.), huminic substances fall into three main groups [6]. Free huminic acids are directly soluble, while bound huminic acids have to be treated with HCl or some other acid in order to turn them from calcium and magnesium salts into free acids and then to dissolve them in alkali. The so-called humine cannot be dissolved. Huminic acids are polyacids [7] that have natural high-molecular macroligand properties containing nitrogen and aromatic structure units. On the basis of their solubility, huminic acids are also distributed into three main gorups. The fraction of humic acids and hymatomelanic acids precipitate from alkaline solutions their acidic treatment. Hymatomelanic acid is separated via ethanol extraction. The obtained acidic solution contains

a fraction of fulvic acids. Huminic acids are polydispersed relative to molecular weight [8]. They have a specific elemental composition, differing from other natural organic compounds. Its basis characteristics are the contents of carbon, hydrogen, oxygen, and nitrogen. The contents of these elements in humic acids depend on their formation place, on the nature of the biochemical processes there, and on the factors causing geochemical transmutations. Humic acids can be characterized by their oxidation state ω

$$\omega = \frac{2/0/ - /\overline{H}/}{/C/}$$

where /0/, /H/ and /C/ denote the content of elements per 100 g of a compound in moles [6].

It is possible on the basis of the elemental content to calculate the combustion heats of huminic acids [6]:

$Q = 90\ (C\ \%) + 34.4\ (H\ \% - 50\ [0.57\ (0\ \%) - 4\ (N\ \%)]$

Q = cal/g

The interaction of elements, oxidation states and combustion heats make it possible to characterize, compare and distribute different humic acids into groups. Acidic and alkaline hydrolysis, mild oxidation and reduction are the main methods used for the determining of the basic structural components of humic acids. The common products of acidic hydrolysis normally are amino acids and monosaccharides, some other compound types (e.g., nucleinic acids / uronic acids aminosaccharides, etc.) being less remarkably represented. The yield of aminoacids from humic acids ranges from 5 % to 10 %, that of carbohydrates being 10–30 % [7].

In several studies dealing with humic acids, the method of derivatography or differential thermogravimetry has successfully been used [9], permitting to register simultaneously weight variations (the TG-curve), the rate of weight variations (the TDC-curve), enthalpy variations (the DTA-curve), temperature variation in time (the T-curve), temperature within the range of 20–1000°C. Derivatograms give significant data about the thermodynamics and kinetics of the processes where either substances or compounds are involved. It is possible to compare objects of research both qualitatively and quantitatively, to differentiate between several stages of the process as a whole and to characterize them quantitatively [9].

Depending on the medium of formation, curative muds contain a

certain amount of mineral components, some of which form finely-dispersed crystalline phase, the rest being colloidal x-ray-amorphous. The role of the latter part in the formation of the colloid chemical properties of curative mud need not be smaller than that of humus substances. The difractometric method enables us to find out the mineral composition of curative mud and the amounts of separate minerals [9]. The same method is applied for a quantitative determination of the amounts of x-ray-amorphous substances.

RESEARCH MATERIAL AND METHODS

Curative Muds

The average samples of the muds of Haapsalu Bay, Suurlaht of Kuressaare and of Värska, were taken from large mud storage tanks in the vicinity of mud cure centres. Similar techniques were applied for the treatment, decomposition and analysis of curative muds.

Elemental Analysis

The quantitative analysis of elements C, H, O, N was carried cut on an automatic analyser "Carlo Erba". A separate weight portion was used for determining the oxygen content. Other elements were determined from one and the same weight sample. Three parallel analyses were carried out [11, 12].

Maximum Shearing Stress

Maximum shearing stress was measured by means of a "GP-4" instrument ("Geolograzvedka") meant for studying fine clayey suspensions. This is a torsional apparatus whose main part is a rifled cylinder suspending on a steel thread. The other end of the thread is fastened to the torsion head. The cylinder is immersed into a cuvette containing the suspension which is being studied. It is kept there until the destroyed structure has been restored. After that the torsion head is turned by an angle enabling steady motion of the cylinder. The value of this torsion angle is fixed and the maximum shearing stress is calculated.

$$\Theta = K \cdot \alpha$$

α – experimentally determined rotation angle,
K – constant of apparatus.

Measurements are carried out at a constant temperature.

Gel Strength

Gel strength, i.e., resistance to test the sample foundering was measured on a Valenti apparatus with a hemispheric standard test unit area of 2 cm^2, its total weight being 71.75 g.

Precipitation Centrifugation

Laboratory centrifuges with angular rotors and suitable capacities were used for the liberation of curative mud from water. If G (acceleration gravity) had a constant value, the necessary duration of centrifugation was fixed, so that the water content of a precipitate would not change. Measurements were made at different G values. The content of water was determined by means of gravimetric analysis. The weighed sample was dried at 110°C.

Derivatography

Derivatograms were taken on a derivatograph of F. Paulik's, J. Paulik's and L. Erdey type (Hungary) within a temperature range of 20–1000°C, at the ratio of 10° min^{-1} [9].

Curative muds were oxidized with the 25 % hydrogen peroxide. The sample was put into a porcelain vessel, an oxidant was poured on it portion by portion until the contents of the vessel had turned light. After the cessation of an active reaction, the reaction vessel was set on a boiling water bath, where it was vapourated until dry.

Difractometry

Difractograms were registered on a modified difractometer DROH-3M [9]. The FeK radiation and Mn filter were used. Sensitivity margin was T-1000 imp/s, time constant 2.5 s. In order to quantitatively determine the crystalline phase, the proportionality relative to pure constants were calculated on the basis of artificial mixtures. The quantitative determination of the x-ray-amorphous portion was carried out by using the method of K. Utsal.

Huminic acids

Raw curative mud was centrifuged at G = 1450. It was dried in the air, extracted exhaustively with bensene: ethanol (1:1) mixture in a Soxlet extractor. The extract was evaporated in a rotating evaporator until dry. The residue (bituminic residue) was weighed. The curative

mud powder liberated from bituminous fraction underwent a 24-hour treatment of constant shaking with the aqueous solution of 0.1 mol sodium hydroxide.

Alkaline extract was separated from the precipitate by means of centrifugation. To separate the finely-dispersed mineral fraction from the solution of huminic acids, the alkaline extract was centrifuged in a super-centrifuge at the speed of 2300 r/min. The centrifuged product was acidified with sulphuric acid until pH = 1. The precipitate was separated by means of centrifugation, it was washed with destilled water to reach the natural reaction, dialysed to liberate it from sulphate ions, and concentrated in a rotator-vaporizer. The obtained mixture of humic acid and hymatomelanic acid why was purified from the residues of mineral matters, and dried. The precipitate of humic acid was dried. The acid solution of fulvic acid was concentrated in a rotatorvaporizer, dialysed and purified according to the methods described in [11, 12].

Amino Acids

The samples to be analysed were hydrolized in a sealed glass ampoule with 6 mol of hydrochloric acid for 30 hours at 100°C. After that they were treated according to the methods [14]. Prepared samples were analysed on an automatic analyser "Hitachi". The data were used for the calculation of the distribution of basic: acidic, OH-polar, and neutral amino acids (the same method as in [14] was used). Minimal molecular weight of a hypothetical "peptide" was also found.

Carbohydrates

A sample of humic, fulvic, and hymatomelanic acid was heated for 30 min at 100°C in 1.0 mol of sulphuric acid in a sealed glass ampoule. The excess of sulphuric acid was neutralized with powdered $BaCO_3$. The precipitate was substantially washed, the solution of carbohydrates was concentrated in a rotator-vaporizer. Varbohydrates underwent chromatography on "Whatman 3" paper three times with the mixture of n-buthanol-acidic acid-water (4:1:1) and once with the mixture of n-buthanol-pyridine-water (5:3:1). Chromatograms were developed with aniline oxalate reactant and then densitometrized. Calibration curves were found on the basis of pure standard carbohydrates. The final result was calculated from five parallel tests [15].

RESULTS

The research results on the curative muds of Haapsalu, Kuressaare Suurlaht and Värska and on their free humic acids are presented in Tables 1–6.

A major problem that one has to tackle when studying these objects is getting an average sample. We found it most appropriate to take average samples out of large amounts of mud stored for curative purposes, as in tanks the mud is more homogenous because it is constantly stirred. We presumed that the composition and properties of the organic fraction and of the anorganic colloidal part do not differ very remarkably within a deposit area. Although, a ratio between the components of the anorganic crystalline stage might vary. The studying of the water content and the ability of the water sorption of mud is a valuable source of data on their colloid chemical properties. Centrifugation experiments have shown that when applying a certain acceleration gravity (G), after a certain period of time such an equilibrium is reached where it is not possible to further condense the precipitate. This margin and the quantity characterizing it are different in different muds (see Table 1). The measurements of the maximum shearing stress of the original and centrifuged samples have revealed that centrifugation changes the reologic properties of curative muds.

Critical shearing stress Θ is another factor showing the character of curative mud (see Table 1).

Table 1 presents only temperatures corresponding to the maximums on the ATC and DTA curves and weight losses at three different temperatures. These data have been taken from the thermograms of curative muds and their products oxidized with hydrogen peroxide. Huminic acids of curative muds are characterized similarly.

The composition of the anorganic part of curative mud was determined as follows. First of all, the mineral and x-ray-amorphous phases of the native muds and after that of a sample heated at 600°C were determined. Muds found in three different deposits can be clearly differentiated from one another. Thus, a difractogram could be one of the factors acting as standard in the qualitative and quantitative description of curative mud (see Table 1). Both organic and inorganic compound groups found in mud solution as well as the compounds being in a equilibrium state between colloidal particles and dispersion medium are significant from the point of view of medicine. Since free humic

acids probably also belong to this group, we have chosen to study them more closely.

There is no standard method for the separation and purification of the huminic acids (free huminic acids included) of curative muds. Owing to that, different researchers do not have similar results, though they have the same objects of research. We have mainly applied methods used in studying sea and lake sediments [12, 16]. For the purposes of a better comparison, all research operations and analyses of curative muds were carried out under possibly similar conditions, with a great number of simultaneous test runs.

The effect of the mineral part contained in the objects of analyses should be taken into account when determining the elemental content (C, H, O, N) [10]. Elemental composition also served as a basis for the calculation of oxidation state ω as well as of combustion heat Q (see Table 1 and 2).

When calculating the content of amino acids in huminic acids, one should bear in mind, that the latter acids also contain plysaccharidic structural units that undergo hydrolysis more easily than the peptide bond. Therefore, the Maillard reaction (a reaction between a monosaccharide and an amino acid) is quite probable here, causing losses of both substances. The results of the analyses are given in Table 3. These data reflect quite well the differences in the total of the contents of different amino acids of different type of huminic acids, and the differences between similar types of huminic acids found in different deposits. As to fulvic acids, their content of the amino acidic fraction is smaller than in the case of hymatomelanic and humic acids [10]. Table 4 presents the distribution of amino acids according to their types. The minimal molecular weight of the hypothetical "polypeptide" part is also to be found there (cf., [14]).

The hydrolysis of the polysaccharidic and glycoprotein parts of huminic acids takes place under milder conditions than that of amino acids. Therefore, the Maillard reaction as a reaction is not so significant for the analysis of carbohydrates. For the quantitative determination of carbohydrates we used the densitimetry of paper chromatograms with monochromatic light (cf. [14]). This method turned out to be quite suitable and reliable for getting comparative information about the carbohydrate contents of different huminic acids. The results are given in Table 5. It should be mentioned that fulvic acids have a remarkably high content of carbohydrates which is in agreement with literature data [10]. On the basis of the results of quantitative determination of C, H.

O, N, amino acids and carbohydrates, we calculated the total balance of carbohydrates, amino acids and the rest of the organic matter and mineral part.

Table 1

Comparison of curative muds

Characteristic feature	Curative mud		
	Haapsalu	Kuressaare Suurlaht	Värska
1. Dry matter (%)	18.12	7.27	8.92
2. Weight loss at 600°C relative to dry matter (%)	16.09	30.54	51.83
3. Weight loss at treatment with 30 % H_2O_2 (%)			
relative to dry matter	8.54	15.72	28.48
relative to sum of elements C, H, O, N	54.19	47.84	57.11
4. Elemental content (%)			
C	5.51	13.77	22.40
H	1.22	2.26	3.09
O	8.29	15.49	22.33
N	0.64	1.35	2.06
Total of elements	15.76	32.86	49.87
5. Heat of combustion Q(cal/g)	1861	2758	3155
6. Oxidtion state	+0.13	-0.25	-0.14
7. Bituminic matter			
in dry matter (%)	1.67	1.32	1.95
relative to sum of elements C, H, O, N	10.60	4.02	3.91
8. Dry matter in mud solution (%)	0.61	0.13	0.07
9. H_2S (%) in native mud	0.018	0.012	0.096
10. Centrifugal sedimentation (1h 1450 g)			
Water in initial mud (%)	81.9	92.7	91.1
Centrifugated mud			
water (%)	71.7	79.9	83.8
dry matter (%)	28.3	20.1	16.2
strength (g/cm^2)	67	77	292
relative strength	1.0	1.2	4.1
11. Free huminic acids in dry matter (%)			
Humic acids (Ha)	0.56	0.41	1.74
Fulvic acids (Fa)	1.16	1.75	1.87
Hymatomelanic acids (Hy)	0.07	0.12	1.38
Total free huminic acids	1.79	2.28	4.99
12. Derivatography			
DTG maxima at (°C)			
initial mud	135	135	140
	275	280	245

Characteristic feature	Curative mud		
	Haapsalu	Kuressaare Suurlaht	Värska
	540	450	(440)
		550	
treated with H_2O_2	125	120	110
	170	175	170
	260	240	290
	550	440	350
		480	430
		540	525
			675
humic acids	140	140	140
	250	240	280
	330	320	375
DTA maxima at (°C) for initial mud			
endothermic	145	135	145
exothermic	310	340	295
	425	450	(440)
	610		
treated with H_2O_2			
endothermic	130	120	100
	170	120	170
exothermic	280	300	280
	420	400	440
	640	450	760
		480	
humic acids			
endothermic	150	155	150
exothermic	280	240	335
	450	370	390
	530	680	520
		780	640
Maximum weight loss (MWL) up to 1000°C (%)			
initial mud	20.09	32.23	45.60
treated with H_2O_2	12.89	15.82	24.14
Weight loss up to 350°C (% relative to MWL)			
initial mud	51.54	50.00	46.67
treated with H_2O_2	51.51	57.14	64.29
Weight loss up to 600°C (% relative to MWL)			
initial mud	86.59	84.29	81.11
treated with H_2O_2	75.75	100.00	78.57
13. Critical shearing stress for mud containing dry matter (%) at 20°C, CSS = 300 mg/cm^2			
fresh	12.6	6.2	7.3

Characteristic feature	Curative mud		
	Haapsalu	Kuressaare Suurlaht	Värska
old	–	9.2	–
fresh centrifugated	–	9.8	–
CSS = 500 mg/cm^2			
fresh	15.0	7.0	8.1
old	15.7	9.4	–
fresh centrifugated	–	11.0	–
CSS = 1000 mg/cm^2			
fresh	17.3	–	8.5
old	–	10.4	–
fresh centrifugated	–	12.3	–
14. Minerals (MinF) and x-ray-amorphous (RAF) in %			
initial mud			
MinF	37.72	47.56	15.60
RAF	62.28	52.44	84.40
Fe_2O_3 (according to hf 45)	10	7	30
minerals (%)			
Quartz	15.67	21.30	5.36
Calcite	–	4.00	–
Dolomite	0.94	4.20	–
Feldspar	4.90	4.00	1.22
Hydromica	11.75	10.01	4.38
Kaolinite	3.13	1.61	1.17
Pyrites	0.82	2.44	3.18
Gypsum	0.51	–	0.29
Total	37.72	47.56	15.60
Mud heated up to 600°C			
MinF	49.87	57.84	49.56
RAF	50.13	42.16	50.44
Fe_2O_3 (according to hf 45)	12	7	35
Amorphous	10.44	5.24	20.75
minerals			
Quartz	18.86	26.93	14.10
Calcite	–	1.88	–
Dolomite	–	2.63	–
Feldspar	7.94	6.56	3.12
Hydromica	19.59	15.80	12.09
Haematite (α-Fe_2O_3)	1.56	1.76	7.05
Maggemite (β-Fe_2O_3)	–	–	7.20
Gypsum	1.92	2.28	6.00
Total	48.87	57.84	49.56

Table 2

Elemental content of free humic acids (%) in ash free matter

Curative muds	C	H	O	N	/C/	/H/	/O/	/N/	C/H	C/O	C/N	H/C	O/C	N/C	H/O	Q_{cal}/g	ω
Haapsalu																	
Ha	45.00	6.66	39.60	8.94	3.75	6.59	2.44	0.64	0.57	1.54	5.86	1.76	0.65	0.20	2.70	4370	-0.46
Fa	38.20	5.59	52.30	3.92	3.18	5.53	3.27	0.28	0.57	0.97	11.36	1.74	1.03	0.10	1.69	2140	+0.32
Hy	45.70	7.40	42.10	4.87	3.81	7.33	2.63	0.35	0.52	1.45	11.17	1.87	0.69	0.11	2.79	3510	-0.54
Kuressaare Suurlaht																	
Ha	45.10	7.03	40.20	7.70	3.76	6.96	2.51	0.55	0.54	1.50	6.84	1.85	0.89	0.17	2.77	4092	-0.50
Fa	42.40	6.33	46.00	5.24	3.53	6.27	2.88	0.37	0.56	1.23	9.54	1.78	1.08	0.12	2.18	3080	-0.14
Hy	48.40	6.62	39.00	6.03	4.03	6.55	2.44	0.43	0.62	1.65	9.37	1.63	0.81	0.12	2.68	4093	-0.41
Värska																	
Ha	37.80	6.35	47.01	6.18	3.15	6.29	2.94	0.44	0.50	1.07	7.16	2.00	0.93	0.14	2.14	2929	-0.13
Fe	42.10	5.40	49.00	3.58	3.50	5.35	3.06	0.26	0.65	1.14	13.46	1.53	0.87	0.74	1.74	2673	+0.22
Hy	42.01	6.22	47.50	4.00	3.50	6.16	2.97	0.29	0.57	1.18	12.07	1.76	0.83	0.08	2.07	2848	-0.06

Table 3

Content of amino acids relative to free huminic acids (%)

Amino acid	Haapsalu			Kuressaare Suurlaht			Värska		
	Ha	Fa	Hy	Ha	Fa	Hy	Ha	Fa	Hy
Lys	0.97	0.46	0.98	1.03	0.62	0.77	0.92	0.48	0.47
His	0.15	0.05	0.13	0.19	0.09	0.11	0.19	0.06	0.11
Arg	0.85	0.25	0.87	0.87	0.43	0.53	0.75	0.16	0.30
Asp	1.78	1.25	2.53	3.29	1.96	3.47	2.17	0.66	1.03
Thr	1.28	1.01	1.48	1.83	1.05	1.63	0.92	0.58	0.67
Ser	1.22	0.65	1.42	1.56	0.98	1.56	1.17	0.55	0.77
Glu	2.61	1.21	3.40	2.86	1.78	2.66	1.98	0.53	1.00
Pro	1.13	0.48	1.82	1.33	0.78	1.16	0.81	0.18	0.42
Gly	1.50	0.77	1.90	1.61	1.30	1.72	1.26	0.69	0.88
Ala	1.57	0.82	1.94	1.70	1.44	1.62	1.10	0.66	0.63
Val	1.43	0.72	2.21	1.50	1.16	1.43	0.92	0.54	0.53
Met	-	0.07	-						
Ile	0.97	0.37	1.27	0.97	0.68	1.08	0.55	0.29	0.38
Leu	1.60	0.53	2.01	1.54	1.08	1.82	0.91	0.41	0.59
Tyr	0.62	0.21	0.72	0.91	0.41	0.77	0.49	0.22	0.24
Phl	1.05	0.33	1.50	1.27	0.63	1.40	0.58	0.21	0.35
Total:	18.73	9.18	24.18	22.46	14.39	21.73	14.73	6.22	8.37

Table 4

Classes of Amino acids (%)
and hypotetical minimum molecul mass (MMM) in Daltons

Amino acids	Ha	Fa	Hy
Haapsalu			
acidic	22.5	24.6	19.3
basic	7.5	4.9	4.4
OH-polar	17.5	21.3	15.2
non-polar	52.5	49.1	60.5
MMM	4612	5417	6612
Kuressaare Suurlaht			
acidic	25.0	22.9	26.4
basic	6.2	4.2	3.8
OH-polar	21.9	16.6	16.9
non-polar	46.7	56.2	52.8
MMM	3792	5346	6034

Amino acids	Ha	Fa	Hy
Värska			
acidic	27.5	14.0	21.2
basic	7.5	6.2	6.4
OH-polar	17.5	20.3	21.2
non polar	47.5	59.2	51.1
MMM	10221	6984	5337

Table 5

Content of saccharides (%)
relative to free huminic acids in investigated muds

Huminic acids	Rham	Xyl	Ara	Man	Glu	Gal	Total
Haapsalu							
Ha	0.5±0.2	traces	0.8±0.1	1.7±0.2	1.0±0.1	0.8±0.1	4.8±0.5
Fa	2.9±0.3	0.83±0.58	2.7±0.2	6.6±0.4	4.6±0.2	3.3±0.3	20.9±1.9
Hy	0.4±0.3	traces	1.2±0.4	4.1±0.5	1.2±0.3	0.5±0.3	7.4±1.8
Kuressaare Suurlaht							
Ha	2.3±0.3	0.20	2.2±0.2	5.3±0.4	3.7±0.4	2.5±0.3	16.2±1.4
Fa	4.2±0.6	1.22	4.9±0.8	9.4±0.9	7.8±0.4	4.9±0.7	32.4±3.4
Hy	1.7±0.7	traces	0.6±0.3	2.7±0.6	1.3±0.2	0.8±0.2	6.8±1.7
Värska							
Ha	0.2±	traces	0.2±0.2	2.0±0.3	0.5±0.2	0.6±0.2	3.0±0.8
Fa	1.3±0.3	traces	2.1±0.2	4.5±0.4	2.6±0.3	1.6±0.3	12.1±1.4
Hy	0.2±0.1	traces	0.4±0.1	2.0±0.3	0.4±0.2	0.4±0.2	3.5±0.8

Table 6

Group content (%) relative to free huminic acids

Huminic acid	Saccharides, S	Amino acids A	S + A	C, H, O, N SUM	Mineral matter MГ= 100--SUM	S+A+M	Residue 100--(S+A+M)	S/A	A/N
Haapsalu									
Ha	4.8	18.6	23.4	54.9	45.1	68.5	31.5	0.3	2.1
Fa	20.9	9.1	30.0	73.7	26.4	56.4	43.7	2.3	2.3
Hy	7.4	24.1	31.4	77.3	22.7	54.1	45.9	0.3	4.9

Humic acid	Saccharides, S	Amino acids A	S + A	C, H, O, N SUM	Mineral matter MГ= 100- -SUM	S+A+M	Residue 100- -(S+A+M)	S/A	A/N
Kuressaare Suurlaht									
Ha	16.2	22.3	38.5	75.2	24.8	63.2	36.8	0.7	2.9
Fa	32.4	14.3	46.7	80.6	19.4	66.1	33.9	2.3	2.7
Hy	6.8	21.6	28.4	84.8	15.2	43.6	56.4	0.3	3.6
Värska									
Ha	3.0	14.6	17.7	69.3	30.7	48.3	51.7	0.2	2.4
Fa	12.1	6.2	18.2	76.9	23.1	41.3	58.7	2.0	1.7
Hy	3.5	8.3	11.8	67.0	33.0	44.8	55.3	0.4	2.1

REFERENCES

1. **Schlossmann, K.** Estonian Curative Sea-Muds and Seaside Health Resorts. London, 1939.
2. **Maide, I.** Estonian Curative Muds. Tallinn, 1940 (in Estonian).
3. **Vadi, V.** Estonian Curative Mud. A balneologic study. Tartu, 1947 (in Estonian).
4. **Veinpalu, E. and L. Veinpalu.** On Curative Mud and Mud Cure. Tallinn, 1976 (in Estonian).
5. **Jefremov, I.** Periodical Colloidal Structures. Leningrad, 1971 (in Russian).
6. **Orlov, D.** Chemistry of Soils. Moscow University Press, 1985 (in Russian).
7. **Zhorobekova, Sh.** Macro-ligand Properties of Huminic Acids. Frunze, 1987 (in Russian).
8. **Shirshova, I.** Polydispersity of Humus Elements of Soils. Moscow, 1991 (in Russian).
9. Physico-chemical Research Methods of Soils. Moscow University Press, 1980 (in Russian).
10. **Orlov, D. and Grishina, L.** A Practival Course in Chemistry of Humus. Moscow University Press, 1981 (in Russian).
11. **Glebova, G.** Hymatomelanic Acids of Soils. Moscow University Press, 1980 (in Russian).
12. **Ishiwatari, R.** Organic Polymers in Recent Sediments – Chemical Nature and Fate in Geological Environment. Tokyo, 1971.
13. **Deveni, T. and Gergei, I.** Amino Acids, Peptides, Proteins. Moscow, 1976 (in Russian).
14. **Ilomets, T., Pärn A., Raidaru, G., Salm, S. and Veermäe, I.** On Chemical Compositions of Humisol. Eesti Rohuteadlane, 3 (1992) 4–10 (in Estonian).

Tartu Ülikooli toimetised. Vihik 966
PUBLICATIONS ON CHEMISTRY XXI
Tartu Ülikool
EE2400 Tartu, Ülikooli 18
T. 50. 500. 14,74. 14,5
TÜ trükikoda. EE2400 Tartu, Tiigi 78